Stochastic models of cell population dynamics and tick-borne virus transmission

Giulia Belluccini

Department of Applied Mathematics

University of Leeds

Submitted in accordance with the requirements for the degree of

Doctor of Philosophy

January 2023

The candidate confirms that the work submitted is her own, except where work which has formed part of jointly authored publications has been included. The contribution of the candidate and the other authors to this work has been explicitly indicated below. The candidate confirms that appropriate credit has been given within the thesis where reference has been made to the work of others.

Almost all of the work in Chapter 3 has been refereed and published, as follows:

- **Belluccini, G**, López-García, M, Lythe, G and Molina-París, C, (2022). Counting generations in birth and death processes with competing Erlang and exponential waiting times. *Scientific Reports*, 12, pp.1–20.

Code availability: GitHub release of codes for Chapter 3.

Additionally, almost all of the work in Chapter 4 and Chapter 5 is in preparation:

- **Belluccini, G**, López-García, M, Lythe, G and Molina-París, C. Two-type branching process to study cell population dynamics with cellular fate decision at birth. *To be submitted.*

- **Belluccini, G**, Lin, Q, Lou, Y, Romero-Severson, E, Leitner, T, López-García, M, Lythe, G and Molina-París, C. Co-infection, co-transmission and co-feeding in segmented viruses: a mathematical model of invasion. *To be submitted.*

Preface

My PhD is funded by the Horizon 2020–Marie Skłodowska-Curie Action as an Early Stage Researcher in the Quantitative T Cell Immunology and Immunotherapy (QuanTII) network. Each PhD student part of QuanTII is required to undertake a secondment in another institution with the aim of receiving specific training relevant to their research project.

According to the original plans of my PhD project, I should have visited the group led by Professor Marc Jenkins in the Department of Microbiology and Immunology at the University of Minnesota in the Summer of 2020. The aim of the visit was to undertake mathematical and computational modelling of the population of $CD4^+$ T cells, based on measurements that would have been made by a post-doctoral research fellow in the Jenkins' laboratory. The work developed in collaboration with Jenkins' laboratory would have constituted the contents of Chapter 5 of my thesis.

Unfortunately, during the SARS-CoV-2 pandemic, the laboratory was closed for several months and consequently, the experiments were not performed.

More recently, the University of Leeds started a new collaboration with Los Alamos National Laboratory (New Mexico) and other institutions around the world to model reassortment at the cellular, clinical, and phylogenetic levels in emerging Bunyaviruses. This project required the development of mathematical models to characterise co-infection dynamics, which is a necessary condition for reassortment. Thus, my PhD supervisors and I thought that I could develop these mathematical

models as work for the final chapter of my thesis. This explains why my thesis contains mathematical models of such different biological processes.

While using some mathematical tools employed also in Chapters 3 and 4 (*e.g.*, branching processes), the work in Chapter 5 allowed me to learn about viral dynamics and epidemiology during my visit to Los Alamos National Laboratory from 10 October to 13 December 2022. Nowadays, these tools are critically important to develop adequate mathematical models for the novel coronavirus and other emerging and re-emerging viruses, which have been prioritised by the World Health Organisation. Thus, I strongly believe that this project has equipped me with useful tools that will enhance my future career as a researcher.

Acknowledgements

My PhD has been a very interesting and challenging journey, which made me grow both scientifically and personally.

First and foremost, I would like to thank my supervisors, Martín López-García, Carmen Molina-París and Grant Lythe, who have supported and inspired me throughout my PhD studies with their curiosity and genuine interest in science. I will be always grateful for everything I learned from you.

My thanks go to the European Union for funding my PhD through the Marie Skłodowska-Curie Innovative Training Network *Quantitative T cell Immunology and Immunotherapy* (QuanTII). As part of QuanTII, I had the opportunity to engage with many PhD students and amazing scientists since the beginning of my studies. From QuanTII, I would like to particularly thank Jessica Brennan, QuanTII administrator, for her incredible support and for organising the QuanTII meetings.

I would like to express my gratitude to all the PhD students of the Mathematical Biology and Medicine group of the University of Leeds for sharing this journey with me. I would not have enjoyed my PhD so much without you! In particular, I would like to thank Polly Anne Jeffrey for the useful discussions throughout my studies.

From Los Alamos National Laboratory, I would like to thank my collaborators for sharing their knowledge and for all the useful discussions during my research visit.

Grazie ai miei genitori, Francesca e Corrado, per avermi sempre incoraggiata a seguire le mie passioni e per avermi sempre sostenuta nelle mie scelte. Senza di voi non sarei quella che sono oggi. Grazie a mia

sorella Benedetta per la generosità e la leggerezza che porta ogni giorno nella mia vita.

I am very grateful to my partner Carlos for all his love, care and support, and for giving me new perspectives. Life with you is more interesting!

Abstract

When modelling cellular population dynamics, many mathematical models consider exponential inter-event times. Despite being the most convenient choice from a mathematical and computational perspective, the exponential distribution overestimates the probability of short division times. In Chapter 3, I consider a multi-stage model of the cell cycle to maintain the advantages of a Markovian model, while improving on exponential times to division. With this structure in place, cell generations are introduced in the model to link theoretical predictions with experimental data. The model with cell generations is parameterised making use of CFSE data and Bayesian methods. Then, in order to study fate correlation of cellular siblings, in Chapter 4, I propose a mathematical model that makes use of the theory of branching processes. Cells are categorised based on their fate, either division or death, which is decided at birth. The applicability of this approach is shown by considering a data set of stimulated B cells produced with time-lapse microscopy.

The last chapter of this thesis aims to shed light on the role of co-feeding and co-transmission in the spread of a vector-borne virus. Thus, a population of ticks interacts with a population of hosts (small or large vertebrates). First, I consider a single infection whose dynamics is modelled through both deterministic and stochastic models. The basic reproduction number is computed by means of the next generation matrix approach. When modelling co-infection with two different viruses (or two strains of the same virus), a deterministic model is proposed to study only co-feeding transmission, accounting also for co-transmission of the virus. A series of stochastic descriptors of interest are computed when considering all the routes of transmission.

Abbreviations

SARS-CoV-2	Severe acute respiratory syndrome coronavirus 2
IL	Interleukin
pdf	Probability density function
pgf	Probability generating function
$\mathbb{N}_0$	$\mathbb{N} \cup \{0\}$
CTMC	Continuous time Markov chain
PH	Phase-type distribution
ODE	Ordinary differential equation
PDE	Partial differential equation
TCR	T cell receptor
CFSE	Carboxyfluorescein succinimidyl ester
ABC	Approximate Bayesian computation
ABC-SMC	Approximate Bayesian computation sequential Monte Carlo
MS	Multi-stage model of cell proliferation and death
MS-G	Multi-stage model of cell proliferation and death tracking generations
AIC	Akaike's information criterion
AIC_C	Corrected Akaike's information criterion
LIP	Lymphopenia-induced proliferation
CCHF	Crimean–Congo hemorrhagic fever

Contents

List of Figures

List of Tables

Chapter 1

Introduction

In this thesis, two different types of population dynamics are studied. Chapters 3 and 4 focus on stochastic models of cell population dynamics, whereas in Chapter 5, a population of ticks interacting with a population of hosts (*e.g.*, small or large vertebrates) is considered to analyse the spread of a vector-borne viral infection.

1.1 Immunological background

Our first line of defence against invaders (*e.g.*, viruses or bacteria) consists of physical barriers, such as skin and mucous membranes (Sompayrac, 2022). Any invader that breaches our physical barriers is greeted by the *innate* immune system, so called because any living being is equipped with it (Sompayrac, 2022). Vertebrates possess also a third line of defence, known as the *adaptive* immune system, whose main characteristic is that it is activated on demand, providing a specific response for different invaders (Sompayrac, 2022). Among the main actors of the adaptive immune response, there are B cells and T cells, also called B lymphocytes and T lymphocytes. They display on their surface molecules called *receptors*, which are used in pathogen recognition. The set of T lymphocytes with the same T cell receptors defines a T cell clonotype (Lythe *et al.*, 2016).
Beyond lymphocytes, the immune system is comprised of other types of cells, such as macrophages and neutrophils. Each type of immune cell has a specific role and is able to communicate and interact with other cells using *cytokines*, which are

small proteins produced by a broad range of cells. Cytokine is a general name; in more specific terms, we can mention for example *lymphokine* (produced by lymphocytes) and *interleukin* (secreted by white blood cells). Some interleukins (IL for short) play an essential role in the development and proliferation of T lymphocytes (Rochman *et al.*, 2009). For example, IL-2 is a T cell growth factor and regulates the proliferation and apoptosis of activated T cells; IL-7 has a central role in the development of T cells in both humans and mice; IL-15 is fundamental to maintaining normal T cell counts (T cell homeostasis). Thus, lack or abundance of these interleukins affects the population size of T lymphocytes.

1.2 Cell population dynamics

Lymphocyte populations stimulated *in vitro* or *in vivo*, grow as cells divide. In particular, during an adaptive immune response, a subset of specific cells, initially a small fraction of the total population, expands as cells undergo multiple rounds of division over a few days (Antia *et al.*, 2005). Mathematical models are fundamental to providing a quantitative characterisation of lymphocyte population expansion. One of the main aims of these models is the estimation of lymphocyte birth and death rates, which vary according to the type of lymphocyte and the stimuli cells receive. Stochastic models are appropriate to describe immune cell dynamics because some cells undergo multiple rounds of division, some die, and others of the same type in the same conditions do not divide at all. If individual cells behave independently, then each cell can be imagined as sampling from a probability density of times to division and death. The exponential density is the most mathematically and computationally convenient choice: it guarantees analytical tractability and computational efficiency of stochastic simulations by means of the Gillespie algorithm (Gillespie, 1976, 1977). However, it does not accurately describe a cell's time to division because it overestimates the probability of short division times (Yates *et al.*, 2017; Zilman *et al.*, 2010). Indeed, cells are cycling through gap, synthesis and mitosis phases. The cell cycle is a complex process that involves DNA replication and chromosome segregation, leading a cell to divide. As depicted in Figure 1.1, different phases comprise the cell cycle:

- the gap phase 1, G1; the cell grows physically larger, copies its organelles and makes molecular building blocks.
- the synthesis, S; the cell synthesises a complete copy of the DNA in its nucleus.
- the gap phase 2, G2; the cell continues to grow, makes proteins and organelles and begins to organise its contents for cell division.
- the dividing phase M, which consists of two main stages:
    1. Mitosis: the nuclear DNA of the cell condenses into visible chromosomes (it is possible to recognise four different mitosis phases).
    2. Cytokinesis: the cytoplasm of the cell is split in two, making two new cells.

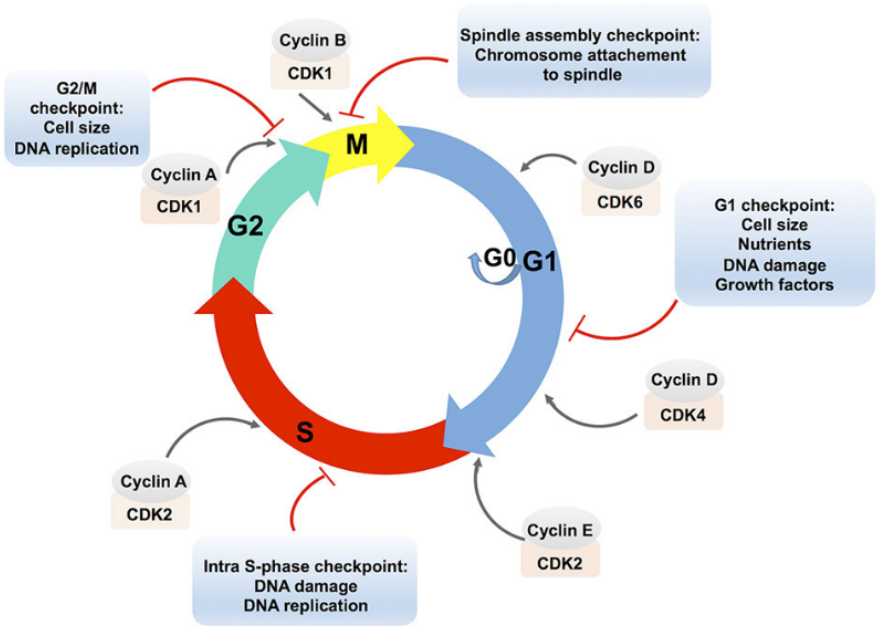

Figure 1.1: Schematic representation of the different phases that comprise the cell cycle from El-Aouar Filho *et al.* (2017).

The phases G1, S, G2 represent together the stage called *interphase*. Cells can also exit the cell cycle and enter a quiescent state, the G0 phase (El-Aouar Filho *et al.*, 2017). Given the complex process that leads a cell to divide, it becomes apparent that daughter cells cannot immediately redivide (Pandit & De Boer, 2019).

With the aim of preserving the advantages of a Markovian framework while improving the representation of experimentally-observed division times, in Chapter 3 a multi-stage representation of cellular division proposed by Yates *et al.* (2017) is extended to account also for cell death. Erlang-distributed (or, more generally, phase-type distributed (He, 2014)) times to division and exponentially distributed times to death are used. The underlying idea is that each cell is required to sequentially visit a given number of stages, denoted by N, before dividing. Each stage is exponentially distributed, and consequently, the Markovian framework is preserved. The rate of progression from a stage to the subsequent one is called *birth rate* and is denoted by λ. The growth rate of the cell population is derived by calculating the fraction of cells in each stage. The exponent describing the long-term cell population growth, and the criterion for extinction of the population, differs from what would be expected if N steps with rate λ were equivalent to a single step of rate λ/N. In order to link theoretical predictions with experimental data, cells are classified into generations (*i.e.*, cells that have divided the same number of times) using the rule that the daughters of cells in generation g are in generation $g+1$. In some circumstances, this representation is equivalent to established models of lymphocyte dynamics (Hawkins *et al.*, 2007). The theoretical predictions of the model are linked with a published experimental data set, where cell counts were reported after T cells were transferred to lymphopenic mice (Hogan *et al.*, 2013), using Approximate Bayesian Computation methods (Toni *et al.*, 2009). Cells at the start of the experiment (before any stimulus has been added) are assumed to be in generation 0. In the comparison, the death rate is assumed to be proportional to the generation and the Erlang time to division for generation 0 is allowed to differ from that of subsequent generations. Our results in Chapter 3 show that the multi-stage representation is preferred to a simple exponential in posterior distributions and the mean time to first division is estimated to be longer than the mean time to subsequent divisions (Belluccini *et al.*, 2022).

Although providing a good description of experimental data (Belluccini *et al.*, 2022), the multi-stage model with cell generations relies on the assumption that cells are independent of each other. In particular, no fate correlation is assumed between daughter cells and their progenitors, or between siblings. However, data sets from time-lapse microscopy of B and T cell families show that division and death times for siblings are correlated (Dowling *et al.*, 2014; Duffy & Hodgkin, 2012; Duffy & Subramanian, 2009; Duffy *et al.*, 2012; Hawkins *et al.*, 2009; Markham *et al.*, 2010; Wellard *et al.*, 2010), and *division destiny* is a familial characteristic (Cheon *et al.*, 2021). As the multi-stage model in Chapter 3 cannot account for such correlations, a two-type branching process is considered in Chapter 4 to model cellular population dynamics with fate decision at birth. A population of cells is split into two pools: cells that are going to divide and cells whose fate is death. When a division occurs, both daughter cells join the division pool with probability p_1, enter the death pool with probability p_2, or have different fates with probability $p_3 = 1 - p_1 - p_2$. After this instantaneous fate decision at birth, cellular fate takes some random time to happen. Exponential and Erlang probability distributions are used to model cellular time to division and death with the aim of preserving the Markov property. In this way, the timescales for cellular division and death are separated from the cellular fate probabilities. The resulting dynamics is a two-type branching process (Athreya *et al.*, 2004). The probability generating function of the number of cells in each pool is derived when working with exponential times, whereas the expected number of cells over time is computed under the assumption of Erlang times to division and death. Cellular fate correlation is introduced in the model through the definition of correlation factors. By means of Approximate Bayesian Computation methods (Toni *et al.*, 2009), the theoretical predictions of the model are compared to a data set of stimulated naive B cells, followed for 120 hours using time-lapse microscopy (Hawkins *et al.*, 2009; Markham *et al.*, 2010). The fate of sibling cells is broken per division: for each generation the fraction of pairs of siblings both dividing, both dying and having different fates is known (Markham *et al.*, 2010). This data representation enables the comparison between the theoretical probabilities of our model and the experimental data. Despite its simplicity, our model qualitatively follows the trends of

the fraction of pairs of siblings both dividing, both dying and having different fates observed in the experiments.

1.3 Tick-borne virus transmission

Segmented viruses are characterised by genomes comprised of multiple RNA strands, called *segments*. A single host cell can be simultaneously infected with two or more segmented viruses (or two or more strains of the same segmented virus) as co-infection of a single host by different pathogens is ubiquitous in nature (Cox, 2001; Lowen, 2017). When co-infection of a single host cell with two or more segmented viruses occurs, genome segments can be exchanged during viral assembly (McDonald *et al.*, 2016). This process of genome segments exchange is known as *reassortment* (Lowen, 2018), and produces progeny with new viral properties, which may lead to more transmissible or more severe diseases. The family of *Bunyavirales* is an order of segmented negative strand RNA-viruses that includes also the Crimean-Congo hemorrhagic fever (CCHF) virus, which has been declared a research and development priority by the World Health Organisation (Mehand *et al.*, 2018). CCHF virus is a tick-borne virus that causes severe disease only in humans.

There are still many questions that remain to be answered about the reassortment process, and in order to provide adequate answers, it is fundamental to understand co-infection dynamics. Indeed, reassortment can only occur when a single host cell is infected by two or more pathogens.

Another aspect that one should take into account when modelling the spread of tick-borne viruses is co-feeding transmission within the tick population (Gonzalez *et al.*, 1992; Matser *et al.*, 2009). This type of transmission occurs when ticks feed in close proximity to each other on the same host (Belli *et al.*, 2017).

To shed light on co-feeding transmission and co-infection dynamics, in Chapter 5 we consider two interacting populations, namely hosts (*e.g.,* small or large vertebrates) and ticks, both susceptible to infection with two distinct strains of the same virus. The infection can be transmitted by infected ticks to susceptible hosts, from infected hosts to susceptible ticks (systemic transmission), and from infected ticks to susceptible ticks through co-feeding (non-systemic transmission). We first

analyse the dynamics of a single infection, proposing both a deterministic and a stochastic model to understand the role of the different routes of virus transmission. In the deterministic setting, the basic reproduction number is computed by making use of the next-generation matrix approach (Van den Driessche, 2017). An approximating branching process is also considered to derive the probability of both the virus-free and endemic states (Allen, 2010). Then, by means of first step arguments (Pinsky & Karlin, 2010), the distribution of the exact number of secondary infections directly caused by a *marked* infected individual is derived (Artalejo & Lopez-Herrero, 2013).

When considering co-infection by two distinct strains (one resident and one invasive), ordinary differential equations are used to model the dynamics of susceptible, infected and co-infected ticks in a deterministic model that accounts only for co-feeding transmission. The invasion reproduction number of the invasive strain is computed by means of the next generation matrix approach (Alizon, 2013a). Using a stochastic approach that considers all the routes of transmission, the probability of (and conditional time to) extinction and establishment of the invasive strain are derived, together with the probability of (and conditional time to) co-infection events.

Chapter 2

Mathematical background

Stochastic models are primarily the tool used in this thesis to study cell population dynamics and tick-borne virus transmission. Some deterministic models have also been proposed to study complementary aspects of these models. Thus, this chapter contains a background of probability theory and stochastic processes, as well as some basic notions of differential equations and deterministic modelling. An overview of the mathematical methods and statistical techniques used throughout the thesis is also provided.

2.1 Generalities of probability theory

In Chapters 3, 4 and 5, I make use of continuous time Markov chains and branching processes to study cell population dynamics and tick-borne virus transmission. The notions required to understand such processes are introduced in this section following the work by Allen (2010); Berger *et al.* (2021); He (2014); Jacod & Protter (2004); Norris (1998); Stirzaker (2005).

2.1.1 Probability

Randomness arises in many everyday activities: flip a coin, make a decision, roll a die, or buy a stock. A person might wonder about the *probability* that a head occurs, or the stock increases its value. In many of these situations the idea of probability is linked to a proportion between favourable outcomes and all the

possible events. Therefore, to formalise mathematically the concept of probability, let $\mathcal{S}$ be the set of all the possible outcomes of an experiment, usually referred as *sample space*. Each subset of $\mathcal{S}$ is called *event*. For example, suppose to roll a die and record the count of spots on the up-face. Then, $\mathcal{S} = \{1, 2, 3, 4, 5, 6\}$, and an event may be $\{3\}$ or $\{4, 6\}$. Let $\mathcal{A}$ denote the family of all events. The set $\mathcal{A}$ must satisfy the following properties.

Definition 2.1. *Let $\mathcal{A}$ be a collection of subsets of $\mathcal{S}$. Then $\mathcal{A}$ is called a* σ-algebra *and the pair $(\mathcal{S}, \mathcal{A})$ is called a* measurable space *if the following properties hold:*

1. $\mathcal{S} \in \mathcal{A}$.
2. *If $A \in \mathcal{A}$, the complement of A, A^C, is in $\mathcal{A}$, that is*
$$A \in \mathcal{A} \implies A^C \in \mathcal{A}.$$
3. *For any sequence $\{A_n\}_{n=1}^{+\infty}$, $A_n \in \mathcal{A}$, the union $\bigcup_{n=1}^{+\infty} A_n \in \mathcal{A}$.*

With each event $A \in \mathcal{A}$ one associates a number denoted by $\mathbb{P}(A)$ and called *probability of A*. This number represents the likelihood of the event A to be realised *a priori*, before the experiment is performed. The probability $\mathbb{P}(A)$ is defined between 0 and 1, where the closer to 1 $\mathbb{P}(A)$ is, the more likely A is to be observed. A probability $\mathbb{P}$ is formally defined on $\mathcal{A}$ as follows.

Definition 2.2. *Let $(\mathcal{S}, \mathcal{A})$ be a measurable space. Let $\mathbb{P}$ be a real-valued set function defined on the σ-algebra $\mathcal{A}$. The set function $\mathbb{P} : \mathcal{A} \to [0, 1]$ is called a* probability measure *if the following properties are satisfied:*

1. $\mathbb{P}(A) \geq 0$ *for all* $A \in \mathcal{A}$.
2. $\mathbb{P}(\mathcal{S}) = 1$.
3. *If $A_i \cap A_j = \emptyset$ for $i, j = 1, 2, \ldots$, $i \neq j$, then*
$$\mathbb{P}\left(\bigcup_{i=1}^{+\infty} A_i\right) = \sum_{i=1}^{+\infty} \mathbb{P}(A_i),$$
where $A_i \in \mathcal{A}, i = 1, 2, \ldots$.

The ordered triple $(\mathcal{S}, \mathcal{A}, \mathbb{P})$ defines a *probability space*.

2.1.2 Conditional probability and independence

When studying a random process, it is interesting to understand the effect that the occurrence of an event B has on the probability of another event A. This leads to the definition of conditional probability and independent events.

Definition 2.3. *Let A and B be events defined in the probability space $(\mathcal{S}, \mathcal{A}, \mathbb{P})$, with $\mathbb{P}(B) > 0$. The* conditional probability of A given B *is defined as*

$$\mathbb{P}(A|B) = \frac{\mathbb{P}(A \cap B)}{\mathbb{P}(B)}. \tag{2.1}$$

It may also happen that the knowledge of B does not affect the probability of A; that is $\mathbb{P}(A|B) = \mathbb{P}(A)$. In this instance, the identity in (2.1) yields

$$\mathbb{P}(A \cap B) = \mathbb{P}(A)\mathbb{P}(B).$$

Definition 2.4. *Two events A and B defined in a probability space $(\mathcal{S}, \mathcal{A}, \mathbb{P})$ are* independent *if*

$$\mathbb{P}(A \cap B) = \mathbb{P}(A)\mathbb{P}(B).$$

2.1.3 Random variables

The mathematical concept of *random variable* formalises the idea of a quantity that depends on the outcome of a random experiment.

Definition 2.5. *Let $(\mathcal{S}, \mathcal{A}, \mathbb{P})$ be a probability space and $(E, \mathcal{E})$ a measurable space. A* random variable X *is defined as a map from the sample space $\mathcal{S}$ to E, $X : \mathcal{S} \to E$ if for each $B \in \mathcal{E}$, one has $\{X \in B\} \in \mathcal{A}$, where*

$$\{X \in B\} := X^{-1}(B) = \{\varsigma \in \mathcal{S} : X(\varsigma) \in B\}.$$

The space E is often the real line $\mathbb{R}$ or $E = \mathbb{R}^n$. The random variable X can be thought of as an element $X(\varsigma)$ of E which depends on the outcome $\varsigma \in \mathcal{S}$ of the random experiment. The *state space* or *support* or *range* Ω_X of the random variable X is defined as the set of all the possible values that X can take

$$\Omega_X = \{x \in E : \exists\ \varsigma \in \mathcal{S} \text{ such that } X(\varsigma) = x\}. \tag{2.2}$$

If Ω_X is finite or countably infinite, then X is said to be a *discrete random variable*, whereas if the support is uncountable, then X is said to be a *continuous random variable*. Throughout the thesis, the subscript referring to the random variable will be omitted to simplify the notation.
For each random variable $X : \mathcal{S} \to E$ it is possible to define the associated *induced probability measure* $\mathbb{P}_X : \mathcal{E} \to [0, 1]$ as

$$\mathbb{P}_X(B) = \mathbb{P}(X \in B), \quad B \in \mathcal{E}.$$

Definition 2.6. *Let X be a real-valued random variable defined on the probability space $(\mathcal{S}, \mathcal{A}, \mathbb{P})$. The* cumulative distribution function *of X is the function $F : \mathbb{R} \to [0, 1]$ defined by*

$$F(x) = \mathbb{P}(X \leq x) = \mathbb{P}_X((-\infty, x]).$$

The induced probability measure defines the probability mass function and the probability density function for discrete and continuous random variables, respectively.

Definition 2.7. *Let X be a discrete random variable. Then the function $f(x) = \mathbb{P}_X(X = x)$ that is defined for each $x \in \Omega$ is called the* probability mass function *of X.*

Definition 2.8. *Let X be a continuous random variable with cumulative distribution function $F(x)$. Suppose there exists a non-negative, integrable function $f : \mathbb{R} \to [0, +\infty)$ such that*

$$F(x) = \int_{-\infty}^{x} f(t)dt.$$

Then the function $f(x)$ is called the probability density function *(pdf for short) of X.*

The *probability distribution* of a random variable X can be specified by either its cumulative distribution function $F(x)$ or its probability density (or probability mass if X is discrete) function $f(x)$.

Example 2.9. *The probability distributions of the main well-known random variables used throughout the thesis are listed below.*

i. A random variable X is said to follow an exponential distribution *with parameter $\lambda > 0$, $X \sim Exp(\lambda)$, if its probability density function is defined as*

$$f(x) = \begin{cases} \lambda e^{-\lambda x}, & x \geq 0, \\ 0 & otherwise. \end{cases}$$

ii. A random variable X is said to follow a uniform distribution *with parameters $a, b \in \mathbb{R}$ and $a < b$, $X \sim U(a, b)$, if its probability density function is defined as*

$$f(x) = \begin{cases} \dfrac{1}{b-a}, & if\ x \in [a, b], \\ 0 & otherwise. \end{cases}$$

iii. A random variable X is said to follow a Gamma distribution *with parameters $\alpha, \beta > 0$, $X \sim \Gamma(\alpha, \beta)$, if its probability density function is defined as*

$$f(x) = \begin{cases} \dfrac{\beta^\alpha}{\Gamma(\alpha)} x^{\alpha-1} e^{-\beta x}, & if\ x \geq 0, \\ 0 & otherwise, \end{cases}$$

where the Gamma function $\Gamma(\cdot)$ is defined as

$$\Gamma(z) = \int_0^{+\infty} x^{z-1} e^{-x} \mathrm{d}x, \tag{2.3}$$

and $\Gamma(n) = (n-1)!$ for any $n \in \mathbb{N}$. The parameter α is referred as shape*, whereas β is called* rate*.*

iv. A random variable X is said to follow an Erlang distribution *with parameters $N \in \mathbb{N}$ and $\lambda > 0$, $X \sim Erlang(N, \lambda)$, if its probability density function is defined as:*

$$f(x) = \begin{cases} \dfrac{\lambda^N x^{N-1} e^{-\lambda x}}{(N-1)!}, & if\ x \geq 0, \\ 0 & otherwise. \end{cases}$$

Note that the Erlang probability density is a particular case of the Gamma where the shape parameter can take only integer values.

v. A non-negative random variable τ is said to follow a phase-type distribution *(PH distribution), $\tau \sim PH(\boldsymbol{\alpha}, \boldsymbol{T})$, if its cumulative distribution function is given by*

$$F(t) = \mathbb{P}(\tau \leq t) = 1 - \boldsymbol{\alpha} \mathrm{e}^{\boldsymbol{T}t} \boldsymbol{e}, \ t \geq 0, \tag{2.4}$$

where

1. *$\boldsymbol{e}$ is a column vector of order $m \in \mathbb{N}$ with all the entries equal to 1;*
2. *$\boldsymbol{\alpha}$ is a row vector of order m such that $\alpha_i \geq 0$ for all $i = 1, \ldots, m$ and $\boldsymbol{\alpha} \cdot \boldsymbol{e} = \sum_{i=1}^{m} \alpha_i \leq 1$. Such a vector is also called* sub-stochastic *vector;*
3. *$\boldsymbol{T}$ is a square matrix of order m such that*
   - *i. $t_{ii} < 0$ for all $i = 1, \ldots, m$,*
   - *ii. $t_{ij} \geq 0$ for all $i, j = 1, \ldots, m$ such that $i \neq j$,*
   - *iii. $\sum_j t_{ij} \leq 0$ for all $i = 1, \ldots, m$,*
   - *iv. $det(\boldsymbol{T}) \neq 0$.*

The matrix $\boldsymbol{T}$ is called PH-generator *and the couple $(\boldsymbol{\alpha}, \boldsymbol{T})$ is referred as* phase-type representation (PH-representation) *of order m for the PH distribution. The related probability density function is given by*

$$f(t) = \boldsymbol{\alpha} \mathrm{e}^{\boldsymbol{T}t}(-\boldsymbol{T}\boldsymbol{e}), \quad t \geq 0. \tag{2.5}$$

Definition 2.10. *Suppose X is a continuous random variable with pdf $f(x)$. Then the* expectation*, or* mean*, of X, denoted as $\mathbb{E}[X]$, is defined as*

$$\mathbb{E}[X] = \int_{\mathbb{R}} x f(x) \mathrm{d}x.$$

Suppose X is a discrete random variable with probability mass function $f(x)$ defined on the space $\Omega = \{a_i\}_{i=1}^{+\infty}$. Then the expectation*, or* mean*, of X is defined as*

$$\mathbb{E}[X] = \sum_{i=1}^{+\infty} a_i f(a_i).$$

Definition 2.11. *The* variance *of the random variable X denoted as σ^2, σ_X^2 or $Var(X)$ is $Var(X) = \mathbb{E}[(X - \mathbb{E}[X])^2]$. The n*th moment of X *about the point a is $\mathbb{E}[(X - a)^n]$.*

For a discrete random variable, it is useful to define its probability generating function (pgf for short).

Definition 2.12. *Let X be a discrete random variable taking non-negative integer values. The* probability generating function *of X is defined as*

$$G(z) = \mathbb{E}\left[z^X\right] = \sum_{n=0}^{+\infty} z^n p_n, \quad |z| \leq 1, \tag{2.6}$$

where $z \in \mathbb{C}$ and $p_n = \mathbb{P}(X = n)$.

Since $\sum_{n=0}^{+\infty} p_n = 1$, the sum in (2.6) converges absolutely for $|z| \leq 1$. Thus, $G(z)$ is well defined for $|z| \leq 1$, and infinitely differentiable for $|z| < 1$ (Karlin & Taylor, 1975). As the name implies, the probability generating function generates the probabilities associated with the distribution of X

$$G(0) = p_0, \quad G'(0) = p_1, \quad G''(0) = 2!p_2,$$

and, in general,

$$G^{(k)}(0) = k!p_k, \quad k \geq 1.$$

The analogous of the probability generating function for a continuous random variable is given by the Laplace-Stieltjes transform.

Definition 2.13. *The* Laplace-Stieltjes transfrom *of a continuous non-negative random variable $X \geq 0$ with probability density function $f(x)$ is denoted by $\phi^X(z)$ and defined as*

$$\phi^X(z) = \mathbb{E}\left[\mathrm{e}^{-zX}\right] = \int_0^{+\infty} \mathrm{e}^{-zx} f(x)dx, \quad Re(z) > 0,$$

*where $z \in \mathbb{C}$. The l*th *moment of X, denoted by $\mathbb{E}\left[X^l\right]$, is obtained by deriving $\phi^X(z)$:*

$$\mathbb{E}\left[X^l\right] = (-1)^l \frac{\mathrm{d}^l}{\mathrm{d}z^l} \phi^X(z)\Big|_{z=0}, \quad l \geq 0.$$

2.2 Stochastic processes

In Section 2.1.3, the idea of a single random variable has been formalised. However, many real phenomena require to be described as random processes evolving in time or space, or both. This leads to the definition of a *stochastic process*. The contents of this section follow Allen (2010); He (2014); Karlin & Taylor (1975); Kulkarni (2016); Stirzaker (2005).

Definition 2.14. *A* stochastic process *is a collection of random variables* $\{X_t(\varsigma) : t \in T, \varsigma \in \mathcal{S}\}$*, where* T *is some index set and* $\mathcal{S}$ *is the common sample space of the random variables. For each fixed* $t \in T$*,* $X_t(\varsigma)$ *denotes a single random variable defined on* $\mathcal{S}$*. For each fixed* $\varsigma \in \mathcal{S}$*,* $X_t(\varsigma)$ *corresponds to a function defined on* T *that is called* sample path *or a* stochastic realisation *of the process.*

Throughout the thesis, the index set T will be a set of times, therefore defined either as $T = \{t \in \mathbb{R} : t \geq 0\}$ in the case of a continuous time stochastic process, or $T = \mathbb{N}_0 = \mathbb{N} \cup \{0\}$ in the instance of a discrete time stochastic process. The common sample space $\mathcal{S}$ will be often omitted hereinafter; therefore, a stochastic process will be simply denoted as $(X(t))_{t\geq 0}$ if continuous, or $(X(k))_{k\in\mathbb{N}_0}$ if discrete.

2.2.1 Continuous time Markov chains

Markov chains are an example of stochastic processes that are utilised to model a wide range of real-world problems that arise from different disciplines, such as finance, biology, chemistry, social sciences, economics and physics.
In this section, continuous time Markov chains are considered, meaning that the time is continuous, whereas the state space of the random variables is discrete. The main feature of a Markov chain is that what happens next depends only on the present, while the past history of the process does not affect its future evolution. The following definition expresses this property in mathematical terms.

Definition 2.15. *Let* $(X(t))_{t\geq 0}$ *be a set of discrete random variables taking values in a finite* $\{0, 1, \dots, N\}$ *or infinite* $\{0, 1, 2, \dots\}$ *state space* Ω*. The stochastic process* $(X(t))_{t\geq 0}$ *is a* continuous time Markov chain *(CTMC) if for any choice of*

$t_0, t_1, \ldots, t_{n+1} \geq 0$ such that $t_0 < t_1 < \cdots < t_{n+1}$

$$\mathbb{P}\left(X(t_{n+1}) = i_{n+1} | X(t_0) = i_0, \ldots, X(t_n) = i_n\right) = \mathbb{P}\left(X(t_{n+1}) = i_{n+1} | X(t_n) = i_n\right), \tag{2.7}$$

for any $i_0, i_1, \ldots, i_{n+1} \in \Omega$.

Equation (2.7) is commonly referred to as *Markov property*. For every $t \in [0, +\infty)$, $X(t)$ is a random variable with probability distribution $\{p_i(t)\}_{i\in\Omega}$, where

$$p_i(t) = \mathbb{P}(X(t) = i), \quad i \in \Omega.$$

The probabilities of the chain to jump from a state i to a state j describe the dynamics of the process and are formally defined as follows.

Definition 2.16. *Let $s, t \in [0, +\infty)$ such that $s < t$. The* transition probabilities *between the random variables $X(t)$ and $X(s)$ are defined as*

$$p_{ij}(s, t) = \mathbb{P}(X(t) = j | X(s) = i), \quad \text{for } i, j \in \Omega.$$

When the transition probabilities do not depend explicitly on t and s, but only on the length of the time interval $t - s$, the Markov process is said to be homogeneous *or* stationary*. Therefore, the transition probabilities can be rewritten as*

$$p_{ij}(t - s) = \mathbb{P}(X(t) = j | X(s) = i) = \mathbb{P}(X(t - s) = j | X(0) = i) \quad \text{for } s < t.$$

The transition matrix*, denoted by $\boldsymbol{P}(t)$, is comprised of the transition probabilities p_{ij}, $\boldsymbol{P}(t) = (p_{ij}(t))_{i,j\in\Omega}$.*

Let $\boldsymbol{\alpha}$ be the initial distribution of the CTMC, which means

$$\mathbb{P}(X(0) = i) = \alpha_i, \quad i \in \Omega.$$

The following result contains the characterization of a homogeneous CTMC (Kulkarni, 2016).

Theorem 2.17. *A CTMC is completely described by its initial distribution $\boldsymbol{\alpha}$ and the set of transition probability matrices $\{\boldsymbol{P}(t) : t \geq 0\}$.*

For most continuous time Markov processes, the following property holds

$$\sum_{j\in\Omega} p_{ij}(t) = 1, \quad t \geq 0, \quad i \in \Omega, \tag{2.8}$$

and such processes are referred as *non-explosive* (see *e.g.*, Norris (1998) for explosive processes). In other words, non-explosive processes have the nice property that the transition matrix $\boldsymbol{P}(t)$, $t \geq 0$, is a stochastic matrix, which means all the row sums are equal to 1. Note that equation (2.8) can be violated only when the state space is infinite (Allen, 2010).
In this thesis, we will consider only homogeneous and non-explosive Markov chains. In order to give an example of a Markov process, the Poisson process will be defined in the following example.

Example 2.18. *Let* $(N(t))_{t\geq 0}$ *be a CTMC with state space* $\Omega = \{0, 1, 2, \dots\}$. $(N(t))_{t\geq 0}$ *is a* Poisson process *if* $N(0) = 0$ *and*

$$p_{ij}(\Delta t) = \mathbb{P}(N(t+\Delta t) = j | N(t) = i) = \begin{cases} \lambda\Delta t + o(\Delta t) & j = i+1, \\ 1 - \lambda\Delta t + o(\Delta t) & j = i, \\ o(\Delta t) & j \geq i+2, \\ 0 & j < i, \end{cases}$$

as $\Delta t \to 0^+$. *Basically the random variable* $N(t)$ *counts the number of jumps which occur in the process, where these jumps occur at rate* λ. *The transition probabilities tell us that in a small time interval* Δt *we can have either one jump or no jumps. The initial conditions and the transition probabilities are used to derive differential equations for the probability distributions* $p_i(t)$ *of* $N(t)$. *The solutions are then shown to represent a Poisson distribution with parameter* λt*; that is, it can be proven that* $N(t) \sim Poisson(\lambda t)$.

Transition matrix

According to Theorem 2.17, given the initial distribution $\boldsymbol{\alpha}$ of the CTMC, the transition matrix $\boldsymbol{P}(t)$ fully describes the process. However, the matrix $\boldsymbol{P}(t)$ might be hard to specify even for simple Markov chains. This is the reason why

other parameters, called *transition rates* q_{ij}, are defined. The transition matrix can be computed from the transition rates.
Suppose that the transition probabilities are differentiable for $t \geq 0$ and at $t = 0$ are given by

$$p_{ij}(0) = 0 \;\forall\; i \neq j \quad \text{and} \quad p_{ii}(0) = 1,$$

i.e., $\boldsymbol{P}(0)$ is equal to the identity matrix. Then, q_{ij} is defined as the rate at which the process can go from state i to state j in a short time interval Δt, which means

$$q_{ij} = \lim_{\Delta t \to 0^+} \frac{p_{ij}(\Delta t) - p_{ij}(0)}{\Delta t} = \lim_{\Delta t \to 0^+} \frac{p_{ij}(\Delta t)}{\Delta t}, \quad i \neq j, \tag{2.9}$$

and

$$q_{ii} = \lim_{\Delta t \to 0^+} \frac{p_{ii}(\Delta t) - p_{ii}(0)}{\Delta t} = \lim_{\Delta t \to 0^+} \frac{p_{ii}(\Delta t) - 1}{\Delta t}. \tag{2.10}$$

Note that $q_{ij} \geq 0, i \neq j$, by definition. As the transition matrix is stochastic, one has

$$1 - p_{ii}(\Delta t) = \sum_{j \in \Omega, j \neq i} p_{ij}(\Delta t) = \sum_{j \in \Omega, j \neq i} \left(q_{ij}\Delta t + o(\Delta t)\right),$$

as $\Delta t \to 0^+$, and therefore

$$q_{ii} = -\lim_{\Delta t \to 0^+} \frac{\sum_{j \in \Omega, j \neq i} \left(q_{ij}\Delta t + o(\Delta t)\right)}{\Delta t} = -\sum_{j \in \Omega, j \neq i} q_{ij},$$

where we used the fact that $\sum_{j \in \Omega, j \neq i} o(\Delta t) = o(\Delta t)$ (Allen, 2010). Therefore, $q_{ii} \leq 0$ and, if q_{ii} is finite, $\sum_{j \in \Omega} q_{ij} = 0$. From (2.9) and (2.10) it follows

$$p_{ij}(\Delta t) = q_{ij}\Delta t + o(\Delta t) + \delta_{ij},$$

as $\Delta t \to 0^+$, where δ_{ij} is Kronecker's delta symbol.
Denoting by $\boldsymbol{P}(\Delta t)$ the infinitesimal transition matrix and by $\boldsymbol{I}$ the identity matrix of the same dimension, the matrix $\boldsymbol{Q}$ is given by

$$\boldsymbol{Q} = \lim_{\Delta t \to 0^+} \frac{\boldsymbol{P}(\Delta t) - \boldsymbol{I}}{\Delta t}. \tag{2.11}$$

Definition 2.19. *The matrix of transition rates* $\boldsymbol{Q} = (q_{ij})_{i,j \in \Omega}$ *defined in (2.9), (2.10), (2.11) is called* infinitesimal generator matrix *and, if* $\Omega = \{0, 1, 2, \dots\}$, $\boldsymbol{Q}$

has the following structure

$$\boldsymbol{Q} = \begin{pmatrix} q_{00} & q_{01} & q_{02} & \cdots \\ q_{10} & q_{11} & q_{12} & \cdots \\ q_{20} & q_{21} & q_{22} & \cdots \\ \vdots & \vdots & \vdots & \end{pmatrix} = \begin{pmatrix} -\sum_{j=0}^{+\infty} q_{0j} & q_{01} & q_{02} & \cdots \\ q_{10} & -\sum_{j=0}^{+\infty} q_{1j} & q_{12} & \cdots \\ q_{20} & q_{21} & -\sum_{j=0}^{+\infty} q_{2j} & \cdots \\ \vdots & \vdots & \vdots & \end{pmatrix}$$

The main features of the infinitesimal generator matrix are that the sum of all the elements of each row is equal to 0 and the diagonal terms q_{ii} are the negative of the sum of the other elements in the same row.

Definition 2.20. *The* Kolmogorov forward equations *are a set of differential equations that describe the rate of change of the transition probabilities:*

$$\frac{\mathrm{d}p_{ij}(t)}{\mathrm{d}t} = \sum_{k \in \Omega} q_{kj} p_{ik}(t), \quad i, j \in \Omega,$$

which can be written in matrix form as

$$\frac{\mathrm{d}\boldsymbol{P}(t)}{\mathrm{d}t} = \boldsymbol{Q}\boldsymbol{P}(t).$$

This system of equations is also known as master equation.

Next result shows how to compute the transition matrix $\boldsymbol{P}(t)$ of a CTMC with a finite state space $\Omega = \{0, 1, \ldots, N\}$ given the infinitesimal generator matrix $\boldsymbol{Q}$.

Theorem 2.21. *The transition probability matrix of a finite-state space CTMC with infinitesimal generator matrix* $\boldsymbol{Q}$ *is given by*

$$\boldsymbol{P}(t) = e^{\boldsymbol{Q}t}, \ t \geq 0.$$

However, computing the exponential of a matrix is usually analytically not possible and numerically challenging (Moler & Van Loan, 1978, 2003).

Inter-event times

The difference between discrete time Markov chains and continuous time Markov ones is that in the first scenario events can occur at time $1, 2, \ldots$, whereas in the second one a jump to a new state can be observed at any time $t \geq 0$. Denoting by W_i the time of the ith event in a CTMC, and assuming $W_0 = 0$, the process will remain in state $X(W_i)$ for a random amount of time and then jump to $X(W_{i+1})$ at time W_{i+1}. The sequence of random variables $(W_i)_{i=0}^{+\infty}$ is usually called *jump times* or *waiting times* series. Another relevant random variable to be considered is the *inter-event time* defined as $T_i = W_{i+1} - W_i$, which represents how long the process remains in state $X(W_i)$. Figure 2.1 illustrates the jump times W_i and the inter-event times T_i for the random variable $X(t)$.

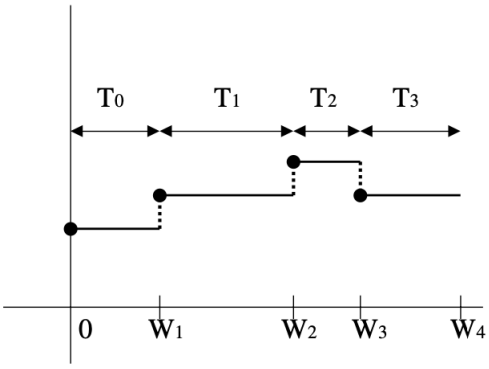

Figure 2.1: Sample path of $X(t)$ that shows the jump times W_i and the inter-event times T_i from Allen (2010).

One of the main features of Markov chains is that the inter-event times T_i are exponentially distributed with rate $\sum_{j \in \Omega, j \neq i} q_{ij}$. As the expected time of an exponentially distributed random variable is the inverse of the rate, the average time spent in state i is given by

$$\mathbb{E}[T_i] = \frac{1}{\sum_{j \in \Omega, j \neq i} q_{ij}}.$$

Furthermore, the probability that the process moves from state i to state j in one

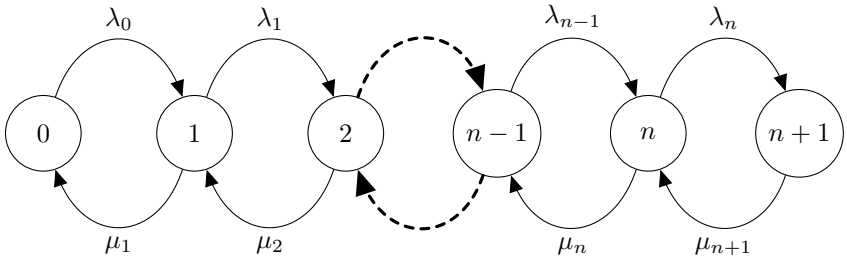

Figure 2.2: A depiction of a birth-and-death process with birth rates λ_j and death rates μ_j, $j \in \Omega$.

jump is computed as

$$p_{ij} = \frac{q_{ij}}{\sum_{l \in \Omega, l \neq i} q_{il}}.$$

Note that the exponential distribution is the only continuous probability distribution characterised by the so-called *memoryless property*:

$$\mathbb{P}\left(T_i \geq t + s | T_i \geq t\right) = \mathbb{P}\left(T_i \geq s\right), \quad \text{for any } t, s > 0. \tag{2.12}$$

2.2.2 Birth-and-death processes

A relevant example of continuous time Markov chain is represented by the family of birth-and-death processes. Consider a continuous time Markov chain $(X(t))_{t \geq 0}$ that might have either finite $\{0, 1, \ldots, N\}$ or infinite $\{0, 1, 2, \ldots\}$ state space Ω. The random variable $X(t)$ expresses the population size at time t. Figure 2.2 depicts a birth-and-death process, where λ_j is the birth rate and μ_j is the death rate from state j.
Transition probabilities for this type of process are

$$\begin{aligned} p_{ij}(\Delta t) &= \mathbb{P}(X(t + \Delta t) = j | X(t) = i) \\ &= \begin{cases} \lambda_i \Delta t + o(\Delta t) & j = i + 1, \\ \mu_i \Delta t + o(\Delta t) & j = i - 1, \\ 1 - (\lambda_i + \mu_i)\Delta t + o(\Delta t) & j = i, \\ o(\Delta t) & \text{otherwise}, \end{cases} \end{aligned}$$

with Δt small enough. Thus, if for example the state space Ω is infinite, the

infinitesimal generator matrix $\boldsymbol{Q}$ has the following structure

$$\boldsymbol{Q} = \begin{pmatrix} -\lambda_0 & \lambda_0 & 0 & 0 & 0 & 0 & \dots \\ \mu_1 & -(\mu_1+\lambda_1) & \lambda_1 & 0 & 0 & 0 & \dots \\ 0 & \mu_2 & -(\mu_2+\lambda_2) & \lambda_2 & 0 & 0 & \dots \\ 0 & 0 & \mu_3 & -(\mu_3+\lambda_3) & \lambda_3 & 0 & \dots \\ \vdots & \vdots & \vdots & \vdots & \vdots & \vdots & \ddots \end{pmatrix}.$$

A particular case of the birth-and-death process is when the birth and death rates are linear, that is $\lambda_i = \lambda i$ and $\mu_i = \mu i$ (Allen, 2010). In this case, $\lambda_0 = 0$ and the state 0 represents an *absorbing state* (that is, a state such that once reached, the system does not leave it).

2.2.3 Waiting times with a phase-type distribution

Exponential and phase-type distributions are very popular in stochastic modelling due to their memoryless property, or quasi memoryless in the case of phase-type. Another reason that justifies the wide use of phase-type distributions in applications is provided by the following result (Asmussen & Albrecher, 2010; He, 2014).

Theorem 2.22. *The set of PH-distributions is dense in the set of probability distributions on the non-negative half-line.*

The previous theorem implies that every probability distribution on the non-negative half-line can be approximated "arbitrarily close" by a sequence of PH distributions, and therefore studied through Markov chains even if that could not have been possible *a priori*. The sequence of PH distributions converges weakly to the non-negative probability distribution under consideration. The reader is referred to Theorem A5.14 of Asmussen & Albrecher (2010) for detailed proof.
It is also possible to provide a probabilistic definition of PH distributions that involves Markov chains. Consider a Markov chain $(X(t))_{t\geq 0}$ such that the state space is comprised of $m+1$ states, $\{1, 2, \dots, m, m+1\}$, and the infinitesimal generator matrix $\boldsymbol{Q}$ has the following structure:

$$\boldsymbol{Q} = \begin{pmatrix} \boldsymbol{T} & \boldsymbol{T^A} \\ \boldsymbol{0} & 0 \end{pmatrix}, \tag{2.13}$$

where $\boldsymbol{T}$ is a PH-generator defined in (2.4). Since the rows of an infinitesimal generator $\boldsymbol{Q}$ sum to 0, $\boldsymbol{T^A}$ and $\boldsymbol{T}$ must be related by the equation $\boldsymbol{T^A} = -\boldsymbol{Te}$. The structure of $\boldsymbol{Q}$ suggests that $m+1$ is an absorbing state. If one sets

$$\tau = \inf\{t \geq 0 : X(t) = m+1\},$$

then $\tau \sim PH(\boldsymbol{\alpha}, \boldsymbol{T})$ will represent the absorption time in state $m+1$ and $\mathbb{P}(\tau \leq t)$ the probability that the process has been absorbed in state $m+1$ before time t. That is, a phase-type distribution can be interpreted as the time until absorption in a CTMC.

Definition 2.23. *Assume that the Markov chain $(X(t))_{t\geq 0}$ defined by the transition matrix (2.13) will be eventually absorbed in state $m+1$ with probability 1. A* phase-type random variable τ *is defined as the absorption time into state $m+1$ of the continuous Markov chain $(X(t))_{t\geq 0}$, given that the initial distribution of the Markov chain is $(\boldsymbol{\alpha}, 1-\boldsymbol{\alpha e})$. The couple $(\boldsymbol{\alpha}, \boldsymbol{T})$ is a PH-representation of τ.*

Definition 2.23 associates a Markov chain to a PH distribution. This Markov chain is called *underlying Markov chain*, has an absorbing state and, before the absorption time, is described by the matrix $\boldsymbol{T}$. The column vector $\boldsymbol{T^A}$ contains the absorption rates from any state of the process to $m+1$. This information enables to compute the distribution of the residual time to absorption. For instance, let us imagine that $X(t) = j$, $1 \leq j \leq m$; then, the residual time to absorption is a PH random variable with PH-representation $(\boldsymbol{\alpha} = (0, \ldots, 1, \ldots, 0), \boldsymbol{T})$, where the 1 in vector $\boldsymbol{\alpha}$ is the jth element. This property of PH distributions is known as *quasi memoryless* property, where the *quasi* underlines the fact that it is necessary to keep track of the process initial state.

Remark 2.24. Both the exponential and the Erlang distributions belong to the family of phase-type distributions.

2.2.4 Branching processes

Branching processes were introduced independently by the French statistician Irénée-Jules Bienaymé, and by the English mathematician Henry William Watson and polymath Francis Galton in the XIX century to study the survival of

family names in aristocracy (Allen, 2010). In later years, the theory of branching processes arose great interest from a theoretical perspective (Athreya *et al.*, 2004; Harris *et al.*, 1963), meanwhile finding numerous applications in biology, immunology, ecology, medicine and epidemiology (Haccou *et al.*, 2005; Kimmel & Axelrod, 2002), among other fields. Let us imagine a population of particles, *e.g.*, humans, cells, or genes, that initially consists of X_0 particles. Each particle gives rise at the end of its life, independently of the others, with probability p_k to k new particles, where

$$p_k \geq 0, \qquad k = 0, 1, 2, \ldots, \qquad \sum_{k=0}^{+\infty} p_k = 1. \tag{2.14}$$

The totality of all the direct descendants of the initial population constitutes the first generation, whose size is denoted by X_1. Each particle of the first generation produces offspring according to the probability distribution (2.14). The descendants of the particles in the first generation constitute the second generation, X_2. The population size of the nth generation is denoted by X_n, and $(X_n)_{n\in\mathbb{N}_0}$ is a Markov chain in discrete time (Norris, 1998). Thus, we have the following definition from Allen (2010):

Definition 2.25. *Three basic assumptions define a* Galton-Watson branching process*:*

i. Each individual in generation n gives birth to ξ_n offspring in the next generation, where ξ_n is a random variable that takes values in $\{0, 1, 2, \ldots\}$ whose offspring distribution is $\{p_k\}_{k=0}^{+\infty}$,

$$p_k = \mathbb{P}(\xi_n = k), \quad k = 0, 1, 2, \ldots.$$

ii. Each individual gives birth independently from all other individuals.

iii. The same offspring distribution applies to each generation n, $\xi_n = \xi$.

In Galton-Watson processes, an individual's lifetime is a fixed length of time, which for convenience is chosen as one unit of time. At the end of its lifetime, the particle is replaced by its progeny. In the analogous continuous time process, an individual's lifetime is not fixed but may have an arbitrary distribution. In the case of exponentially distributed lifetimes, the branching process $(X(t))_{t\geq 0}$ is

a continuous time Markov chain, where $X(t)$ represents the population size at time t (Allen, 2010). If the individual's lifetime is not exponential, $(X(t))_{t\geq 0}$ is an age-dependent process known as *Bellman-Harris branching process* (Allen, 2010; Harris *et al.*, 1963; Kimmel & Axelrod, 2002).

In order to model biological processes, we may need to define different types of individuals within the same population. This leads to the definition of *multi-type branching processes*. Assume there are N types of individuals, where $X_j(t)$ is the discrete random variable for the number of individuals of type j, $j = 1, \ldots, N$, at time t. Each individual type produces offspring according to a probability distribution. The process $X(t) = (X_1(t), \ldots, X_N(t))_{t\geq 0}$ is a continuous time multi-type branching process. In particular, in Chapters 4 and 5 we will make use of two-type branching processes to model cell population dynamics and tick-borne virus transmission.

2.2.5 Gillespie algorithm

The Gillespie algorithm was originally formulated by Daniel Gillespie to simulate chemical or biochemical systems of reactions efficiently (Gillespie, 1976, 1977). Suppose that a Markov chain $(X(t))_{t\geq 0}$ has infinitesimal generator matrix $\boldsymbol{Q} = (q_{ij})_{i,j\in\Omega}$. Algorithm 1 shows how to obtain stochastic realisations of $(X(t))_{t\geq 0}$.

2.3 Bayesian statistics background

Bayesian inference is a statistical method which aims to estimate the parameters $\boldsymbol{\theta}$ in a mathematical model by updating the knowledge of the parameters as more data $\boldsymbol{D}$ are observed according to *Bayes' theorem*, which states

$$\mathbb{P}(A|B) = \frac{\mathbb{P}(B|A)\mathbb{P}(A)}{\mathbb{P}(B)},$$

where A and B are two events such that $\mathbb{P}(A) > 0$ and $\mathbb{P}(B) > 0$. Note that the assumption $\mathbb{P}(A) > 0$ and $\mathbb{P}(B) > 0$ guarantees that the conditional probabilities $\mathbb{P}(A|B)$ and $\mathbb{P}(B|A)$ are well defined. In a statistical framework, this yields

$$\pi\left(\boldsymbol{\theta}|\boldsymbol{D}\right) = \frac{\pi\left(\boldsymbol{D}|\boldsymbol{\theta}\right)\pi(\boldsymbol{\theta})}{\int_{\boldsymbol{\theta}} \pi\left(\boldsymbol{D}|\boldsymbol{\theta}\right)\pi(\boldsymbol{\theta})\mathrm{d}\boldsymbol{\theta}}, \tag{2.15}$$

Algorithm 1 Gillespie algorithm

1: Choose $t_{\max}$, the maximum time point for which a stochastic realisation of $(X(t))_{t\geq 0}$ will be constructed. Set the initial state $i = X(0)$.
2: **while** $t < t_{\max}$ **do**:
3: Sum all the transition rates to the states where the process can jump to from i in a single step, $R = \sum_{j\neq i} q_{ij}$.
4: Assign a number from 1 to n to the possible n states where the process can jump to from i in a single step, $j_1, \ldots, j_n$.
5: Sample $u_1 \sim U(0,1)$. The process will move to state j_k such that $\sum_{l=1}^{k-1} \frac{q_{ij_l}}{R} \leq u_1 \leq \sum_{l=1}^{k} \frac{q_{ij_l}}{R}$.
6: Update the current state of the process to $i = j_k$.
7: Sample $u_2 \sim U(0,1)$. Set $t \to t - \frac{\log u_2}{R}$. This is equivalent to adding a time exponentially distributed with rate R.
8: **end while**

where $\pi(\boldsymbol{\theta})$ is the *prior distribution*, which encodes our beliefs about the parameters before observing the data, $\pi(\boldsymbol{D}|\boldsymbol{\theta})$ is the *likelihood*, which is the probability of obtaining the data $\boldsymbol{D}$ given the value of the parameters $\boldsymbol{\theta}$ and $\pi(\boldsymbol{\theta}|\boldsymbol{D})$ is the *posterior distribution* and represents the knowledge of the parameters after observing the data. As the integral in (2.15) is a normalisation constant, a simpler formula than equation (2.15) can be used to estimate the posterior distribution:

$$\pi(\boldsymbol{\theta}|\boldsymbol{D}) \propto \pi(\boldsymbol{D}|\boldsymbol{\theta})\,\pi(\boldsymbol{\theta}),$$

where $\propto$ stands for "proportional to". In many mathematical models, the estimation of the likelihood function represents a challenge. Approximate Bayesian Computation (ABC for short) methods have been developed to deal with likelihood functions which are not tractable from a computational point of view or require too many resources to be evaluated (Csilléry *et al.*, 2010). Two ABC methods are presented in Sections 2.3.1 and 2.3.2.

2.3.1 ABC with rejection algorithm

Given a mathematical model which generates predictions (*e.g.*, number of individuals over time) based on some parameters $\boldsymbol{\theta}$ and a data set $\boldsymbol{D}$, the ABC method

based on a rejection algorithm aims to estimate the posterior distributions of the parameters $\pi(\boldsymbol{\theta}|\boldsymbol{D})$ by updating the prior beliefs making use of the experimental data $\boldsymbol{D}$ and Algorithm 2 (Pritchard *et al.*, 1999). To this end, a tolerance threshold ε is fixed. Parameters are sampled from the prior distributions $\pi(\boldsymbol{\theta})$ and are used to simulate the mathematical model. A function $d(\cdot,\cdot)$ is utilised to measure a distance between the simulated model predictions and the experimental data. The sampled parameters are accepted if the measured distance is smaller than ε. The method is reiterated until a fixed sample size N of the approximated posterior distribution is reached.

Algorithm 2 ABC with rejection algorithm.

1: Fix the tolerance threshold ε and the sample size N, and set $n = 0$.
2: **while** $n < N$ **do**:
3: Sample the parameters $\boldsymbol{\theta}^*$ from the prior distributions $\pi(\boldsymbol{\theta})$.
4: Simulate the model predictions $\boldsymbol{D}^*$ using the parameter values $\boldsymbol{\theta}^*$.
5: Compute the distance $d(\boldsymbol{D}^*, \boldsymbol{D})$ between $\boldsymbol{D}^*$ and the observed data $\boldsymbol{D}$.
6: **if** $d(\boldsymbol{D}^*, \boldsymbol{D}) \leq \varepsilon$ **then**:
7: Accept and store $\boldsymbol{\theta}^*$ and $n \to n + 1$.
8: **end if**
9: **end while**

If ε is sufficiently small, the output $\pi(\boldsymbol{\theta}|d(\boldsymbol{D}^*, \boldsymbol{D}) \leq \varepsilon)$ will be a good approximation of the posterior distribution.

2.3.2 ABC sequential Monte Carlo

Algorithm 2 can be computationally inefficient when the parameter space to explore is large due to either a large number of parameters in the model or prior distributions defined over large intervals. Indeed, in these cases, it is more challenging to sample a set of parameters that generate a small distance when the parameter space to explore is large. Thus, Algorithm 2 may take a long time to converge. In order to overcome this issue and to more efficiently explore the parameter space, Toni *et al.* (2009) proposed an ABC algorithm that uses sequential Monte Carlo methods (ABC SMC for short). Maintaining the same notation of the previous

section, the idea behind the ABC SMC algorithm is that the posterior distributions of the parameters in the model, $\pi(\boldsymbol{\theta}|\boldsymbol{D})$, are obtained through intermediate distributions, called *populations*, which converge to the final posterior distributions. To this end, the sample size N and the tolerance thresholds $\varepsilon_1 > \varepsilon_2 > \cdots > \varepsilon_T$ are defined, with T representing the number of iterations required to obtain the posterior distributions. Note that the tolerance threshold is reduced iteration by iteration. In the first iteration, the parameters (or *particles*) are sampled from the prior distributions $\pi(\boldsymbol{\theta})$ and are used to simulate model predictions $\boldsymbol{D}^*$ from the model described by $\pi(\boldsymbol{D}|\boldsymbol{\theta}^*)$. A distance $d(\boldsymbol{D}^*, \boldsymbol{D})$ is computed between the simulated predictions and the experimental data. If $d(\boldsymbol{D}^*, \boldsymbol{D}) \leq \varepsilon_1$, then $\boldsymbol{\theta}^*$ are accepted. The process continues until the sample size N has been reached. The accepted parameters constitute the population $\pi(\boldsymbol{\theta}|d(\boldsymbol{D}^*, \boldsymbol{D}) \leq \varepsilon_1)$, and for all the accepted particles the weights $w_1 = 1/N$ are computed. For the subsequent iterations, the prior distributions are the posteriors obtained from the previous iteration. Thus, the parameters $\boldsymbol{\theta}^*$ are sampled from $\pi(\boldsymbol{\theta}|d(\boldsymbol{D}^*, \boldsymbol{D}) \leq \varepsilon_1)$ with weights w_1 and then perturbed according to a perturbation kernel to get $\boldsymbol{\theta}^{**}$. The model predictions $\boldsymbol{D}^*$ are simulated from $\pi(\boldsymbol{D}|\boldsymbol{\theta}^{**})$. If $d(\boldsymbol{D}^*, \boldsymbol{D}) \leq \varepsilon_2$, then the parameters $\boldsymbol{\theta}^{**}$ are accepted. The process stops when a number of parameter values equal to the sample size N has been achieved. The weights w_2 are computed for all the accepted particles. The procedure is repeated T times and the set of the accepted parameters of the last iteration $\pi(\boldsymbol{\theta}|d(\boldsymbol{D}^*, \boldsymbol{D}) \leq \varepsilon_T)$ comprises the posterior distribution of the parameters in the model. Therefore, the ABC SMC algorithm requires the definition of the prior distribution, distance, tolerance thresholds and perturbation kernel. The method is summarised in Algorithm 3.

Note that in the ABC methods illustrated in this section, users have the freedom to choose the distance function between the experimental data sets and the model simulations. For a specifically chosen distance function, the ABC inference can be equivalent to a full likelihood inference for a deterministic system. Indeed, if the distance function is chosen to be the Euclidean distance, *i.e.*, the sum of squared errors, then the ABC inference is equivalent to the maximum likelihood problem for deterministic models for which normally distributed errors are assumed (see Appendix C of Toni *et al.* (2009)).

Algorithm 3 ABC sequential Monte Carlo algorithm (Toni *et al.*, 2009).

1: Set the number of iterations T, define the tolerance thresholds $\varepsilon_1 > \varepsilon_2 > \cdots > \varepsilon_T$ and the sample size N. Set the population indicator $i = 1$.
2: **while** $i < T$ **do**:
3: Initialise the sample size $n = 0$.
4: **while** $n < N$ **do**:
5: **if** $i = 1$ **then**
6: Sample $\boldsymbol{\theta}^{**}$ from $\pi(\boldsymbol{\theta})$.
7: **else**
8: Sample $\boldsymbol{\theta}^{*}$ from the previous iteration posterior distribution, $\{\boldsymbol{\theta}_{i-1}^{(k)}\} = \pi\left(\boldsymbol{\theta}|d(\boldsymbol{D}^{*}, \boldsymbol{D}) \leq \varepsilon_{i-1}\right)$, $k = 1, \ldots, N$, with weights w_{i-1}. Perturb $\boldsymbol{\theta}^{*}$ to obtain $\boldsymbol{\theta}^{**} \sim K_i(\boldsymbol{\theta}|\boldsymbol{\theta}^{*})$. If $\pi(\boldsymbol{\theta}^{**}) = 0$, re-sample $\boldsymbol{\theta}^{*}$ until $\pi(\boldsymbol{\theta}^{**}) \neq 0$.
9: **end if**
10: Simulate the model predictions $\boldsymbol{D}^{*}$ from $\pi\left(\boldsymbol{D}|\boldsymbol{\theta}^{**}\right)$.
11: If $d(\boldsymbol{D}^{*}, \boldsymbol{D}) \leq \varepsilon_i$, set $\boldsymbol{\theta}_i^{(n)} = \boldsymbol{\theta}^{**}$ and set $n \to n + 1$. Calculate the weights of the particles $\boldsymbol{\theta}_i^{(n)}$ as

$$w_i^{(n)} = \begin{cases} 1 & \text{if } i = 1, \\ \dfrac{\pi(\boldsymbol{\theta}_i^{(n)})}{\sum_{j=1}^{N} w_{i-1}^{(j)} K_i(\boldsymbol{\theta}_i^{(n)}|\boldsymbol{\theta}_{i-1}^{(j)})} & \text{if } i > 1, \end{cases}$$

12: **end while**
13: Normalise the weights and set $i \to i + 1$.
14: **end while**

2.4 Deterministic models

The mathematical models presented in this thesis are mainly stochastic. In particular, I worked with continuous time Markov chains to model cell population dynamics (Chapters 3 and 4) and transmission of tick-borne infection (Chapter 5). Thus, the quantities of interest of such models, *e.g.*, the number of cells in a given stage of the cell cycle in Chapter 3 or the number of infected individuals in Chapter 5, are random variables. If one considers the expected values of such variables, their dynamics over time can be described by ordinary differential equations. This leads to a *deterministic* model for the means of the stochastic variables. The main difference between a stochastic and a deterministic model is that, given a set of parameter values, the stochastic model output is a collection of different realisations of the process, whereas the output resulting from the deterministic model is always the same. Thus, stochastic models account for uncertainty and random fluctuations of the variables of interest, which are ubiquitous in many biological processes. However, stochastic models can introduce many mathematical details and consequently complexity. Deterministic models may help to gain useful insights analysing an approximated, simpler, process.
To better understand the setting of Chapters 3 and 4, consider a family of random variables $X_j(t)$, $j = 1, \dots, N$, and let $M_j(t) = \mathbb{E}[X_j(t)]$ be their expected values. The evolution of $M_j(t)$ over time can be described as

$$\frac{\mathrm{d}M_j(t)}{\mathrm{d}t} = f(M_i(t), \boldsymbol{\theta}), \quad i, j = 1, \dots, N,$$

where $\boldsymbol{\theta}$ is the vector of the parameters in the model and $f(\cdot, \cdot)$ is a function of the parameters and the variables of the model. In order to find $f(\cdot, \cdot)$, one can consider the probability master equation and the generating functions of the random variables $X_j(t)$, $j = 1, \dots, N$. Alternatively, it is possible to look at the events that can occur in the stochastic process in a short time interval Δt. The use of ordinary differential equations to model mean quantities in a stochastic process is useful to link the theoretical predictions of the model to experimental data, as shown in Chapters 3 and 4. This stochastic approach enables to define also higher moments of the random variables $X_j(t)$, *i.e.*, $\mathbb{E}[(X_j(t))^l], l \geq 1$, which

could potentially be used when parameterising the model if adequate data sets were available.

Chapter 3

Multi-stage models of cell proliferation and death: tracking cell divisions with Erlang distributions

Cells of the immune system patrol our bodies for months or years (den Braber *et al.*, 2012; Westera *et al.*, 2013). During an adaptive immune response, a subset of specific cells, initially a small fraction of the total population, expands as cells undergo multiple rounds of division over a few days (Antia *et al.*, 2005). Although most of these cells die as the infection is overcome, lasting immunity is ensured by the transformation, or "differentiation" of individual cells to a memory phenotype. Stochastic models are appropriate here because some cells undergo multiple rounds of division, some die, and others of the same type in the same conditions do not divide at all (Deenick *et al.*, 2003; Pereira *et al.*, 2003). If individual cells behave independently, then each cell can be imagined as sampling from a probability density of times to division and death. Given its unique memoryless property described in equation (2.12), the exponential density is the most mathematically and computationally convenient choice. It ensures analytical tractability, at least in some scenarios, and computational efficiency of stochastic simulations using the Gillespie algorithm (Gillespie, 1976, 1977). In particular, the consideration of exponentially distributed inter-event times leads to a Markovian framework,

which is capable to account for heterogeneity at the single-cell level, identifying different types of cells. In these models, the variables describe the number of cells of each type as a function of time, and cellular events such as division, death or differentiation are defined by their associated rates; each event corresponds to a possible fate of an individual cell. Since the inter-event times are exponentially-distributed random variables, their probability density is maximised at zero.

The rapid expansion of cohorts of lymphocytes is recreated in laboratories, either by stimulation *in vitro* or by transferring cells to lymphopenic mice. By labelling cells with carboxyfluorescein succinimidyl ester (CFSE) (Lyons & Parish, 1994) or cell trace violet (Quah & Parish, 2012) at the beginning of an experiment, and then using flow cytometry at a later time, a cohort of cells can be classified into *generations*; that is the number of rounds of divisions a cell undergoes over the course of the experiment. Indeed, each round of division dilutes the intracellular dye, which is equally distributed from the mother to the two daughter cells (De Boer *et al.*, 2006; Gett & Hodgkin, 2000; Hasbold *et al.*, 1999; Lee & Perelson, 2008; Lyons & Parish, 1994; Wellard *et al.*, 2011). At the beginning of an experiment, when cells are labelled, it is considered that all cells are in generation 0.

In more recent years, time-lapse microscopy experiments allowed to track individual cells and identified correlations within family trees of immune cells (Dowling *et al.*, 2014; Duffy & Subramanian, 2009; Duffy *et al.*, 2012; Hawkins *et al.*, 2009; Kinjyo *et al.*, 2015; Markham *et al.*, 2010; Wellard *et al.*, 2010). Over the timescales of such experiments, hours to days, it is not appropriate to treat cell division as an instantaneous event. Rather, cells are "cycling" through gap, synthesis and mitosis phases (G_1/G_2, S and M), and daughter cells cannot immediately redivide (Pandit & De Boer, 2019). To improve on the exponential distribution, Smith and Martin proposed a model in which the time between divisions is the sum of a fixed time spent in phase B, corresponding to $S/G_2/M$, and a variable time spent in phase A, corresponding to G_1 (Smith & Martin, 1973). In the "single stochastic division" model of Hogan *et al.* (2013), the rate of transition from A to B phase depends on the T cell clonotype and on the number of cells competing for the same resources (Hogan *et al.*, 2013). If there is a common molecular mechanism controlling the time spent in all phases of the cell cycle, then phase B may, instead, occupy a fixed proportion of the total time (Dowling *et al.*, 2014). Takahashi (1966,

1968) divided the cell cycle into four phases, with the duration of each drawn from a Pearson type III distribution. Weber *et al.* (2014) postulated a delayed exponential waiting time for each of the three phases, corresponding to G_1, S and G_2/M. Kendall (1948) introduced the idea of cell division occurring at the end of a sequence of k phases, with an exponentially-distributed time spent in each phase. Luzyanina *et al.* (2007) made use of a similar model, where each phase identifies a cell generation to study methodological and computational issues related to CFSE labelling data. Gamma and Erlang distributions have been considered to model a cell's time to division (León *et al.*, 2004; Zilman *et al.*, 2010). Yates *et al.* (2017) incorporated the idea of a sequence of exponentially-distributed phases, also referred as *stages*, before division in a multi-stage representation of a population of dividing cells. This yields an Erlang distribution of times to division, while retaining some of the mathematical and computational advantages of the exponential distribution (Yates *et al.*, 2017). The number of stages N and their mean duration $1/\lambda$ can be used as free parameters to compare with experimental data (Chao *et al.*, 2019; Vittadello *et al.*, 2019). On the other hand, the internal stages are a mathematical construct that do not directly correspond to biological phases.

With a particular focus on modelling proliferating lymphocytes, Hawkins *et al.* (2007) proposed a general framework, called cyton model, based on the idea that each cell has a set of competing clocks, determining its fate. Cellular division and death times are modelled making use of right-skewed probability distributions, such as gamma, log-normal and Weibull. A number of features are incorporated in the model: generation-dependent parameters, heritable factors, or correlations between cells of the same generation (Cheon *et al.*, 2021; Duffy & Subramanian, 2009; Markham *et al.*, 2010). When the fate of an individual cell is determined by competing internal clocks, the probability density of observed times between divisions is not the same as that of the division clock because division only happens if another fate does not. The probability density of division times is said to be "censored" (Duffy & Hodgkin, 2012). When all clocks have exponential probability densities, the probability density of observed division times is also exponential due to the memoryless property of exponential random variables; this conservation of shape does not hold for non-exponential distributions, including the log-normal and Erlang distributions.

3. MULTI-STAGE MODELS OF CELL PROLIFERATION AND DEATH: TRACKING CELL DIVISIONS WITH ERLANG DISTRIBUTIONS

In this chapter, we aim to preserve the advantages of a Markovian framework while improving the representation of experimentally-observed division times. To this end, we adopt a multi-stage representation of the cell cycle, building on the approach of Yates *et al.* (2017), where cell death is included as a competing fate. Phase-type distributed times to division, and exponentially distributed times to death are used. In the simplest case, obtained by assuming identical birth and death rates across stages, the analytical expression for the expected number of cells in each stage as a function of time is derived, and the limiting behaviour of the system is studied as $t \to +\infty$. The growth rate of the cell population is derived by calculating the proportions of cells by stage. The exponent describing the long-term cell population growth, and the criterion for extinction of the population, differs from what would be expected if N steps with rate λ were equivalent to a single step of rate λ/N. Cell generations are also included in the model in order to make theoretical predictions comparable to CFSE experimental data (Hogan *et al.*, 2013). The expected number of cells in each generation is found in the case of constant birth and death rates, and number of stages across generations. Although arising from different motivations, the multi-stage model with cell generations can be accommodated within the cyton framework, with the progressor fraction equal to one, and division and death clocks following Erlang and exponential distributions, respectively. The applicability of our stochastic approach is shown by calibrating the multi-stage model with cell generations and its exponential version with CFSE data from two populations of murine T cells (Hogan *et al.*, 2013). Model calibration is performed making use of Approximate Bayesian Computation sequential Monte Carlo (ABC-SMC) approaches (Toni *et al.*, 2009) described in detail in Section 2.3.

The chapter is structured as follows. In Section 3.1, the multi-stage model including cell death is presented and cell generations are incorporated in the representation. In Section 3.2, analytical results for the multi-stage framework are derived under some conditions on the model parameters. Furthermore, the multi-stage model with generations is compared to the cyton framework. In Section 3.3, the multi-stage model with cell generations is calibrated by making use of CFSE data from Hogan *et al.* (2013). Its performance is compared with a simple exponential model of cell division. A final discussion is provided in Section 3.4.

3.1 Multi-stage models of cell division and death: a Markovian framework

A multi-stage (MS) model of the time between cell divisions is presented. Cells pass through a sequence of N stages before dividing. Hereinafter, stages and compartments will be used as synonyms. The stages are not directly related to the biological phases of the cellular cycle. The time to progress from stage j to the next one, $j+1$, is an exponentially-distributed random variable with mean $1/\lambda^{(j)}$. These rates, $\lambda^{(j)}$, $j = 1, \ldots, N$, will be referred to as *birth* rates. Times to death are also distributed exponentially, with per cell *death* rate μ. Thus, at each stage, each cell may either proceed to the next one, with probability $\lambda^{(j)}/(\lambda^{(j)}+\mu)$, or die, with probability $\mu/(\lambda^{(j)}+\mu)$. The inter-event time is a random variable, following the exponential distribution with mean $1/(\lambda^{(j)}+\mu)$. When a cell in stage N divides, its daughters enter the first stage.

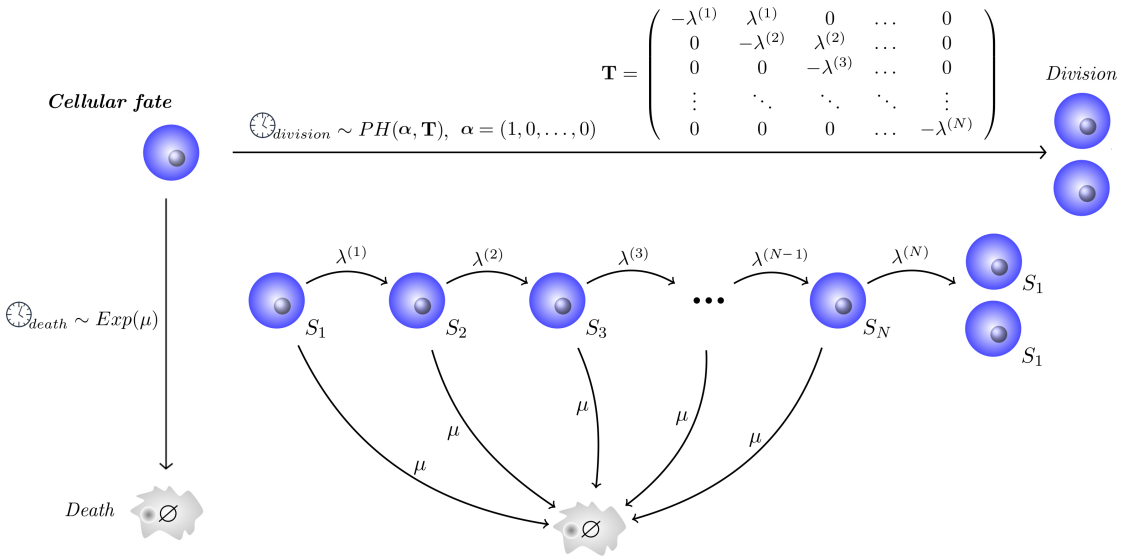

Figure 3.1: Multi-stage model of cell division and death (**MS model**). The cell cycle is divided into N different stages. A cell has to visit N stages in order to divide. At each stage j, $j = 1, \ldots, N$, the cell may proceed to the next stage, with birth rate $\lambda^{(j)}$, or die, with death rate μ.

Figure 3.1 illustrates the dynamics. This multi-stage model is equivalent to considering two independent clocks for cell division and death, which compete to decide the cellular fate. The time-to-death clock follows an exponential distribution with rate μ, while the division time follows a continuous phase-type distribution with parameters $\boldsymbol{\alpha}$ and $\mathbf{T}$ (see Section 2.2.3). A particular choice of phase-type distribution is the $Erlang(N, \lambda)$, which is a concatenation of N identically distributed exponential steps, where all birth rates are equal: $\lambda^{(j)} = \lambda$, $j = 1, \dots, N$. The case $\mu = 0$ has been considered by Yates *et al.* (2017).

The number of cells in stage j at time t, is the random variable $S_j(t)$, $j = 1, \dots, N$. Let $M_j(t) = \mathbb{E}[S_j(t)]$, be the expected value of $S_j(t)$. In a short time interval Δt the following events can happen:

$$M_j(t + \Delta t) = \begin{cases} M_1(t) + \Delta t(2\lambda^{(N)} M_N(t) - (\lambda^{(1)} + \mu) M_1(t)), & \text{if } j = 1, \\ M_j(t) + \Delta t(\lambda^{(j-1)} M_{j-1}(t) - (\lambda^{(j)} + \mu) M_j(t)), & \text{if } j = 2, \dots, N. \end{cases} \tag{3.1}$$

Indeed, in the case of the first stage, two daughter cells can arrive following the division of an individual in stage N, or a cell loss may occur because a cell either moves to stage 2 or dies. For all the other stages, a cell might join from the previous stage, proceed to the next one or die. Letting $\Delta t \to 0^+$ in (3.1), one obtains

$$\frac{\mathrm{d}M_j(t)}{\mathrm{d}t} = \begin{cases} 2\lambda^{(N)} M_N(t) - (\lambda^{(1)} + \mu) M_1(t), & \text{if } j = 1, \\ \lambda^{(j-1)} M_{j-1}(t) - (\lambda^{(j)} + \mu) M_j(t), & \text{if } j = 2, \dots, N. \end{cases} \tag{3.2}$$

When the MS model is extended to assign a generation to each cell, the model is referred to as the MS-G model. In this way, model predictions can be compared with CFSE experimental data (Lyons & Parish, 1994). CFSE is an intracellular dye that dilutes two-fold when a cell divides. At the beginning of the experiment cells are labelled with the dye. Then, harvesting the cells and measuring CFSE intensity by flow cytometry at particular time instants generates cellular profiles, and by quantifying the fluorescent intensity of any given cell, one can ascertain the *generation* that this cell belongs to. CFSE data typically display a number of *intensity peaks*, which reflect the number of divisions that cells of that peak have undergone. An example of CFSE profile is displayed in Figure 3.2. The maximum number of peaks is usually 9 or 10 due to the fact that after 10 divisions, the

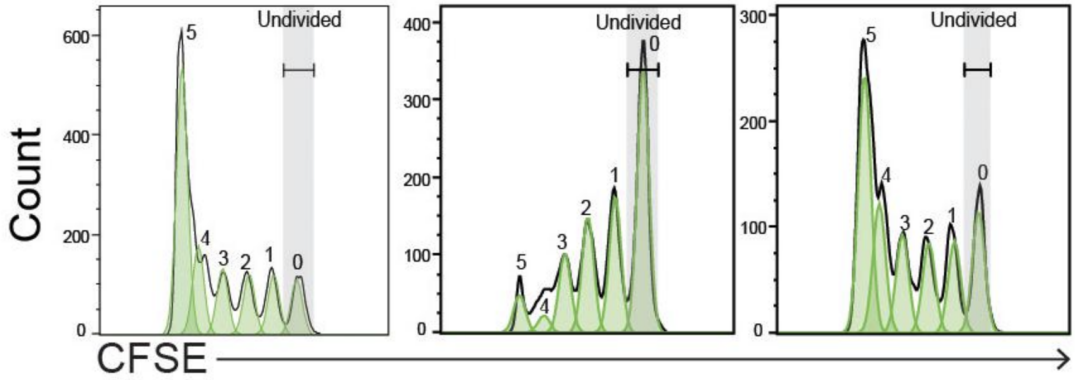

Figure 3.2: CFSE dilution of CD4$^+$ T cells cultured with monocyte-derived cells from the CD4$^+$ T cell-monocyte cultures from Figure 1 of Zhang *et al.* (2020).

intensity of the dye is 2^{10} fold lower than that of the initial one, and comparable to the auto-florescence of cells (Ganusov *et al.*, 2007).

In the MS-G model, generation $g \geq 0$ is split into N_g different stages. The notation N_g reflects the fact that the number of stages may depend on the generation g. A cell in generation g has to sequentially visit all N_g compartments to divide. On the other hand, cells might also die at any stage of the cycle. As depicted in Figure 3.3, if a cell belongs to generation g and is in compartment j, $j = 1, \ldots, N_g - 1$, it may proceed to the following stage, with birth rate λ_g, or die with death rate μ_g. Again the notation reflects the potential for these rates to depend on the generation. When a cell reaches the last stage, N_g, of generation g and divides, its two daughters will join the first compartment of generation $g+1$. In summary, given a cell in generation g, its time to division follows an Erlang distribution with parameters (N_g, λ_g), whereas its time to death follows an exponential distribution with rate μ_g. These distributions correspond to two independent competing clocks to control cellular fate, similarly to those considered in Figure 3.1.

The number of cells in stage j of generation g at time t is the random variable $S_j^g(t)$, $g \geq 0$, $j = 1, \ldots, N_g$. Let $M_j^g(t) = \mathbb{E}[S_j^g(t)]$ be the expected value of $S_j^g(t)$. To obtain the dynamics of $M_j^g(t)$ over time, the events that can happen in a short

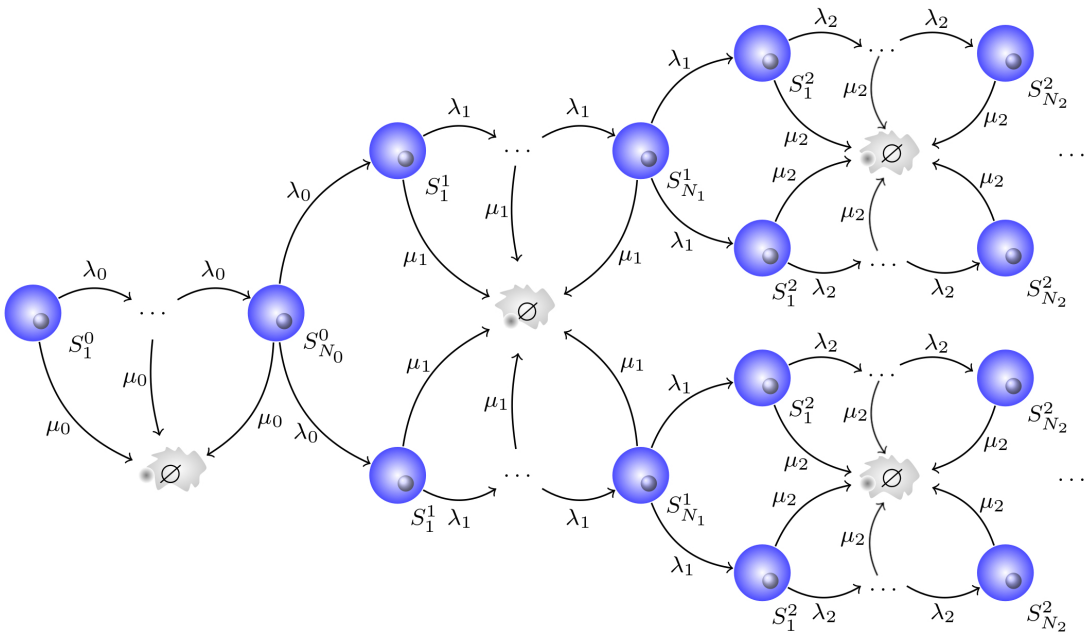

Figure 3.3: Multi-stage model with cell generations (**MS-G model**). Each cell in the first stage of generation 0 has to visit all the N_0 compartments in order to divide. When cells arrive at the last stage of generation 0, N_0, they may divide with birth rate λ_0, or die with death rate μ_0. If a cell divides, its daughter cells join the first stage of the next generation, and the process continues.

time interval Δt are considered:

$$M_j^g(t+\Delta t) = \begin{cases} M_1^0(t) + \Delta t(-(\lambda_0+\mu_0)M_1^0(t)), & \text{if } g=0,\ j=1, \\ M_j^g(t) + \Delta t(\lambda_g M_{j-1}^g(t) - (\lambda_g+\mu_g)M_j^g(t)), & \text{if } g\geq 0,\ j\neq 1, \\ M_j^g(t) + \Delta t(2\lambda_{g-1}M_{N_{g-1}}^{g-1}(t) - (\lambda_g+\mu_g)M_j^g(t)) & \text{if } g\geq 1,\ j=1. \end{cases} \tag{3.3}$$

Indeed, the only possible events affecting cells in stage 1, generation 0, is either one of these cells moving to the next stage, or dying. If instead one looks at the first stage of all generations but 0, two cells may arrive following a division in the last stage of the previous generation, or a cell might die or proceed to the following stage. Lastly, at any intermediate stage ($j = 2, \ldots, N_g$) within a generation g, a cell may join from the previous stage, proceed to next one, die, or divide if $j = N_g$. The set of differential equations below follows from equation (3.3) letting $\Delta t \to 0^+$:

$$\frac{\mathrm{d}M_j^g(t)}{\mathrm{d}t} = \begin{cases} -(\lambda_0+\mu_0)M_1^0(t), & \text{if } g=0,\ j=1, \\ \lambda_g M_{j-1}^g(t) - (\lambda_g+\mu_g)M_j^g(t), & \text{if } g\geq 0,\ j=2,\ldots,N_g, \\ 2\lambda_{g-1}M_{N_{g-1}}^{g-1}(t) - (\lambda_g+\mu_g)M_1^g(t), & \text{if } g\geq 1,\ j=1. \end{cases} \tag{3.4}$$

One aims to compute the mean number of cells over time for the MS and MS-G models. Specifically the MS-G model will provide the mean number of cells in each generation, and thus, can be used together with CFSE data to obtain division and death rates. When division times are Erlang distributed (MS model), or if one considers that those Erlang distributions are identical across generations (MS-G model), it is possible to carry out a comprehensive analytical study. This is shown in Section 3.2.

When convenient analytical solutions cannot be obtained, (3.2)-(3.4) can be solved numerically in different ways. For example, for the MS-G model, and keeping in mind our interest in modelling CFSE data, it is assumed there exists a maximum generation G that can be measured by the dye. Thus, one might be interested in following cells within generations $g = 0, \ldots, G$. For these generations, equations (3.4) can be solved by making use of the matrix exponential. To this end, let $\boldsymbol{M}(t)$ be the column vector of the mean number of cells in each stage and

generation as time evolves, *i.e.*,

$$\begin{aligned}\boldsymbol{M}(t) &= \left(M_1^0(t),\ldots,M_{N_0}^0(t),M_1^1(t),\ldots,M_{N_1}^1(t),\ldots,M_1^G(t),\ldots,M_{N_G}^G(t)\right)^T \\ &= (\mathbf{M}_0(t)^T,\mathbf{M}_1(t)^T,\ldots,\mathbf{M}_G(t)^T)^T,\end{aligned}$$

which has length $\sum_{g=0}^{G} N_g$, and where the column sub-vectors $\mathbf{M}_g(t)$ contain the mean number of cells across stages in generations $g = 0,\ldots,G$. Also, the coefficient matrix is defined as

$$\mathbf{A} = \begin{pmatrix} \mathbf{A}_{00} & \mathbf{0}_{N_0\times N_1} & \mathbf{0}_{N_0\times N_2} & \cdots & \mathbf{0}_{N_0\times N_{G-1}} & \mathbf{0}_{N_0\times N_G} \\ \mathbf{A}_{10} & \mathbf{A}_{11} & \mathbf{0}_{N_1\times N_2} & \cdots & \mathbf{0}_{N_1\times N_{G-1}} & \mathbf{0}_{N_1\times N_G} \\ \vdots & \ddots & \ddots & \ddots & \vdots & \vdots \\ \mathbf{0}_{N_{G-1}\times N_0} & \mathbf{0}_{N_{G-1}\times N_1} & \mathbf{0}_{N_{G-1}\times N_2} & \cdots & \mathbf{A}_{G-1,G-1} & \mathbf{0}_{N_{G-1}\times N_G} \\ \mathbf{0}_{N_G\times N_0} & \mathbf{0}_{N_G\times N_1} & \mathbf{0}_{N_G\times N_2} & \cdots & \mathbf{A}_{G,G-1} & \mathbf{A}_{G,G} \end{pmatrix},$$

where

$$\mathbf{A}_{gg} = \begin{pmatrix} -(\lambda_g+\mu_g) & 0 & 0 & 0 & \cdots & 0 \\ \lambda_g & -(\lambda_g+\mu_g) & 0 & 0 & \cdots & 0 \\ 0 & \lambda_g & -(\lambda_g+\mu_g) & 0 & \cdots & 0 \\ \vdots & \ddots & \ddots & \ddots & \ddots & \vdots \\ 0 & \cdots & 0 & \lambda_g & -(\lambda_g+\mu_g) & 0 \\ 0 & \cdots & 0 & 0 & \lambda_g & -(\lambda_g+\mu_g) \end{pmatrix},$$

$$\mathbf{A}_{g,g-1} = \begin{pmatrix} 0 & \cdots & 0 & 2\lambda_{g-1} \\ 0 & \cdots & 0 & 0 \\ \vdots & \ddots & \vdots & \vdots \\ 0 & \cdots & 0 & 0 \end{pmatrix}.$$

$\mathbf{A}_{gg}$ is a square $N_g \times N_g$ matrix, whereas $\mathbf{A}_{g,g-1}$ is a $N_g \times N_{g-1}$ matrix. $\boldsymbol{A}$ is then a real square matrix of dimension $\sum_{g=0}^{G} N_g$, and $\mathbf{0}_{a\times b}$ represents a null matrix with dimension $a \times b$. Given the vector of the initial conditions $\boldsymbol{n}_0$, which has length $\sum_{g=0}^{G} N_g$, the system of equations (3.4) can be rewritten as the following Cauchy problem

$$\begin{cases} \dfrac{\mathrm{d}\boldsymbol{M}(t)}{\mathrm{d}t} = \boldsymbol{A}\cdot\boldsymbol{M}(t), \\ \boldsymbol{M}(0) = \boldsymbol{n_0}. \end{cases}$$

The solution of the system is given by $\boldsymbol{M}(t) = \mathrm{e}^{\boldsymbol{A}t}\boldsymbol{n_0}$, where

$$\mathrm{e}^{\boldsymbol{A}t} = \sum_{k=0}^{+\infty} \frac{(\boldsymbol{A}t)^k}{k!}$$

represents the matrix exponential. For efficient ways of computing this matrix, see Refs. Gómez-Corral & García (2014); Gómez-Corral & López García (2013); Moler & Van Loan (1978, 2003). Finally, since CFSE data describe the number of cells in each generation, one can then compute the mean number of cells in each generation over time as

$$M^g(t) = \sum_{j=1}^{N_g} M_j^g(t), \qquad g \geq 0. \tag{3.5}$$

Using (3.4) and (3.5), the time evolution of $M^g(t)$ is computed as follows

$$\begin{aligned} \frac{\mathrm{d}M^0(t)}{\mathrm{d}t} &= -\lambda_0 M^0_{N_0}(t) - \mu_0 M^0(t), \\ \frac{\mathrm{d}M^g(t)}{\mathrm{d}t} &= 2\lambda_{g-1} M^{g-1}_{N_{g-1}}(t) - \lambda_g M^g_{N_g}(t) - \mu_g M^g(t), \qquad g \geq 1. \end{aligned} \tag{3.6}$$

In a related approach by Zilman *et al.* (2010), a cell's time to division is a gamma-distributed random variable, and time to death is exponentially distributed. Solutions are given in terms of integral equations. Here, with Erlang-distributed division times, a set of linear differential equations is found for the expected number of cells in each stage.

3.2 Exact mean number of cells in each stage and generation

In this section, it is shown how the Markovian framework of the proposed multi-stage models provides analytical tractability under some simplifying assumptions. The aim is to compute the mean number of cells in each stage and generation over time, and then to study the long-term behaviour as $t \to +\infty$.

3.2.1 MS model with Erlang division time

In this section, a simple case of the MS model, where identical birth rates are assumed across different stages, is considered; that is, $\lambda^{(j)} = \lambda,\ j = 1, \ldots, N$. The phase-type distribution for the time to division in Figure 3.1 is $Erlang(N, \lambda)$ and the mean time to division is given by $\frac{N}{\lambda}$. Note that when $N = 1$ the MS model becomes a Markovian linear birth-and-death process (see Section 2.2.2), with birth rate, λ, and death rate, μ. Equations (3.2) become

$$\frac{\mathrm{d}M_j(t)}{\mathrm{d}t} = \begin{cases} 2\lambda M_N(t) - (\lambda + \mu)\, M_1(t), & \text{if } j = 1, \\ \lambda M_{j-1}(t) - (\lambda + \mu)\, M_j(t), & \text{if } j = 2, \ldots, N. \end{cases} \tag{3.7}$$

As in Yates *et al.* (2017), new variables are introduced to derive the solutions of (3.7). In particular, the system is rewritten in terms of $m_j(t) = \mathrm{e}^{(\lambda+\mu)t} M_j(t)$, $j = 1, \ldots, N$, which satisfy the following ODEs:

$$\frac{\mathrm{d}m_j(t)}{\mathrm{d}t} = \begin{cases} 2\lambda m_N(t), & \text{if } j = 1, \\ \lambda m_{j-1}(t), & \text{if } j = 2, \ldots, N. \end{cases} \tag{3.8}$$

An N^{th}-order homogeneous differential equation for $m_N(t)$ that does not depend on μ is derived:

$$\frac{\mathrm{d}^N m_N(t)}{\mathrm{d}t^N} = 2\lambda^N m_N(t), \tag{3.9}$$

together with a set of ODEs that relate $m_j(t)$ to the derivatives of $m_N(t)$ with respect to time

$$m_j(t) = \left(\frac{1}{\lambda}\right)^{N-j} \frac{\mathrm{d}^{N-j} m_N(t)}{\mathrm{d}t^{N-j}}, \quad j = 1, \ldots, N-1. \tag{3.10}$$

The characteristic polynomial associated to (3.9) is

$$P(x) = x^N - 2\lambda^N,$$

and its roots in $\mathbb{C}$ are given by

$$x_k = 2^{\frac{1}{N}} \lambda \left(\cos\left(\frac{2k\pi}{N}\right) + i\ \sin\left(\frac{2k\pi}{N}\right) \right), \quad k = 0, \ldots, N-1,$$

which can be written in the exponential form as

$$x_k = 2^{\frac{1}{N}} \lambda e^{\frac{2k\pi}{N} i}, \quad k = 0, \ldots, N-1.$$

Hence, the solution of (3.9) is given by

$$m_N(t) = \sum_{k=0}^{N-1} c_k e^{2^{\frac{1}{N}} \lambda z^k t}, \tag{3.11}$$

where $z = e^{\frac{2\pi i}{N}}$ is the first Nth root of unity and c_k are yet undetermined constants which depend on the initial conditions. If, at time $t = 0$, there are C_0 cells in the first stage and zero cells in any other stage, then

$$c_k = \frac{C_0}{2N} 2^{\frac{1}{N}} z^k, \qquad k = 0, \ldots, N-1. \tag{3.12}$$

In order to prove this, $m_N(t)$ is first differentiated with respect to time to derive the analytical expression of $m_j(t)$ according to equation (3.10). As $z^{kN} = 1$ for all $k = 0, \ldots, N-1$, one obtains

$$m_j(t) = \sum_{k=0}^{N-1} c_k \left(2^{\frac{1}{N}} z^k\right)^{N-j} e^{2^{\frac{1}{N}} \lambda z^k t} = 2^{1-\frac{j}{N}} \sum_{k=0}^{N-1} c_k z^{-kj} e^{2^{\frac{1}{N}} \lambda z^k t}. \tag{3.13}$$

It is now shown by substitution that the constants c_k are given by (3.12). For $j = 1$ one gets

$$m_1(0) = 2^{1-\frac{1}{N}} \sum_{k=0}^{N-1} \frac{C_0}{2N} 2^{\frac{1}{N}} z^k z^{-k} = C_0,$$

and if $j = 2, \ldots, N$

$$m_j(0) = 2^{1-\frac{j}{N}} \sum_{k=0}^{N-1} \frac{C_0}{2N} 2^{\frac{1}{N}} z^k z^{-jk} = \frac{C_0}{N} 2^{\frac{1-j}{N}} \sum_{k=0}^{N-1} z^{k(1-j)}.$$

To prove that $m_j(0) = 0$, the summation $\sum_{k=0}^{N-1} z^{k(1-j)}$ is studied. The sum of the Nth roots of unity is equal to zero. Indeed, from $z^N = 1$ one obtains

$$0 = z^N - 1 = (z-1)(z^{N-1} + z^{N-2} + \cdots + z + 1) = (z-1) \sum_{k=0}^{N-1} z^k.$$

Since $z \neq 1$, it is proved that $\sum_{k=0}^{N-1} z^k = 0$. On the other hand $z^{N(1-j)} = 1$ for all $j = 2, \ldots, N$, so that one concludes $\sum_{k=0}^{N-1} z^{k(1-j)} = 0$ and therefore $m_j(0) = 0$, $j = 2, \ldots, N$. Replacing the expression of the constants (3.12) in (3.13) and going

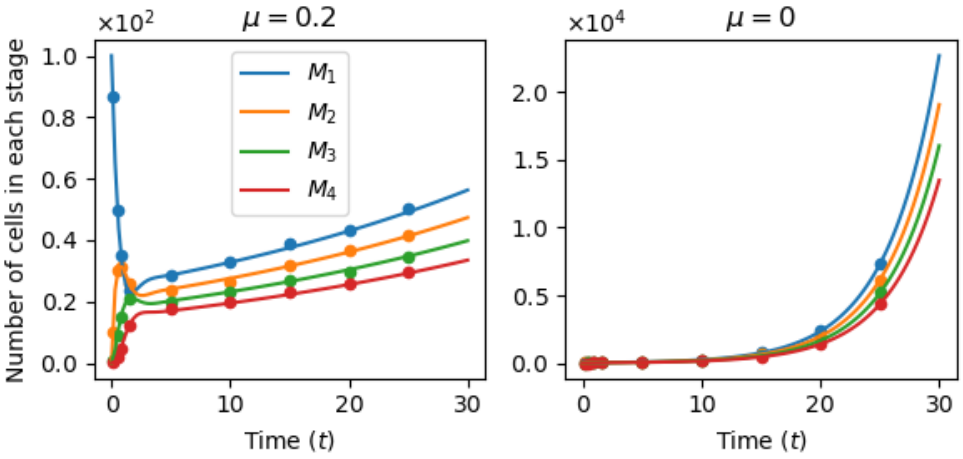

Figure 3.4: Analytical solutions derived in equations (3.14) (solid lines) are compared with stochastic simulations (dots) realised using the Gillespie algorithm. Each dot is the mean value of 200 realisations. The number of stages is $N = 4$ and the birth and death rates are $\lambda = 1.2$ and $\mu = 0.2$ (on the left), $\mu = 0$ (on the right) with units of inverse time t^{-1}.

back to the original variables $M_j(t), j = 1, \ldots, N$, the solutions of system (3.7) are

$$M_j(t) = C_0 \, \frac{2^{\frac{1-j}{N}}}{N} \, \mathrm{e}^{-\mu t} \sum_{k=0}^{N-1} z^{(1-j)k} \mathrm{e}^{\left(2^{\frac{1}{N}} z^k - 1\right)\lambda t}, \qquad j = 1, \ldots, N. \tag{3.14}$$

In Figure 3.4, the analytical solutions obtained for $M_j(t), j = 1, \ldots, N$ are compared with stochastic simulations of the process realised making use of the Gillespie algorithm (Gillespie, 1976, 1977). The solutions and the stochastic realisations agree. The expected number of cells in each stage $M_j(t), j = 1, \ldots, N$ are plotted when the death rate is $\mu = 0.2$ (on the left) and $\mu = 0$ (on the right). One notes that in the latter case, corresponding to the model considered by Yates *et al.* (2017), the cell population grows significantly faster. Furthermore, the inclusion of cell death makes population extinction possible (as shown in Figure 3.6), conversely to the model proposed by Yates *et al.* (2017), where the population of cells always grows exponentially.

The total number of cells in the population at time $t \geq 0$ is defined as $S(t) = \sum_{i=1}^{N} S_i(t)$, so that $M(t) = \mathbb{E}[S(t)]$ is expected total number of cells in the popu-

lation at time t. From (3.14), $M(t)$ can be derived as

$$M(t) = \sum_{j=1}^{N} M_j(t) = C_0 \frac{2^{\frac{1}{N}}}{2N} \mathrm{e}^{-\mu t} \sum_{k=0}^{N-1} \frac{z^k}{2^{\frac{1}{N}} z^k - 1} \mathrm{e}^{\left(2^{\frac{1}{N}} z^k - 1\right)\lambda t}, \tag{3.15}$$

where the final expression is obtained recalling that the sum of the first $N+1$ terms of a geometric series is given by $\sum_{i=0}^{N} x^i = \frac{1-x^{N+1}}{1-x}$. One also notes that the time evolution of $M(t)$ can be easily derived from (3.7) as

$$\frac{\mathrm{d}M(t)}{\mathrm{d}t} = \lambda M_N(t) - \mu M(t). \tag{3.16}$$

Mean fraction of cells at each stage

As in Yates *et al.* (2017), the mean fraction of cells in each stage, $P_j(t)$, is defined as the ratio between the mean number of cells in compartment j and the expected total number of cells in the population, *i.e.*,

$$P_j(t) = \frac{M_j(t)}{M(t)}, \quad j = 1, \ldots, N. \tag{3.17}$$

Making use of (3.7) and (3.16), the dynamics over time of $P_j(t), j = 1, \ldots, N$ obey the differential equations

$$\frac{\mathrm{d}P_j(t)}{\mathrm{d}t} = \begin{cases} \lambda(2P_N(t) - P_1(t) - P_1(t)P_N(t)), & \text{if } j = 1, \\ \lambda(P_{j-1}(t) - P_j(t) - P_j(t)P_N(t)), & \text{if } j = 2, \ldots, N, \end{cases} \tag{3.18}$$

which have the following steady state solution

$$P_1^* = \frac{2P_N^*}{1 + P_N^*}, \quad P_j^* = \frac{P_{j-1}^*}{1 + P_N^*}, \ j = 2, \ldots, N. \tag{3.19}$$

One observes that $P_j^* < P_{j-1}^*$, $j = 1, \ldots, N-1$, which means (on average) the fraction of cells decreases stage by stage, independently of the initial distribution of cells. In fact, one can solve (3.19) to determine P_j^*, as follows

$$P_j^* = \left(\sqrt[N]{2}\right)^{N-j} \left(\sqrt[N]{2} - 1\right), \ j = 1, \ldots, N, \tag{3.20}$$

which interestingly does not depend on λ or μ. Thus, at late times the fraction of cells in each stage only depends on the number of stages considered; the parameter λ sets the timescale of the dynamical system, and all cells are equally susceptible to death, regardless of the stage they are in. Figure 3.5 shows the values of $P_j^*, j = 1, \ldots, N$ for different values of N.

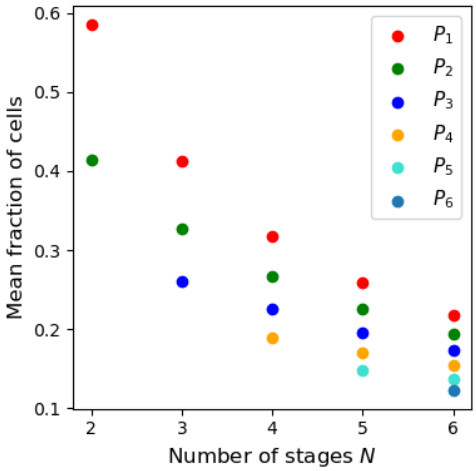

Figure 3.5: Mean fraction of cells in each stage in the long term derived in equation (3.20) as a function of the number of stages N.

Population extinction versus unlimited growth

In order to study the long-term behaviour of the population of cells, the MS model with Erlang division time is considered. One can define

$$p_j^{(m)} = \lim_{t\to+\infty} \mathbb{P}(S(t) = 0 \mid S_j(0) = m,\ S_k(0) = 0,\ k \neq j), \quad j = 1, \ldots, N,$$

the probability of population extinction at late times, for m cells initially in stage j at time $t = 0$. Since cells behave independently, it is clear that $p_j^{(m)} = \left(p_j^{(1)}\right)^m$, so I omit the super-index hereinafter and denote $p_j^{(1)} \equiv p_j$. A first-step argument leads to

$$\begin{aligned} p_i &= \frac{\mu}{\lambda+\mu} + \frac{\lambda}{\lambda+\mu}\, p_{i+1}, \quad i = 1, \ldots, N-1, \\ p_N &= \frac{\mu}{\lambda+\mu} + \frac{\lambda}{\lambda+\mu}\, p_1^2. \end{aligned}$$

These equations can be solved recursively, leading to

$$p_1 = \begin{cases} \frac{1}{(1-r)^N} - 1, & \text{if } \mu < (2^{1/N} - 1)\lambda, \\ 1, & \text{if } \mu \geq (2^{1/N} - 1)\lambda, \end{cases} \tag{3.21}$$

where $r = \frac{\mu}{\mu+\lambda}$. When $N = 1$, $p_1 = \frac{\mu}{\lambda}$, that is the extinction probability of a birth-and-death process (Allen, 2010); when $N = 2$, $p_1 = \frac{\mu^2+2\mu\lambda}{\lambda^2}$.

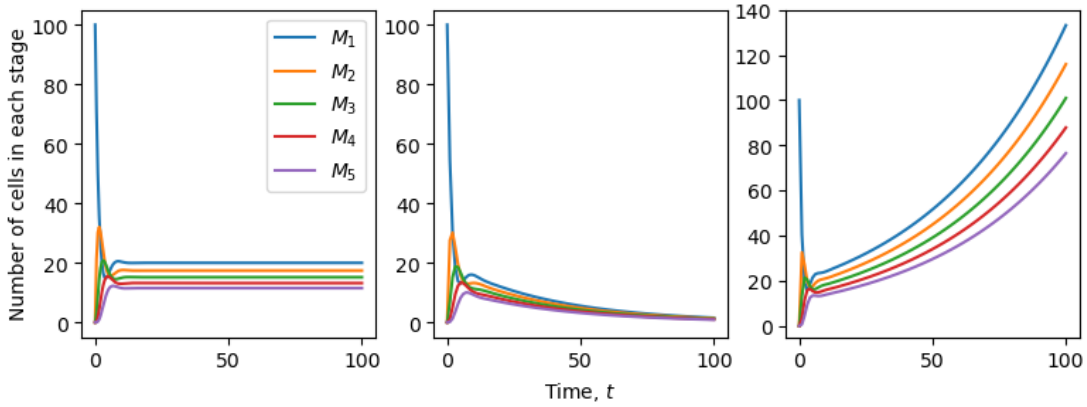

Figure 3.6: Long-term behaviour when $t \to +\infty$ of a population with an initial number of cells, $C_0 = 10^2$. Birth and death rates, λ and μ, have units of inverse time, t^{-1}. **Left.** Parameters: $N = 5$, $\lambda = 0.6$, $\mu = (2^{1/N} - 1)\lambda$. The population of cells in stage j levels out to $2^{\frac{1-j}{N}} C_0/N$ for sufficiently large times. **Centre.** Parameters: $N = 5$, $\lambda = 0.5$, $\mu = 0.1$, so that $\mu > (2^{1/N} - 1)\lambda$. The population of cells at any stage becomes extinct at late times. **Right.** Parameters: $N = 5$, $\lambda = 0.8$, $\mu = 0.1$, so that $\mu < (2^{1/N} - 1)\lambda$. The populations grow according to (3.25) and the relation between M_1 and M_5 given by equation (3.24) is satisfied. For example, at $t = 100$, $M_1(t) \simeq 2^{4/5} M_5(t)$.

The analytical solutions (3.14)-(3.15) provide another route to study the limiting behaviour as $t \to +\infty$. The terms of the summation in (3.14) are considered in order to explore if there exists a dominant term. When $k = 0$, the exponent is given by $(2^{1/N} - 1)\lambda - \mu$, which can be positive, if $\mu < (2^{1/N} - 1)\lambda$ or negative, when $\mu > (2^{1/N} - 1)\lambda$, or zero if $\mu = (2^{1/N} - 1)\lambda$. When $k > 0$, one notices that

$$\mathrm{Re}\left(\left(2^{\frac{1}{N}} z^k - 1\right)\lambda - \mu\right) = \left(2^{\frac{1}{N}} \cos\left(\frac{2\pi k}{N}\right) - 1\right)\lambda - \mu. \tag{3.22}$$

Since the cosine function is always less or equal to 1, the right hand side of (3.22) is dominated by $\left(2^{1/N} - 1\right)\lambda - \mu$ for all $k = 1, \ldots, N-1$. This means that the leading term in the summation of (3.14) is the one corresponding to $k = 0$. To conclude the analysis, three cases are distinguished:

1. $\mu = (2^{1/N} - 1)\lambda$. The exponent of the term corresponding to $k = 0$ is

zero. For $k > 0$, the exponents become $2^{1/N}\lambda(z^k - 1)$, which have negative real part for all $k = 1, \ldots, N-1$. Therefore, the long-term behaviour of $M_j(t), j = 1, \ldots, N$ and $M(t)$ is derived as

$$\lim_{t\to+\infty} M_j(t) = \frac{2^{\frac{1-j}{N}} C_0}{N}, \ j = 1, \ldots, N, \quad \text{and} \quad \lim_{t\to+\infty} M(t) = \frac{2^{\frac{1}{N}} C_0}{N},$$

as shown in Figure 3.6 (left).

2. $\mu > (2^{1/N} - 1)\lambda$. The exponent of the term corresponding to $k = 0$ is negative. Since it is the dominant term, the exponent is also negative for $k = 1, \ldots, N-1$. Thus, extinction of the cell population is certain, that is $\lim_{t\to+\infty} M_j(t) = 0$ for all $j = 1, \ldots, N$. Figure 3.6 (centre) shows an example of extinction when $N = 5, \lambda = 0.5\ t^{-1}, \mu = 0.1\ t^{-1}$ – where t is the unit of time – and the initial number of cells is $C_0 = 10^2$.

3. $\mu < (2^{1/N} - 1)\lambda$. Since the dominant term corresponds to $k = 0$, as $t \to +\infty$,

$$M_j(t) \simeq \frac{2^{\frac{1-j}{N}} C_0}{N} \mathrm{e}^{\left((2^{\frac{1}{N}}-1)\lambda - \mu\right)t}, \qquad j = 1, \ldots, N, \tag{3.23}$$

and

$$\lim_{t\to+\infty} \frac{M_1(t)}{M_N(t)} = 2^{\frac{N-1}{N}}, \tag{3.24}$$

which is illustrated in Figure 3.6 (right).

The leading term in the summation of (3.15) is the one corresponding to $k = 0$. Therefore, as $t \to +\infty$,

$$M(t) \simeq C_0 \, \frac{2^{\frac{1}{N}}}{2N\left(2^{\frac{1}{N}} - 1\right)} \, \mathrm{e}^{(\sigma_N \lambda - \mu)t}, \qquad \text{where } \sigma_N = 2^{\frac{1}{N}} - 1. \tag{3.25}$$

The exponent $\sigma_N = 2^{\frac{1}{N}} - 1$, describing the long-term cell population growth, plotted in Figure 3.7, is lower than would be expected if N steps with rate λ were equivalent to a single step of rate λ/N. As $N \to +\infty$, we have $N\sigma_N \to \log 2$. In terms of (3.20), $\lambda\sigma_N < \lambda/N$ because $P_N(t) < 1/N$ as $t \to +\infty$. Because the cell population is unevenly distributed across stages, with a bias towards earlier stages in the long run as shown in equation (3.20), N steps with rate λ are not equivalent to a single step of rate λ/N.

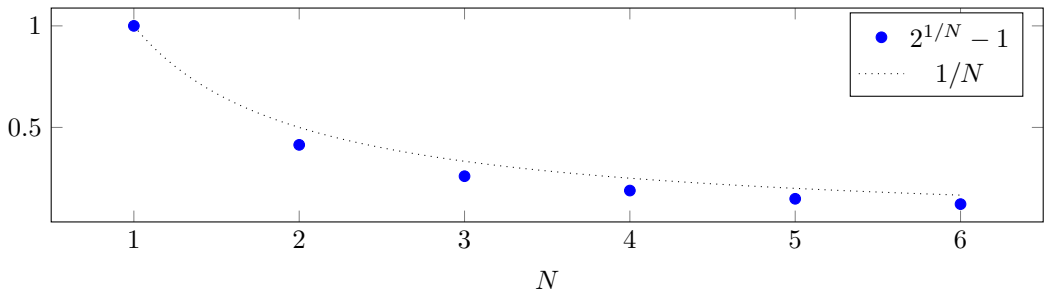

Figure 3.7: The exponent σ_N that determines the asymptotic growth rate of the population is shown against the number of stages. The dotted line would be expected if N steps with rate λ were equivalent to a single step of rate λ/N.

3.2.2 MS-G model with identical Erlang division times across generations

The solutions of the system (3.4) can be written in a closed analytical form in particular cases. For example, one may consider a simplified scenario where the number of stages is equal to 1 for all the generations, *i.e.*, $N_g = 1$ for all $g \geq 0$. Thus, system (3.6) becomes

$$\frac{\mathrm{d}M^g(t)}{\mathrm{d}t} = \begin{cases} -(\lambda_0 + \mu_0)M^0(t), & \text{if } g = 0, \\ 2\lambda_{g-1}M^{g-1}(t) - (\lambda_g + \mu_g)M^g(t), & \text{if } g \geq 1. \end{cases} \tag{3.26}$$

Then, if at time $t = 0$, there are C_0 cells in generation 0, so that $\mathbf{n}_0^T = (C_0, 0, \ldots, 0)$, this leads by recursion to the following solutions:

$$\begin{aligned} M^0(t) &= C_0 \mathrm{e}^{-(\lambda_0+\mu_0)t}, \\ M^g(t) &= 2^g\, C_0 \left(\prod_{l=0}^{g-1} \lambda_l\right) \sum_{i=0}^{g} \mathrm{e}^{-(\lambda_i+\mu_i)t} \prod_{k=0,k\neq i}^{g} \frac{1}{\lambda_k + \mu_k - \lambda_i - \mu_i}, \quad g \geq 1. \end{aligned} \tag{3.27}$$

In this case the MS-G model becomes a birth-and-death process tracking cell generations, and becomes identical to that considered in Refs. De Boer & Perelson (2005); Luzyanina & Bocharov (2018); Luzyanina *et al.* (2007); Revy *et al.* (2001), where the inter-event times of cell death and division are modelled as exponential random variables, rather than Erlang distributions.

Another particular case is when one considers identical number of stages, N, and rates, λ and μ, across generations, so that division times are Erlang-distributed in each generation. Under these assumptions, it is possible to obtain an analytical expression for the mean number of cells in each generation. In particular, system (3.4) becomes

$$\frac{\mathrm{d}M_j^g(t)}{\mathrm{d}t} = \begin{cases} -(\lambda+\mu)M_1^0(t), & \text{if } g=0,\ j=1, \\ \lambda M_{j-1}^g(t) - (\lambda+\mu)M_j^g(t), & \text{if } g\geq 0,\ j=2,\ldots,N, \\ 2\lambda M_N^{g-1}(t) - (\lambda+\mu)M_1^g(t), & \text{if } g\geq 1,\ j=1. \end{cases} \tag{3.28}$$

These equations can be rewritten in terms of the new variables $m_j^g(t) = \mathrm{e}^{(\lambda+\mu)t}M_j^g(t)$, for $g\geq 0$, $j=1,\ldots,N$. This is equivalent to multiplying (3.28) by the integrating factor $e^{(\lambda+\mu)t}$. Thus, (3.28) become

$$\frac{\mathrm{d}m_j^g(t)}{\mathrm{d}t} = \begin{cases} 0, & \text{if } g=0,\ j=1, \\ \lambda m_{j-1}^g(t), & \text{if } g\geq 0,\ j=2,\ldots,N, \\ 2\lambda m_N^{g-1}(t), & \text{if } g\geq 1,\ j=1. \end{cases} \tag{3.29}$$

To determine the solutions of (3.29), we focus here on the case $M_1^0(0) = m_1^0(0) = C_0$, while all the other compartments are empty at time $t=0$. This implies that $m_1^0(t) = C_0$ for $t\geq 0$, and by solving (3.29) recursively one gets

$$m_j^0(t) = C_0\lambda^{j-1}\frac{t^{j-1}}{(j-1)!},\quad j=1,\ldots,N.$$

This expression allows one then to determine the mean number of cells in each stage of generation 1,

$$m_j^1(t) = 2C_0\lambda^{N+j-1}\frac{t^{N+j-1}}{(N+j-1)!},\quad j=1,\ldots,N. \tag{3.30}$$

By recursion of (3.29) the mean number of cells in each compartment j of generation g is given by

$$m_j^g(t) = 2^g C_0\lambda^{gN+j-1}\frac{t^{gN+j-1}}{(gN+j-1)!} \text{ for } g\geq 0,\ j=1,\ldots,N.$$

Going back to the original variables, $M_j^g(t)$, the solutions of (3.28) are

$$M_j^g(t) = 2^g C_0\lambda^{Ng+j-1}\frac{t^{Ng+j-1}}{(Ng+j-1)!}\mathrm{e}^{-(\lambda+\mu)t},\quad g\geq 0,\ j=1,\ldots,N. \tag{3.31}$$

From the previous equations, one can show that

$$\lim_{t\to+\infty} M_j^g(t) = 0, \text{ for all } g \geq 0, \ j = 1, \ldots, N,$$

since cells in each generation and compartment either proceed to the next stage within their generation, divide (proceeding to the next generation), or die.
Once the mean number of cells in each compartment for a given generation is at hand, the expected number of cells in each generation can be determined according to (3.5). It can be written

$$M^g(t) = \sum_{j=1}^{N} M_j^g(t) = 2^g C_0 (\lambda t)^{Ng} \mathrm{e}^{-(\lambda+\mu)t} \sum_{j=1}^{N} \frac{(\lambda t)^{j-1}}{(Ng+j-1)!}, \ g \geq 0. \tag{3.32}$$

This equation is consistent with the results of the exponential model ($N = 1$) (see Section 3.2 of Luzyanina *et al.* (2007)). On the other hand, if one is interested in the mean number of cells in each compartment, $M_j(t)$ for $j = 1, \ldots, N$, regardless of the generation they belong to, this can be computed as follows

$$\begin{aligned} M_j(t) &= \sum_{g=0}^{+\infty} M_j^g(t) = \sum_{g=0}^{+\infty} 2^g \ C_0 \ \lambda^{gN+j-1} \ \frac{\mathrm{e}^{-(\lambda+\mu)t} \ t^{gN+j-1}}{(gN+j-1)!} \\ &= C_0 \ \mathrm{e}^{-(\lambda+\mu)t} \ 2^{\frac{1-j}{N}} \ \sum_{g=0}^{+\infty} \frac{\left(2^{\frac{1}{N}}\lambda t\right)^{gN+j-1}}{(gN+j-1)!}, \end{aligned} \tag{3.33}$$

for $j = 1, \ldots, N$ and $t \geq 0$. In practice, one could truncate the series above to get an approximation of the mean number of cells in each stage. However, one can use instead the solution provided by (3.14), since the dynamics of the MS-G model is equivalent to the dynamics of the MS model, when the parameters N, λ and μ are generation-independent. It can be numerically checked, that this indeed provides equivalent results as shown in Figure 3.8. The analytical solutions of the MS model derived in (3.14) (solid lines) are compared with stochastic simulations of the MS-G model realised with the Gillespie algorithm (Gillespie, 1976, 1977). The two models agree.
Moreover, when $N = 1$ or $N = 2$, one can analytically show the equivalence. In the former case ($N = 1$), it is enough to recall the power series of the exponential

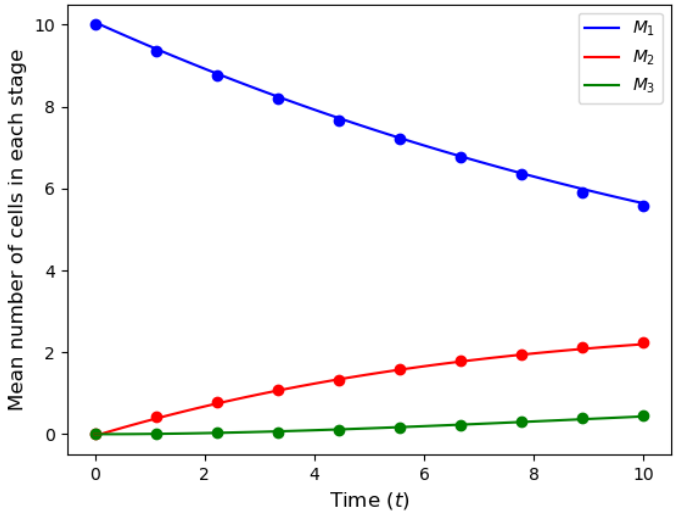

Figure 3.8: Equivalence between the analytical solutions of the MS model (solid lines) and stochastic simulations of the MS-G model (dots) to compute the expected number of cells in each stage under the assumption of identical number of stages N, birth and death rates, λ and μ, across generations. The number of stages is $N = 3$, the rates are fixed as $\lambda = 0.04$, $\mu = 0.01$ and have unit of inverse time t^{-1}. The simulations consider a maximum number of generations $G = 5$. Each dot is the mean value of 500 realisations realised with the Gillespie algorithm.

function. In the latter case ($N = 2$), we derive from (3.14)

$$\begin{aligned} M_1(t) &= \frac{C_0}{2}\mathrm{e}^{-(\lambda+\mu)t}\left(\mathrm{e}^{\sqrt{2}\lambda t} + \mathrm{e}^{-\sqrt{2}\lambda t}\right), \\ M_2(t) &= \frac{C_0}{2\sqrt{2}}\mathrm{e}^{-(\lambda+\mu)t}\left(\mathrm{e}^{\sqrt{2}\lambda t} - \mathrm{e}^{-\sqrt{2}\lambda t}\right), \end{aligned}$$

using the fact that $z = \mathrm{e}^{\pi i} = -1$. On the other hand, from (3.33) one obtains

$$\begin{aligned} M_1(t) &= C_0\mathrm{e}^{-(\lambda+\mu)t}\cosh\left(\sqrt{2}\lambda t\right) = C_0\mathrm{e}^{-(\lambda+\mu)t}\frac{\mathrm{e}^{\sqrt{2}\lambda t} + \mathrm{e}^{-\sqrt{2}\lambda t}}{2}, \\ M_2(t) &= C_0\mathrm{e}^{-(\lambda+\mu)t}\sinh\left(\sqrt{2}\lambda t\right) = \frac{C_0}{\sqrt{2}}\mathrm{e}^{-(\lambda+\mu)t}\frac{\mathrm{e}^{\sqrt{2}\lambda t} - \mathrm{e}^{-\sqrt{2}\lambda t}}{2}. \end{aligned}$$

This shows that the two models lead to the same expected number of cells in each stage.

3.2.3 Comparison between the MS-G model and the cyton model

The *cyton model* is a stochastic model proposed by Hawkins *et al.* (2007) to describe the population dynamics of B and T lymphocytes. Division and death times are regulated by two independent clocks, and the competition between both clocks determines the fate of the cell. In the cyton model, each clock is described by a probability density function, and the parameters that define these probabilities are the free parameters in the model. Right skewed distributions, such as log-normal or gamma, are usually adopted to characterise the two independent clocks that regulate cell division and death. When a cell divides, these clocks, which depend on the number of divisions the cell has undergone, are reset for each daughter cell. However, when analysing an *in vitro* experiment with this type of cells, there is evidence that not all cells either divide or die. For instance, a portion of them may not respond to the stimulation (Pereira *et al.*, 2003), or may respond without division (Deenick *et al.*, 2003). This is the reason why a progressor fraction is defined in the cyton model. This progressor fraction represents for a given generation, the fraction of cells that are capable of undergoing further division. In summary, the cyton model is based on the following assumptions:

- death and division are random events, characterised by a probability density function for the time to divide or die, respectively,
- these processes are independent, and compete to determine the fate of the cell,
- the clocks responsible for these processes are reset in the daughter cells when a cell divides,
- only a fraction of the cells in each generation are capable to undergo further divisions, and
- the intra-cellular mechanisms that regulate cellular fate depend on the cell's generation.

In order to translate these assumptions into mathematical terms, let γ_g be the progressor fraction characterising cells having undergone g divisions, and let $\phi_g(\cdot)$ and $\psi_g(\cdot)$ represent the probability density functions for the time to division and death, respectively, for cells in generation g. The number of cells dividing for the first time, or dying, per unit time at time $t \geq 0$ can be calculated, respectively, as (Hawkins *et al.*, 2007):

$$n_0^{div}(t) = \gamma_0 \, C_0 \left(1 - \int_0^t \psi_0(s)\mathrm{d}s\right) \phi_0(t), \tag{3.34}$$

$$n_0^{die}(t) = C_0 \left(1 - \gamma_0 \int_0^t \phi_0(s)\mathrm{d}s\right) \psi_0(t), \tag{3.35}$$

where C_0 is the initial number of cells in the population. Consequently, the time evolution of the expected number of cells in generation 0, $\widetilde{M}^0(t)$, obeys the differential equation

$$\frac{\mathrm{d}\widetilde{M}^0(t)}{\mathrm{d}t} = -\left[n_0^{div}(t) + n_0^{die}(t)\right]. \tag{3.36}$$

The number of cells in generation g dividing, or dying, per unit time at time t can be computed, respectively, as

$$n_g^{div}(t) = 2\gamma_g \int_0^t n_{g-1}^{div}(s) \left[1 - \int_0^{t-s} \psi_g(l)\mathrm{d}l\right] \phi_g(t-s)\mathrm{d}s, \tag{3.37}$$

$$n_g^{die}(t) = 2 \int_0^t n_{g-1}^{div}(s) \left[1 - \gamma_g \int_0^{t-s} \phi_g(l)\mathrm{d}l\right] \psi_g(t-s)\mathrm{d}s. \tag{3.38}$$

Hence, the dynamics of the average number of cells in each generation, $\widetilde{M^g}(t)$, is governed by the differential equations

$$\frac{\mathrm{d}\widetilde{M^g}(t)}{\mathrm{d}t} = 2n_{g-1}^{div}(t) - n_g^{div}(t) - n_g^{die}(t),\ g \geq 1. \tag{3.39}$$

In the next sections we show how the cyton model is equivalent to our model for particular choices of the probability density functions of the division and death clocks, $\phi_g(\cdot)$ and $\psi_g(\cdot)$, and the progressor faction γ_g.

Exponential time to division and death

Here the MS-G model is considered with number of stages across generations equal to one, *i.e.*, $N_g = 1$ for all $g \geq 0$. This means that cells in generation g divide after an exponentially distributed time with rate λ_g, and die with rate μ_g. This is different to a Markovian linear birth-and-death process, since rates are generation-dependent. The evolution through time of $M^g(t), g \geq 0$, obeys the differential equations derived in (3.26). In this case, the MS-G model is equivalent to the cyton model with exponential times for division and death, and progressor fraction $\gamma_g = 1$, $g \geq 0$. One can show this equivalence by proving that $n_g^{div}(t) = \lambda_g M^g(t)$ and $n_g^{die}(t) = \mu_g M^g(t)$, by induction on g. In the cyton model, the assumption of exponential time to division and death implies that $\phi_g(t) = \lambda_g \mathrm{e}^{-\lambda_g t}$ and $\psi_g(t) = \mu_g \mathrm{e}^{-\mu_g t}$, $g \geq 0$. Therefore, according to (3.34) and (3.35), the number of cells at time t dividing for the first time or dying to exit generation 0 per unit time is given by

$$n_0^{div}(t) \ = \ C_0\lambda_0 \mathrm{e}^{-(\lambda_0+\mu_0)t}, \quad n_0^{die}(t) \ = \ C_0\mu_0 \mathrm{e}^{-(\lambda_0+\mu_0)t}.$$

From (3.27), one knows that $M^0(t) = C_0 \mathrm{e}^{-(\lambda_0+\mu_0)t}$. Therefore, it is possible to write $n_0^{div}(t) = \lambda_0 M^0(t)$ and $n_0^{die}(t) = \mu_0 M^0(t)$, which proves the case $g = 0$. Following induction, one assumes $n_g^{div}(t) = \lambda_g M^g(t)$ and $n_g^{die}(t) = \mu_g M^g(t)$ hold for generation g and needs to show they also hold for generation $g + 1$. Making

use of (3.27) and (3.37), it follows

$$\begin{aligned} n_{g+1}^{div}(t) &= 2\int_0^t \lambda_g 2^g C_0 \prod_{l=0}^{g-1}\lambda_l \sum_{i=0}^{g} \mathrm{e}^{-\nu_i s} \prod_{k=0,k\neq i}^{g} \frac{1}{\nu_k-\nu_i}\lambda_{g+1}\mathrm{e}^{-\nu_{g+1}(t-s)}\mathrm{d}s \\ &= \lambda_{g+1}2^{g+1}C_0 \prod_{l=0}^{g}\lambda_l \sum_{i=0}^{g}\mathrm{e}^{-\nu_{g+1}t}\int_0^t \prod_{k=0,k\neq i}^{g}\frac{\mathrm{e}^{(\nu_{g+1}-\nu_g)s}}{\nu_k-\nu_i}\mathrm{d}s \\ &= \lambda_{g+1}M^{g+1}(t), \end{aligned}$$

where $\nu_i = \lambda_i + \mu_i$. For the number of cells in generation $g+1$ dying, equation (3.38), together with (3.27) lead to

$$\begin{aligned} n_{g+1}^{die}(t) &= 2\int_0^t \lambda_g 2^g C_0 \prod_{l=0}^{g-1}\lambda_l \sum_{i=0}^{g} \mathrm{e}^{-\nu_i s} \prod_{k=0,k\neq i}^{g} \frac{1}{\nu_k-\nu_i}\mu_{g+1}\mathrm{e}^{-(\nu_{g+1})(t-s)}\mathrm{d}s \\ &= \mu_{g+1}2^{g+1}C_0 \prod_{l=0}^{g}\lambda_l \sum_{i=0}^{g}\mathrm{e}^{-\nu_{g+1}t}\int_0^t \prod_{k=0,k\neq i}^{g}\frac{\mathrm{e}^{(\nu_{g+1}-\nu_g)s}}{\nu_k-\nu_i}\mathrm{d}s \\ &= \mu_{g+1}M^{g+1}(t), \end{aligned}$$

which concludes the proof. With the identities $n_g^{div}(t) = \lambda_g M^g(t)$ and $n_g^{die}(t) = \mu_g M^g(t)$ in (3.36) and (3.39), one shows that $M^g(t)$ and $\widetilde{M}^g(t)$ obey the same differential equations for all $g \geq 0$. Thus, the two models are equivalent.

Erlang time to division and exponential time to death

I now consider the more interesting case where the number of stages in each generation is greater than one, and the cell cycle can be described as a multi-stage process. The focus here is on the case where identical number of stages N and birth and death rates, λ and μ, respectively, are considered across generations. Similarly to the previous case, one can show that $n_g^{div}(t) = \lambda M_N^g(t)$ and $n_g^{die}(t) = \mu M^g(t)$ by induction on g. Since a cell's time to division is Erlang distributed and a cell's time to death is exponentially distributed, $\psi_g(t) = \mu \mathrm{e}^{-\mu t}$ for all $g \geq 0$ and

$$\phi_g(t) = \frac{\lambda^N t^{N-1}\mathrm{e}^{-\lambda t}}{(N-1)!},\ g \geq 0,$$

where the progressor fraction is again set to 1 for each generation. Note that in this case the parameters in $\phi_g(\cdot)$ and $\psi_g(\cdot)$ are independent of the generation

g, since the number of stages and the birth and death rates are identical for all generations. From (3.34) and (3.35), the number of cells dividing for the first time or dying to exit generation 0 per unit time at time t is

$$n_0^{div}(t) = \frac{C_0\lambda^N t^{N-1}}{(N-1)!}\mathrm{e}^{-(\lambda+\mu)t}, \quad n_0^{die}(t) = C_0\mu\mathrm{e}^{-(\lambda+\mu)t}\sum_{j=0}^{N-1}\frac{(\lambda t)^j}{j!}.$$

The dynamics of the expected number of cells in generation 0 is given by (3.36), as in the previous case. Using (3.31) and (3.32), one observes that

$$M^0(t) = C_0\mathrm{e}^{-(\lambda+\mu)t}\sum_{j=0}^{N-1}\frac{(\lambda t)^j}{j!}, \quad M_N^0(t) = \frac{\lambda^N t^{N-1}}{(N-1)!}\mathrm{e}^{-(\lambda+\mu)t}.$$

Therefore, $n_0^{div}(t) = \lambda M_N^0(t)$ and $n_0^{die}(t) = \mu M^0(t)$, which concludes the case $g = 0$. Making use of these identities in (3.36) one obtains

$$\frac{\mathrm{d}\widetilde{M}^0(t)}{\mathrm{d}t} = -\lambda M_N^0(t) - \mu M^0(t),$$

which is the differential equation derived in (3.6) for $M^0(t)$. Now, let us suppose that the identities $n_g^{div}(t) = \lambda M_N^g(t)$ and $n_g^{die}(t) = \mu M^g(t)$ hold for generation g and we prove them for generation $g+1$. Using (3.37) and the induction hypothesis, we have

$$\begin{aligned}
n_{g+1}^{div}(t) &= 2\int_0^t \lambda 2^g C_0 \frac{(\lambda s)^{Ng+N-1}}{(Ng+N-1)!}\mathrm{e}^{-(\lambda+\mu)s}\mathrm{e}^{-\mu(t-s)}\frac{\lambda^N(t-s)^{N-1}\mathrm{e}^{-\lambda(t-s)}}{(N-1)!}\mathrm{d}s \\
&= 2^{g+1}\frac{\lambda^{N(g+2)}}{(N(g+1)-1)!}C_0\mathrm{e}^{-(\lambda+\mu)t}\frac{1}{(N-1)!}\int_0^t s^{N(g+1)-1}(t-s)^{N-1}\mathrm{d}s \\
&= 2^{g+1}\frac{\lambda^{N(g+2)}}{(N(g+1)-1)!}C_0\mathrm{e}^{-(\lambda+\mu)t}\sum_{j=0}^{N-1}\frac{(-1)^j t^{N-1-j}}{j!(N-1-j)!}\int_0^t s^{N(g+1)-1+j}ds \\
&= \lambda 2^{g+1}\frac{(\lambda t)^{N(g+1)+N-1}}{(N(g+1)+N-1)!}C_0\mathrm{e}^{-(\lambda+\mu)t} = \lambda M_N^{g+1}(t),
\end{aligned}$$

where we have used (3.31) for the last step. The same arguments can be used to look at the number of cells in generation $g+1$ dying per unit of time given by

equation (3.38). Together with the induction hypothesis, we can write

$$\begin{aligned} n_{g+1}^{die}(t) &= 2\int_0^t \lambda 2^g C_0 \frac{(\lambda s)^{Ng+N-1}}{(Ng+N-1)!} \mathrm{e}^{-(\lambda+\mu)s} \mathrm{e}^{-\lambda(t-s)} \sum_{j=0}^{N-1} \frac{\lambda^j (t-s)^j}{j!} \mu \mathrm{e}^{-\mu(t-s)} \mathrm{d}s \\ &= 2^{g+1}\lambda^{Ng+N} C_0 \frac{\mathrm{e}^{-(\lambda+\mu)t}\mu}{(Ng+N-1)!} \sum_{j=0}^{N-1} \frac{\lambda^j}{j!} \int_0^t s^{Ng+N-1}(t-s)^j \mathrm{d}s \\ &= 2^{g+1}\lambda^{Ng+N} C_0 \mathrm{e}^{-(\lambda+\mu)t}\mu \sum_{j=0}^{N-1} \lambda^j \sum_{k=0}^{j} \frac{t^j}{k!(j-k)!} \frac{t^{k+N+Ng}}{k+N+Ng} \frac{(-1)^k}{(Ng+N-1)!} \\ &= \mu 2^{g+1} C_0 \mathrm{e}^{-(\lambda+\mu)t} \sum_{j=0}^{N-1} \frac{(\lambda t)^{N(g+1)+j}}{(N(g+1)+j)!} \quad = \quad \mu M^{g+1}(t), \end{aligned}$$

where the last identity was obtained making use of (3.32). Hence, (3.39) becomes

$$\frac{\mathrm{d}\widetilde{M}^g(t)}{\mathrm{d}t} = 2\lambda M_N^{g-1}(t) - \lambda M_N^g(t) - \mu M^g(t), \ g \geq 1,$$

which is identical to (3.6) for $M^g(t)$, $g \geq 1$. This concludes the proof of the equivalence between the cyton model and the multi-stage model with generations when a cell's time to divide is Erlang distributed with parameters λ and N, and a cell's time to die is exponential with rate μ. In summary, the analysis presented in this section for the multi-stage model with Erlang division time and exponential death time leads to novel analytical solutions for the cyton model with the previous choice of clocks.

3.3 Case study: lymphopenia-induced proliferation

In this section, I illustrate the applicability of the MS-G model to CFSE data, making use of an experimental study of lymphopenia-induced proliferation (Hogan *et al.*, 2013). In particular, the performance of the MS-G model is compared to that of a simple exponential (or single stage) model with generations, which is equivalent to making $N_g = 1$ for all g in the MS-G model. The statistical comparison is realised by means of the corrected version of the Akaike Information

Criterion (AIC_C) (Anderson & Burnham, 2004; Burnham & Anderson, 2004). See Appendix A for the derivation of the AIC_C.

Lymphopenia is defined as an abnormally low or reduced level of lymphocytes in the peripheral blood and can occur due to viral infections, chemical and physical lympho-depleting agents, autoimmune-related systemic diseases, genetic factors, cancers, sepsis and other severe injuries (Guo *et al.*, 2021). This condition results in an abundance of available resources for T cells (such as IL-7). Consequently, a process called lymphopenia-induced proliferation (LIP) can occur to restore the normal number of lymphocytes. Differences in T cell response to lymphopenia have been observed to vary between distinct T cell clonotypes (*i.e.*, the set of T cells with the same T cell receptor). Thus, Hogan *et al.* (2013) considered T lymphocytes belonging to two different T cell clonotypes, namely OT-I and F5 T cells, which are characterised by different rates of LIP. In particular, F5 T cells show a relatively slow rate of LIP, whereas OT-I T lymphocytes undergo a significantly more rapid LIP (Hogan *et al.*, 2013). CFSE-labelled OT-I or F5 T cells were transferred intravenously to lymphopenic mice. A certain number of days (3, 4, 5, 6, 7, 10, 12 and 18 days) after the transfer, spleens and lymph nodes were recovered from the mice and analysed by flow cytometry to quantify the expression levels of CD8, CD5, CD44, and CFSE dilution (Hogan *et al.*, 2013). For each time point, the number of mice analysed was between 3 and 7. Two independent transfer experiments, carried out under identical conditions, were performed: one for OT-I cells and a second one for F5. In Figure 3.9, both data sets are shown: for each time point the number of cells is plotted for each mouse and generation (identified via CFSE dilution measurement). On the left (right), OT-I (F5) cells are represented by the green (blue) histograms. In order to infer model parameters, all cells which have divided five or more times will be considered as a single class, denoted 5^+. This is similar to the approach considered in Refs. De Boer *et al.* (2006); Ganusov *et al.* (2007); Zilman *et al.* (2010). The rationale behind this choice is to reduce errors in the quantification of labelled cells with low CFSE fluorescence, as is the case for five or more divisions.

Figure 3.9 clearly shows that OT-I T cells proliferate faster than F5 cells, so that by day 7 there are OT-I cells in generation 10, whereas for F5 cells the maximum generation observed at day 7 is 6. This greater proliferative capacity of

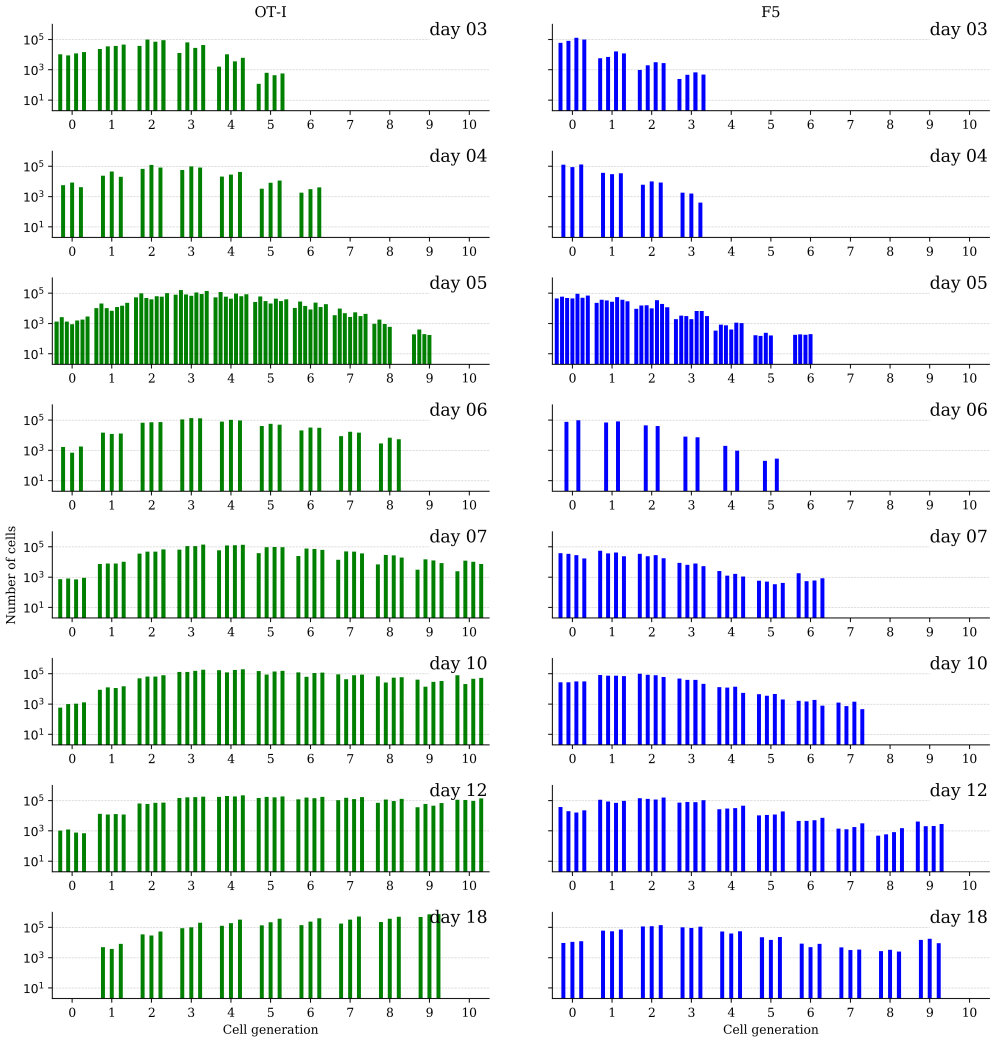

Figure 3.9: Data set of murine T lymphocytes from Hogan *et al.* (2013). **Left**: OT-I T cells. **Right**: F5 T cells. For each time point, the number of cells is plotted for each mouse and generation.

OT-I cells eventually leads, after one week, to competition for resources (*e.g.,* IL-7 cytokine) and the OT-I population approaching its carrying capacity (Hogan *et al.*, 2013). Since our model does not account for competition, it can only appropriately describe the dynamics of OT-I cells during the first week of the experiment. Thus, for OT-I cells we will only make use of the data set up to that time (one week). Yet for the F5 population we will use the entire data set since that effect (carrying capacity) is not observed. In Hogan *et al.* (2013) this competition was incorporated with a density-dependent birth rate, $\lambda(P)$, as follows

$$\lambda(P) = \bar{\lambda}\, \mathrm{e}^{-\delta P}, \tag{3.40}$$

where $\bar{\lambda}$ is the rate of growth under unlimited resources, δ the size of reduction caused by the expansion of competing cells, and P is the size of the population (Hogan *et al.*, 2013). Figure 3.10 shows the density-dependent birth rate, $\lambda(P)$, as a function of the population size P. It suggests that the competition for resources is greater in the case of OT-I T cells. In the experiments the number of OT-I cells after one week (about 5×10^5) is larger than the population of F5 T cells at day 18 (about 4×10^5). Therefore, the population of F5 T cells never reaches its carrying capacity and the role of competition for resources can be neglected.
We aim to model the dynamics in Figure 3.9 by using the MS-G model, for which we need to estimate a number of model parameters. These model parameters are estimated by means of the ABC-SMC method illustrated in Algorithm 3 (Toni *et al.*, 2009). Thus, the posterior distribution of the parameters is obtained by T sequential applications of the ABC algorithm, where the posterior obtained in each iteration is used as prior for the next one. Algorithm 3 requires the definition of prior distributions for the first iteration, a distance function, a tolerance threshold for each iteration, and a perturbation kernel (Toni *et al.*, 2009). Uniform prior distributions are assumed for all the parameters in the model, which means for each parameter a credible interval, where the parameter is believed to lie, is defined. Since further information is not added and the structure of the prior distribution does not favour any particular parameter value, all the knowledge that one will obtain from the calibration will actually come from the experimental data. The ranges of the prior distributions are described in Table 3.1. When a prior distribution spans several orders of magnitude, the uniform distribution is taken over the

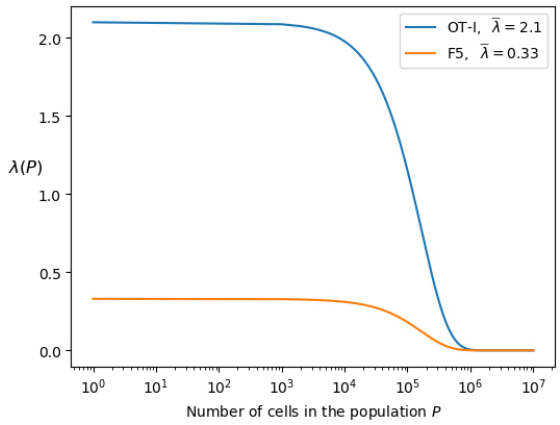

Figure 3.10: Density-dependent birth rate, $\lambda(P)$, as a function of the population size, P. The parameter $\bar{\lambda}$, with units of $cell \cdot day^{-1}$, represents the rate of growth under no competition and δ quantifies the level of reduction caused by the expansion of competing cells. Values for $\bar{\lambda}$ (shown in the inset) and $\delta = 6.0 \times 10^{-6}$ are taken from Table 1 of Hogan *et al.* (2013).

exponent to efficiently explore parameter space. Given $x_D^g(t)$, the experimentally determined mean number of cells in generation g at time t, for $g \in \{0, 1, 2, 3, 4, 5^+\}$, and its corresponding model prediction, $x_M^g(t) = M^g(t)$ for a particular choice of parameters $\boldsymbol{\theta} = (C_0, N_0, N, \lambda_0, \lambda, \alpha)$, the distance function is defined as

$$d(\text{model,data} \mid \boldsymbol{\theta}) = \sqrt{\sum_{g=0}^{G} \sum_{t \in \mathscr{T}} \left[\frac{x_M^g(t) - x_D^g(t)}{\sigma_D^g(t)} \right]^2}, \tag{3.41}$$

where $\mathscr{T}$ is the set of time points and depends on the clonotype of interest (either OT-I or F5), $\sigma_D^g(t)$ represents the standard deviation of the experimental data at time t and generation g, and G is the merged (and maximum) generation, $G = 5^+$. In practice, the first tolerance threshold, ε_1, in the ABC-SMC algorithm is defined as the median value of the distances obtained from 10^4 preliminary realisations, with the parameters sampled from the prior distributions in Table 3.1. The subsequent tolerance thresholds, ε_j, $j = 2, \ldots, T$ can be then defined as the median of the distance values obtained from the previous iterations of the algorithm. Finally, a uniform perturbation kernel is used to perturb the parameters during the sequence of iterations (Toni *et al.*, 2009), and the algorithm is implemented for

$T = 16$ in the case of the multi-stage model and $T = 7$ for the single stage one. Before performing the Bayesian inference, some assumptions are made based on the experimental set-up. Several studies have shown that the time to first division is larger than the time to subsequent divisions, since cells require time to become activated before they divide (Hawkins *et al.*, 2007; Kinjyo *et al.*, 2015; Markham *et al.*, 2010). Thus, I assume that all generations but 0 are comprised of the same number of stages N, whereas generation 0 is characterised by N_0 stages. Similarly, cells in generation 0 proceed to divide with birth rate λ_0, whilst all the other generations have a birth rate λ. Therefore, in contrast to the inference in Zilman *et al.* (2010), the number of stages N_0 and N are free parameters in the model. On the other hand, the per cell death rate in a given generation is assumed to be linear on the number of cell divisions that the cell has undergone (Ganusov *et al.*, 2007; Mazzocco *et al.*, 2017). That is

$$\mu_g = \alpha\, g, \;\; g \geq 0, \tag{3.42}$$

where α is a parameter to estimate. These linear death rates encode the fact that cells are more likely to die when they have already undergone several divisions (Ganusov *et al.*, 2007; Mazzocco *et al.*, 2017). Finally, the initial number of cells, C_0, is considered a parameter to be estimated, since the actual number of transferred cells which make it to the lymph nodes or spleen cannot be measured. The calibration of the simple exponential model is carried out similarly, but just with the constraint $N_0 = N = 1$.

Model parameter	Description	Prior distribution
C_0	Initial number of cells	$C_0 = 10^x$, $x \sim U(4, 6)$
N_0, N	Number of stages	$U_{\text{discrete}}(1, 50)$
λ_0, λ	Birth rate	$\lambda_0 = 10^y$, $\lambda = 10^z$, $y, z \sim U(-3, 1)$
α	Death rate slope	$\alpha = 10^w$, $w \sim U(-5, -1)$

Table 3.1: Prior distributions for parameters in the multi-stage model with cell generations. Units for λ_0, λ and α are inverse hours (h^{-1}).

The calibrated model predictions obtained for each model, and for each clonotype (OT-I or F5), are shown in Figure 3.11. I run the model with the parameters

being sampled from the estimated posterior distributions and compute the median of all the model predictions, which corresponds to the solid magenta (multi-stage model) and turquoise (exponential model) lines in Figure 3.11. The bands around median predictions represent 95% confidence intervals, which are calculated as the central 95% intervals of the model predictions for those parameter values. Thus, the lower bound of the confidence interval is given by the 2.5th percentile of all the model predictions, whereas the upper bound corresponds to the 97.5th percentile. Data points are plotted with the standard deviation from the multiple experimental replicates. As shown in Figure 3.11, the calibrated MS-G model successfully captures the dynamics of the proliferating T-cell populations (OT-I and F5), whereas the single stage model significantly underestimates the expected number of cells beyond generation 1, particularly in the case of OT-I T cells. The corrected version of the Akaike Information Criterion (AIC_C) (Anderson & Burnham, 2004; Burnham & Anderson, 2004) was used to quantify the better fit of the MS-G model accounting for the extra parameters N_0 and N in the multi-stage model. The values of AIC_C for each model and clonotype are listed in Table 3.2. Despite the two extra parameters, the values of AIC_C corresponding to the multi-stage model are significantly lower for both clonotypes. Overall, the MS-G model is able to explain the data from the OT-I transfer experiment better, since this data set is less noisy than the F5 set.

Mathematical model	Cell type	Value of AIC_C
Multi-stage	OT-I T cells	50.4
Exponential	OT-I T cells	283
Multi-stage	F5 T cells	206
Exponential	F5 T cells	317

Table 3.2: AIC_C values for the exponential and multi-stage models with cell generations calibrated with CFSE data of murine T lymphocytes.

The marginal posterior distributions for each parameter are shown in green and blue in Figures 3.12 and 3.13, for the multi-stage and exponential models, respectively, and the (uniform) prior distributions are plotted in red. Summary statistics of these posterior distributions are shown in Tables 3.3-3.6. Cell death is governed

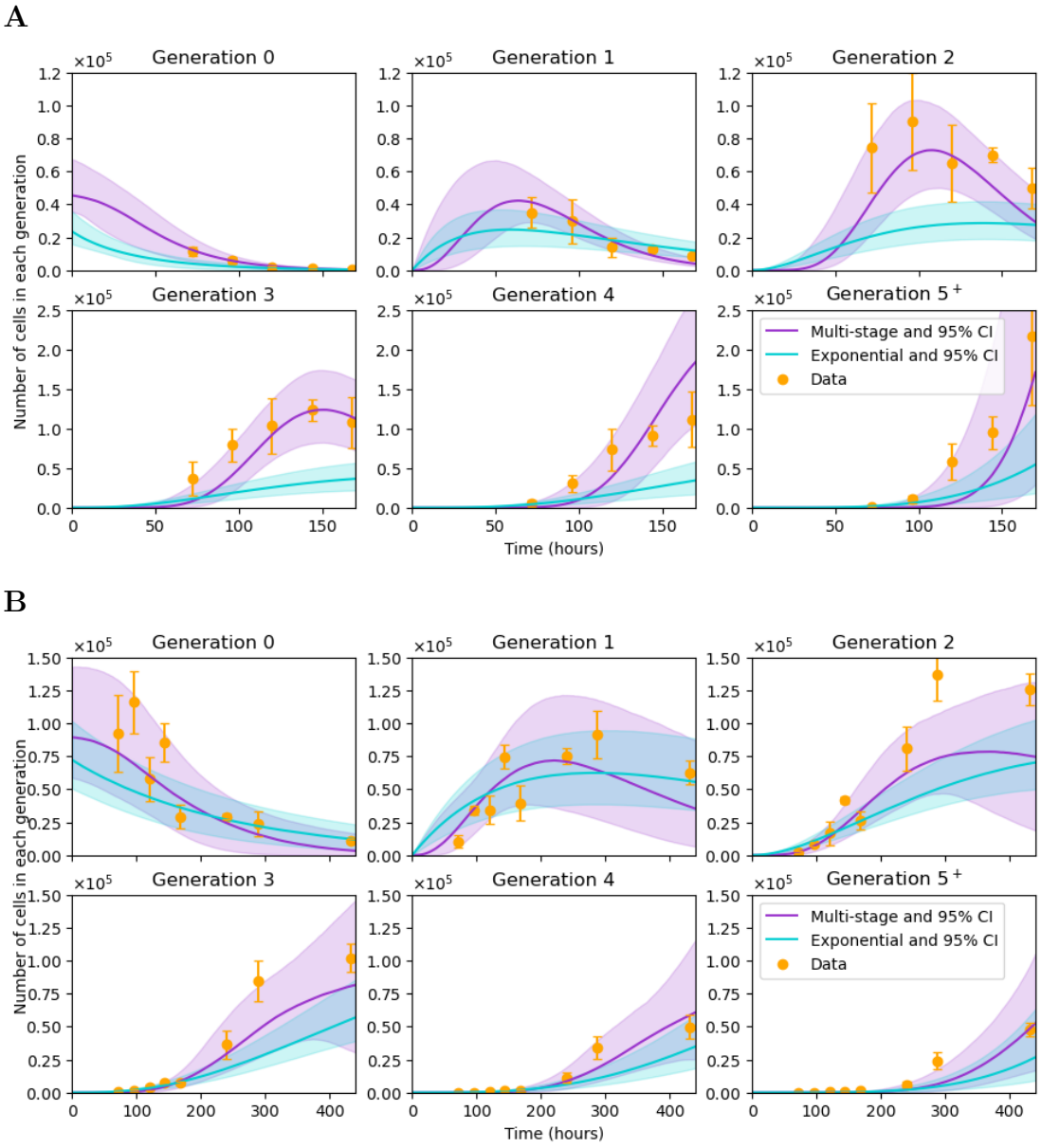

Figure 3.11: Exponential (solid turquoise line) and multi-stage (solid magenta line) model predictions compared to the data sets (orange dots) for OT-I (**A**) and F5 (**B**) T cells. Bars on data points represent their standard deviation. The expected number of cells in each generation is plotted as a function of time. These predictions represent the median value of 10^4 simulations with the accepted parameter values from the posterior distributions. Shaded areas represent 95% confidence intervals.

by the parameter α, and is estimated to be low for both models and clonotypes, suggesting that cell death does not have a significant impact on the dynamics during lymphopenia, which is in fact dominated by cell division. This result is in agreement with Hogan *et al.* (2013), where the death rate is assumed to be zero. The initial number of cells can be estimated with relative success, and does not seem to depend heavily on the model considered. On the other hand, cell division is governed by parameters $(N_0, \lambda_0, N, \lambda)$, with $N_0 = N = 1$ in the exponential model. One notes that in both models, $\frac{N_0}{\lambda_0}$ and $\frac{N}{\lambda}$ represent the mean time to the first and subsequent divisions, respectively. Although all division-related parameters can be estimated from the data, for both models and clonotypes, a correlation between the division rate and the number of stages is seen in the scatter plots of Figure 3.14. Instead of plotting the marginal posterior distributions for these parameters, one can consider the posterior distribution for the mean times $\frac{N_0}{\lambda_0}$ and $\frac{N}{\lambda}$ (see Figure 3.14). The fact that $N = 1$ is never chosen as an accepted parameter value in the posterior distribution for the multi-stage model and the OT-I clonotype already suggests that a multi-stage representation of cell division is preferred for this clonotype. On the other hand, for the F5 clonotype the marginal distribution for N shows a non-zero frequency for the value 1, but larger values of N are also represented in its posterior distribution. The mean time to both first and subsequent divisions, $\frac{N_0}{\lambda_0}$ and $\frac{N}{\lambda}$, are significantly longer for the F5 clonotype than the OT-I. In fact, our results estimate that F5 T cells divide slowly compared to OT-I cells, requiring on average 192 hours to carry out a first division (59 hours taken by OT-I T cells), as shown in Figure 3.14 for the multi-stage model. The time to subsequent divisions is represented by the blue histograms. Interestingly, my estimation of the mean time to first division of OT-I cells, on average 59 hours, is close to the value obtained by Hogan *et al.* (2013) (52 hours when considering the best fit parameter estimates). In the case of F5 cells, my results predict an average of 192 hours to undergo their first division, whereas Hogan *et al.* obtained a value of 137 hours. Still, one notes that the value 137 hours is within the range covered by the predicted posterior distribution.

Results here indicate that OT-I T lymphocytes require on average 59 hours for their first division, and a bit less, 46 hours, for subsequent divisions (see upper left plot of Figure 3.14). Based on the ABC-SMC approach, one concludes that

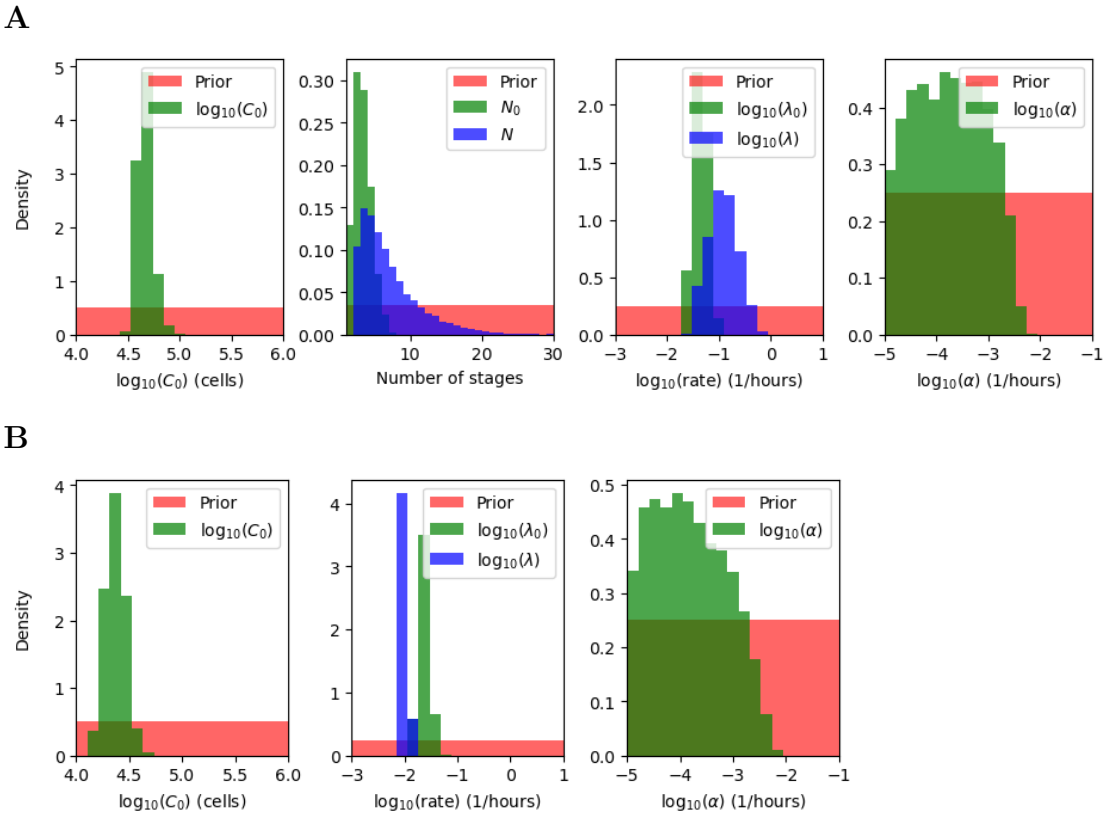

Figure 3.12: Posterior distributions (green and blue) for the parameters in the multi-stage (**A**) and exponential (**B**) model for OT-I T cells. In the exponential model, the number of stages for all generations is equal to 1, *i.e.*, $N_0 = N = 1$. Prior distributions are shown in red.

Param.	Minimum	Maximum	Mean	Median	Std dev
C_0	3.00×10^4	1.03×10^5	4.67×10^4	4.54×10^4	8.03×10^3
N_0	1	7	2.83	3	1.23
N	2	34	6.59	5	4.30
λ_0	1.98×10^{-2}	1.08×10^{-1}	4.64×10^{-2}	4.56×10^{-2}	1.45×10^{-2}
λ	2.80×10^{-2}	8.08×10^{-1}	1.48×10^{-1}	1.20×10^{-1}	1.01×10^{-1}
α	1.00×10^{-5}	5.97×10^{-3}	5.06×10^{-4}	1.76×10^{-4}	7.47×10^{-4}

Table 3.3: Summary statistics of OT-I clonotype posterior distributions for the multi-stage model. Although N_0 and N are integers, the means of their posterior distributions are non-integers.

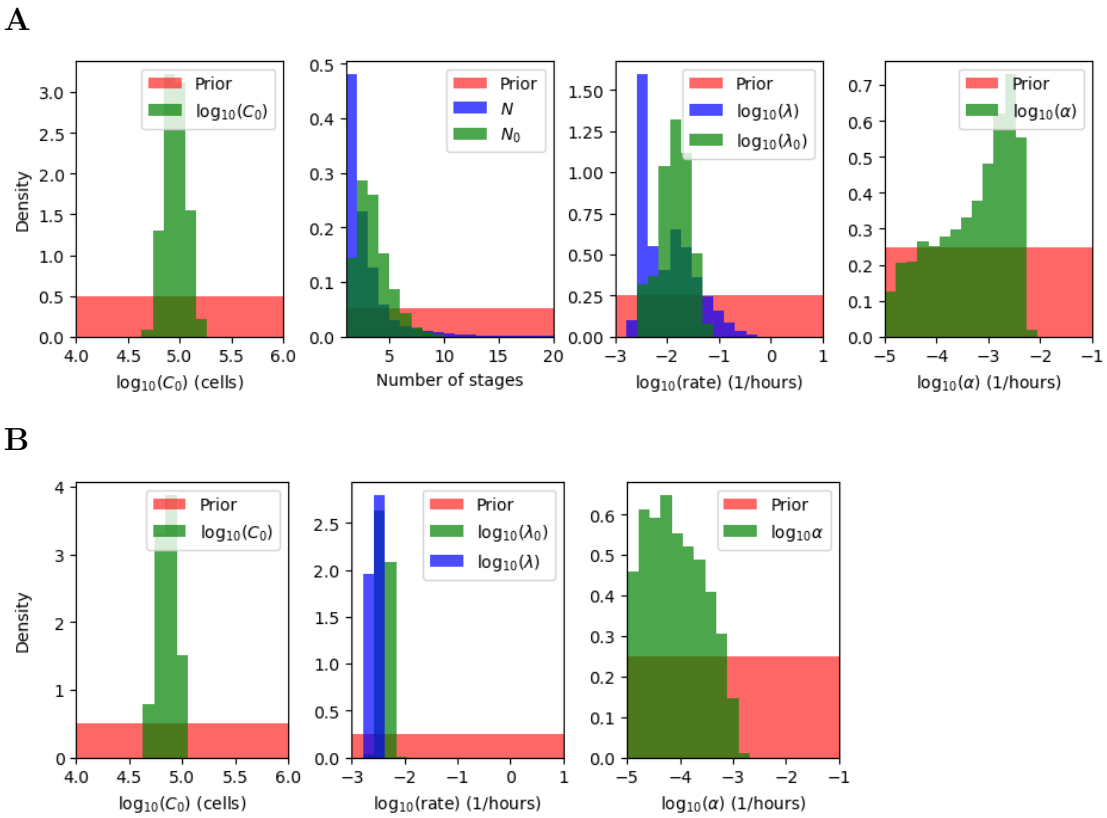

Figure 3.13: Posterior distributions (green and blue) for the parameters in the multi-stage (**A**) and exponential (**B**) model for F5 T cells. In the exponential model, the number of stages for all generations is equal to 1, *i.e.*, $N_0 = N = 1$. Prior distributions are shown in red.

Param.	Minimum	Maximum	Mean	Median	Std dev
C_0	4.74×10^4	1.85×10^5	9.26×10^4	8.94×10^4	2.22×10^4
N_0	1	10	3.01	3	1.53
N	1	35	2.42	2	2.57
λ_0	2.68×10^{-3}	7.20×10^{-2}	1.70×10^{-2}	1.47×10^{-2}	1.07×10^{-2}
λ	2.06×10^{-3}	5.88×10^{-1}	2.20×10^{-2}	9.54×10^{-3}	3.90×10^{-2}
α	1.00×10^{-5}	6.21×10^{-3}	1.35×10^{-3}	8.19×10^{-4}	1.40×10^{-3}

Table 3.4: Summary statistics of F5 clonotype posterior distributions for the multi-stage model. Although N_0 and N are integers, the means of their posterior distributions are non-integers.

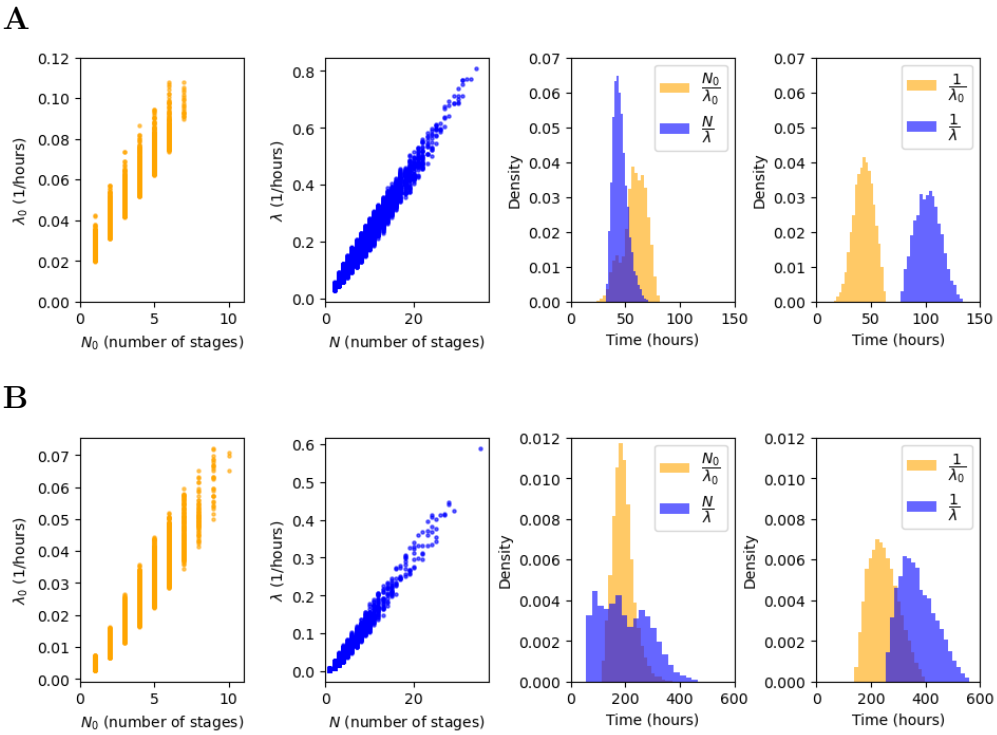

Figure 3.14: Joint posterior distributions (**left two columns**) of the number of stages N_0, N and the birth rates λ_0, λ. Marginal posterior distributions (**right two columns**) for the mean time to first and subsequent divisions estimated from the multi-stage model (third column) and the exponential model (fourth column). Panel **A** for OT-I T cells and **B** for F5 T cells.

Param.	Minimum	Maximum	Mean	Median	Std dev
C_0	1.43×10^4	5.46×10^5	2.40×10^4	2.34×10^4	5.28×10^3
λ_0	1.56×10^{-2}	6.19×10^{-2}	2.40×10^{-2}	2.28×10^{-2}	5.69×10^{-3}
λ	7.45×10^{-3}	1.29×10^{-2}	9.88×10^{-3}	9.78×10^{-3}	1.10×10^{-3}
α	1.00×10^{-5}	7.23×10^{-3}	4.76×10^{-4}	1.32×10^{-4}	8.17×10^{-4}

Table 3.5: Summary statistics for the posterior distributions of the exponential model for the OT-I clonotype.

Param.	Minimum	Maximum	Mean	Median	Std dev
C_0	4.54×10^3	1.10×10^5	7.33×10^4	7.22×10^4	1.39×10^4
λ_0	2.50×10^{-3}	7.18×10^{-3}	4.24×10^{-3}	4.13×10^{-3}	9.28×10^{-4}
λ	1.79×10^{-3}	3.92×10^{-3}	2.77×10^{-3}	2.76×10^{-3}	4.66×10^{-4}
α	1.00×10^{-5}	1.52×10^{-3}	1.72×10^{-4}	7.30×10^{-5}	2.23×10^{-4}

Table 3.6: Summary statistics for the posterior distributions of the exponential model for the F5 clonotype.

a multi-stage model with a constant division rate after the first division event, is a suitable description of lymphopenia-induced proliferation (De Boer & Perelson, 2005; Gett & Hodgkin, 2000; Zilman *et al.*, 2010). The MS-G model estimates that F5 cells take on average slightly less than 200 hours to divide, both for the first or subsequent division rounds, as shown in the lower left plot of Figure 3.14. This dissimilarity can be explained by the different characteristics in terms of proliferative capacity of OT-I and F5 T cells, and was previously observed by Hogan *et al.* (2013). The posterior distributions of the expected time to subsequent divisions in the MS-G model, $\frac{N}{\lambda}$, and in the exponential one, $\frac{1}{\lambda}$, shown as blue histograms in Figure 3.14, indicate that the exponential model predicts a longer division time than the multi-stage model for both clonotypes. This can be explained by the implementation of the ABC-SMC algorithm. Indeed, when parameterising the exponential model, the algorithm tries to keep the distance between the model predictions and the experimental observations low. This leads to the choice of parameter sets which limit cell proliferation, as shorter division times in the exponential model would lead to an increase in cell numbers not observed in the data set, and thus, larger distance values. This is why the estimated birth rates in the exponential model are lower than the ones in the multi-stage representation. As a result, the exponential model predicts a greater average division time than the multi-stage model for both clonotypes. Finally, my results indicate that for both clonotypes the exponential model (see Figure 3.14) found a shorter time to first division than to subsequent ones, contradicting previous findings (Hawkins *et al.*, 2007; Kinjyo *et al.*, 2015; Markham *et al.*, 2010), which support longer first division times. This is related to the fact that, overall, the exponential model is

not able to capture the observed cell dynamics for neither of the clonotypes, as can be seen in Figure 3.11.

3.4 Discussion

A multi-stage model of cell proliferation and death, tracking cell generations, is proposed in this chapter, leading to a modelling framework which retains the benefits of a Markov process. With particular choices of rates, the models in this chapter are equivalent to previously published models used to study lymphocyte proliferation (De Boer & Perelson, 2005; Hawkins *et al.*, 2007; Luzyanina & Bocharov, 2018; Luzyanina *et al.*, 2007; Revy *et al.*, 2001; Zilman *et al.*, 2010). In the case study of Section 3.3, the MS-G model performs better than the exponential model of time to division. The model implemented here provides a flexible framework for estimating the birth and death rates that describe the dynamics of lymphocyte populations (Callard & Hodgkin, 2007; De Boer & Perelson, 2013). The representation retains the advantages of a Markovian approach, including analytical tractability in some cases, and computational efficiency of numerical simulations with the Gillespie algorithm (Gillespie, 1976, 1977). The expected number of cells in each generation satisfies a set of linear differential equations. Further statistical comparison of the models in this chapter with other published models (De Boer & Perelson, 2005; Hawkins *et al.*, 2007; Luzyanina & Bocharov, 2018; Luzyanina *et al.*, 2007; Revy *et al.*, 2001; Zilman *et al.*, 2010) and with different experimental data sets is the aim of future work.

It has been observed by Hawkins *et al.* (2007); Kinjyo *et al.* (2015); Markham *et al.* (2010) that immune cells typically need longer to divide for the first time, whereas later divisions require shorter times (see *e.g.* Gett & Hodgkin (2000)). It is possible to assume that divided and undivided cells have different probability densities of time to cell division in exponential and Smith-Martin models (Ganusov *et al.*, 2007; Lee & Perelson, 2008; Mazzocco *et al.*, 2017). With the multi-stage model introduced here, the separation need not be explicit because it is incorporated in the generation-dependent parameters. A longer mean time to first division, $\frac{N_0}{\lambda_0}$, than mean time to subsequent divisions, $\frac{N}{\lambda}$, is a natural feature of the framework. Extension of the mathematical analysis in Section 3.2 to the case $\lambda_0 \neq \lambda$, $N_0 \neq N$

and possibly generation-dependent death rate μ_g, $g \geq 0$, would be desirable to compute analytically the expected number of cells in each generation also in this more general setting.

My calculations rely on the assumption that cells are independent of each other. In particular, no fate correlation is assumed between daughter cells and their progenitors, or between siblings. However, data sets from time-lapse microscopy of B and T cell families (Dowling *et al.*, 2014; Duffy & Hodgkin, 2012; Duffy & Subramanian, 2009; Duffy *et al.*, 2012; Hawkins *et al.*, 2009; Markham *et al.*, 2010; Wellard *et al.*, 2010) show that division and death times for siblings are correlated, and "division destiny" is a familial characteristic (Cheon *et al.*, 2021). A Markovian mathematical model that accounts for siblings fate correlation will be presented in Chapter 4.

A further potential extension of the MS-G model is the introduction of a population carrying capacity. In the model as described in Section 3.2, the mean number of cells over time either increases without bound, dies out or reaches a steady-state, depending on the relation between division-related parameters (birth rate and number of stages in the cell cycle), and the death rate. Competition for resources may be modelled using density-dependent birth and/or death rates (Callard *et al.*, 2003; Dessalles *et al.*, 2021; Hogan *et al.*, 2013), or by rates that depend on the time-dependent availability of resources (Hart *et al.*, 2014).

Chapter 4

Two-type branching process to study cellular dynamics with cell fate decision at birth

Mathematical models of population dynamics are often required to account for different types of individuals within the same population. For instance, in cancer biology, mutant cells may lead to tumour growth or acquired drug resistance (Antal & Krapivsky, 2011; Cheek & Antal, 2018; Gunnarsson *et al.*, 2020); in epidemiology, it might be important to consider age-dependent risk profiles when modelling the spread of a disease (Lovell-Read *et al.*, 2022), and to track exposed and infectious individuals to determine the probability of an outbreak (Allen, 2015). The theory of branching processes provides a powerful mathematical tool, the so-called *multi-type branching processes*, to model dynamics that involve non-identical individuals (Athreya *et al.*, 2004).

Till *et al.* (1964) made use of a two-type branching process classifying cells based on their *proliferative potential* to model colony growth from a single cell in mice spleens. Thus, the population of cells is divided into two pools: stem cells with unlimited proliferative potential, from which a colony is formed, and differentiated cells that cannot give rise to a colony. Since the interest was in studying the process of colony formation, only the dynamics of stem cells (*i.e.*, a birth-and-death process) was considered. In the following years this model was extended by Mackillop *et al.* (1983) with the incorporation of a third pool of cells to study

tumour growth. Therefore, the population is comprised of three distinct types of cells: cells with unlimited proliferative potential (also called stem cells), cells that can undergo a limited number of divisions, and cells incapable of further divisions. When a cell division occurs, daughter cells join each pool with a given probability. Coldman *et al.* (1985) and Coldman & Goldie (1986) used this model to study the emergence of drug resistance assuming that stem cells are initially sensitive to drug delivery. However, they can then generate either two sensitive cells or one sensitive and one drug resistant cell upon division with a given probability. The resulting dynamics of drug sensitive and resistant stem cells is a two-type branching process.

The underlying idea of these models, where cells are classified in different types and decide which pool to enter at birth (*i.e.*, daughter cells decide which pool they join when a division occurs), has been adapted here to describe the dynamics of a population of cells over time with the aim of investigating the role of fate correlation of siblings making use of a Markovian model. Cells are categorised according to their fate, either division or death. Thus, the population is divided into two pools defined by cellular fate. In the division pool, there are cells whose fate is division, whereas the death pool consists of cells that are going to die. Hawkins *et al.* (2009) and Markham *et al.* (2010) suggest that cellular fate is determined at, or soon after, birth. Therefore, when a division occurs, both daughter cells enter the division pool with probability p_1, both join the death pool with probability p_2, or have different fates with probability $p_3 = 1 - p_1 - p_2$. Conversely to the model proposed by Till *et al.* (1964), we follow the dynamics of both types of cells, and in contrast to Mackillop *et al.* (1983), our mathematical model does not account for cells with a limited proliferative potential. On the other hand, the approach proposed here allows for the generation of two cells in the death pool from a cell in the division pool, whereas two drug resistant cells cannot arise from a division of a sensitive cell (Coldman & Goldie, 1986; Coldman *et al.*, 1985).

After the instantaneous decision at birth, cellular fate (*i.e.*, either division or death) takes some random time to happen. As a first approach, cellular times to division and death are modelled making use of exponential random variables. In this instance, the analytical expression of the probability generating function (pgf for short) of the number of cells in each pool is derived. The expected time

to extinction of the division pool is computed making use of the theory of birth-and-death processes (Allen, 2010). We note that a particular case of this model under the assumption $p_1 = p_2$ and exponential times to division and death has been considered by Antal & Krapivsky (2010) to study cell dynamics in skin tissue. Thus, some of our work here generalises the analysis carried by Antal & Krapivsky (2010).

As discussed in Chapter 3, despite being the most convenient choice from both a mathematical and a computational perspective, the exponential distribution does not provide an accurate representation of a cell's time to division when studying cellular proliferation. Therefore, we also consider in this chapter the Erlang distribution to model a cell's time to division or death. In this case, each cell is required to visit a sequence of identical and independent exponentially distributed stages before dividing or dying. With this structure in place, the expected number of cells in each pool is computed as a function of time, and the long-term behaviour of the system is studied when $t \to +\infty$.

Interestingly, the model with cellular fate decision at birth presented here separates the cell population timescale – and therefore its rate of growth – from the cellular fate probability and long-term behaviour, which depend on the same parameters in many mathematical models of cell population dynamics. For example, in the classic birth-and-death process, a cell's time to division is exponentially distributed with birth rate λ ($T_{\text{div}} \sim Exp(\lambda)$) and a cell's time to death is an exponential random variable with death rate μ ($T_{\text{death}} \sim Exp(\mu)$) (Allen, 2010; Pinsky & Karlin, 2010). Thus, the inter-event times are exponentially distributed with rate $\lambda + \mu$, and each cell's fate is decided as a competition between these times, where the probability that a cell divides is given by $\mathbb{P}(T_{\text{div}} < T_{\text{death}}) = \frac{\lambda}{\lambda+\mu}$, whereas the probability that a cell dies corresponds to $\mathbb{P}(T_{\text{death}} < T_{\text{div}}) = \frac{\mu}{\lambda+\mu}$. Therefore, both cellular fate probabilities and population timescales are encapsulated into the parameters λ and μ. Similarly, in the multi-stage model of the cell cycle proposed in Chapter 3 (Belluccini *et al.*, 2022), a cell's division time is an Erlang random variable with N stages and birth rate λ ($T_{\text{div}} \sim Erlang(N, \lambda)$), whereas a cell's death time is exponentially distributed with rate μ ($T_{\text{death}} \sim Exp(\mu)$). The fate of each cell is decided by the competition between these times; in particular, the probability that a cell divides is $\mathbb{P}(T_{\text{div}} < T_{\text{death}}) = \left(\frac{\lambda}{\lambda+\mu}\right)^N$, and the probability

that a cell dies is computed as $\mathbb{P}(T_{\text{death}} < T_{\text{div}}) = 1 - \left(\frac{\lambda}{\lambda+\mu}\right)^N$. Thus, as in the birth-and-death process, both cellular fate probabilities and population timescales are determined by the parameters N, λ and μ. On the other hand, the mathematical model of cell population dynamics proposed here separates population timescales and cellular fate probabilities, by means of splitting the cell population into two pools, and incorporating the new parameters p_1, p_2 and $p_3 = 1 - p_1 - p_2$. In particular, p_1 and p_2 encapsulate the cellular fate probabilities and determine the population asymptotic behaviour, whereas p_3 and the parameters that characterise a cell's time to division and death (*i.e.*, birth and death rates, and number of stages in the case of Erlang distributions) set the population rate of growth.

The Markovian nature of the model presented here ensures analytical tractability, as shown by the results in Section 4.1, and computational efficiency of stochastic simulation realised with the Gillespie algorithm (Gillespie, 1976, 1977). An additional feature of the model proposed here is that the choice of the probabilities p_1 and p_2 allows one to account for *sibling fate correlation*. This is an important feature as time-lapse microscopy experiments, allowing tracking individual cells, identified correlations in terms of cellular fate within family trees of immune cells, *e.g.*, between cell siblings (Cheon *et al.*, 2021; Hawkins *et al.*, 2007; Kinjyo *et al.*, 2015; Markham *et al.*, 2010; Wellard *et al.*, 2010). In particular, when a division occurs, daughter cells are more likely to have the same fate, either division or death (Markham *et al.*, 2010). In order to include sibling fate correlation into our stochastic model of cell proliferation, *correlation factors* are defined. The applicability of this approach is shown in Section 4.3 by considering a published data set of B cell families observed with time-lapse microscopy (Hawkins *et al.*, 2009). The fate of siblings is broken down per division by Markham *et al.* (2010), allowing the comparison of the experimental data with the theoretical probabilities p_1, p_2 and $p_3 = 1 - p_1 - p_2$ computed in the stochastic model.

The chapter is structured as follows. Section 4.1 describes the mathematical model, and contains the analytical results in the instance of exponential times to division and death (Section 4.1.1) and Erlang times to division and death (Section 4.1.2). Section 4.2 contains the sensitivity analysis carried out to study how the probability p_3, the birth and death rates, and the number of stages of the division and

death processes affect the population dynamics. Finally, in Section 4.3, the role of sibling fate correlation is studied. Section 4.4 provides a final discussion.

4.1 The two-type branching process

A population of cells is divided into two pools based on cellular fate, either division or death. The division pool contains cells whose ultimate fate is division, whereas the death pool is comprised of cells whose destiny is death. As suggested by Hawkins *et al.* (2009) and Markham *et al.* (2010), cellular fate is decided at, or soon after, birth. Thus, we consider that, when a division occurs, daughter cells instantaneously join the division pool with probability p_1, enter the death pool with probability p_2, or have different fates with probability $p_3 = 1 - p_1 - p_2$. Cellular dynamics is depicted in Figure 4.1, where cells in the division and death pools are represented in green and red, respectively.

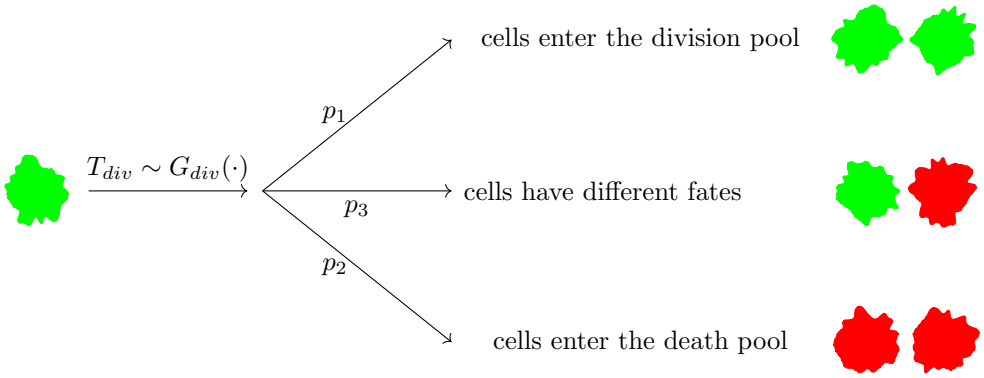

Figure 4.1: Three different outcomes of a cell division event. A cell in the division pool (green) divides after a random time T_{div}, generated from a given probability distribution $G_{div}(\cdot)$. Upon division, both daughters enter the division pool (green cells) with probability p_1, or the death pool (red cells) with probability p_2. Daughter cells have different fates with probability $p_3 = 1 - p_1 - p_2$.

After the instantaneous decision at birth, cellular fate takes some random time to actually occur. Here, we consider the exponential (Section 4.1.1) and Erlang (Section 4.1.2) probability densities as candidates to model these inter-event times. We note that, by considering these distributions, our stochastic model is Markovian.

4.1.1 Exponential times to division and death

Cellular times to division and death are assumed to be exponential random variables with rates λ and μ, respectively; $T_{div} \sim G_{div}(\cdot) \equiv Exp(\lambda)$, $T_{death} \sim G_{death}(\cdot) \equiv Exp(\mu)$. As the fate decision is instantaneous at birth, the expected time to division for a cell in the division pool is $\frac{1}{\lambda}$, whereas a cell in the death pool takes on average $\frac{1}{\mu}$ units of time to die. Under this hypothesis, the approach presented here amounts to a generalisation of the mathematical model proposed by Antal & Krapivsky (2010) to study cell dynamics in skin tissue, where the particular case $p_1 = p_2$ (or $r = p_1 = p_2$, $p_3 = 1 - 2r$ adopting the notation in the paper) is considered.
The random variables $\mathbb{B}(t)$ and $\mathbb{D}(t)$ are defined:

- $\mathbb{B}(t)$ is the number of cells in the division pool at time t, and
- $\mathbb{D}(t)$ is the number of cells in the death pool at time t.

Since we assume that cells in a given pool behave identically and independently from each other, the resulting dynamics is a two-type branching process, or a 2-dimensional continuous-time Markov chain, $(\mathbb{B}(t), \mathbb{D}(t))_{t\geq 0}$, with state space $\mathbb{N}_0 \times \mathbb{N}_0$, where $\mathbb{N}_0 = \mathbb{N} \cup \{0\}$.

Mean number of cells in each pool and long-term behaviour

To study the dynamics of the expected number of cells in each pool as a function of time, let $B(t) = \mathbb{E}[\mathbb{B}(t)]$ and $D(t) = \mathbb{E}[\mathbb{D}(t)]$ be the expected values of $\mathbb{B}(t)$ and $\mathbb{D}(t)$, respectively. The total mean number of cells in the population at time t, $P(t)$, is computed as $P(t) = B(t) + D(t)$. During a short time interval Δt, in the division pool one has

$$B(t + \Delta t) = B(t) + \Delta t \left(\lambda p_1 B(t) - \lambda p_2 B(t)\right),$$

where the first term in brackets reflects the possibility that a cell divides and both daughters enter the division pool, whereas the second one corresponds to the event that a cell divides and both daughters' fate is death. One notices that the case when a division occurs and daughter cells have different fates does not affect the

number of cells in the division pool. Therefore, the evolution through time of $B(t)$ is given by

$$\frac{\mathrm{d}B(t)}{\mathrm{d}t} = \lambda(p_1 - p_2)B(t),$$

from which the analytical expression of $B(t)$ is obtained as

$$B(t) = B(0)e^{\lambda(p_1-p_2)t}. \tag{4.1}$$

From here, we can already note that the division pool population will grow for $p_1 > p_2$, remain constant if $p_1 = p_2$, and decay if $p_1 < p_2$; and that this is not affected by the probability p_3, beyond the fact that these probabilities need to satisfy the condition $p_1 + p_2 + p_3 = 1$.

Let us now consider the death pool. The mean number of cells in this pool, $D(t)$, obeys the equation

$$D(t + \Delta t) = D(t) + \Delta t \left(2\lambda p_2 B(t) + \lambda(1 - p_1 - p_2)B(t) - \mu D(t)\right),$$

where the first term in brackets reflects the event that a cell divides and the offsprings enter the death pool, the second term accounts for the possibility that a cell undergoes a division and the two daughters have different fates, and the last term refers to a cell death. Hence,

$$\frac{\mathrm{d}D(t)}{\mathrm{d}t} = 2\lambda p_2 B(t) + \lambda(1 - p_1 - p_2)B(t) - \mu D(t),$$

which can be solved by multiplying both sides by the integrating factor $e^{\mu t}$. Assuming $D(0)$ as initial condition at time $t = 0$, the evolution through time of $D(t)$ is given by

$$D(t) = \frac{\lambda(1 - p_1 + p_2)}{\lambda(p_1 - p_2) + \mu} B(0) \left(e^{\lambda(p_1-p_2)t} - e^{-\mu t}\right) + D(0)e^{-\mu t}, \tag{4.2}$$

so that

$$P(t) = B(0)e^{\lambda(p_1-p_2)t} + \frac{\lambda(1 - p_1 + p_2)}{\lambda(p_1 - p_2) + \mu} B(0) \left(e^{\lambda(p_1-p_2)t} - e^{-\mu t}\right) + D(0)e^{-\mu t}. \tag{4.3}$$

From (4.1) and (4.2), it is clear that the long-term behaviour of the mean of the population as $t \to +\infty$ depends only on the relationship between the probabilities p_1 and p_2, whereas the birth and death rates λ and μ set the population dynamics timescale. In particular, the population will grow when $p_1 > p_2$, go extinct when $p_1 < p_2$, and reach a steady state at $\left(\frac{\lambda}{\mu} + 1\right) B(0)$ when $p_1 = p_2$, as shown in Figure 4.2.

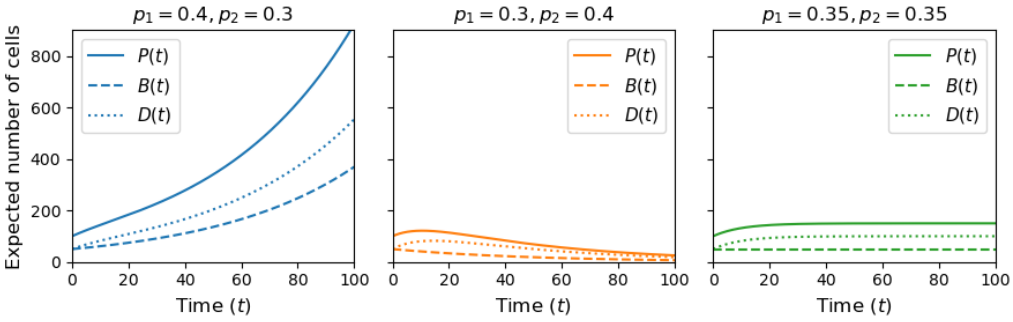

Figure 4.2: Long-term behaviour of the expected number of cells in the division pool (dashed lines), the death pool (dotted lines) and the whole population (solid lines) when $t \to +\infty$ under the assumption of exponential times to division and death derived in equations (4.1), (4.2) and (4.3), respectively. Three cases are distinguished: $p_1 > p_2$ (left), $p_1 < p_2$ (centre), and $p_1 = p_2$ (right). The initial condition provides a total number of 10^2 cells, half in the division pool and half in the death pool. The birth and death rates are fixed as $\lambda = 0.2$ and $\mu = 0.1$ with units inverse of time, t^{-1}.

Probability generating function

As the probability generating function characterises completely a discrete random variable, the aim of this section is to derive the analytical expression of the pgf of the number of cells in each pool. Let $p_{(i,j)}(t)$ denote the probability that the process is in state (i, j), with $i, j \in \mathbb{N}_0$, at time t given the initial conditions $(\mathbb{B}(0), \mathbb{D}(0)) = (1, 0)$, *i.e.*,

$$p_{(i,j)}(t) = \mathbb{P}\big((\mathbb{B}(t), \mathbb{D}(t)) = (i, j) | (\mathbb{B}(0), \mathbb{D}(0)) = (1, 0)\big), \quad t \geq 0.$$

Note that we are omitting the initial conditions in this notation. The expression of the Kolmogorov forward equation (or master equation) is

$$\begin{aligned} \frac{\mathrm{d}p_{(i,j)}(t)}{\mathrm{d}t} = {} & \lambda p_1(i-1)p_{(i-1,j)}(t) + \lambda p_2(i+1)p_{(i+1,j-2)}(t) \\ & + \lambda(1-p_1-p_2)ip_{(i,j-1)}(t) + \mu(j+1)p_{(i,j+1)}(t) \\ & - (\lambda i + \mu j)p_{(i,j)}(t), \end{aligned} \tag{4.4}$$

where the first term represents the event that a cell divides and both daughters' fate is division, the second one accounts for the possibility that a cell divides and

the offsprings enter the death pool, the third one refers to the probability that a division occurs and the daughters have different fates, the fourth one corresponds to the event that a cell dies and the last term contains rates for all the events that can occur from state (i, j).

Let $G(x, y; t)$ be the probability generating function of the number of cells in each pool defined as

$$G(x, y; t) = \sum_{i=0}^{+\infty} \sum_{j=0}^{+\infty} p_{(i,j)}(t) x^i y^j, \quad x, y \in \mathbb{C}, |x|, |y| \leq 1, \tag{4.5}$$

for the initial conditions $(\mathbb{B}(0), \mathbb{D}(0)) = (1, 0)$. Equation (4.4) enables the derivation of a partial differential equation (PDE) for the pgf $G(x, y; t)$. To this end, let us consider the partial derivatives of $G(x, y; t)$:

$$\begin{aligned}
\frac{\partial G(x, y; t)}{\partial x} &= \sum_{i=1}^{+\infty} \sum_{j=0}^{+\infty} p_{(i,j)}(t) i x^{i-1} y^j, \\
\frac{\partial G(x, y; t)}{\partial y} &= \sum_{i=0}^{+\infty} \sum_{j=1}^{+\infty} p_{(i,j)}(t) x^i j y^{j-1}, \\
\frac{\partial G(x, y; t)}{\partial t} &= \sum_{i=0}^{+\infty} \sum_{j=0}^{+\infty} \frac{\mathrm{d} p_{(i,j)}(t)}{\mathrm{d} t} x^i y^j.
\end{aligned}$$

Replacing equation (4.4) in the partial derivative with respect to time, one obtains

$$\frac{\partial G}{\partial t} = \lambda p_1 x^2 \frac{\partial G}{\partial x} + \lambda p_2 y^2 \frac{\partial G}{\partial x} + \lambda(1 - p_1 - p_2) xy \frac{\partial G}{\partial x} + \mu \frac{\partial G}{\partial y} - \lambda x \frac{\partial G}{\partial x} - \mu y \frac{\partial G}{\partial y},$$

which can be rewritten as

$$\lambda\big(p_1 x^2 + p_2 y^2 + (1 - p_1 - p_2) xy - x\big) \frac{\partial G}{\partial x} + \mu(1 - y) \frac{\partial G}{\partial y} - \frac{\partial G}{\partial t} = 0, \tag{4.6}$$

with boundary condition $G(x, y; 0) = x$ for the initial conditions $(\mathbb{B}(0), \mathbb{D}(0)) = (1, 0)$. One could attempt to solve equation (4.6) making use of the methods of characteristics; see *e.g.*, Ref. Pinchover *et al.* (2005). However, its expression involves all the three partial derivatives of $G(x, y; t)$. Instead, one can derive another equation satisfied by $G(x, y; t)$ that involves only the partial derivative with respect to time. To this end, let $d_j(t)$ denote the probability that there are j

cells in the death pool at time t given the initial conditions $(\mathbb{B}(0), \mathbb{D}(0)) = (0, 1)$, *i.e.*,

$$d_j(t) = \mathbb{P}\big(\mathbb{D}(t) = j | (\mathbb{B}(0), \mathbb{D}(0)) = (0, 1)\big).$$

The probability generating function of cells in the death pool, $H(y; t)$, is defined as

$$H(y; t) = \sum_{j=0}^{+\infty} d_j(t) y^j, \quad y \in \mathbb{C}, |y| \leq 1,$$

with initial condition $H(y; 0) = y$ given that $(\mathbb{B}(0), \mathbb{D}(0)) = (0, 1)$. As $(\mathbb{B}(0), \mathbb{D}(0)) = (0, 1)$, in a short time interval Δt, $\Delta t \to 0^+$, one has

$$(\mathbb{B}(\Delta t), D(\Delta t)) = \begin{cases} (0, 0) & \text{with probability } \mu \Delta t, \\ (0, 1) & \text{with probability } 1 - \mu \Delta t. \end{cases}$$

Therefore

$$H(y; t + \Delta t) = \mu \Delta t + (1 - \mu \Delta t) H(y; t),$$

from which $H(y; t)$ obeys the differential equation

$$\frac{\partial H}{\partial t} = \mu - \mu H, \tag{4.7}$$

with initial condition $H(y; 0) = y$. Thus, the solution of (4.7) is given by

$$H(y; t) = 1 - e^{-\mu t} + y e^{-\mu t}, \tag{4.8}$$

which corresponds to the probability generating function of a pure death process (Allen, 2010), as one would expect.

Let us now consider the initial conditions $(\mathbb{B}(0), \mathbb{D}(0)) = (1, 0)$. In a short time interval Δt, $\Delta t \to 0^+$, the following scenarios are possible:

$$(\mathbb{B}(\Delta t), \mathbb{D}(\Delta t)) = \begin{cases} (2, 0) & \text{with probability } \lambda p_1 \Delta t, \\ (0, 2) & \text{with probability } \lambda p_2 \Delta t, \\ (1, 1) & \text{with probability } \lambda(1 - p_1 - p_2) \Delta t, \\ (1, 0) & \text{with probability } 1 - \lambda \Delta t. \end{cases}$$

Therefore

$$\begin{aligned} G(x, y; t + \Delta t) = G(x, y; t)(1 - \lambda \Delta t) + \lambda p_1 G^2(x, y; t) \Delta t + \lambda p_2 H^2(x, y; t) \Delta t \\ + \lambda(1 - p_1 - p_2) G(x, y; t) H(y; t) \Delta t, \end{aligned}$$

from which another PDE for the probability generating function $G(x, y; t)$ is derived as

$$\frac{\partial G}{\partial t} = -\lambda G + \lambda p_1 G^2 + \lambda p_2 H^2 + \lambda(1 - p_1 - p_2)GH, \tag{4.9}$$

with boundary condition $G(x, y; 0) = x$ for the initial conditions $(\mathbb{B}(0), \mathbb{D}(0)) = (1, 0)$. Hereinafter, the arguments used in Antal & Krapivsky (2010) will be extended to solve (4.9). Replacing the expression of (4.8) in (4.9), one gets

$$\frac{\partial G}{\partial t} = \lambda p_1 G^2 + \lambda((1-p_1-p_2)(1-e^{-\mu t}+ye^{-\mu t})-1)G + \lambda p_2(1-e^{-\mu t}+ye^{-\mu t})^2, \tag{4.10}$$

which seems easier to solve than equation (4.6) since only the partial derivative with respect to time appears. Indeed, its expression takes the form of a Riccati equation (Bittanti *et al.*, 2012), *i.e.*, a first-order ordinary differential equation that is quadratic in the unknown function:

$$Y'(t) = A(t)Y^2(t) + B(t)Y(t) + C(t).$$

Without loss of generality, the birth rate is assumed to be $\lambda = 1$, which means that the unit of time is set as the average time for a cell in the division pool to divide. Let $h(t) = 1 - e^{-\mu t} + ye^{-\mu t}$. Rewritten in terms of $h \equiv h(t)$, equation (4.10) becomes

$$\mu(1 - h)\frac{\partial G}{\partial h} = p_1 G^2 + p_2 h^2 - (p_1 + p_2)hG - (1 - h)G, \tag{4.11}$$

with initial conditions $G(x, y; h(0) = y) = x$ at time $t = 0$. Equation (4.11) is then rewritten in terms of the new variable $u \equiv u(t) = 1 - h(t) = (1 - y)e^{-\mu t}$ as

$$-\mu u\frac{\partial G}{\partial u} = p_1 G^2 + p_2(1 - u)^2 - (p_1 + p_2)(1 - u)G - uG,$$

and its initial condition is $G(x, y; u(0) = 1 - y) = x$. Hence, if $u \neq 0$, one has

$$\frac{\partial G}{\partial u} = -\frac{p_1}{\mu u}G^2 + \frac{p_1(1 - u) + p_2(1 - u) + u}{\mu u}G - \frac{p_2(1 - u)^2}{\mu u}. \tag{4.12}$$

When $u = 0$, that is $y = 1$ (or equivalently $t = 0$), equation (4.10) becomes

$$\frac{\partial G}{\partial t} = p_1 G^2 - (p_1 + p_2)G + p_2, \tag{4.13}$$

with boundary condition $G(x,1;0)=x$ at time $t=0$. Equation (4.13) is a Riccati equation with constant coefficients. Thus, one considers the classical change of variables adopted in the case of a Riccati equation, *i.e.*, $G(t)=-s'(t)/\left(p_1 s(t)\right)$. It follows

$$s''(t)+(p_1+p_2)s'(t)+p_1p_2s(t)=0, \tag{4.14}$$

with initial conditions $s(0)=1, s'(0)=-p_1x$. The characteristic polynomial associated to (4.14) is

$$\Lambda^2+(p_1+p_2)\Lambda+p_1p_2=0,$$

which has two distinct real roots $\Lambda_1=-p_1, \Lambda_2=-p_2$. The solution of (4.14) is therefore

$$s(t)=C_1e^{-p_1t}+C_2e^{-p_2t},$$

where the constants C_1 and C_2 are yet to be determined. Making use of the initial conditions $s(0)=1, s'(0)=-p_1x$, one obtains

$$C_1=\frac{p_2-p_1x}{p_2-p_1}, \qquad \text{and} \qquad C_2=\frac{p_1x-p_1}{p_2-p_1}.$$

Thus, the solution of (4.13) is given by

$$G(x,1;t)=\frac{C_1p_1e^{-p_1t}+C_2p_2e^{-p_2t}}{p_1\left(C_1e^{-p_1t}+C_2e^{-p_2t}\right)}.$$

The aim is now to solve equation (4.12), which is a Riccati equation with coefficients

$$\begin{aligned}
A(u)&=-\frac{p_1}{\mu u},\\
B(u)&=\frac{p_1(1-u)+p_2(1-u)+u}{\mu u},\\
C(u)&=\frac{p_2(1-u)^2}{\mu u}.
\end{aligned}$$

As shown above, one considers the classical change of variables adopted in the case of a Riccati equation, *i.e.*, $G(u)=-z'(u)/(A(u)z(u))$, or equivalently $G(u)=-(\log z(u))'/A(u)$, and obtains the homogeneous second-order differential equation

$$z''(u)+\alpha(u)z'(u)+\beta(u)z(u)=0, \tag{4.15}$$

where

$$\alpha(u) = -\left(B(u) + \frac{A(u)}{A'(u)}\right) = \frac{\mu - p_1(1-u) - p_2(1-u) - u}{\mu u},$$
$$\beta(u) = C(u)A(u) = \frac{p_1 p_2 (1-u)^2}{\mu^2 u^2}.$$

Let $\Phi(u) = \mathrm{e}^{-\frac{1}{2}\left(\int \alpha(u)\mathrm{d}u\right)}$. Thus, $\Phi' = -\alpha(u)\Phi/2$. Considering $Z = z/\Phi$, or equivalently, $z = \Phi Z$, the first derivative in (4.15) disappears yielding

$$Z'' + \left(L_1 + \frac{L_2}{u} + \frac{L_3}{u^2}\right) Z = 0, \tag{4.16}$$

with

$$L_1 = \frac{2(p_1+p_2) - 1 - (p_1-p_2)^2}{4\mu^2},$$
$$L_2 = \frac{(p_1-p_2)^2 - (p_1+p_2)(\mu+1) + \mu}{2\mu^2},$$
$$L_3 = \frac{\mu^2 - (p_1-p_2)^2}{4\mu^2}.$$

In order to solve equation (4.16), two cases are distinguished: $p_1 = \left(1-\sqrt{p_2}\right)^2$ and $p_1 \neq \left(1-\sqrt{p_2}\right)^2$.

Case $p_1 \neq \left(1-\sqrt{p_2}\right)^2$. Re-scaling equation (4.16) using

$$v = \sqrt{p_1^2 + (p_2-1)^2 - 2p_1(p_2+1)},$$
$$w = \frac{p_1^2 + (p_2-1)(p_2-\mu) - p_1(1+2p_2+\mu)}{2v\mu},$$
$$\eta = \frac{p_1 - p_2}{2\mu},$$
$$g = \frac{uv}{\mu},$$

one obtains the canonical Whittaker differential equation (Whittaker, 1903)

$$\frac{\mathrm{d}^2 Z}{\mathrm{d}g^2} + \left(-\frac{1}{4} + \frac{w}{g} + \frac{\frac{1}{4} - \eta^2}{g^2}\right) Z = 0. \tag{4.17}$$

Notice that w is well defined as $v \neq 0$ since $p_1 \neq \left(1-\sqrt{p_2}\right)^2$. The solution of (4.17) up to an irrelevant constant is given by

$$Z(g) = M(w,\eta,g) + CW(w,\eta,g),$$

where $M(w,\eta,g)$ and $W(w,\eta,g)$ are the Whittaker functions (Abramowitz *et al.*, 1988) and C is a constant yet to be computed making use of the initial conditions. My aim is to write the pgf $G(x,y;u)$ in terms of its original variables $(x,y;t)$. One has

$$\begin{aligned} G(x,y;u) &= -\frac{(\log z(u))'}{A(u)} = \frac{\mu u}{p_1}\left(\log Z(u) + \log \Phi(u)\right)' \\ &= \frac{\mu u}{p_1}\left(\frac{\partial_g M(w,\eta,g) + C\partial_g W(w,\eta,g)}{M(w,\eta,g) + CW(w,\eta,g)}\frac{v}{\mu} - \frac{\alpha(u)}{2}\right) \\ &= \frac{uv}{p_1}\frac{\partial_g M(w,\eta,g) + C\partial_g W(w,\eta,g)}{M(w,\eta,g) + CW(w,\eta,g)} - \frac{\mu - (p_1+p_2)(1-u) - u}{2p_1}, \end{aligned}$$

where ∂_g denotes the partial derivative with respect to g and

$$\begin{aligned} \partial_g M(w,\eta,g) &= \frac{(g-2w)M(w,\eta,g) + (1+2w+2\eta)M(1+w,\eta,g)}{2g}, \\ \partial_g W(w,\eta,g) &= \frac{(g-2w)W(w,\eta,g) - 2W(1+w,\eta,g)}{2g}. \end{aligned}$$

Therefore,

$$\begin{aligned} G(x,y;u) =& \frac{uv - 2\mu w - \mu + (p_1+p_2)(1-u) + u}{2p_1} \\ &+ \frac{\mu}{2p_1}\frac{(1+2w+2\eta)M(1+w,\eta,g) - 2CW(1+w,\eta,g)}{M(w,\eta,g) + CW(w,\eta,g)}. \end{aligned} \tag{4.18}$$

The initial condition $G(x,y;u=1-y) = x$ is replaced in (4.18) to compute the constant C:

$$\begin{aligned} x =& -\frac{(1-y)v - 2\mu w - \mu + (p_1+p_2)y + 1 - y}{2p_1} \\ &+ \frac{\mu}{2p_1}\frac{(1+2w+2\eta)M(1+w,\eta,\hat{g}) - 2CW(1+w,\eta,\hat{g})}{M(w,\eta,\hat{g}) + CW(w,\eta,\hat{g})}, \end{aligned}$$

where $\hat{g} = \frac{(1-y)v}{\mu}$. Solving the previous equation with respect to C and denoting

$$\theta = \hat{g} - 2w - 1 + \frac{(p_1+p_2)y + 1 - y - 2p_1 x}{\mu},$$

it follows that

$$C = \frac{\theta M(w,\eta,\hat{g}) + (1+2w+2\eta)M(1+w,\eta,\hat{g})}{-\theta W(w,\eta,\hat{g}) + 2W(1+w,\eta,\hat{g})}. \tag{4.19}$$

Replacing (4.19) in (4.18), and recalling the definition of u as $u(t) = (1-y)e^{-\mu t}$, one gets the analytical expression of the probability generating function $G(x, y; u)$ in terms of the original variables $(x, y; t)$. We note that when we set $p_1 = p_2$ in equation (4.18), we recover equation (59) in Antal & Krapivsky (2010), as one would expect. Figure 4.3 shows the comparison between the numerical solution of (4.9) and its analytical expression derived in (4.18), which agree.

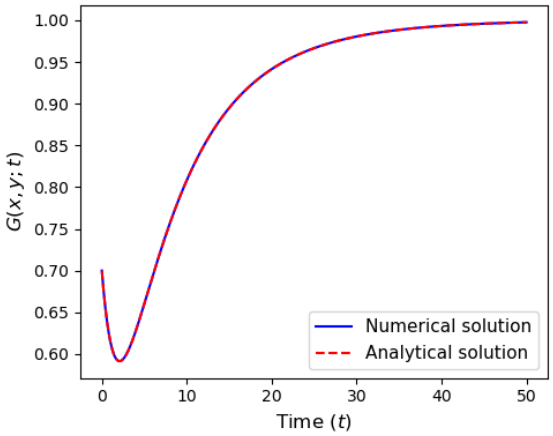

Figure 4.3: Comparison between the numerical solution of (4.9) and its analytical expression derived in (4.18) for the following choice of parameter values: $p_1 = 0.4$, $p_2 = 0.5$, $\mu = 0.3$, $x = 0.7$, $y = 0.8$. The death rate μ has units of inverse time, t^{-1}.

Case $p_1 = \left(1 - \sqrt{p_2}\right)^2$. In this instance, equation (4.16) simplifies as

$$Z'' + \left(\frac{(1-\mu)(p_2 - \sqrt{p_2})}{\mu^2 u} + \frac{\mu^2 - (1 - 2\sqrt{p_2})^2}{4\mu^2 u^2} \right) Z = 0.$$

The previous equation is re-scaled through the definition of

$$\widetilde{w} = \frac{(1-\mu)(p_2 - \sqrt{p_2})}{\mu^2},$$
$$\widetilde{\eta} = \frac{(1 - 2\sqrt{p_2})}{2\mu},$$

yielding

$$Z'' + \left(\frac{\widetilde{w}}{u} + \frac{\frac{1}{4} - \widetilde{\eta}^2}{u^2} \right) Z = 0. \tag{4.20}$$

The Frobenius method (see *e.g.*, Chapter 4 of Ref. Teschl (2012)) is used here to solve (4.20). This method searches for a solution in the form of a power series. In particular, one considers

$$Z(u) = u^r \sum_{k=0}^{+\infty} A_k u^k = \sum_{k=0}^{+\infty} A_k u^{k+r}, \quad A_0 \neq 0, \tag{4.21}$$

where the parameter $r \in \mathbb{R}$ and the coefficients A_k, $k \geq 0$, are yet to be determined. A function defined as power series is analytic in the region of convergence of the power series, so the first and second derivatives of $Z(u)$ are well defined and computed as

$$\begin{aligned} Z'(u) &= \sum_{k=0}^{+\infty} (k+r) A_k u^{k+r-1}, \\ Z''(u) &= \sum_{k=0}^{+\infty} (k+r)(k+r-1) A_k u^{k+r-2}. \end{aligned}$$

Replacing $Z(u)$ and $Z''(u)$ in (4.20), it follows

$$\sum_{k=0}^{+\infty} (k+r)(k+r-1) A_k u^{k+r-2} + \left(\frac{\widetilde{w}}{u} + \frac{\frac{1}{4} - \widetilde{\eta}^2}{u^2} \right) \sum_{k=0}^{+\infty} A_k u^{k+r} = 0,$$

from which we obtain the equation

$$\begin{aligned} &\left((r-1)r + \left(\frac{1}{4} - \widetilde{\eta}^2 \right) \right) A_0 u^{r-2} \\ &+ \sum_{k=1}^{+\infty} \left((k+r-1)(k+r) + \left(\frac{1}{4} - \widetilde{\eta}^2 \right) \right) A_k u^{k+r-2} \\ &+ \sum_{k=1}^{+\infty} \widetilde{w} A_{k-1} u^{k+r-2} = 0. \end{aligned}$$

For the previous equation to hold, the coefficients of each power of u must be null, that is

$$\left((r-1)r + \left(\frac{1}{4} - \widetilde{\eta}^2 \right) \right) A_0 = 0 \tag{4.22}$$

$$\left((k+r-1)(k+r) + \left(\frac{1}{4} - \widetilde{\eta}^2 \right) \right) A_k + \widetilde{w} A_{k-1} = 0, \quad k \geq 1. \tag{4.23}$$

Since $A_0 \neq 0$ by construction, from (4.22) two values of r are derived, $r = \frac{1\pm 2\eta}{2}$, which will lead to two independent solutions of (4.20). Replacing the values of r in (4.23), one obtains

$$\begin{aligned} A_k &= -\frac{\widetilde{w}}{(k\pm\widetilde{\eta})^2 - \frac{1}{4} + \frac{1}{4} - \widetilde{\eta}^2} A_{k-1} \\ &= -\frac{\widetilde{w}}{k\,(k\pm 2\widetilde{\eta})} A_{k-1}. \end{aligned}$$

In order to write the solution of equation (4.20) in terms of the Bessel function of the first kind, $J_\nu(z)$, (Abramowitz *et al.*, 1988), we choose $A_0 = \widetilde{w}^{\frac{1}{2}\pm\widetilde{\eta}}$. Thus, the general expression of A_k is given by

$$A_k = (-1)^k \frac{\widetilde{w}^{k+\frac{1}{2}\pm\widetilde{\eta}}}{k!(k\pm 2\widetilde{\eta})(k-1\pm 2\widetilde{\eta})\cdots(1+\pm 2\widetilde{\eta})},$$

which replaced in (4.21) yields

$$Z_\pm(u) = \sum_{k=0}^{+\infty} (-1)^k \frac{\widetilde{w}^{k+\frac{1}{2}\pm\widetilde{\eta}}}{k!(k\pm 2\widetilde{\eta})(k-1\pm 2\widetilde{\eta})\cdots(1\pm 2\widetilde{\eta})} u^{k+\frac{1}{2}\pm\widetilde{\eta}}.$$

The functions $Z_\pm(u)$ can be rewritten in terms of the Bessel function of the first kind, $J_\nu(z)$ as

$$Z_\pm(u) = \Gamma\left(1\pm 2\widetilde{\eta}\right)\sqrt{u}\sqrt{\widetilde{w}} J_{\pm 2\widetilde{\eta}}\left(2\sqrt{u}\sqrt{\widetilde{w}}\right),$$

where $\Gamma(z)$ is the Gamma function defined in equation (2.3). Thus, the general solution of (4.20) is given by

$$\begin{aligned} Z(u) &= c_1 Z_-(u) + c_2 Z_+(u) \\ &= \sqrt{u}\sqrt{\widetilde{w}}\left(c_1\Gamma(1-2\widetilde{\eta})\; J_{-2\widetilde{\eta}}\left(2\sqrt{u}\sqrt{\widetilde{w}}\right) + c_2\Gamma(1+2\widetilde{\eta}) J_{2\widetilde{\eta}}\left(2\sqrt{u}\sqrt{\widetilde{w}}\right)\right), \end{aligned}$$

where c_1 and c_2 are constants yet to be determined depending on the initial conditions. Hence,

$$\begin{aligned} G(x,y;u) &= -\frac{(\log z(u))'}{A(u)} = \frac{\mu u}{p_1}\left(\log Z(u) + \log\Phi(u)\right)' \\ &= \frac{\mu u}{\left(1-\sqrt{p_2}\right)^2}\left(\frac{Z(u)}{Z'(u)} - \frac{\alpha}{2}\right), \end{aligned} \tag{4.24}$$

where

$$Z'(u) = \frac{1}{2}(\sqrt{u}\sqrt{\widetilde{w}})^{-1-2\widetilde{\eta}}\widetilde{w}\Bigg((1+2\widetilde{\eta})c_1\ {}_0F_1(1-2\widetilde{\eta};-u\widetilde{w}) - 4\widetilde{\eta}c_1\ {}_0F_1(-2\widetilde{\eta};-u\widetilde{w}) \\ +(\sqrt{u}\sqrt{\widetilde{w}})^{4\widetilde{\eta}}c_2\Gamma(1+2\widetilde{\eta})\left(\frac{2\ {}_0F_1(2\widetilde{\eta};-u\widetilde{w})}{\Gamma(2\widetilde{\eta})} + (1-2\widetilde{\eta})\frac{{}_0F_1(1+2\widetilde{\eta};-u\widetilde{w})}{\Gamma(1+2\widetilde{\eta})}\right)\Bigg),$$

where ${}_0F_1(a;z)$ denotes the generalised hypergeometric function (Andrews *et al.*, 1999). Indeed, the Bessel function can be expressed in terms of the generalised hypergeometric function ${}_0F_1(a;z)$ as

$$J_\nu(z) = \frac{\left(\frac{1}{2}z\right)^\nu}{\Gamma(\nu+1)}\ {}_0F_1\left(\nu+1;-\frac{1}{4}z^2\right).$$

See for example equation (9.1.69) of Abramowitz *et al.* (1988) for reference. Defining $c = \frac{c_1}{c_2}$ and introducing the functions

$$\begin{aligned}
d(x,y,t) &= 2\frac{{}_0F_1\left(2\widetilde{\eta};e^{-\mu t}(y-1)\widetilde{\eta}\right)}{\Gamma(2\widetilde{\eta})} + (1-2\widetilde{\eta})\frac{{}_0F_1\left(1+2\widetilde{\eta};e^{-\mu t}(y-1)\widetilde{\eta}\right)}{\Gamma(1+2\widetilde{\eta})},\\
f(x,y,t) &= (1+2\widetilde{\eta})\ {}_0F_1\left(1-2\widetilde{\eta};e^{-\mu t}(y-1)\widetilde{\eta}\right) - 4\widetilde{\eta}\ {}_0F_1\left(-2\widetilde{\eta};e^{-\mu t}(y-1)\widetilde{\eta}\right)\\
&\quad + c\left(\sqrt{e^{-\mu t}(1-y)}\sqrt{\widetilde{\eta}}\right)^{4\widetilde{\eta}}\Gamma(1+2\widetilde{\eta})d(x,y,t),\\
g(x,y,t) &= {}_0F_1\left(1-2\widetilde{\eta};e^{-\mu t}(y-1)\widetilde{\eta}\right)\\
&\quad + c\left(\sqrt{e^{-\mu t}(1-y)}\sqrt{\widetilde{\eta}}\right)^{4\widetilde{\eta}}\ {}_0F_1\left(1+2\widetilde{\eta};e^{-\mu t}(y-1)\widetilde{\eta}\right),
\end{aligned}$$

allows one to rewrite $G(x,y;u)$ in (4.24) in terms of the original variables $(x,y;t)$ as

$$G(x,y;t) = \frac{1+2\left(p_2-\sqrt{p_2}\right)\left(1-e^{-\mu t}+ye^{-\mu t}\right)-\mu+\dfrac{\mu f(x,y,t)}{g(x,y,t)}}{2\left(\sqrt{p_2}-1\right)^2},$$

where

$$\begin{aligned}
c &= \frac{\kappa_1\kappa_2\ {}_0F_1\left(1-2\widetilde{\eta};(y-1)\widetilde{\eta}\right)+4\widetilde{\eta}\mu\ {}_0F_1\left(-2\widetilde{\eta};(y-1)\widetilde{\eta}\right)}{4\widetilde{\eta}\mu\ {}_0F_1\left(2\widetilde{\eta};(y-1)\widetilde{\eta}\right)+\kappa_3\ {}_0F_1\left(1+2\widetilde{\eta};(y-1)\widetilde{\eta}\right)},\\
\kappa_1 &= \left(\sqrt{1-y}\sqrt{\widetilde{\eta}}\right)^{-4\widetilde{\eta}},\\
\kappa_2 &= 2\left(\sqrt{p_2}-1\right)^2x + 2\sqrt{p_2}y - 2p_2y - 2\widetilde{\eta}\mu - 1,\\
\kappa_3 &= 1-2\left(\sqrt{p_2}-1\right)^2x - 2\sqrt{p_2}y + 2p_2y - 2\widetilde{\eta}\mu.
\end{aligned}$$

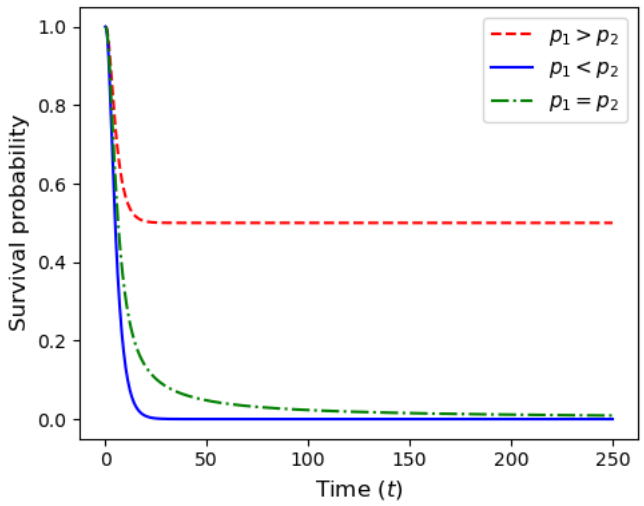

Figure 4.4: Survival probabilities in the three scenarios $p_1 = 0.6 > p_2 = 0.3$, $p_1 = 0.3 < p_2 = 0.6$, and $p_1 = p_2 = 0.45$. The death rate is fixed at $\mu = 0.5$ with units of inverse time, t^{-1}.

Once the probability generating function is at hand, the survival probability at time t can be computed as $S(t) = 1 - G(0, 0; t)$, *i.e.*,

$$S(t) = 1 - \mathbb{P}((\mathbb{B}(t), \mathbb{D}(t)) = (0, 0) | (\mathbb{B}(0), \mathbb{D}(0)) = (1, 0))), \quad t \geq 0.$$

Figure 4.4 shows an example of the probability of survival when $p_1 > p_2$, $p_1 = p_2$, and $p_1 < p_2$.
Another quantity of interest is the probability of having a total number of $i + j$ cells in the population at time t, $\Pi_n(t)$, that is

$$\Pi_n(t) = \mathbb{P}(B(t) + D(t) = n | (\mathbb{B}(0), \mathbb{D}(0)) = (1, 0)), \quad n \in \mathbb{N}_0,$$

or equivalently

$$\Pi_n(t) = \sum_{i+j=n} p_{(i,j)}(t).$$

As in Ref. Antal & Krapivsky (2010), one observes that

$$G(z, z; t) = \sum_{i=0}^{+\infty} \sum_{j=0}^{+\infty} p_{(i,j)}(t) z^i z^j = \sum_{n=0}^{+\infty} \Pi_n(t) z^n,$$

which means that the probability $\Pi_n(t)$ is the coefficient of the power series that defines $G(z,z;t)$. Thus, $\Pi_n(t)$ can be extracted making use of the Cauchy's integral formula and its derivatives (Ablowitz *et al.*, 2003; Antal & Krapivsky, 2010)

$$\Pi_n(t) = \frac{1}{2\pi i}\oint_\gamma \frac{G(z,z;t)}{z^{n+1}}\mathrm{d}z, \tag{4.25}$$

where γ is any simple closed contour in the domain where $G(z,z;t)$ is analytical. Similarly, recalling the definition of $G(x,y;t)$ in (4.5), one obtains

$$p_{(i,j)}(t) = -\frac{1}{4\pi^2}\oint_\gamma \frac{1}{y^{j+1}}\oint_\gamma \frac{G(x,y;t)}{x^{i+1}}\mathrm{d}x\mathrm{d}y. \tag{4.26}$$

Note that the probabilities $p_{(i,j)}(t)$ fully determine the dynamics of the stochastic process $(\mathbb{B}(t),\mathbb{D}(t))_{t\geq 0}$ for the initial conditions $(\mathbb{B}(0),\mathbb{D}(0)) = (1,0)$. The integrals in (4.25) and (4.26) can be approximated making use of the fast Fourier transform method, as discussed in Antal & Krapivsky (2010).

Probability and expected time to extinction

The aim of this section is to derive the probability of extinction of the total cell population and the expected time to extinction of the cells in the division pool. Indeed, cells in the death pool will eventually die and therefore do not contribute to the probability of population extinction in the long-term. To this end, define

$$\begin{aligned} p_B^{(b_0)} &= \lim_{t\to+\infty} \mathbb{P}\big((\mathbb{B}(t),\mathbb{D}(t)) = (0,0)|(\mathbb{B}(0),\mathbb{D}(0)) = (b_0,0)\big), \\ p_D^{(d_0)} &= \lim_{t\to+\infty} \mathbb{P}\big((\mathbb{B}(t),\mathbb{D}(t)) = (0,0)|(\mathbb{B}(0),\mathbb{D}(0)) = (0,d_0)\big). \end{aligned} \tag{4.27}$$

If cells are independent of each other, $p_B^{(b_0)} = \left(p_B^{(1)}\right)^{b_0}$ and $p_D^{(d_0)} = \left(p_D^{(1)}\right)^{d_0}$. We make use of the following notation: $p_B = p_B^{(1)}$ and $p_D = p_D^{(1)}$. A first-step argument leads to

$$p_B = p_1 p_B^2 + p_2 p_D^2 + (1-p_1-p_2)p_D p_B.$$

Obviously $p_D = 1$ as cells in the death pool can only die. Thus, it follows

$$p_B = \begin{cases} 1 & \text{if } p_1 \leq p_2, \\ \dfrac{p_2}{p_1} & \text{if } p_1 > p_2, \end{cases} \tag{4.28}$$

in agreement with the survival probabilities depicted in Figure 4.4 and the well known results of classic birth-and-death process (see *e.g.*, Refs. Allen (2010); Pinsky & Karlin (2010)). Indeed, the process $(\mathbb{B}(t))_{t\geq 0}$ is a linear birth-and-death process with birth rate $\lambda_i = i\lambda p_1$ and death rate $\mu_i = i\lambda p_2$. Furthermore, the condition of extinction $p_1 < p_2$ agrees with the results of the study of the long-term behaviour of the population in the deterministic case illustrated in Figure 4.2. To derive the expected time to extinction, let $T_{a,b}$, $a, b \in \mathbb{N}_0$, $a < b$, be the random variable for the time it takes for the population of cells in the division pool to go from size a to size b, that is

$$T_{a,b} = \inf\{t \geq 0 : B(t) = b \mid B(0) = a\}.$$

The expected time to extinction beginning from m cells in the division pool is defined as $\tau_m := \mathbb{E}[T_{m,0}]$, $m \in \mathbb{N}$. Clearly $\tau_0 = 0$ from its definition. From Theorem 6.3 of Allen (2010),

$$\begin{aligned} \tau_1 &= \frac{1}{\lambda p_2} + \sum_{i=2}^{+\infty} \frac{\lambda_1\lambda_2\ldots\lambda_{i-1}}{\mu_1\mu_2\ldots\mu_i} = \sum_{i=1}^{+\infty} \frac{(i-1)!(\lambda p_1)^{i-1}}{i!(\lambda p_2)^i} \\ &= \frac{1}{\lambda p_1}\sum_{i=1}^{+\infty}\frac{1}{i}\left(\frac{p_1}{p_2}\right)^i = -\frac{1}{\lambda p_1}\log\left(1-\frac{p_1}{p_2}\right). \end{aligned} \tag{4.29}$$

Regarding the expected time to extinction starting with m cells in the division pool, τ_m, from the same Theorem 6.3 of Allen (2010), it follows that

$$\begin{aligned} \tau_m &= \tau_1 + \sum_{s=1}^{m-1}\left(\frac{\mu_1\ldots\mu_s}{\lambda_1\ldots\lambda_s}\sum_{i=s+1}^{+\infty}\frac{\lambda_1\ldots\lambda_{i-1}}{\mu_1\ldots\mu_i}\right) \\ &= \tau_1 + \sum_{s=1}^{m-1}\left(\frac{s!(\lambda p_2)^s}{s!(\lambda p_1)^s}\sum_{i=s+1}^{+\infty}\frac{(i-1)!(\lambda p_1)^{i-1}}{i!(\lambda p_2)^i}\right) \\ &= \tau_1 + \frac{1}{\lambda p_1}\sum_{s=1}^{m-1}\left(\frac{p_2}{p_1}\right)^s\left[-\log\left(1-\frac{p_1}{p_2}\right) - \sum_{i=1}^{s}\frac{(\frac{p_1}{p_2})^i}{i}\right]. \end{aligned} \tag{4.30}$$

For instance, if $m = 2$, the expected time to extinction is

$$\tau_2 = -\frac{1}{\lambda p_1^2}\left[p_1\log\left(1-\frac{p_1}{p_2}\right) + p_2\log\left(1-\frac{p_1}{p_2}\right) + p_1\right].$$

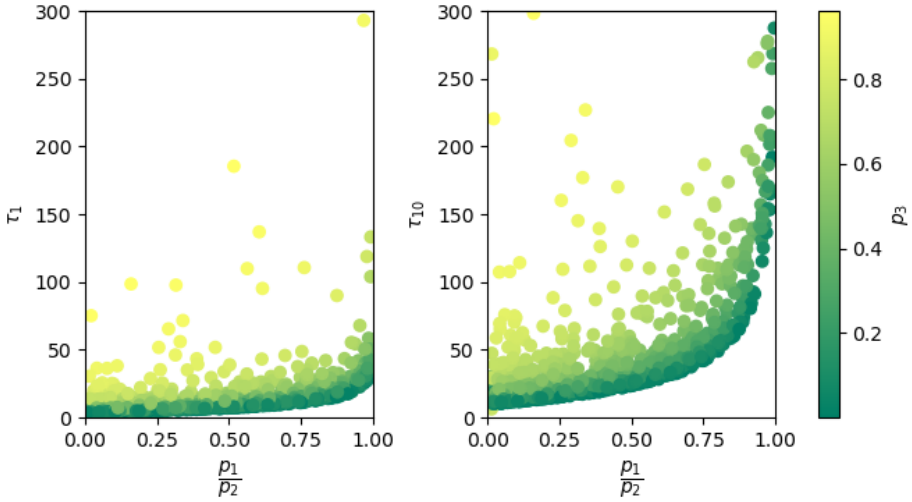

Figure 4.5: How the ratio $\frac{p_1}{p_2}$ affects the expected times to extinction τ_1 derived in equation (4.29) and τ_{10} computed from equation (4.30) with $m = 10$ and $\lambda = 0.3$ with units inverse of time, t^{-1}.

Figure 4.5 shows how the expected times to extinction τ_1 and τ_{10} are affected by the ratio $\frac{p_1}{p_2}$. As derived in equation (4.28), population extinction occurs when $p_1 \leq p_2$. Moreover, in our model $0 \leq p_1 + p_2 \leq 1$. Thus, the values of p_1 and p_2 must be sampled from the region where $0 \leq p_1 \leq p_2 \leq 1$ and $0 \leq p_1 + p_2 \leq 1$. We adopt the approach illustrated by Goggans *et al.* (2014) to sample uniformly in such region. In Figure 4.5, it is interesting to notice that both τ_1 and τ_{10} increase as the ratio $\frac{p_1}{p_2}$ grows, and higher values of p_3 generally imply longer expected time to extinction. This is explained by the role that p_3 plays on cellular dynamics, which is studied in detail in Section 4.2. I underline the fact that τ_m, with $m \geq 1$, represents the expected time to extinction of the cells in the division pool, which will imply the extinction of the total population of cells since the fate of the cells in the death pool is death. However, at time τ_m, some cells may still populate the death pool.

Figure 4.6 shows the distribution of the time to extinction starting with 10 cells in the division pool for different values of the ratio $\frac{p_1}{p_2}$, which varies across rows:

in the first row, $\frac{p_1}{p_2} = 0.25$, in the second $\frac{p_1}{p_2} = 0.5$ and in the third $\frac{p_1}{p_2} = 0.75$. The vertical line represents the expected time to extinction τ_{10}. In the first row, $p_2 = 4p_1$. Since $p_1 + p_2 \leq 1$, the maximum value that p_1 can take is $p_{1,\max} = 1/5$ (right plot). In the left plot, $p_1 = p_{1,\max}/4$ and in the central one $p_1 = p_{1,\max}/2$. The choice of p_1 in the second and third rows follows the same logic. Thus, the value of p_3 decreases across columns, reaching $p_3 = 0$ on the right column. We observe that the time to extinction becomes shorter as p_3 decreases, according to the results in Figure 4.5. Interestingly, a larger value of the ratio $\frac{p_1}{p_2}$ implies a longer time to extinction. Indeed, for the same value of p_1, when $\frac{p_1}{p_2}$ increases, p_2 becomes smaller, while p_3 grows.

4.1.2 Erlang times to division and death

In this section, the multi-stage model of the cell cycle described in detail in Chapter 3 is adopted for the division process, and extended also to death events. As in Yates *et al.* (2017) and Belluccini *et al.* (2022), the cell cycle is divided into N stages, which a cell has to sequentially visit before dividing. The time to progress from stage j to the next one, $j + 1$, is an exponentially distributed random variable with mean $\frac{1}{\lambda_j}$. I will refer to these rates, λ_j, $j = 1, \ldots, N$, as *birth* rates. Thus, the division time follows a continuous phase-type distribution. A particular choice of phase-type distribution is the Erlang (N, λ), which is a concatenation of N identically distributed and independent exponential steps, where all birth rates are equal: $\lambda_j = \lambda, j = 1, \ldots, N$. Therefore, $T_{div} \sim G_{div}(\cdot) \equiv Erlang(N, \lambda)$ and the expected time to division is $\frac{N}{\lambda}$. In a similar manner, the death process is comprised of K stages, which the cell has to visit sequentially before dying. The time to progress from stage i to the next one, $i+1$, is an exponentially distributed random variable with mean $\frac{1}{\mu_i}$. These rates, μ_i, $i = 1, \ldots, K$, will be called *death* rates. If the death rate is identical across stages, *i.e.*, $\mu_i = \mu, i = 1, \ldots, K$, a cell's time to death is a random variable with an Erlang distribution of parameters (K, μ). Thus, $T_{death} \sim G_{death}(\cdot) \equiv Erlang(K, \mu)$ and the expected time to death is $\frac{K}{\mu}$.

We note that the Erlang distribution can be thought of as a sum of exponential distributions, and consequently the Markovian property is maintained.

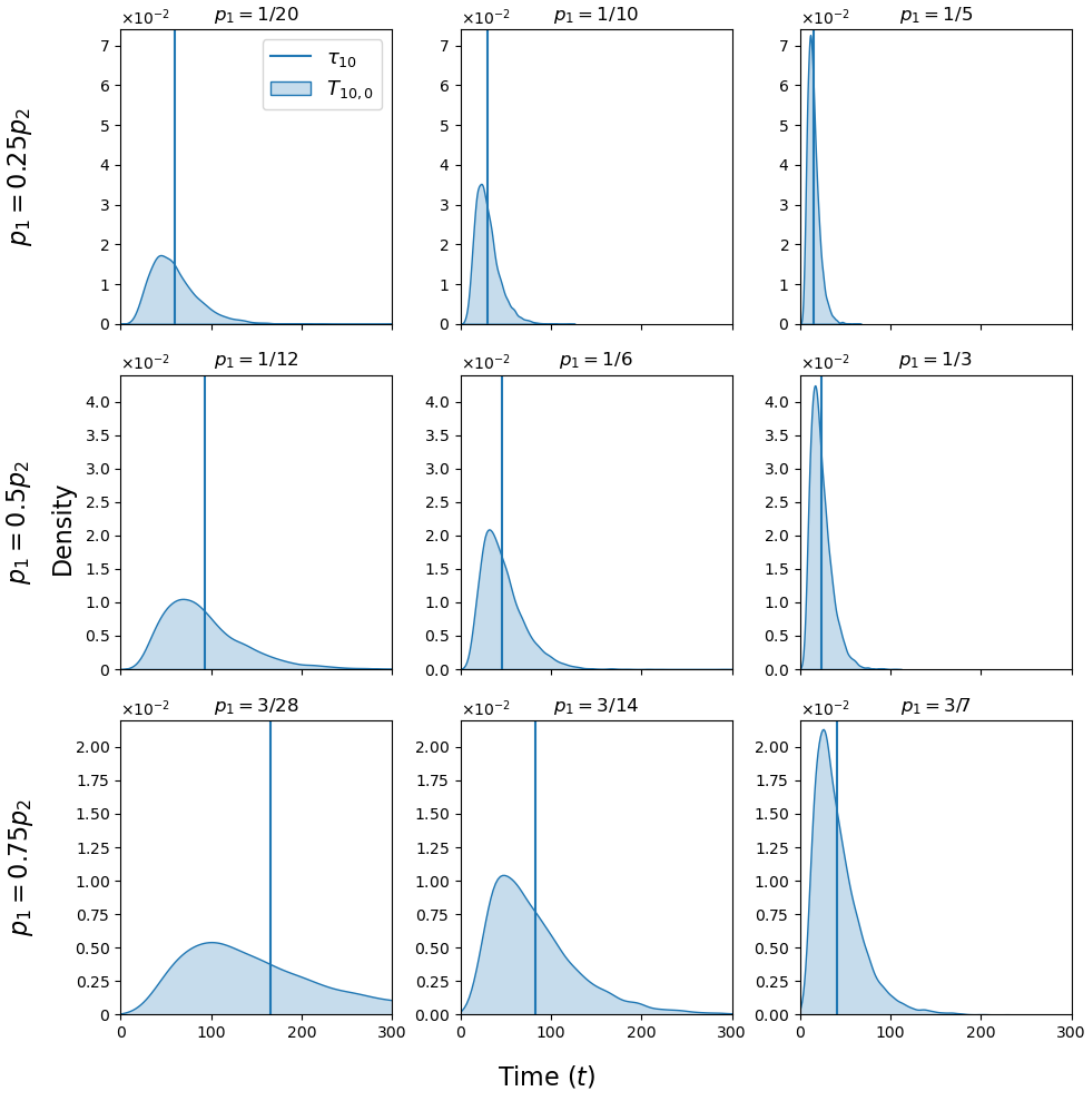

Figure 4.6: Distribution of the time to extinction $T_{10,0}$ for different values of the ratio $\frac{p_1}{p_2}$, which varies across rows: in the first row, $\frac{p_1}{p_2} = 0.25$, in the second $\frac{p_1}{p_2} = 0.5$ and in the third $\frac{p_1}{p_2} = 0.75$. The birth rate λ is 0.3 with units inverse of time, t^{-1}. The probability densities are obtained from 10^4 simulations of a birth-and-death process with birth rate λp_1 and death rate λp_2 realised with the Gillespie algorithm (Algorithm 1).

We aim to study the evolution through time of the mean number of cells in each pool. To this end, the following random variables are defined:

- $\mathbb{B}_j(t)$ to count the number of cells at stage j of the division process at time t, $j = 1, \ldots, N$.

- $\mathbb{D}_i(t)$ to count the number of cells at stage i of the death process at time t, $i = 1, \ldots, K$.

Thus, the resulting mathematical process is a multi-dimensional Markov chain $(\mathbb{B}_1(t), \ldots, \mathbb{B}_N(t), \mathbb{D}_1(t), \ldots, \mathbb{D}_K(t))_{t\geq 0}$ with space state $\mathbb{N}_0^N \times \mathbb{N}_0^K$, or a 2-type branching process with Erlang inter-event times. To describe the state where the process is at time t, a tuple of dimension $N+K$ is needed to count the number of cells in each stage of the division and death processes.
One notes that, at time t, the total number of cells in the division pool is $\sum_{j=1}^{N} \mathbb{B}_j(t)$, whereas in the death pool there are $\sum_{i=1}^{K} \mathbb{D}_i(t)$ cells. Consequently, the total population size at time t is given by $\sum_{j=1}^{N} \mathbb{B}_j(t) + \sum_{i=1}^{K} \mathbb{D}_i(t)$.

Mean number of cells in each pool

Denote by $B_j(t)$, $j = 1, \ldots, N$, and $D_i(t)$, $i = 1, \ldots, K$, the expected values of the random variables $\mathbb{B}_j(t), j = 1, \ldots, N$, and $\mathbb{D}_i(t), i = 1, \ldots, K$, respectively; that is $B_j(t) = \mathbb{E}[\mathbb{B}_j(t)]$ and $D_i(t) = \mathbb{E}[\mathbb{D}_i(t)]$. The total expected number of cells in the birth stages at time t is $B(t) = \sum_{j=1}^{N} B_j(t)$, whereas the total expected number of cells in the death stages at time t is given by $D(t) = \sum_{i=1}^{K} D_i(t)$. Thus, the total mean number of cells in the population at time t, $P(t)$, is computed as $P(t) = B(t) + D(t)$. To understand the dynamics of the mean number of cells in each stage, consider what can happen in a short time interval Δt, starting with one cell that proceeds to divide. One has

$$B_j(t + \Delta t) = B_j(t) + \Delta t \left(\lambda B_{j-1}(t) - \lambda B_j(t)\right), \ j = 2, \ldots, N.$$

Therefore, the evolution through time of $B_j(t)$ is given by

$$\frac{\mathrm{d}B_j(t)}{\mathrm{d}t} = \lambda B_{j-1}(t) - \lambda B_j(t), \ j = 2, \ldots, N, \tag{4.31}$$

where the first term accounts for the event of a cell arriving at stage j from stage $j-1$, and the second one refers to the possibility of a cell moving from stage j to $j+1$. Let us now consider the first stage of the division process, $j=1$. In a short time interval Δt, three different events can occur which affect the mean number of cells in division stage 1 (that is, $B_1(t)$): two new cells arrive into division stage 1 when a cell divides and the offsprings join the division pool, only one cell lands into division stage 1 when a division occurs and the siblings select different fates, or a cell in division stage 1 proceeds to stage 2. In mathematical terms,

$$B_1(t+\Delta t) = B_1(t) + \Delta t \left(2\lambda p_1 B_N(t) + \lambda(1-p_1-p_2)B_N(t) - \lambda B_1(t)\right).$$

Simplifying, one finds that the evolution of $B_1(t)$ over time is given by

$$\frac{\mathrm{d}B_1(t)}{\mathrm{d}t} = \lambda(1+\rho)B_N(t) - \lambda B_1(t), \tag{4.32}$$

where $\rho = p_1 - p_2$. Let us now determine the dynamics of the cells in the death pool, considering first a cell in stage i, $i=2,\ldots,K$, of the death process. In a short time interval, one has

$$D_i(t+\Delta t) = D_i(t) + \Delta t \left(\mu D_{i-1}(t) - \mu D_i(t)\right), \quad i=2,\ldots,K.$$

Therefore, the expected number of cells in stage i of the death process, $D_i(t)$, obeys the differential equation

$$\frac{\mathrm{d}D_i(t)}{\mathrm{d}t} = \mu D_{i-1}(t) - \mu D_i(t), \quad i=2,\ldots,K. \tag{4.33}$$

The last stage that remains to be analysed is the first one of the death branch. Its dynamics is affected by three distinct events: a cell in the Nth stage of the division process divides and its daughters have different fates, a cell divides and its offsprings enter the death pool, and a cell in the death stage 1 proceeds towards death stage 2. This means

$$D_1(t+\Delta t) = D_1(t) + \Delta t \left(2\lambda p_2 B_N(t) + \lambda(1-p_1-p_2)B_N(t) - \mu D_1(t)\right),$$

which leads to the differential equation

$$\frac{\mathrm{d}D_1(t)}{\mathrm{d}t} = \lambda(1-\rho)B_N(t) - \mu D_1(t). \tag{4.34}$$

The set of equations (4.31), (4.32), (4.33) and (4.34) fully describes the cellular dynamics in our model. To obtain their analytical solutions, I first focus on equations (4.31) and (4.32) that describe the division process as they do not depend on the death pool dynamics. The steps illustrated in Yates *et al.* (2017) and Chapter 3 (Belluccini *et al.*, 2022) are adapted here. The core idea is to rewrite equations (4.31) and 4.32 in terms of the new variables

$$X_j(t) = B_j(t)e^{\lambda t}, \quad j = 1, \dots, N.$$

Therefore, the new set of equations

$$\frac{\mathrm{d}X_j(t)}{\mathrm{d}t} = \begin{cases} (1+\rho)\lambda X_N(t), & \text{if } j = 1, \\ \lambda X_{j-1}(t), & \text{if } j = 2, \dots, N, \end{cases}$$

is obtained, from which the equation below follows

$$\frac{\mathrm{d}^N X_N(t)}{\mathrm{d}t^N} = (1+\rho)\lambda^N X_N(t), \tag{4.35}$$

together with a set of ODEs that relate $X_j(t)$ to the derivative of $X_N(t)$ with respect to time

$$X_j(t) = \left(\frac{1}{\lambda}\right)^{N-j} \frac{\mathrm{d}^{N-j} X_N}{\mathrm{d}t^{N-j}}, \quad j = 1, \dots, N-1. \tag{4.36}$$

Equation (4.35) is an N^{th} order homogeneous differential equation; its associated characteristic polynomial is

$$P(x) = x^N - (1+\rho)\lambda^N,$$

whose roots in $\mathbb{C}$ are given by

$$x_k = (1+\rho)^{\frac{1}{N}}\lambda \left(\cos\left(\frac{2k\pi}{N}\right) + i \ \sin\left(\frac{2k\pi}{N}\right)\right), \quad k = 0, \dots, N-1,$$

which can be written in exponential form as

$$x_k = (1+\rho)^{\frac{1}{N}}\lambda e^{\frac{2k\pi}{N}i}, \quad k = 0, \dots, N-1.$$

Hence, the solution of (4.35) is given by

$$X_N(t) = \sum_{k=0}^{N-1} a_k e^{x_k t} = \sum_{k=0}^{N-1} a_k e^{(1+\rho)^{\frac{1}{N}}\lambda z^k t},$$

where $z = e^{\frac{2\pi i}{N}}$ is the first Nth root of unity and a_k are yet undetermined constants. In order to compute a_k, consider the initial conditions $B_1(0) = b_0$, $B_k(0) = 0$ for $k = 2, \ldots, N$, and $D_i(0) = 0$, for $i = 1, \ldots, K$, representing b_0 cells (for some $b_0 \geq 1$) in the first division stage and no cells in all the other stages. Given the identity in equation (4.36), $X_N(t)$ is differentiated with respect to time to obtain the analytical expression of $X_j(t)$, $j = 1, \ldots, N$, as

$$\begin{aligned} X_j(t) &= \sum_{k=0}^{N-1} a_k \left((1+\rho)^{\frac{1}{N}} z^k \right)^{N-j} e^{(1+\rho)^{\frac{1}{N}} \lambda z^k t} \\ &= (1+\rho)^{1-\frac{j}{N}} \sum_{k=0}^{N-1} a_k z^{-kj} e^{(1+\rho)^{\frac{1}{N}} \lambda z^k t}, \end{aligned} \tag{4.37}$$

since $z^{kN} = 1$ for all $k = 0, \ldots, N-1$. It can be proven by substitution that the constants a_k are given by

$$a_k = \frac{b_0}{(1+\rho)N} (1+\rho)^{\frac{1}{N}} z^k. \tag{4.38}$$

Indeed, for $j = 1$ one obtains

$$X_1(0) = (1+\rho)^{1-\frac{1}{N}} \sum_{k=0}^{N-1} \frac{b_0}{(1+\rho)N} (1+\rho)^{\frac{1}{N}} z^k z^{-k} = b_0,$$

and if $j = 2, \ldots, N$

$$\begin{aligned} X_j(0) &= (1+\rho)^{1-\frac{j}{N}} \sum_{k=0}^{N-1} \frac{b_0}{(1+\rho)N} (1+\rho)^{\frac{1}{N}} z^k z^{-jk} \\ &= \frac{b_0}{N} (1+\rho)^{\frac{1-j}{N}} \sum_{k=0}^{N-1} z^{k(1-j)}. \end{aligned}$$

To prove that $X_j(0) = 0$, the summation $\sum_{k=0}^{N-1} z^{k(1-j)}$ is considered, observing that the sum of the Nth roots of unity is equal to zero. Indeed, from $z^N = 1$ one obtains

$$0 = z^N - 1 = (z-1)(z^{N-1} + z^{N-2} + \cdots + z + 1) = (z-1) \sum_{k=0}^{N-1} z^k.$$

Since $z \neq 1$, it follows $\sum_{k=0}^{N-1} z^k = 0$. On the other hand $z^{N(1-j)} = 1$ for all $j = 2, \ldots, N$, so that one can conclude $\sum_{k=0}^{N-1} z^{k(1-j)} = 0$, and therefore $X_j(0) = 0$.

Replacing the expression of the constants (4.38) in (4.37) and going back to the original variables $B_j(t)$, the solution of the equations (4.31) and (4.32) can be rewritten as

$$B_j(t) = \frac{(1+\rho)^{\frac{1-j}{N}} b_0}{N} \sum_{k=0}^{N-1} z^{(1-j)k} e^{\lambda t\left((1+\rho)^{\frac{1}{N}} z^k - 1\right)}, \quad j = 1, \ldots, N. \tag{4.39}$$

Note that, if $N = 1$, *i.e.*, a cell's time to division is exponentially distributed, equation (4.39) agrees with the result derived in equation (4.1).
Equations (4.33) and (4.34), that describe the dynamics of cells whose fate is death, remain to be solved. To this end, firstly equation (4.34) will be solved making use of an integrating factor, and then one will proceed with the other equations (4.33) from $i = 2$ to $i = K$ adopting the same technique. This is due to the fact that the time evolution of $D_i(t)$ depends on $D_{i-1}(t)$, $i = 2, \ldots, K$. Multiplying (4.34) by the integrating factor $e^{\mu t}$ and rearranging the order of the terms, one gets

$$\frac{\mathrm{d}(D_1(t)e^{\mu t})}{\mathrm{d}t} = \lambda(1-\rho)B_N(t)e^{\mu t}. \tag{4.40}$$

Replacing the expression of $B_N(t)$ derived in (4.40) in the differential equation (4.40), and integrating the result with respect to time, it follows

$$D_1(t) = \frac{\lambda(1-\rho)(1+\rho)^{\frac{1}{N}-1} b_0}{N} \sum_{k=0}^{N-1} \frac{z^k e^{\lambda t\left((1+\rho)^{\frac{1}{N}} z^k - 1\right)}}{\lambda(1+\rho)^{\frac{1}{N}} z^k - \lambda + \mu} + d_1 e^{-\mu t}, \tag{4.41}$$

where d_1 is an integration constant to be determined. In order to compute d_1, one makes use of the initial condition $D_1(0) = 0$. Thus, d_1 is given by

$$d_1 = -\frac{\lambda(1-\rho)(1+\rho)^{\frac{1}{N}-1} b_0}{N} \sum_{k=0}^{N-1} \frac{z^k}{\lambda(1+\rho)^{\frac{1}{N}} z^k - \lambda + \mu}.$$

Replacing the value of d_1 in (4.41), $D_1(t)$ is given by

$$D_1(t) = \frac{\lambda(1-\rho)(1+\rho)^{\frac{1}{N}-1} b_0}{N} \sum_{k=0}^{N-1} z^k \frac{e^{\lambda t\left((1+\rho)^{\frac{1}{N}} z^k - 1\right)} - e^{-\mu t}}{\lambda(1+\rho)^{\frac{1}{N}} z^k - \lambda + \mu}.$$

Consider the subsequent stage of the death process, $D_2(t)$. It obeys the differential equation

$$\frac{\mathrm{d}D_2(t)}{\mathrm{d}t} = \mu D_1(t) - \mu D_2(t), \tag{4.42}$$

with initial condition $D_2(t) = 0$. The same approach illustrated for $D_1(t)$ is adopted here by multiplying the equation above by the integrating factor $e^{\mu t}$. Then, the expression of $D_1(t)$ is replaced in (4.42) and the equation is integrated with respect to time t. One obtains

$$D_2(t) = \frac{\lambda\mu(1-\rho)(1+\rho)^{\frac{1}{N}-1}b_0}{N}\sum_{k=0}^{N-1}\frac{z^k}{q_k}\left(\frac{e^{\lambda t\left((1+\rho)^{\frac{1}{N}}z^k-1\right)}}{q_k} - te^{-\mu t}\right) + d_2e^{-\mu t}, \tag{4.43}$$

where $q_k = \lambda(1+\rho)^{\frac{1}{N}}z^k - \lambda + \mu$. The constant d_2 is found making use of the initial condition $D_2(0) = 0$, and its expression is replaced in (4.43). This leads to the expected number of cells in the second stage of the death pool $D_2(t)$, *i.e.*,

$$D_2(t) = \frac{\lambda\mu(1-\rho)(1+\rho)^{\frac{1}{N}-1}b_0}{N}\sum_{k=0}^{N-1}\frac{z^k}{q_k}\left(\frac{e^{\lambda t\left((1+\rho)^{\frac{1}{N}}z^k-1\right)} - e^{-\mu t}}{q_k} - te^{-\mu t}\right). \tag{4.44}$$

Repeating the same procedure for D_i, $i = 3, \ldots, K$, the general analytical solutions of (4.33) are obtained as

$$D_i(t) = \frac{\lambda\mu^{i-1}(1-\rho)(1+\rho)^{\frac{1}{N}-1}b_0}{N}\sum_{k=0}^{N-1}z^k\left(\frac{e^{\lambda t\left((1+\rho)^{\frac{1}{N}}z^k-1\right)} - e^{-\mu t}}{q_k^i} - \sum_{l=1}^{i-1}\frac{t^le^{-\mu t}}{l!q_k^{i-l}}\right), \tag{4.45}$$

where $i = 1, \ldots, K$. Note that, when $K = 1$, *i.e.*, a cell's time to death is exponentially distributed, equation (4.45) agrees with the result derived in equation (4.2). In order to verify the accuracy of equations (4.39) and (4.45), cellular dynamics is simulated making use of the Gillespie algorithm (Gillespie, 1976, 1977). The realisations are then compared to the deterministic solutions. The results agree, as shown in Figure 4.7.

Long-term behaviour

Here, the focus is on the long-term behaviour of the cell population as $t \to +\infty$, finding a condition for its extinction and growth, which one expects to depend on the probabilities p_1 and p_2 as in the exponential case.

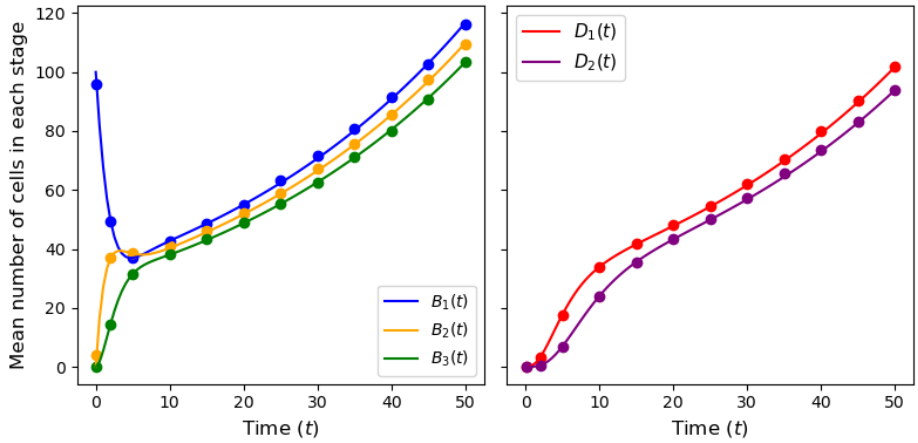

Figure 4.7: Comparison between the analytical solutions derived in (4.39) and (4.45) (solid lines) and stochastic realisations (dots) obtained using the Gillespie algorithm as mean value of 5×10^2 simulations. The initial condition represents 10^2 cells in the first stage of the division process and no cells in all the other stages. The parameters in the model are fixed as $N = 3$, $K = 2$, $p_1 = 0.5$, $p_2 = 0.3$, $p_3 = 0.2$, $\lambda = 0.4$ and $\mu = 0.3$. The birth and death rates λ and μ have units of inverse time, t^{-1}.

From the mean number of cells in stage j of the division process at time t, $B_j(t), j = 1, \ldots, N$, derived in (4.39), the expected total number of cells in the birth stages, $B(t) = \sum_{j=1}^{N} B_j(t)$, can be computed summing equation (4.39) from $j = 1$ to $j = N$, *i.e.*,

$$B(t) = \sum_{k=0}^{N-1} \frac{(1+\rho)^{\frac{1}{N}} b_0}{N} z^k e^{\lambda t\left((1+\rho)^{\frac{1}{N}} z^k - 1\right)} \sum_{j=1}^{N} (1+\rho)^{-\frac{j}{N}} z^{-jk}. \tag{4.46}$$

Let us simplify the last summation in equation (4.46). The sum of the first $N+1$ terms of a geometric series is given by $\sum_{i=0}^{N} x^i = \frac{1-x^{N+1}}{1-x}$. Hence,

$$\begin{aligned}
\sum_{j=1}^{N} \left((1+\rho)^{-\frac{1}{N}} z^{-k}\right)^j &= \frac{1 - \left((1+\rho)^{-\frac{1}{N}} z^{-k}\right)^{N+1}}{1 - (1+\rho)^{-\frac{1}{N}} z^{-k}} - 1 \\
&= \frac{-(1+\rho)^{-\frac{1}{N}-1} z^{-k} + (1+\rho)^{-\frac{1}{N}} z^{-k}}{(1+\rho)^{\frac{1}{N}} z^k - 1} (1+\rho)^{\frac{1}{N}} z^k \\
&= \frac{\rho}{(1+\rho)\left((1+\rho)^{\frac{1}{N}} z^k - 1\right)}.
\end{aligned}$$

Therefore, the expected total number of cells in the division pool is given by

$$B(t) = \frac{(1+\rho)^{\frac{1}{N}} b_0 \rho}{(1+\rho) N} \sum_{k=0}^{N-1} \frac{z^k}{(1+\rho)^{\frac{1}{N}} z^k - 1} e^{\lambda t\left((1+\rho)^{\frac{1}{N}} z^k - 1\right)}. \tag{4.47}$$

Moreover, from (4.31) and (4.32) the evolution through time of $B(t)$ can be easily derived as

$$\frac{\mathrm{d}B(t)}{\mathrm{d}t} = \lambda \rho B_N(t). \tag{4.48}$$

In order to study the limiting behaviour of the population size as $t \to +\infty$, one observes that in the analytical expression of $B_j(t)$ given by equation (4.39), the dominant term is always the first, which corresponds to $k = 0$. The other terms related to $k \geq 1$ are analysed in order to justify this statement. In the exponent of the second term of the summation in (4.39), which means $k = 1$, the coefficient of t has its real part equal to

$$\mathrm{Re}\left(\left((1+\rho)^{\frac{1}{N}} z - 1\right)\lambda\right) = \left((1+\rho)^{\frac{1}{N}} \cos\left(\frac{2\pi}{N}\right) - 1\right)\lambda. \tag{4.49}$$

If $\cos\left(\frac{2\pi}{N}\right) < 0$, then the quantity in (4.49) is negative; otherwise, since

$$1 + \rho \leq 2,$$

and $f(y) = y^{1/N}$ is an increasing function,

$$(1+\rho)^{\frac{1}{N}} \cos\left(\frac{2\pi}{N}\right) - 1 \leq 2^{\frac{1}{N}} \cos\left(\frac{2\pi}{N}\right) - 1,$$

where the right hand side is negative for any integer N in the interval $[2, 28]$ (Yates *et al.*, 2017). In practice, one would not consider a number of stages in the division pool larger than $N = 28$, which is the case for all the numerical results presented in Chapter 3. Therefore, it is proved that the second term in the summation of (4.39) decays as $t \to +\infty$. The same conclusion cannot be drawn for the rest of the terms since some exponents are positive. However, the dominant term is always the first one given that

$$\left((1+\rho)^{\frac{1}{N}} - 1\right)\lambda > \left((1+\rho)^{\frac{1}{N}} \cos\left(\frac{2\pi k}{N}\right) - 1\right)\lambda \quad \text{for } k = 2, \ldots, N-1,$$

where the term on the left is the real part of the coefficient of t when $k = 0$ and the right hand side corresponds to the same quantity for all the other values of k, but $k = 1$. Hence, as $t \to +\infty$, one has

$$\lim_{t\to+\infty} B_j(t) = \lim_{t\to+\infty} \frac{(1+\rho)^{\frac{1-j}{N}} b_0}{N} e^{\left((1+\rho)^{\frac{1}{N}} - 1\right)\lambda t}, \quad j = 1, \ldots, N. \tag{4.50}$$

Equation (4.50) gives an approximation of the expected number of cells in each birth stage $B_j(t)$, $j = 1, \ldots, N$ for large values of t. Using again the well known sum of the first $N + 1$ terms of a geometric series, it follows that

$$\lim_{t\to+\infty} B(t) = \lim_{t\to+\infty} \frac{(1+\rho)^{\frac{1}{N}-1} b_0 \rho}{N\left((1+\rho)^{\frac{1}{N}} - 1\right)} e^{\left((1+\rho)^{\frac{1}{N}} - 1\right)\lambda t}, \tag{4.51}$$

which is equal to 0 when $(1+\rho)^{\frac{1}{N}} < 1$, *i.e.*, if $p_1 < p_2$, and goes to $+\infty$ when $p_1 > p_2$, as the intuition would suggest.

Note that we studied the late time behaviour of the division pool as cells in the death pool will eventually die and therefore do not contribute to the probability of population extinction.

Finally, one can consider the special case when $p_1 = p_2$. The differential equations (4.31), (4.32), (4.33) and (4.34) that define the cellular dynamics simplify as

$$\begin{aligned}
\frac{\mathrm{d}B_1(t)}{\mathrm{d}t} &= \lambda B_N(t) - \lambda B_1(t),\\
\frac{\mathrm{d}B_j(t)}{\mathrm{d}t} &= \lambda B_{j-1}(t) - \lambda B_j(t),\ j = 2,\dots,N,\\
\frac{\mathrm{d}D_1(t)}{\mathrm{d}t} &= \lambda B_N(t) - \mu D_1(t),\\
\frac{\mathrm{d}D_i(t)}{\mathrm{d}t} &= \mu D_{i-1}(t) - \mu D_i(t),\ i = 2,\dots,K.
\end{aligned}$$

Their solutions are given by

$$B_j(t) = \frac{b_0}{N}\sum_{k=0}^{N-1} z^{(1-j)k} e^{\lambda t\left(z^k-1\right)}, \quad j = 1,\dots,N, \tag{4.52}$$

and

$$D_i(t) = \frac{\lambda\mu^{i-1}b_0}{N}\sum_{k=0}^{N-1} z^k \left(\frac{e^{\lambda t\left(z^k-1\right)} - e^{-\mu t}}{\left(\lambda z^k - \lambda + \mu\right)^i} - \sum_{l=1}^{i-1}\frac{t^l e^{-\mu t}}{l!\left(\lambda z^k - \lambda + \mu\right)^{i-l}}\right),\ i = 1,\dots,K.$$

Repeating the same steps shown for the cases $p_1 < p_2$ and $p_1 > p_2$, the long-term behaviour of $B_j(t)$ can be determined also when $p_1 = p_2$. As $t \to +\infty$, the leading term in the summation in (4.52) is the one corresponding to $k = 0$, which means

$$\lim_{t\to+\infty} B_j(t) = \frac{b_0}{N}, \quad j = 1,\dots,N. \tag{4.53}$$

Equation (4.53) tells us that the population size of the division pool remains constant ($B_1(0) = b_0$ and $B_j(0) = 0$ if $j > 1$) and the cells in this pool are distributed homogeneously among the stages.

Similarly, as $t \to +\infty$, the leading term in the summation in equation (4.1.2) is the one corresponding to $k = 0$. Thus, one obtains

$$\lim_{t\to+\infty} D_i(t) = \lim_{t\to+\infty}\frac{\lambda\mu^{i-1}b_0}{N\mu^i}\left(1 - e^{-\mu t} - \sum_{l=1}^{i-1}\frac{t^l e^{-\mu t}}{l!\mu^{-l}}\right) = \frac{\lambda b_0}{\mu N}, \quad i = 1,\dots,K. \tag{4.54}$$

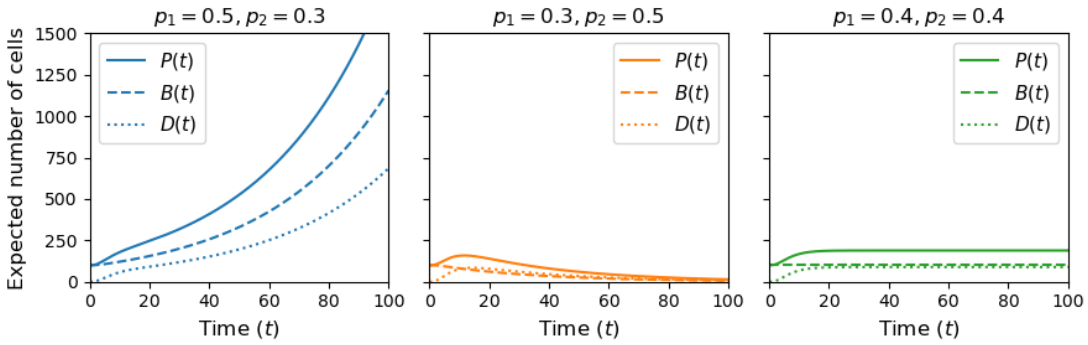

Figure 4.8: Long-term behaviour of the expected number of cells in the division stages $B(t)$ (dashed lines), the death stages $D(t)$ (dotted lines) and the whole population $P(t)$ (solid lines) when $t \to +\infty$ under the assumption of Erlang times to division and death. Three cases are distinguished: $p_1 > p_2$ (left), $p_1 < p_2$ (centre), and $p_1 = p_2$ (right). The number of stages of the birth process is $N = 3$, whereas the death branch is comprised of $K = 2$ stages. The birth and death rates are $\lambda = 0.4$ and $\mu = 0.3$, respectively, with units of inverse time, t^{-1}. The initial conditions provide 10^2 cells in the first stage of the division stage and no cells in the other stages.

Thus, if $\lambda > \mu$ cells accumulate in the death pool, where they are homogeneously distributed among the stages. Conversely, if $\mu > \lambda$ cells leave quickly the death pool.
In summary, the total number of cells in the population tends to

$$\lim_{t \to +\infty} P(t) = \left(1 + \frac{\lambda}{\mu}\frac{K}{N}\right) b_0, \tag{4.55}$$

where $\frac{\lambda}{\mu}\frac{K}{N}$ is the ratio between the expected time to death $\frac{K}{\mu}$ and the expected time to division $\frac{N}{\lambda}$. The larger this ratio is, the larger the total population size is for late times. Note that when $N = 1 = K$, the steady state in equation (4.55) agrees with the one obtained in the case of exponential times to division and death. Figure 4.8 shows the long-term behaviour of the system as $t \to +\infty$ in the three cases $p_1 < p_2$ (on the left), $p_1 > p_2$ (in the centre), $p_1 = p_2$ (on the right). These results are in agreement with the ones obtained in the exponential case.

Probability of extinction

In order to derive the probability of extinction of the population of cells, define for $j = 1, \ldots, N$ and $i = 1, \ldots, K$

$$p_{B_j}^{(b_0)} = \lim_{t\to+\infty} \mathbb{P}\big(P(t) = 0 | B_j(0) = b_0, B_l(t) = 0 \text{ if } l \neq j, D_i(t) = 0 \text{ for } i = 1, \ldots, K\big),$$
$$p_{D_i}^{(d_0)} = \lim_{t\to+\infty} \mathbb{P}\big(P(t) = 0 | D_i(0) = d_0, B_j(t) = 0 \text{ for } j = 1, \ldots, N, D_l(t) = 0 \text{ if } l \neq i\big). \tag{4.56}$$

Since cells are independent of each other, $p_{B_j}^{(b_0)} = \left(p_{B_j}^{(1)}\right)^{b_0}$ and $p_{D_i}^{(d_0)} = \left(p_{D_i}^{(1)}\right)^{d_0}$. I will denote $p_{B_j} = p_{B_j}^{(1)}$ and $p_{D_i} = p_{D_i}^{(1)}$. A first-step argument leads to

$$p_{B_N} = p_1 p_{B_1}^2 + p_2 p_{D_1}^2 + (1 - p_1 - p_2) p_{D_1} p_{B_1}.$$

Notice that $p_{B_j} = p_{B_{j+1}}, j = 1, \ldots, N-1$ and obviously $p_{D_i} = 1$ for all $i = 1, \ldots, K$ as cells in the death pool can only die. Hence, the same probability of extinction derived in the exponential case is obtained, *i.e.*,

$$p_{B_j} = \begin{cases} 1 & \text{if } p_1 \leq p_2, \\ \dfrac{p_2}{p_1} & \text{if } p_1 > p_2. \end{cases}$$

This means, as one would expect, that the consideration of an Erlang distribution for the division and death times, instead of the exponential one, only affects the timescales of the process, and not its asymptotic fate (*i.e.*, population survival versus extinction). Notice that these results are in agreement with the conditions of population growth and extinction derived in the previous section when studying the long-term behaviour of the deterministic system for $t \to +\infty$.

4.2 Sensitivity analysis

In the mathematical analysis presented in Section 4.1, I proved that the long-term behaviour of the system depends on the relationship between the parameters p_1 and p_2, regardless of the probability distribution adopted to model a cell's time to division and death. In particular, if $p_1 > p_2$ the population grows, if $p_1 < p_2$ the

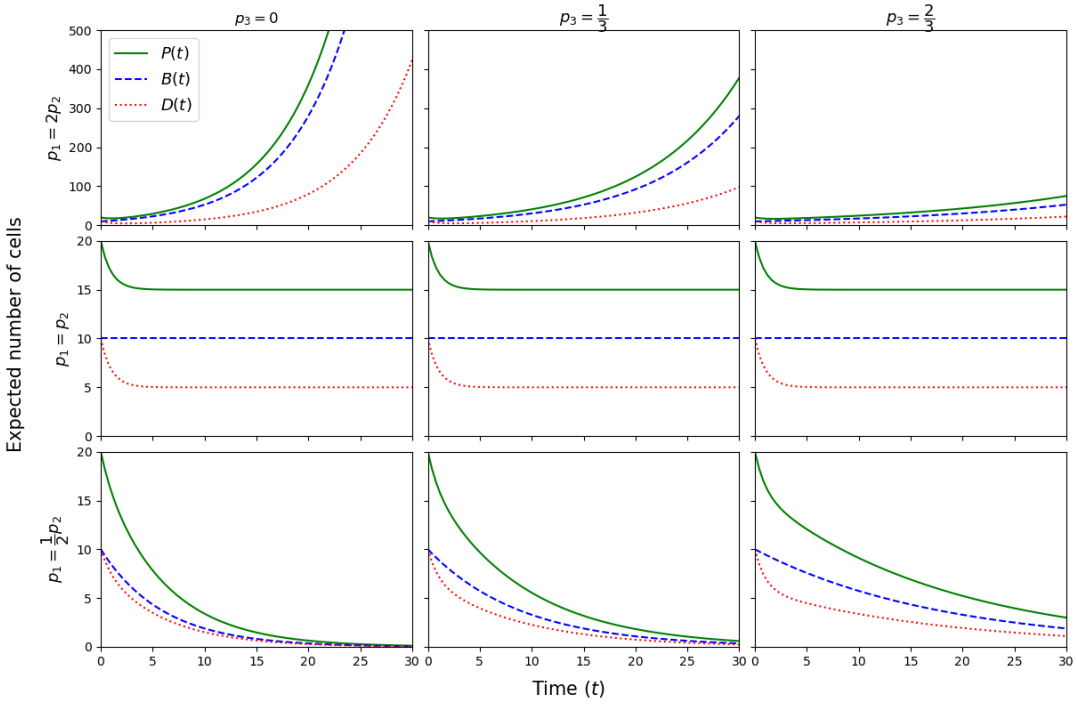

Figure 4.9: Effect of the probability $p_3 = 1 - p_1 - p_2$ on the expected number of cells over time, calculated via equations (4.1), (4.2) and (4.3). The birth and death rates are fixed as $\lambda = 0.5$ and $\mu = 1$ with units of inverse time, t^{-1}, and a cell's time to division and death is an exponential random variable. In all cases, the initial condition is $(B(0), D(0)) = (10, 10)$.

population goes extinct and if $p_1 = p_2$ the population reaches a steady state, as shown in Figures 4.2 and 4.8.

After understanding the role of p_1 and p_2, the interest is in studying how the probability $p_3 = 1-p_1-p_2$, and the birth and death rates λ and μ affect the cellular dynamics. Another aim is to analyse the impact that the type of distribution (exponential or Erlang) used to model cell's time to division and death has on population dynamics.

In Figure 4.9 the role of p_3 is explored. To this end, the death rate μ is fixed equal to 1 t^{-1}, therefore the unit of time is the average life-span of a cell in the death pool. On the other hand, the birth rate is assumed to be the half of the death rate, *i.e.*, $\lambda = 0.5\ t^{-1}$. Figure 4.9 shows the time evolution of the expected number of cells in each pool and in the whole population for different values of p_3. In particular, the probability p_3 varies as $p_3 = 0$ (left column), $p_3 = 1/3$ (central column) and $p_3 = 2/3$ (right column). At the same time, three scenarios are considered in Figure 4.9: $p_1 > p_2$ (first row), $p_1 = p_2$ (second row), $p_1 < p_2$ (third row). The ratio between p_1 and p_2 is constant for the different values of p_3. First, it is observed that higher values of p_3 lead to slower cellular dynamics. For instance, the first row of Figure 4.9 shows the case $p_1 > p_2$, which corresponds to population growth. When $p_3 = 0$, cell population increases significantly faster than in the scenario $p_3 = 2/3$. The same behaviour is observed when $p_1 < p_2$ (third row of Figure 4.9): the population requires a longer time to become extinct for increasing values of p_3. Interestingly, the value of p_3 does not affect cellular dynamics when $p_1 = p_2$. This is explained by the equations (4.1) and (4.2) of the expected number of cells in the division and death pools. Indeed, they both depend on the quantity $\rho = p_1 - p_2$, which vanishes when $p_1 = p_2$, explaining the behaviour observed in the central row of Figure 4.9. When $p_1 < p_2$, larger values of p_3 increase the population time to extinction. In summary, the probability p_3 does not determine the asymptotic behaviour of the system, although it affects the population rate of growth or time to extinction.

In Figure 4.10, we explore how the birth and death rates impact the timescales of the population dynamics. When the probabilities p_1 and p_2 are fixed, together with the number of stages N and K, and the death rate μ (left panel of Figure 4.10), the larger λ is, the faster the dynamics is. This is due to the shorter expected time to

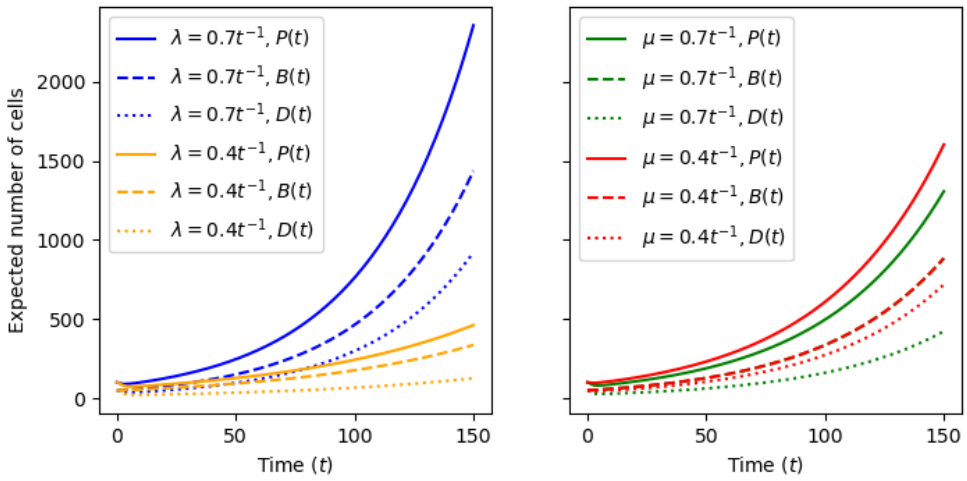

Figure 4.10: Effect of the variation of the birth and death rates λ (on the left) and μ (on the right) on cell population dynamics. On the left $\mu = 0.6$, on the right $\lambda = 0.6$ with units of inverse time t^{-1}. The probabilities p_1, p_2 and the number of stages of the birth-and-death processes are fixed as $p_1 = 0.4, p_2 = 0.3, N = 3, K = 2$.

division that corresponds to larger values of λ. When all the parameters are fixed, but the death rate μ (right panel of Figure 4.10), one notices that the number of cells in the division pool does not vary according to different values of μ (the red and green dashed curves overlap), in agreement with what one would expect from the theoretical study of the system being $B_j(t)$, $j = 1, \ldots, N$, independent of μ. Instead, for larger values of μ, one observes a smaller size of the population in the death pool, and consequently of the whole population of cells. Indeed, if μ increases, a cell's death time will become shorter, implying that cells leave the population quicker.

In Figure 4.11, we aim to understand the role that the number of stages of the division and death processes, N and K respectively, introduced in Section 4.1.2, play on the cellular dynamics. To this end, the dynamics of cells over time is simulated assuming first exponential times to division and death (which is equivalent to $N = 1 = K$). Then, $N = 10$ stages are considered for the division process while keeping $K = 1$, and vice-versa, exponential time to division and $K = 10$ stages for the death process are considered. Finally, the case $N = K = 10$ is simulated. The outcomes are compared in Figure 4.11. In order to obtain a fair comparison, the stages N and K in the division and death processes are introduced while maintaining the expected time to division $\frac{N}{\lambda}$ and death $\frac{K}{\mu}$ the same as in the exponential case (*i.e.*, when varying N or K, the rates λ and μ are varied as well so that those expected times remain the same in Figure 4.11). When $p_1 > p_2$ (left panel of Figure 4.11) and cell's time to division is exponential (green dashed-dotted line and blue dotted line), the total number of cells in the population is larger than the one predicted by the model with Erlang distributed times to division (red dashed-dotted line and orange dashed line). Indeed, while the expected times remain the same, the exponential distribution overestimates the probability of shorter division times. This is explained by the shape of the exponential probability density function compared to the Erlang one depicted in Figure 4.12, where different values of the number of stages N are considered. One notes that the shape of the Erlang probability density function becomes narrower as the number of stages N increases. Furthermore, the Erlang distribution becomes deterministic as the number of stages increases to infinity, $N \to +\infty$.

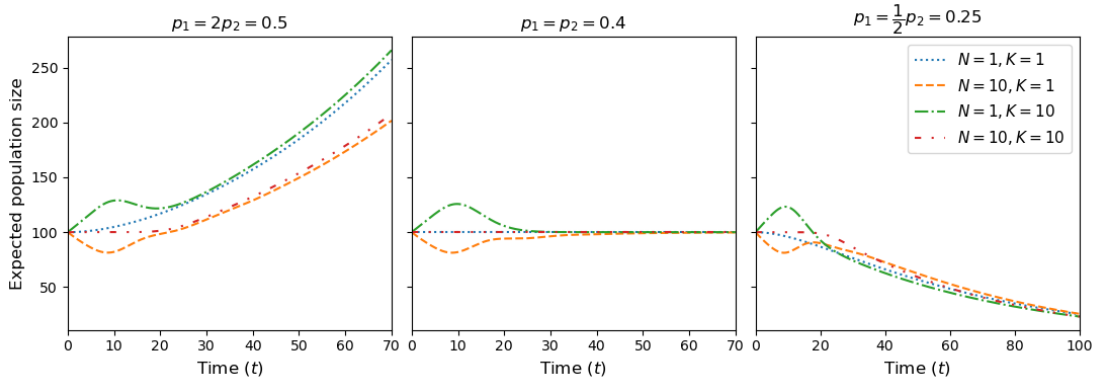

Figure 4.11: Expected number of cells in the population when considering exponential and/or Erlang times to division and death. The expected times to division and death are fixed at 15 units of time, and birth and death rates are computed given the number of stages N and K.

Similarly, for equal times to division, the case with Erlang distributed times to death predicts a larger number of cells. This is justified by the fact that the exponential distribution estimates shorter times to death. The behaviour observed in the central plot of Figure 4.11 when $p_1 = p_2$ confirms the results found in equation (4.55). In the instance of $p_1 < p_2$, the number of stages in the division and death processes does not have a significant impact on the population dynamics. The sensitivity analysis carried out in this section shows that my model separates the cell population timescales – and consequently its rate of growth – from the cellular fate probability and asymptotic behaviour, which often depend on the same parameters, as in the case of the classic birth-and-death process and the multi-stage model proposed in Chapter 3. Indeed, the long-term behaviour is determined by the relationship between the probabilities p_1 and p_2, whereas the other parameters p_3, λ, μ and the number of stages N and K in the instance of Erlang times to division and death set the population rate of growth. Table 4.1 contains a comparison of the conditions for population extinction and explosion in the instances of my model with cellular fate decision at birth, the birth-and-death process and the multi-stage model of cell proliferation and death presented in Chapter 3.

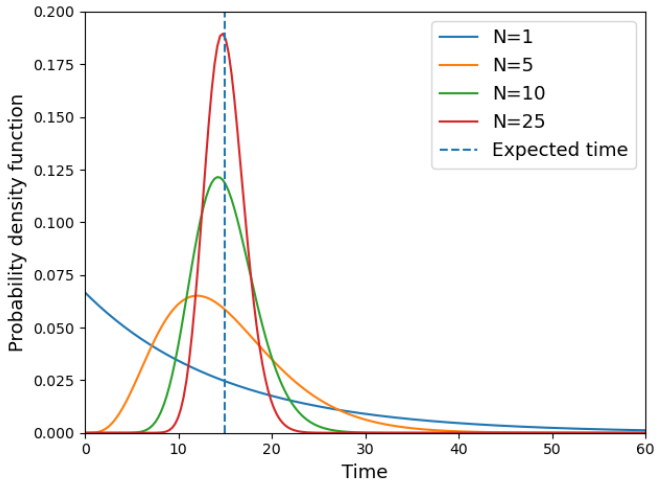

Figure 4.12: Erlang probability densities (solid lines) with expected time fixed at 15 units of time (dashed line) and different number of stages N. $N = 1$ corresponds to the exponential probability density function.

Mathematical model	Explosion	Extinction	Steady state	Reference
Fate decision at birth	$p_1 > p_2$	$p_1 < p_2$	$p_1 = p_2$	Sections 4.1.1 and 4.1.2
Multi-stage	$\mu < (2^{1/N} - 1)\lambda$	$\mu > (2^{1/N} - 1)\lambda$	$\mu = (2^{1/N} - 1)\lambda$	Belluccini *et al.* (2022)
Birth and death	$\lambda > \mu$	$\lambda < \mu$	$\lambda = \mu$	Allen (2010)

Table 4.1: Model comparison. The mathematical model with cellular fate decision at birth presented in this chapter is compared with the classic birth-and-death process and the multi-stage model of cell proliferation and death introduced in Chapter 3. Three different parameter regimes have been considered: population explosion, extinction and steady state.

4.3 Role of cellular fate correlation

In recent years, time-lapse microscopy experiments allowed to track individual cells (Hawkins *et al.*, 2009). The study of these data sets of B and T cell families showed that division and death times for siblings are correlated (Dowling *et al.*, 2014; Duffy & Hodgkin, 2012; Duffy & Subramanian, 2009; Duffy *et al.*, 2012; Hawkins *et al.*, 2009; Markham *et al.*, 2010; Wellard *et al.*, 2010), and "division destiny" is a familial characteristic (Cheon *et al.*, 2021). Hawkins *et al.* (2009) have produced a data set of CpG-stimulated naive B cells, followed for 120 hours using time-lapse microscopy. A total of 107 and 89 pedigrees were observed in two distinct experiments, Fam2 and Fam3. In Markham *et al.* (2010), the data set published in Hawkins *et al.* (2009) is further studied, and new quantitative representations of cellular fate correlation are provided. The fate of siblings (*i.e.*, two daughter cells arising from the same mother upon division) is broken down per division event (see Figure 1 of Ref. Markham *et al.* (2010)). Thus, for each generation, the fraction of pairs of siblings that both divide, both die, and have different fates is experimentally estimated, and can be compared with the theoretical probabilities p_1, p_2 and p_3 in my model. Figure 4.13 summarises this representation for Fam2 and Fam3.

These results suggest that, when a division occurs, daughter cells are more likely to either both divide or both die. This trend varies with generations. Indeed, in early generations both siblings almost always divide (green triangles), whereas after some divisions both daughters' fate is increasingly likely to be death (red triangles). It is interesting to observe that the fraction of pairs of siblings with different fates (blue triangles) always remains below 20%, reaching its maximum at generation 3. The aim here is to try to compare these experimental results with theoretical predictions. In Section 4.3.1, cell independence is assumed and it is shown that the model predictions cannot reproduce the trends of the experimental data under this assumption. Thus, Section 4.3.2 contains a first attempt to incorporate sibling fate correlation in the model through the definition of *correlation factors*.

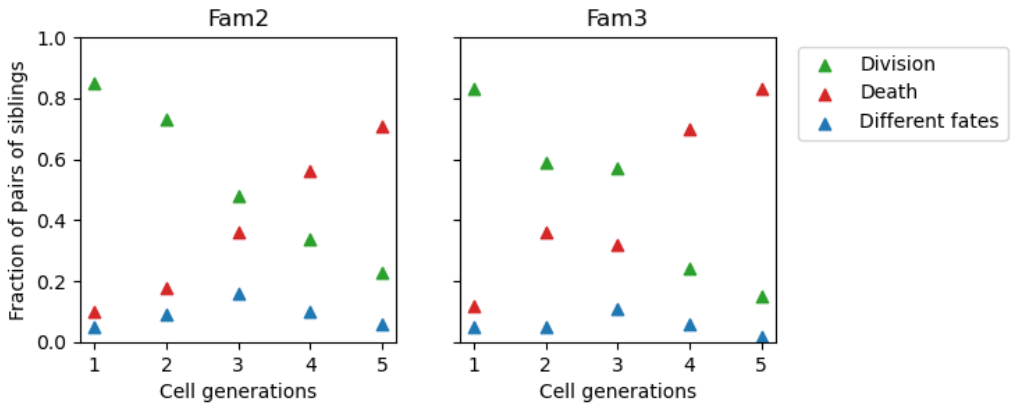

Figure 4.13: Fate of siblings is broken down per division in Markham *et al.* (2010) for experiments Fam2 (on the left) and Fam3 (on the right). A cell generation represents the number of divisions that those cells have undergone. For all division events involving cells in a given generation, the fraction of events leading to each possible pair of siblings fates (both siblings decide to divide, both decide to die or each one has a different fate) has been experimentally estimated.

4.3.1 Cells are independent of each other

In order to understand the role of cellular fate correlation when studying the expansion phase of lymphocytes populations stimulated *in vitro*, cells are assumed to be independent of each other and the theoretical model predictions are compared to the data set studied in Markham *et al.* (2010). To this end, the probabilities that determine cellular fate are assumed to be generation-dependent, as the trends of the data plotted in Figure 4.13 would suggest. When a cell in the division pool in generation $g-1$ divides, we consider that siblings belong to generation g. We denote by ε_g the probability that a cell belonging to generation g divides. As cell fate is either division or death, the probability that a cell in generation g will die is $1-\varepsilon_g$. Given the independence amongst cells in the population, the probability that a pair of siblings generated by a cell in generation $g-1$ both divide is given by $p_1^g = \varepsilon_g^2$, and, in a similar manner, the probability that both daughters' fate is death is $p_2^g = (1-\varepsilon_g)^2$. Therefore, the possibility that a pair of siblings coming from a cell in generation $g-1$ have different fates is quantified by the probability

$p_3^g = 1 - p_1^g - p_2^g = 2\varepsilon_g(1-\varepsilon_g)$. One can directly estimate $p_1^g, g = 1, \ldots, 5$, from the data set shown in Figure 4.13 (by setting p_1^g equal to the values given by the green triangles). Then, the probability ε_g is derived as $\varepsilon_g = \sqrt{p_1^g}$, and thus, p_2^g and p_3^g are computed under the assumption of cell independence as

$$p_2^g = \left(1 - \sqrt{p_1^g}\right)^2 \qquad \text{and} \qquad p_3^g = 2\sqrt{p_1^g}(1 - \sqrt{p_1^g}), \qquad g = 1, \ldots, 5. \tag{4.57}$$

The comparison between the experimental data of Fam2 and Fam3 and the theoretical probabilities computed in (4.57) is plotted in Figure 4.14, on the left and right column, respectively. The red triangles correspond to the fraction of pairs of siblings whose fate is death, whereas the blue triangles refer to pairs of daughters with different fates. The theoretical probabilities p_2^g and p_3^g, $g = 1, \ldots, 5$, derived according to equation (4.57) are plotted as dots in red and blue, respectively. In both Fam2 and Fam3, it is straightforward to notice that, under the assumption of cell independence, the mathematical model with cellular fate decision at birth cannot explain the experimental data. This is particularly evident in the case of pairs of siblings with different fates: the model predictions show an increasing trend across generations, reaching a maximum between 70% and 80% at generation 4, in contrast with the experimental data that always stay below 20%. It becomes apparent that a different choice of p_1 and p_2 that incorporates cellular fate correlation is necessary to link theoretical predictions and experimental data sets, as suggested in Ref. Duffy & Hodgkin (2012). This will be discussed in the next section.

4.3.2 Introducing sibling fate correlation

In this section, a first attempt to introduce *correlation factors* in the model to account for sibling fate correlation is presented. In order to understand the role of these factors in cellular dynamics, imagine that, when a division occurs, the first daughter joins the division pool with probability ε, whereas its fate is death with probability $1 - \varepsilon$. The fate of the second daughter is determined taking into account the destiny of its sibling as follows:

- $\mathbb{P}(2^{\text{nd}}$ daughter divides $\mid 1^{\text{st}}$ daughter divides$) = f\varepsilon$, where $1 < f \leq \frac{1}{\varepsilon}$.

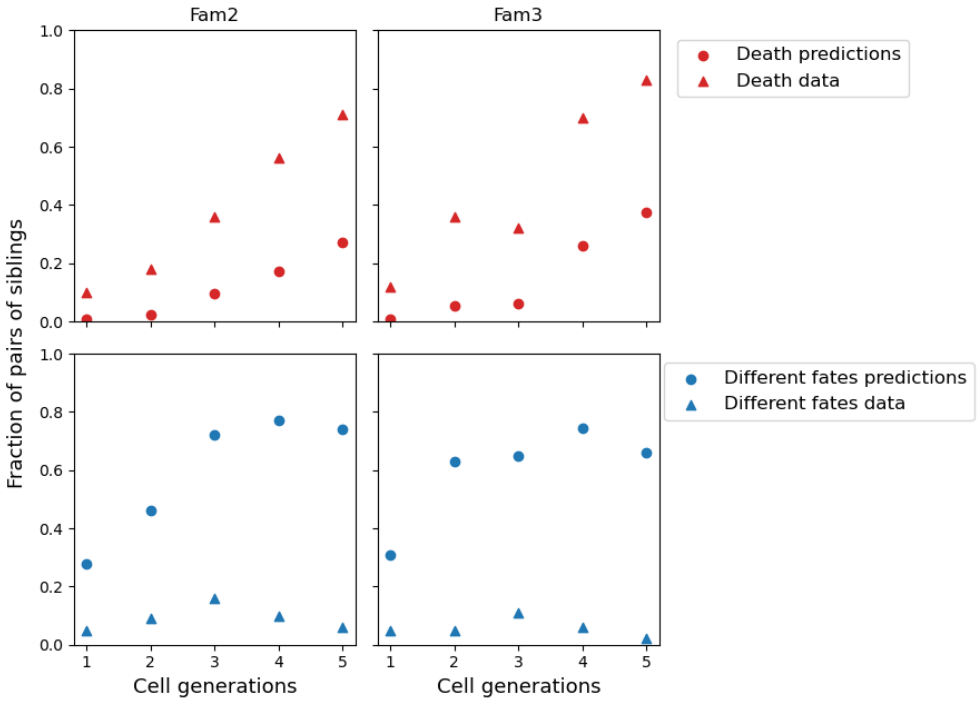

Figure 4.14: Comparison between the data set analysed in Markham *et al.* (2010) and our theoretical predictions derived according to (4.57) under the assumption of cell independence for experiments Fam2 (left column) and Fam3 (right column). The data points are represented by the triangles, whereas the dots identify our theoretical predictions.

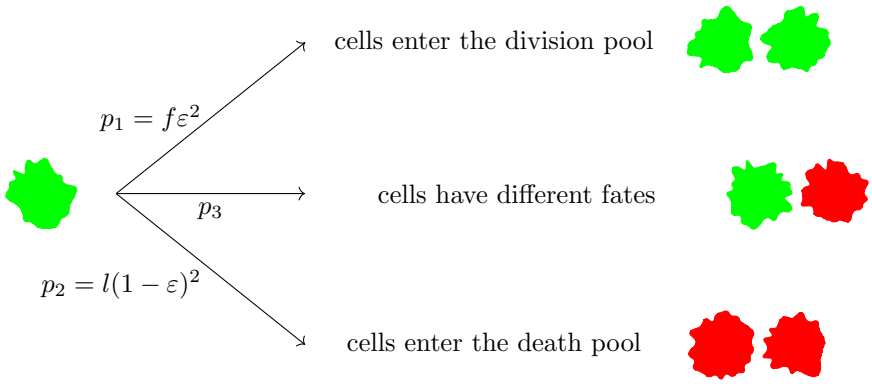

Figure 4.15: Three different outcomes following a cell division in presence of sibling fate correlation. Both daughters enter the division pool with probability $p_1 = f\varepsilon^2$ or the death pool with probability $p_2 = l(1-\varepsilon)^2$. Daughter cells have different fates with probability $p_3 = 1 - f\varepsilon^2 - l(1-\varepsilon)^2$.

- $\mathbb{P}(2^{\text{nd}}$ daughter dies $\mid 1^{\text{st}}$ daughter divides$) = 1 - f\varepsilon$.
- $\mathbb{P}(2^{\text{nd}}$ daughter dies $\mid 1^{\text{st}}$ daughter dies$) = l(1-\varepsilon)$, where $1 < l \leq \frac{1}{1-\varepsilon}$.
- $\mathbb{P}(2^{\text{nd}}$ daughter divides $\mid 1^{\text{st}}$ daughter dies$) = 1 - l(1-\varepsilon)$.

Note that, $f = l = 1$ leads to the case of cell independence analysed in the previous section, while correlation factors f and l greater than 1 introduce fate correlation between siblings as their definition increases the probability of a pair of siblings having the same fate. In this setting, the probabilities p_1 and p_2 are computed as $p_1 = f\varepsilon^2$ and $p_2 = l(1-\varepsilon)^2$. Thus, $p_3 = 1 - f\varepsilon^2 - l(1-\varepsilon)^2$. Figure 4.15 depicts the possible outcomes of a cell division event when sibling fate correlation is introduced in the model.

As described for the general mathematical model discussed in Section 4.1, after the decision at birth, cellular fate takes some random time to happen. Although not needed to compare with Figure 4.13, I note that one could compute analytically the expected number of cells in each pool over time in the case of exponential and Erlang times to division and death retracing the steps described in Sections 4.1.1 and 4.1.2. As the exponential distribution can be thought of as a Erlang distribution with a single stage (*i.e.*, $N = 1$ and $K = 1$), only the case of Erlang

times to division and death is considered in this section. Replacing $p_1 = f\varepsilon^2$ and $p_2 = l(1-\varepsilon)^2$ in (4.32) and (4.34), one gets the set of ordinary differential equations that describe the dynamics of cells across stages as

$$\begin{aligned}
\frac{\mathrm{d}B_1(t)}{\mathrm{d}t} &= \lambda(1 + f\varepsilon^2 - l(1-\varepsilon)^2)B_N(t) - \lambda B_1(t), \\
\frac{\mathrm{d}B_j(t)}{\mathrm{d}t} &= \lambda B_{j-1}(t) - \lambda B_j(t), && j = 2, \dots, N, \\
\frac{\mathrm{d}D_1(t)}{\mathrm{d}t} &= \lambda(1 - f\varepsilon^2 + l(1-\varepsilon)^2)B_N(t) - \mu D_1(t), \\
\frac{\mathrm{d}D_i(t)}{\mathrm{d}t} &= \mu D_{i-1}(t) - \mu D_i(t), && i = 2, \dots, K.
\end{aligned}$$

From Section 4.1.2, the expected number of cells in each stage of the division process over time is equal to

$$B_j(t) = \frac{(1+\widetilde{\rho})^{\frac{1-j}{N}} b_0}{N} \sum_{k=0}^{N-1} z^{(1-j)k} e^{\lambda t\left((1+\widetilde{\rho})^{\frac{1}{N}} z^k - 1\right)}, \quad j = 1, \dots, N, \tag{4.58}$$

where $\widetilde{\rho} = f\varepsilon^2 - l(1-\varepsilon)^2$. On the other hand, the evolution through time of the mean number of cells in the death pools is computed as

$$D_i(t) = \frac{\lambda\mu^{i-1}(1-\widetilde{\rho})(1+\widetilde{\rho})^{\frac{1}{N}-1} b_0}{N} \sum_{k=0}^{N-1} z^k \left(\frac{e^{\lambda t\left((1+\widetilde{\rho})^{\frac{1}{N}} z^k - 1\right)} - e^{-\mu t}}{\widetilde{q_k}^{\,i}} - \sum_{m=1}^{i-1} \frac{t^m e^{-\mu t}}{m! \widetilde{q_k}^{\,i-m}} \right), \tag{4.59}$$

$i = 1, \dots, K$, with $\widetilde{q_k} = \left(\lambda(1+\widetilde{\rho})^{\frac{1}{N}} z^k - \lambda + \mu\right)$.

In order to compare the theoretical predictions of our model with the data set illustrated in Figure 4.13, the probabilities of joining the division or death pool are assumed to depend on the number of cell divisions. This reflects the fact that cells are more likely to die when they have already undergone several divisions (Belluccini *et al.*, 2022; Ganusov *et al.*, 2007; Mazzocco *et al.*, 2017). Thus, it is not restrictive to assume that ε_g, $g = 1, \dots, 5$ decreases as cell generation increases; that is $\varepsilon_1 \geq \varepsilon_2 \geq \cdots \geq \varepsilon_5$. On the other hand, one can consider that the correlation factors f and l do not vary across generations to limit the number of parameters in the model. In particular, the parameters in my model with fate correlation are the probabilities $\varepsilon_g, g = 1, \dots, 5$, and the correlation factors f and l. It is

important to note that, since the data set in Figure 4.13 does not incorporate any information about the timescales of the process or the evolution of the number of cells over time, parameters μ and λ (and the number of stages N and K in the case of Erlang times to division and death) are irrelevant here. The parameters in the model are inferred making use of the data set in Figure 4.13 and Algorithm 2. The prior distributions are uniform between $[0, 1]$ for the probabilities $\varepsilon_g, g = 1, \ldots, 5$, and also for the correlation factors in their range of definition. However, as the interval of existence of f and l depends on $\varepsilon_g, g = 1, \ldots, 5$, the approach illustrated in Goggans *et al.* (2014) is adopted here to explore efficiently the parameter space. In order to do so, observe that

$$0 \leq \frac{l-1}{l} \leq \varepsilon_5 \leq \varepsilon_4 \leq \varepsilon_3 \leq \varepsilon_2 \leq \varepsilon_1 \leq f\varepsilon_1 \leq 1,$$

where the first and the last two inequalities follow directly from the definition of f and l, whereas the others reflect the assumption that cells are more likely to die (and therefore less likely to divide) when they have already undergone several divisions, trends that are clearly exhibited also by the data set in Figure 4.13. Figure 4.16 contains the theoretical predictions of the mathematical model (dots) compared to the experimental data (triangles) described in Figure 4.13. Despite its simplicity, my model is able to replicate the trends shown by the data for both experiments Fam2 and Fam3, especially when comparing to results in Figure 4.14. Three different colours identify the fate of pairs of siblings: green corresponds to both daughters dividing, red represents the case where both daughters' fate is death, and lastly, blue corresponds to siblings with different fates. In Figure 4.16, one notices that, in both experiments, the model predictions still overestimate the probability of siblings having different fates, particularly in the case of experiment Fam3 (right panel of Figure 4.16). In some instances, this corresponds to an underestimation of the fraction of pairs of siblings that either divide or die. This may be related to the fact that the model ignores inheritable features from the mother cell, accounting only for sibling fate correlation. As suggested by Markham *et al.* (2010), another parameter might be required for vertical inheritance. Figure 4.17 contains the posterior distributions of model parameters, which indicate overall good learning from the data sets given the mathematical model. In the case of experiment Fam2, the correlation factor l is higher than f, whereas they are very

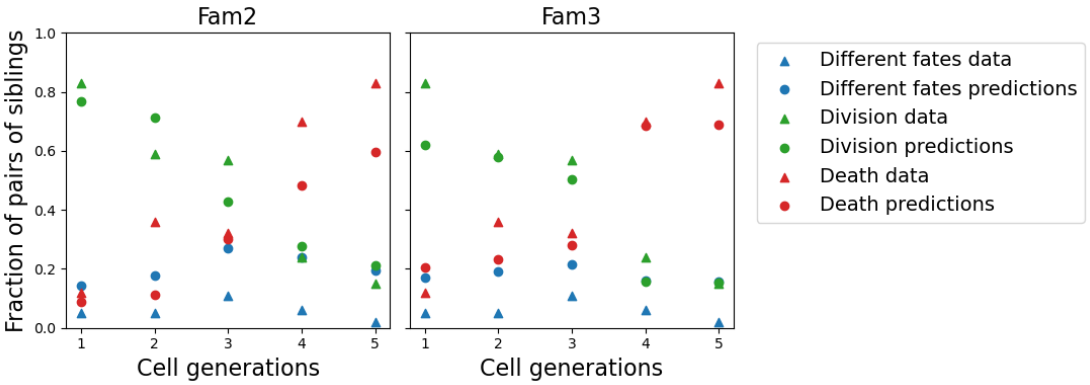

Figure 4.16: Model predictions (triangles) compared with experimental data (dots) from Fam2 (left) and Fam3 (right).

similar in the instance of Fam3. It is also interesting to observe that, in Figure 4.17 **B**, ε_4 and ε_5 are significantly smaller than the other probabilities ε_g, $g = 1, 2, 3$. This can be explained by the data set: looking at the data of Fam3 (Figure 4.13, right plot), there is a remarkable decrease of the fraction of pairs of siblings that divide between generation 3 and generation 4.

On the other hand, one could assume that both the probabilities and the correlation factors depend on cell generations. In this instance, choosing one of the correlation factors equal to 1, for example $l_g = 1, g = 1, \ldots, 5$, the parameters in the model are $\varepsilon_g, f_g, g = 1, \ldots, 5$. Thus, the probabilities are computed as $p_1^g = f_g \varepsilon_g^2$ and $p_2 = (1 - \varepsilon_g)^2$, $g = 1, \ldots, 5$, from which one can derive for each generation the exact values of ε_g and f_g that reproduce the experimental data. The same conclusion follows from the assumption $f_g = 1, g = 1, \ldots, 5$. Although under this assumption it is possible to replicate exactly the data, the fact that the number of parameters equals the number of data points suggests that over-fitting issues may arise.

A

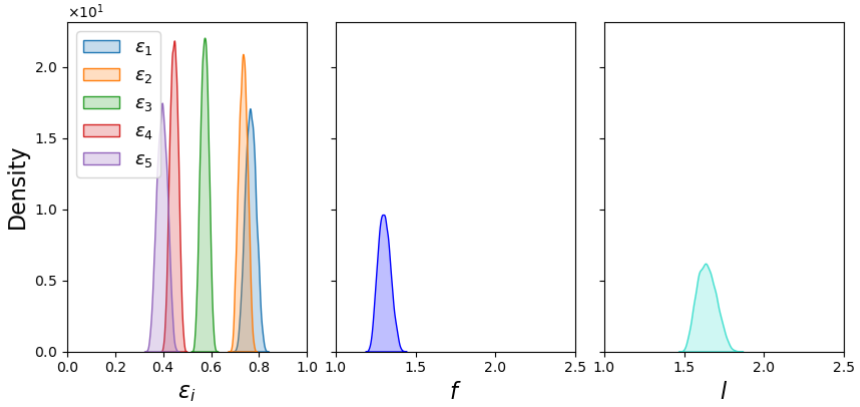

B

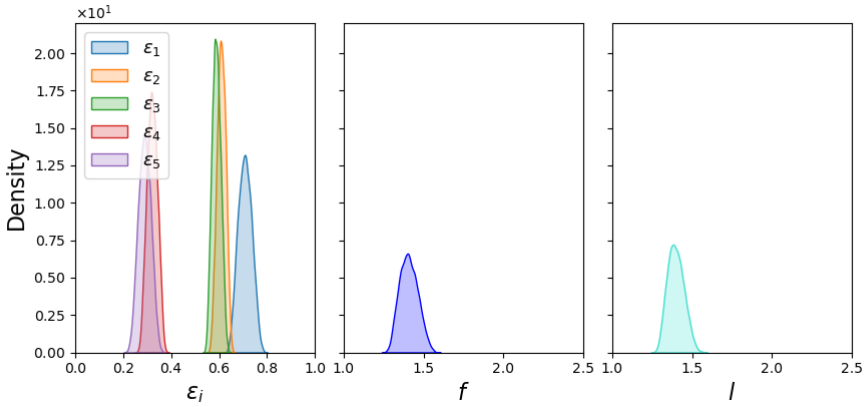

Figure 4.17: Posterior distributions for model parameters, obtained with the data sets Fam2 (**A**) and Fam3 (**B**).

4.4 Discussion

A mathematical model that makes use of two-type branching processes is proposed here to study the dynamics of a population of cells over time, and to investigate the role that cellular fate correlation plays on the evolution of the population. A family of cells is divided into two pools based on cellular fate, which is either division or death. The underlying idea is that cells decide their fate at birth, and after this instantaneous decision, the fate takes some random time to happen. A cell's times to division and death have been modelled as exponential and Erlang random variables. Hence, the stochastic approach presented in this chapter yields a Markovian model. Obviously, other probability densities may be adopted to model division and death times, such as gamma, Weibull and log-normal distributions (Cheon *et al.*, 2021; Zilman *et al.*, 2010). However, these choices would not guarantee the advantages of the Markovian models, which ensure analytical tractability, as shown by the results in Section 4.1, and computational efficiency of stochastic simulations with the Gillespie algorithm (Gillespie, 1976, 1977). When considering exponential times to division and death, the probability generating function of the number of cells in each pool is derived, generalising the analysis carried out by Antal & Krapivsky (2010) to study cell dynamics in skin tissue.

Interestingly, the model with cellular fate decision at birth presented here separates the cell population timescales – and therefore its rate of growth – from the cellular fate probability and asymptotic behaviour (*i.e.*, population survival versus extinction), which often depend on the same parameters, as in the case of the classic birth-and-death process (Allen, 2010) and the multi-stage model proposed in Chapter 3 (Belluccini *et al.*, 2022). In particular, in our model p_1 and p_2 encapsulate the cellular fate probabilities and determine the asymptotic behaviour of the cell population. On the other hand, the parameters p_3, the birth and death rates λ and μ, and the number of stages N and K in the case of Erlang times to division and death, set the population timescales and rate of growth.

After studying the model under the assumption of cell independence, a preliminary attempt to include sibling fate correlation in the model is proposed through the definition of correlation factors. The applicability of this approach is shown by considering a time-lapse microscopy data set of B cell families (Hawkins *et al.*,

2009; Markham *et al.*, 2010), where the fate of sibling pairs is broken down per division. Despite its simplicity, the model is able to replicate the trend of the experimental data, although overestimating the fraction of pairs of siblings with different fates. This might be related to the possibility that only one factor accounting for sibling fate correlation is not enough to explain cellular dynamics, as suggested by Markham *et al.* (2010). Another parameter may be required to account for inheritable features from the mother cell.

An extension of my stochastic model to track the number of divisions that cells undergo over time would be desirable, both with and without cellular fate correlation. This would allow one to link theoretical predictions with other types of experimental data, *e.g.*, CFSE data (De Boer & Perelson, 2005; De Boer *et al.*, 2006; Ganusov *et al.*, 2007), making use of the expected number of cells in each pool derived in Sections 3.2 and 4.3.2. This is the aim of future work.

Depending on the relationship between the probabilities p_1 and p_2, the population of cells expands without bounds, dies out or reaches a steady state, as shown in Section 4.1. Competitions for resources may be introduced making use of resource-dependent branching processes (Bruss & Duerinckx, 2015) or logistic branching processes (Lambert, 2005).

In the model presented in this chapter only two possible fates, either division or death, are considered. However, the flexibility of the approach enables the incorporation of other fates, such as cellular differentiation (Míguez, 2015), through the introduction of other events at birth. The analysis of the expected number of cells in each pool can be carried out following the steps shown in Section 4.1.

Chapter 5

Mathematical models of tick-borne virus transmission

The genomes of segmented viruses are comprised of multiple RNA strands, called *segments*, each of which is a self-contained genetic element, carrying the required protein components for its expression and replication. Although segmented viruses can differ significantly in their virion structure, pathology, or genome architecture, they all have in common the capability of exchanging genome segments during viral assembly in a co-infected host cell (McDonald *et al.*, 2016). Indeed, a host can be simultaneously infected by two (or more) distinct pathogens, or two (or more) strains of the same virus, which might enter the same cell (Cox, 2001; Lowen, 2017). The process of genome segments exchange is known as *reassortment* (Lowen, 2018), and produces progeny with new viral properties, such as accelerated replication kinetics or altered pathogenicity (Ma *et al.*, 2009; Zhu *et al.*, 2011).

Established in 2017, *Bunyavirales* is an order of segmented negative strand RNA-viruses which is comprised of more than 330 viruses classified within fourteen virus families (Abudurexiti *et al.*, 2019). These viruses possess genomes of between two and eight RNA segments, although those with tripartite genomes represent the majority. The three segments are named small (S), medium (M) and large (L); the S segment encodes the nucleocapsid protein, the M segment encodes the membrane glycoproteins and the L segment encodes the RNA polymerase (Ariza *et al.*, 2013). Bunyaviruses that cause diseases in humans include the Crimean–Congo

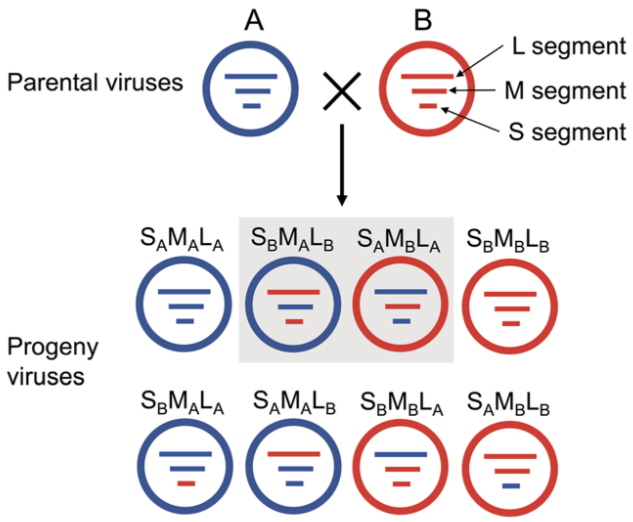

Figure 5.1: Schematic representation from Klempa (2018) of all potential reassortants resulting from the co-infection of a cell by two hypothetical parental viruses A (blue) and B (red). S, M, and L capital letters stand for the S, M, and L genomic segments. Subscripted A and B indicate the origin of the given segment to one of the two parents.

hemorrhagic fever (CCHF) virus, which has been declared a research and development priority pathogen by the World Health Organisation (Mehand *et al.*, 2018). CCHF is a tick-borne virus with fatality rate ranging from less than 5% to more than 30% depending on the size of the outbreak and the region (Spengler *et al.*, 2019). In recent years, a reassortant of CCHF virus caused severe disease in Spain (Negredo *et al.*, 2021). Several questions remain to be answered about reassorment, for instance, if there is any mechanism that promotes the establishment of one reassortant over the possible $2^3 = 8$ (for two strains and three segments) segment combinations summarised in Figure 5.1 (Michalakis & Blanc, 2020). In order to shed light on these issues, it is necessary to take a step back to understand the co-infection dynamics in hosts and ticks, as well as the role that different routes of transmission play in the spread of the virus. These two aspects represent the focus of the work presented in this chapter.

After contracting the CCHF virus, humans are the only species to develop a severe

disease characterised by fever, myalgia, dizziness, neck pain and stiffness, backache, headache, sore eyes and photophobia. Human infections occur through tick bites, handling parts of viremic animals, or exposure to the blood and body fluids of infected patients (Spengler & Estrada-Peña, 2018; Spengler *et al.*, 2019). On the other hand, transmission between ticks and livestock occurs during blood meals (Bhowmick *et al.*, 2022; Matser *et al.*, 2009). Infection amongst ticks may also be trans-stadial (*i.e.*, transmitted across the different life stages of the tick, which are egg, larvae, nymph and adult, as depicted in Figure 5.2), transovarial (*i.e.*, from female adults to eggs) or occur during co-feeding through saliva contact (Gonzalez *et al.*, 1992; Matser *et al.*, 2009). The transmission of the infection via co-feeding between ticks occurs when the vectors feed in close proximity to each other on the same host and at the same time (Belli *et al.*, 2017). Since the infection through co-feeding does not involve the host bloodstream, it can occur when the vectors are feeding on a vertebrate that is not necessarily infected. Once a tick becomes infected, the infection lasts for its lifetime (Gargili *et al.*, 2017), whereas viremia is cleared in about a week in livestock (Gonzalez *et al.*, 1998; Hoch *et al.*, 2018). The short-lasting viremia in vertebrates and the fact that vertebrate animals develop only quite mild symptoms make the detection of CCHF virus in livestock rather challenging. The transmission tick-to-vertebrate and vice-versa involves blood contact and is usually referred to as systemic, while co-feeding is regarded as non-systemic transmission (Bhowmick *et al.*, 2022).

Several mathematical models account for the different life stages of ticks (Lou *et al.*, 2014; Ogden *et al.*, 2005; Rosà *et al.*, 2003). Conversely, the models presented in this chapter do not distinguish egg, larva, nymphs and adults to avoid hyper-parametrisation. The aim is to provide analytical results to clarify the role of different transmission routes, and co-transmission in the instance of co-infection dynamics.

Ticks represent vectors and reservoirs for CCHF virus, and vertebrate animals, in particular livestock, are critical for the maintenance of the virus (Spengler & Estrada-Peña, 2018; Spengler *et al.*, 2016). In order to understand the role of the different routes of transmission, the spread of a single infection (*i.e.*, a single virus or viral strain) amongst two interacting populations, *i.e.*, vertebrate animals and ticks, is modelled in Section 5.1. A system of ordinary differential equations is used

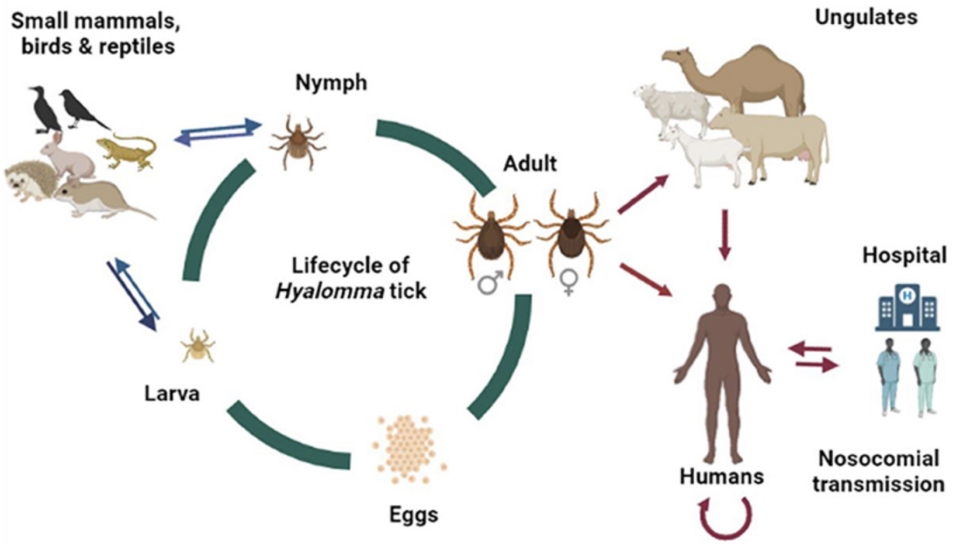

Figure 5.2: Life cycle of Hyalomma ticks and vertical and horizontal transmission of Crimean-Congo hemorrhagic fever virus from Perveen & Khan (2022).

to describe the dynamics of susceptible and infected individuals. The basic reproduction number is computed making use of the next generation matrix approach (Diekmann *et al.*, 2010; Van den Driessche, 2017). Moreover, if the populations of susceptible individuals are large, one can assume that infected individuals behave independently of each other. Thus, the dynamics of infected hosts and ticks can be approximated making use of a two-type branching process, as shown in Section 5.1.2. This approach enables the computation of the probability of epidemic extinction. On the other hand, when considering depletion of susceptible individuals, the probability of epidemic extinction versus virus establishment, as well as the conditional times to such events, can be computed by means of first step arguments (Pinsky & Karlin, 2010). Furthermore, the distribution of the exact number of secondary infections caused by an infected individual is derived (Artalejo & Lopez-Herrero, 2013).

In order to study co-infection dynamics, the populations of vertebrates and ticks are assumed to be in an endemic equilibrium due to a resident viral strain V_1. An invasive viral strain, V_2, is then introduced in the system through a given number of hosts and/or ticks infected with V_2. In the instance of CCHF virus, the invasive viral strain can be thought of as a mutant or reassortant strain of the same virus.

First, in Section 5.2.1 we propose a deterministic model that accounts only for co-feeding transmission. In this setting, the invasion reproduction number of the invasive viral strain V_2 in an endemic equilibrium of the resident viral strain V_1 is computed by means of the next generation matrix approach (Allen *et al.*, 2019; Gao *et al.*, 2016). Then, a stochastic model is introduced to describe the dynamics of hosts and ticks infected with the invasive viral strain V_2. As our interest is in studying the early dynamics of V_2, the population of susceptible individuals, as well as the populations of hosts and ticks infected by V_1, are assumed to be large and constant over time. Thus, individuals infected with V_2 are independent of each other. Hence, the stochastic model presented in Section 5.2.2 enables the computation of some stochastic descriptors of interest making use of first step arguments: probability of extinction of the invasive strain V_2, establishment of V_2, and co-infection events (*i.e.*, co-infection of either a vertebrate or a vector). The conditional times to such events are also computed. We focus on analysing summary statistics related to co-infection events since co-infection is a necessary (but not sufficient) condition for reassortment to occur. Thus, our interest is in studying the different factors affecting the probability and timescales of co-infection events occurring.
The chapter is structured as follows. Section 5.1 contains a deterministic and a stochastic model of the single infection dynamics aimed to understand the role of different routes of transmission. In Section 5.2, we propose a deterministic model of co-feeding transmission, and also a stochastic approach to study the infection dynamics in the presence of two distinct viral strains, V_1 and V_2, referred to as resident and invasive strain, respectively. Section 5.3 provides a final discussion.

5.1 Single infection dynamics

Consider a population of ticks interacting with a population of hosts, which may be small or large vertebrates. Both species are susceptible to the infection of a viral strain V_1. The virus is transmitted from tick-to-vertebrate and vice-versa through contact with infected blood. Within the tick population, tick-to-tick transmission may also happen through co-feeding (Gonzalez *et al.*, 1992; Matser *et al.*, 2009). Vertebrate animals are characterised by short lasting viremia (Gonzalez *et al.*,

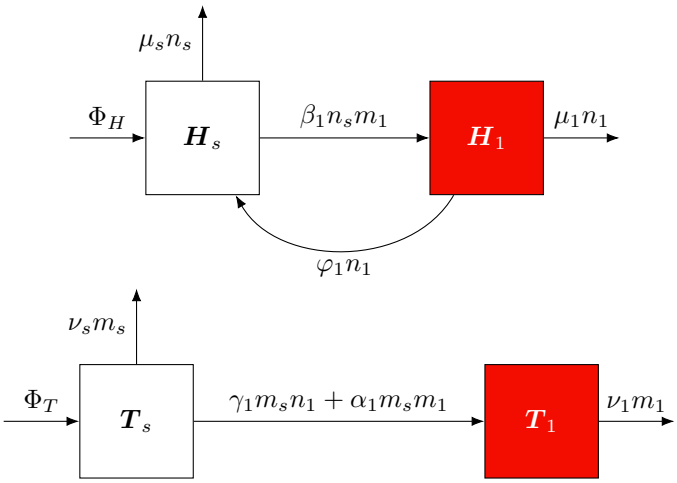

Figure 5.3: Diagram for the dynamics of susceptible and infected hosts (**top**) and ticks (**below**). The model parameters are summarised in Table 5.1.

1998; Hoch *et al.*, 2018), whereas once a tick contracts the virus, the infection lasts for its lifetime (Gargili *et al.*, 2017). This assumption reflects the fact the virus usually survives the moulting process through to the subsequent developmental stage of ticks (trans-stadial transmission) (Dohm *et al.*, 2014; Gargili *et al.*, 2017; Norman *et al.*, 1999).

Let us denote the number of susceptible and infected hosts at time t as $n_s(t)$ and $n_1(t)$, respectively. Similarly, susceptible and infected ticks at time t are $m_s(t)$ and $m_1(t)$, respectively. Thus, the sub-index s indicates susceptible individuals and the sub-index 1 denotes species infected by the viral strain V_1. Figure 5.3 illustrates the dynamics considered in this mathematical model. In particular, susceptible hosts immigrate in the population with rate Φ_H, are infected by an infected tick with transmission parameter β_1, and die with rate μ_s; infected hosts clear the virus on average in $1/\varphi_1$ units of time and die with rate μ_1. On the other hand, susceptible ticks immigrate with rate Φ_T, contract the virus due to systemic transmission with transmission parameter γ_1, or through co-feeding with transmission parameter α_1, and live on average $1/\nu_s$ units of time; infected ticks have an average lifespan of $1/\nu_1$ units of time.

Parameter	Event	Range	Units	Reference
β_1	$T_1 + H_s \rightarrow T_1 + H_1$	$[10^{-4}, 10^{-1}]$	1/Days/Tick	Norman *et al.* (2004)
γ_1	$H_1 + T_s \rightarrow H_1 + T_1$	$[10^{-4}, 10^{-1}]$	1/Days/Host	Norman *et al.* (2004)
α_1	$T_1 + T_s \rightarrow T_1 + T_1$	$[10^{-6}, 10^{-3}]$	1/Days/Tick	Norman *et al.* (2004)
ν_s	Death rate of T_s	$[6 \times 10^{-3}, 3.8 \times 10^{-2}]$	1/Days	Lou *et al.* (2014)
ν_1	Death rate of T_1	$[6 \times 10^{-3}, 3.8 \times 10^{-2}]$	1/Days	Lou *et al.* (2014)
μ_s	Death rate of H_s	$[1/3600, 1/360]$	1/Days	Mpeshe *et al.* (2011)
μ_1	Death rate of H_1	$[1/3600, 1/360]$	1/Days	Mpeshe *et al.* (2011)
Φ_T	Arrival of ticks	$[0.5, 3.5]$	Tick/Days	Sutton *et al.* (2012)
Φ_H	Arrival of hosts	$[0.5, 1.5]$	Host/Days	Mpeshe *et al.* (2011)
φ_1	$H_1 \rightarrow H_s$	$[1/7, 1/5]$	1/Days	Hoch *et al.* (2018)

Table 5.1: Summary of the parameters in the single infection model.

5.1.1 A deterministic approach

The events described in Figure 5.3 are combined in the following system of ordinary differential equations to obtain the evolution of susceptible and infected hosts and ticks over time as

$$\begin{aligned}
\frac{\mathrm{d}n_s}{\mathrm{d}t} &= -\mu_s n_s - \beta_1 n_s m_1 + \varphi_1 n_1 + \Phi_H, \\
\frac{\mathrm{d}m_s}{\mathrm{d}t} &= -\nu_s m_s - \gamma_1 m_s n_1 - \alpha_1 m_s m_1 + \Phi_T, \\
\frac{\mathrm{d}n_1}{\mathrm{d}t} &= -\mu_1 n_1 + \beta_1 n_s m_1 - \varphi_1 n_1, \\
\frac{\mathrm{d}m_1}{\mathrm{d}t} &= -\nu_1 m_1 + \gamma_1 m_s n_1 + \alpha_1 m_s m_1.
\end{aligned} \tag{5.1}$$

The basic reproduction number, R_0, is the average number of secondary infections generated by one infected individual in a completely susceptible population (Diekmann *et al.*, 1990; Van den Driessche & Watmough, 2002), and represents a threshold parameter for the epidemic. In particular, if $R_0 < 1$, on average an infected individual produces fewer than one new infection during its infectious period; thus, the infection does not become endemic. Conversely, when $R_0 > 1$, an infectious individual transmits the virus to more than one individual; hence, the infection invades the population. If there is only one species of infected individuals in the model, R_0 is given by the product of the infection rate and the average duration of the infection (Van den Driessche & Watmough, 2002). However, when

the model presents more than one type of infectious individuals, as in the instance of our model defined in equations (5.1), or when different stages of infectiousness are taken into account (Anderson & Watson, 1980), a more general method is required to compute R_0. The next generation matrix approach, proposed by Diekmann *et al.* (1990) and then elaborated by Diekmann *et al.* (2010); Van den Driessche (2017); Van den Driessche & Watmough (2002), provides a tool to compute the basic reproduction number "as the number of new infections produced by a typical infected individual in a population at the virus-free equilibrium" (Van den Driessche & Watmough, 2002).

Here, R_0 is computed considering all the routes of transmission and in some simplified scenarios (*i.e.*, when some parameters are set equal to zero) making use of the next generation matrix approach. The first step is to distinguish between infected and uninfected individuals (Van den Driessche & Watmough, 2002), which is straightforward in the case of the model defined in equations (5.1): n_s and m_s are the uninfected individuals, whereas n_1 and m_1 are the infected ones. Thus, the virus-free equilibrium is derived from the system of equations (5.1) in the absence of infected hosts or ticks, *i.e.*, considering only the uninfected individuals n_s and m_s:

$$\begin{aligned} \frac{\mathrm{d}n_s}{\mathrm{d}t} &= -\mu_s n_s + \Phi_H, \\ \frac{\mathrm{d}m_s}{\mathrm{d}t} &= -\nu_s m_s + \Phi_T. \end{aligned} \tag{5.2}$$

The virus-free steady state can be written as $(n_s^\star, m_s^\star, 0, 0)$, where

$$\begin{aligned} n_s^\star &= \frac{\Phi_H}{\mu_s}, \\ m_s^\star &= \frac{\Phi_T}{\nu_s}. \end{aligned} \tag{5.3}$$

The Jacobian matrix of system (5.1) linearised at $(n_s^\star, m_s^\star, 0, 0)$ is computed as

$$\begin{pmatrix} -\mu_s & 0 & \varphi_1 & 0 \\ 0 & -\nu_s & -\gamma_1 \frac{\Phi_T}{\nu_s} & -\alpha_1 \frac{\Phi_T}{\nu_s} \\ 0 & 0 & -\mu_1 - \varphi_1 & \beta_1 \frac{\Phi_H}{\mu_s} \\ 0 & 0 & \gamma_1 \frac{\Phi_T}{\nu_s} & -\nu_1 + \alpha_1 \frac{\Phi_T}{\nu_s} \end{pmatrix}.$$

The sub-system of the infected species is given by

$$\begin{aligned}\frac{\mathrm{d}n_1}{\mathrm{d}t} &= -\mu_1 n_1 + \beta_1 n_s m_1 - \varphi_1 n_1,\\ \frac{\mathrm{d}m_1}{\mathrm{d}t} &= -\nu_1 m_1 + \gamma_1 m_s n_1 + \alpha_1 m_s m_1,\end{aligned}$$

which, linearised at the virus-free steady state $(n_s^\star, m_s^\star, 0, 0)$, becomes

$$\begin{aligned}\frac{\mathrm{d}n_1}{\mathrm{d}t} &= -\mu_1 n_1 + \beta_1 \frac{\Phi_H}{\mu_s} m_1 - \varphi_1 n_1,\\ \frac{\mathrm{d}m_1}{\mathrm{d}t} &= -\nu_1 m_1 + \gamma_1 \frac{\Phi_T}{\nu_s} n_1 + \alpha_1 \frac{\Phi_T}{\nu_s} m_1.\end{aligned}$$

The system thus obtained is used to determine the fate of a small number of infected individuals introduced in a virus-free population. Adopting the notation in Van den Driessche & Watmough (2002), in order to compute the basic reproduction number R_0, the previous linearised system of ODEs is written as $\dot{x} = (F - V)x$, where $x = (n_1, m_1)^T$, F is the transmission component which accounts for the production of new infections, and V is the transition component that considers the changes in the state of the infected populations. Thus, the matrix F is given by

$$F = \begin{pmatrix} 0 & \beta_1 \dfrac{\Phi_H}{\mu_s} \\ \gamma_1 \dfrac{\Phi_T}{\nu_s} & \alpha_1 \dfrac{\Phi_T}{\nu_s} \end{pmatrix},$$

whereas V is defined as

$$V = \begin{pmatrix} \mu_1 + \varphi_1 & 0 \\ 0 & \nu_1 \end{pmatrix}.$$

The value of R_0 is then given by $\rho(FV^{-1})$, that is the largest eigenvalue of the matrix FV^{-1}, called *next generation matrix* (Van den Driessche & Watmough, 2002), which is computed as

$$FV^{-1} = \begin{pmatrix} 0 & \beta_1 \dfrac{\Phi_H}{\mu_s \nu_1} \\ \gamma_1 \dfrac{\Phi_T}{\nu_s(\mu_1 + \varphi_1)} & \alpha_1 \dfrac{\Phi_T}{\nu_s \nu_1} \end{pmatrix}. \tag{5.4}$$

This definition of R_0 is due to the fact that the largest eigenvalue of a matrix represents the largest possible stretch that a vector can undergo when multiplied

by the matrix. As explained by Brouwer (2022), "the first couple of generations of a new epidemic will quickly converge to a specific pattern, with the size of each generation increasing (or decreasing) by a factor of $\rho(FV^{-1})$ and the distribution among infected compartments given by ν", where ν is the eigenvector of the next generation matrix corresponding to $\rho(FV^{-1})$. In order to interpret the entries of FV^{-1}, consider the fate of an infected individual introduced into a susceptible population. For example, if an infected host is introduced in a population of susceptible hosts, the expected number of secondary infections produced by the infected host is $R_{HH} = (FV^{-1})_{11} = 0$ because the infection cannot be directly transmitted from host-to-host. If the infected host is introduced among susceptible ticks, then the mean number of secondary infections is

$$R_{HT} = (FV^{-1})_{21} = \gamma_1 \frac{\Phi_T}{\nu_s(\mu_1 + \varphi_1)}.$$

On the other hand, if an infected tick is introduced in a population of susceptible hosts, the expected number of secondary infections is given by

$$R_{TH} = (FV^{-1})_{12} = \beta_1 \frac{\Phi_H}{\mu_s \nu_1}.$$

Finally, if an infected tick is introduced in a population of susceptible ticks, the average number of new infections among ticks produced by the infected tick is

$$R_{TT} = (FV^{-1})_{22} = \alpha_1 \frac{\Phi_T}{\nu_s \nu_1}.$$

The following values of R_0 are computed considering particular transmission scenarios where some parameters are set equal to zero:

- Non-systemic transmission, *i.e.*, co-feeding only and $\gamma_1 = \beta_1 = 0$:

  $$R_0 = \frac{\alpha_1 \Phi_T}{\nu_s \nu_1} = R_{TT}.$$

  An epidemiological interpretation of R_0 here is that an infected tick transmits the virus to susceptible ticks at a rate of $\alpha_1 \Phi_T / \nu_s$ during its lifetime $1/\nu_1$, so that the average number of secondary infections is $\frac{\alpha_1 \Phi_T}{\nu_s \nu_1}$.

- Transmission only from infected tick to susceptible host, thus $\gamma_1 = \alpha_1 = 0$: $R_0 = 0$. Therefore, this type of transmission cannot generate an outbreak.

- Transmission only from infected host to susceptible tick, that is $\beta_1 = \alpha_1 = 0$: $R_0 = 0$. As in the case above, this type of transmission cannot generate an outbreak.

- Co-feeding and from tick-to-host transmissions, which means $\gamma_1 = 0$:

$$R_0 = \frac{\alpha_1 \Phi_T}{\nu_s \nu_1}.$$

  Notice that this is the same R_0 as the one computed in the case of only non-systemic transmission.

- Co-feeding and from host-to-tick transmissions, therefore $\beta_1 = 0$:

$$R_0 = \frac{\alpha_1 \Phi_T}{\nu_s \nu_1}.$$

  Notice that this is the same R_0 as the one computed in the case of only non-systemic transmission.

- Systemic transmission, that is from infected host to susceptible tick and from infected tick to susceptible host, while $\alpha_1 = 0$:

$$R_0 = \sqrt{\frac{\beta_1 \gamma_1 \Phi_H \ \Phi_T}{\mu_s \ \nu_1 \ \nu_s(\mu_1 + \varphi_1)}} = \sqrt{R_{HT} R_{TH}}.$$

  An epidemiological interpretation of R_0 in this case is that an infected tick transmits the virus to susceptible hosts at a rate $\beta_1 \Phi_H / \mu_s$ during its lifetime $1/\nu_1$; on the other hand, an infected host can infect susceptible ticks at a rate $\gamma_1 \Phi_T / \nu_s$ during the time frame $1/(\mu_1 + \varphi_1)$ it is infected. Note that the square root in the expression of R_0 represents a geometric mean (Van den Driessche, 2017). As discussed in Roberts & Heesterbeek (2003); Van den Driessche (2017), in the literature the square root is often omitted, giving the same threshold for stability at 1, but considering R_0^2 as the expected number of secondary infected hosts that result from a single infected host (or tick) as two generations are required to transmit an infection from host-to-host (or tick-to-tick, respectively), the first being from host-to-tick (or tick-to-host) and the second being from tick-to-host (or host-to-tick). For example, Allen

et al. (2019) define the basic reproduction numbers without the square root. The quantity R_0^2 can also be referred to as *type* reproduction number (Shutt *et al.*, 2017). Note that, in the case of only systemic transmission, ticks and vertebrates are characterised by the same type reproduction number.

- Transmission by any route:

$$\begin{aligned} R_0 &= \frac{1}{2}\left(\frac{\alpha_1\Phi_T}{\nu_s\nu_1} + \sqrt{\frac{\alpha_1^2\Phi_T^2}{\nu_s^2\nu_1^2} + \frac{4\beta_1\gamma_1\Phi_H\ \Phi_T}{\mu_s\ \nu_1\ \nu_s(\mu_1+\varphi_1)}}\right) \\ &= \frac{1}{2}\left(R_{TT} + \sqrt{R_{TT}^2 + 4R_{HT}R_{TH}}\right). \end{aligned} \tag{5.5}$$

  Since $R_0 > 0$, one has $R_0 \leq 1 \iff R_0^2 \leq 1$. The last inequality can be rewritten as

$$\frac{\alpha_1^2\Phi_T^2}{\nu_s^2\nu_1^2} + \frac{4\beta_1\gamma_1\Phi_H\ \Phi_T}{\mu_s\ \nu_1\ \nu_s(\mu_1+\varphi_1)} \leq \left(2 - \frac{\alpha_1\Phi_T}{\nu_s\nu_1}\right)^2.$$

  After simplifying, one obtains the condition

$$\frac{\beta_1\gamma_1\Phi_T\Phi_H}{\nu_1(\mu_1+\varphi_1)\nu_s\mu_s} + \frac{\alpha_1\Phi_T}{\nu_1\nu_s} \leq 1, \tag{5.6}$$

  which is more intuitive to interpret from an epidemiological point of view. In particular, it is straightforward to observe that the left hand side of equation (5.6) is comprised of two components, the first of which accounts for systemic transmission and the second is due to co-feeding.

The study of the basic reproduction number highlights that co-feeding represents a special route of transmission, which is totally distinguished from the systemic transmission and is able to maintain an epidemic on its own. On the other hand, the systemic transmission requires both the tick-to-host and host-to-tick routes to produce an outbreak.

Figure 5.4 shows how the value of the basic reproduction number R_0 in the presence of all routes of transmission derived in equation (5.5) is affected by varying the transmission parameters tick-to-tick α_1 (across rows), tick-to-host β_1 (varied along the y-axis) and host-to-tick γ_1 (varied along the x-axis), as well as the number of susceptible ticks at virus-free equilibrium, given by the ratio $\frac{\Phi_T}{\nu_s}$ (varied across

columns). The number of susceptible hosts at equilibrium, represented by $\frac{\Phi_H}{\mu_s}$, is normalised at 1. It is also assumed that infection does not affect the death rate of hosts and ticks, *i.e.*, $\mu_s = \mu_1$ and $\nu_s = \nu_1$ (Gao *et al.*, 2016). The red line in the plots represents the threshold value $R_0 = 1$. Note that, for increasing values of α_1 and susceptible number of ticks at virus-free equilibrium, the basic reproduction number becomes larger. In particular, when $\alpha_1 \geq 10^{-3}$ (1/Days/Tick) and $\frac{\Phi_T}{\nu_s} = 6$ or $\frac{\Phi_T}{\nu_s} = 8$, the co-feeding transmission becomes predominant and R_0 is never smaller than 1. As our intuition would suggest, the largest values of R_0 correspond to the largest values of the transmission parameters α_1, β_1 and γ_1.

5.1.2 Branching process approximation

The theory of branching processes has been used to model the propagation of infectious diseases to shed light, for example, on the extinction of the epidemic outbreaks, their extinction time and the effect of possible control measures (Bartoszyński, 1967; Jacob, 2010). These models assume independence between infected individuals, meaning that infected individuals transmit the virus to susceptible ones independently of each other. Therefore, a branching process approximation provides an adequate description of the system when the susceptible populations are large, for instance at the beginning of an outbreak. When the depletion of susceptible individuals due to infection can be neglected and the population is not saturated with infectious individuals, one can assume that the infected populations behave as a branching process (*i.e.*, an infected individual infects a susceptible, generating two infected individuals in the next generation).
Assuming that the populations of susceptible ticks and vertebrates are large, in this section the dynamics of infected ticks and hosts is approximated making use of a two-type branching process. To this end, define the following random variables:

- $H_1(t)$ is the number of infected hosts at time t;
- $T_1(t)$ is the number of infected ticks at time t.

Imagine that one infected host is introduced in a population of susceptible hosts and ticks, that is $(H_1(0), T_1(0)) = (1, 0)$. Following the events illustrated in Fig-

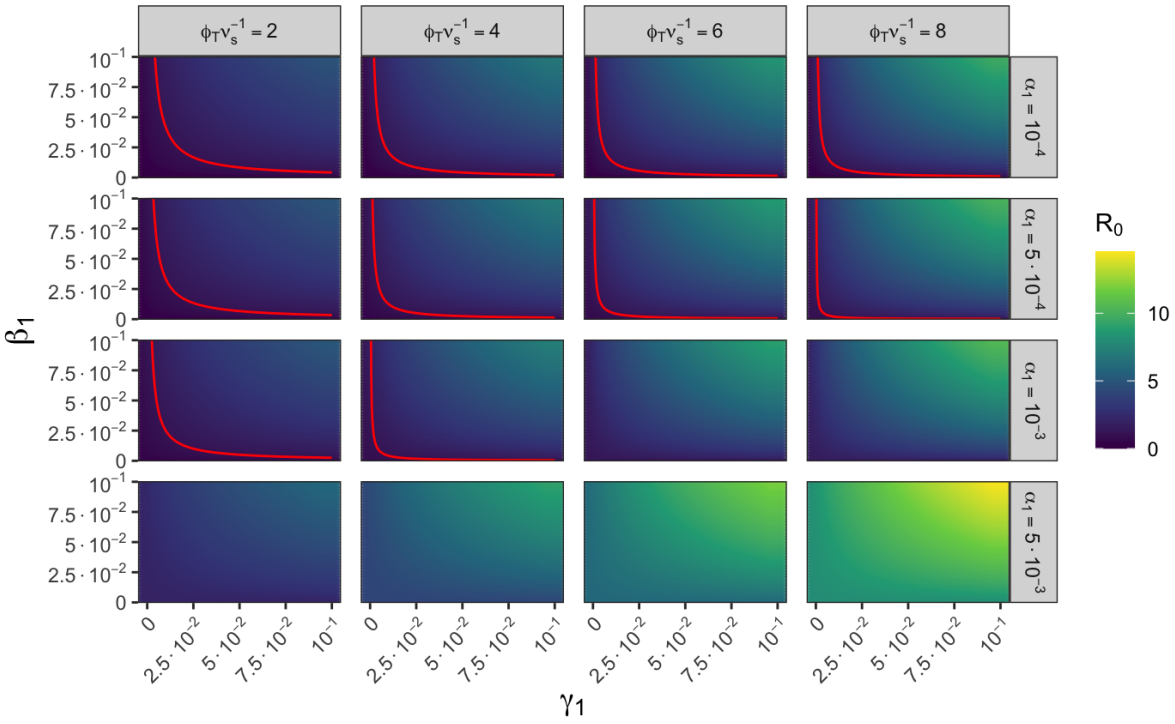

Figure 5.4: How the basic reproduction number computed in equation (5.5) is affected by varying the transmission parameters tick-to-tick α_1 (across rows), tick-to-host β_1 (varied along the y-axis) and host-to-tick γ_1 (varied along the x-axis), as well as the number of susceptible ticks at virus-free equilibrium, given by the ratio $\frac{\Phi_T}{\nu_s}$ (varied across columns). The number of susceptible hosts at equilibrium, represented by $\frac{\Phi_H}{\mu_s}$, is normalised at 1. The death rates of hosts and ticks are not affected by the infection, that is $\mu_s = \mu_1 = 1/(4\times365)$ per day and $\nu_s = \nu_1 = 1/200$ per day. The viral clearance rate of an infected host is 1/6 per day. The red lines represent the threshold value $R_0 = 1$.

ure 5.3, in a short time interval Δt one has

$$(H_1(\Delta t), T_1(\Delta t)) = \begin{cases} (1,1) & \text{with probability } \gamma_1 m_s \Delta t, \\ (0,0) & \text{with probability } (\mu_1 + \varphi_1)\Delta t, \\ (1,0) & \text{with probability } 1 - (\gamma_1 m_s + \mu_1 + \varphi_1)\Delta t. \end{cases} \tag{5.7}$$

Instead, if an infected tick is introduced in a population of susceptible ticks and hosts, *i.e.*, $(H_1(0), T_1(0)) = (0,1)$, the following cases are possible

$$(H_1(\Delta t), T_1(\Delta t)) = \begin{cases} (1,1) & \text{with probability } \beta_1 n_s \Delta t, \\ (0,2) & \text{with probability } \alpha_1 m_s \Delta t, \\ (0,0) & \text{with probability } \nu_1 \Delta t, \\ (0,1) & \text{with probability } 1 - (\beta_1 n_s + \alpha_1 m_s + \nu_1)\Delta t. \end{cases} \tag{5.8}$$

Thus, the pair $(H_1(t), T_1(t))_{t\geq 0}$ defines a two-type branching process in continuous time (Athreya *et al.*, 2004). Note that, as the susceptible populations of ticks and hosts are assumed to be large and depletion due to infection is ignored, the number of susceptible hosts and ticks, n_s and m_s respectively, is considered constant. In order to study the probability of extinction of the infected species, one considers the embedded discrete time branching process; see page 418 of Karlin & Taylor (1975) for reference. The embedded discrete time branching process is defined as $(H_1(kt_0), T_1(kt_0))_{k\in\mathbb{N}}$, where t_0 is any fixed positive number. Making use of the theory of discrete time branching processes, one can easily determine the probability of virus-free and endemic states in the continuous case. To this end, the steps illustrated in Section 4.7 of Allen (2010) will be adapted here.

Suppose $(H_1(0), T_1(0)) = (1,0)$ and denote by $p_{H_1}(i,j)$ the probability of having i infected hosts and j infected ticks in one generation (or in one time step) starting with one infected host at time $t = 0$. From equation (5.7), one obtains

$$p_{H_1}(1,1) = \frac{\gamma_1 m_s}{\gamma_1 m_s + \mu_1 + \varphi_1},$$
$$p_{H_1}(0,0) = \frac{\mu_1 + \varphi_1}{\gamma_1 m_s + \mu_1 + \varphi_1}.$$

The probability generating function associated with the offspring distribution of

one infected host, $f_{H_1}(x,y)$, is defined as

$$\begin{aligned} f_{H_1}(x,y) &= \sum_{i=0}^{+\infty}\sum_{j=0}^{+\infty} p_{H_1}(i,j)x^i y^j \\ &= \frac{\gamma_1 m_s}{\gamma_1 m_s + \mu_1 + \varphi_1}xy + \frac{\mu_1 + \varphi_1}{\gamma_1 m_s + \mu_1 + \varphi_1}, \end{aligned}$$

where $x, y \in \mathbb{C}$ and $|x|, |y| < 1$.

Similarly, starting with one infected tick and denoting by $p_{T_1}(i,j)$ the probability of having i infected hosts and j infected ticks in one generation (or in one time step) starting with one infected tick at time $t = 0$, equation (5.8) yields

$$\begin{aligned} p_{T_1}(1,1) &= \frac{\beta_1 n_s}{\beta_1 n_s + \alpha_1 m_s + \nu_1}, \\ p_{T_1}(0,2) &= \frac{\alpha_1 m_s}{\beta_1 n_s + \alpha_1 m_s + \nu_1}, \\ p_{T_1}(0,0) &= \frac{\nu_1}{\beta_1 n_s + \alpha_1 m_s + \nu_1}. \end{aligned}$$

The probability generating function associated with the offspring distribution of one infected tick, $f_{T_1}(x,y)$, is defined as

$$\begin{aligned} f_{T_1}(x,y) &= \sum_{i=0}^{+\infty}\sum_{j=0}^{+\infty} p_{T_1}(i,j)x^i y^j \\ &= \frac{\beta_1 n_s}{\beta_1 n_s + \alpha_1 m_s + \nu_1}xy + \frac{\alpha_1 m_s}{\beta_1 n_s + \alpha_1 m_s + \nu_1}y^2 + \frac{\nu_1}{\beta_1 n_s + \alpha_1 m_s + \nu_1}, \end{aligned}$$

where $x, y \in \mathbb{C}$ and $|x|, |y| < 1$.

Let $F(x,y) = (f_{H_1}(x,y), f_{T_1}(x,y))$ be the vector of the probability generating functions. Given its definition, $F(x,y)$ has a fixed point at $(1,1)$. The probability of extinction depends on the existence of another fixed point of $F(x,y)$ in $[0,1]^2$. To investigate this, consider the mean number of infected ticks (or hosts) caused by an infected host (or tick) in one generation, *i.e.*, in one time step, that is

$$\begin{aligned} m_{H_1H_1} &= \mathbb{E}\left[H_1(1)|(H_1(0),T_1(0)) = (1,0)\right], \\ m_{H_1T_1} &= \mathbb{E}\left[H_1(1)|(H_1(0),T_1(0)) = (0,1)\right], \\ m_{T_1H_1} &= \mathbb{E}\left[T_1(1)|(H_1(0),T_1(0)) = (1,0)\right], \\ m_{T_1T_1} &= \mathbb{E}\left[T_1(1)|(H_1(0),T_1(0)) = (0,1)\right]. \end{aligned}$$

These expected values can be defined in terms of the probability generating functions as

$$\begin{aligned}
m_{H_1H_1} &= \left.\frac{\partial f_{H_1}(x,y)}{\partial x}\right|_{x=1,y=1} = \frac{\gamma_1 m_s}{\gamma_1 m_s + \mu_1 + \varphi_1},\\
m_{H_1T_1} &= \left.\frac{\partial f_{H_1}(x,y)}{\partial y}\right|_{x=1,y=1} = \frac{\gamma_1 m_s}{\gamma_1 m_s + \mu_1 + \varphi_1},\\
m_{T_1H_1} &= \left.\frac{\partial f_{T_1}(x,y)}{\partial x}\right|_{x=1,y=1} = \frac{\beta_1 n_s}{\beta_1 n_s + \alpha_1 m_s + \nu_1},\\
m_{T_1T_1} &= \left.\frac{\partial f_{T_1}(x,y)}{\partial y}\right|_{x=1,y=1} = \frac{\beta_1 n_s + 2\alpha_1 m_s}{\beta_1 n_s + \alpha_1 m_s + \nu_1},
\end{aligned}$$

from which the expectation matrix M is built to derive the condition of virus extinction and virus establishment (see page 180 of Allen (2010)):

$$M = \begin{pmatrix} \dfrac{\gamma_1 m_s}{\gamma_1 m_s + \mu_1 + \varphi_1} & \dfrac{\beta_1 n_s}{\beta_1 n_s + \alpha_1 m_s + \nu_1} \\ \dfrac{\gamma_1 m_s}{\gamma_1 m_s + \mu_1 + \varphi_1} & \dfrac{\beta_1 n_s + 2\alpha_1 m_s}{\beta_1 n_s + \alpha_1 m_s + \nu_1} \end{pmatrix}.$$

Since all its entries are positive, the matrix M is regular, which means all the entries of M^p are positive for some $p > 0$. Thus, M has a simple eigenvalue of maximum modulus, that will be denoted by λ; see page 180 of Allen (2010). It is straightforward to compute

$$\lambda = \frac{1}{2}\left(A^+ + B + \sqrt{(A^+)^2 + B^2 + 2A^-B}\right), \tag{5.9}$$

where

$$\begin{aligned}
A^{\pm} &= \frac{\beta_1 n_s \pm 2\alpha_1 m_s}{\alpha_1 m_s + \beta_1 n_s + \nu_1},\\
B &= \frac{\gamma_1 m_s}{\gamma_1 m_s + \mu_1 + \varphi_1}.
\end{aligned} \tag{5.10}$$

From Theorem 4.5 of Allen (2010), one has

i. If $\lambda \leq 1$, then

$$\begin{aligned}
\lim_{k\to+\infty} \mathbb{P}\Big((H_1(k), T_1(k)) = (0,0) | (H_1(0), T_1(0)) = (1,0)\Big) = 1,\\
\lim_{k\to+\infty} \mathbb{P}\Big((H_1(k), T_1(k)) = (0,0) | (H_1(0), T_1(0)) = (0,1)\Big) = 1.
\end{aligned}$$

ii. If $\lambda > 1$, then

$$\lim_{k\to+\infty} \mathbb{P}\Big((H_1(k), T_1(k)) = (0,0) | (H_1(0), T_1(0)) = (1,0)\Big) = \overline{x},$$
$$\lim_{k\to+\infty} \mathbb{P}\Big((H_1(k), T_1(k)) = (0,0) | (H_1(0), T_1(0)) = (0,1)\Big) = \overline{y},$$

where $(\overline{x}, \overline{y})$ is the fixed point of $F(x, y)$.

The expression of the fixed point $(\overline{x}, \overline{y})$, which gives the probability of extinction when $\lambda > 1$, can be found for this system using the software Mathematica. As observed by Allen (2010), if the process starts with n_1 infected hosts and m_1 infected ticks, *i.e.*, $(H_1(0), T_1(0)) = (n_1, m_1)$, the probability of extinction is given by

$$\lim_{k\to+\infty} \mathbb{P}\Big((H_1(k), T_1(k)) = (0,0) | (H_1(0), T_1(0)) = (n_1, m_1)\Big) = \overline{x}^{n_1}\overline{y}^{m_1}.$$

5.1.3 Equivalence of deterministic model and branching process approximation

We aim to show here that the condition $\lambda \leq 1$ (or $\lambda > 1$) derived from the branching process approximation in (5.9) is equivalent to the condition $R_0 \leq 1$ (or $R_0 > 1$, respectively) obtained from the deterministic model, where R_0 is defined by equation (5.5). The condition $\lambda \leq 1$, where λ is defined in equation (5.9), can be rewritten as

$$\sqrt{(A^+)^2 + B^2 + 2A^-B} \leq 2 - A^+ - B.$$

Taking the square of both sides and simplifying, we obtain

$$A^-B + 2A^+ + 2B - A^+B \leq 2.$$

Replacing the definitions of $A^\pm$ and B as in equation (5.10) in the previous inequality and simplifying yields

$$\frac{\beta_1\gamma_1 m_s n_s}{\nu_1(\mu_1 + \varphi_1)} + \frac{\alpha_1 m_s}{\nu_1} \leq 1.$$

Evaluating the previous condition at the virus-free equilibrium $(n_s^\star, m_s^\star, 0, 0)$ defined in (5.3), we derive the condition

$$\frac{\beta_1\gamma_1\Phi_T\Phi_H}{\nu_1(\mu_1 + \varphi_1)\nu_s\mu_s} + \frac{\alpha_1\Phi_T}{\nu_1\nu_s} \leq 1, \tag{5.11}$$

which is the same inequality obtained in equation (5.6) from the deterministic model. Thus, the deterministic model and the branching process approximation provide equivalent conditions for the virus extinction or establishment, as one would expect. While the equivalence is shown only when all the routes of transmission are considered, it can be easily proven also in the other special cases considered in Section 5.1.1. From an epidemiological perspective, the left hand side of (5.11) can be interpreted as follows: the first term represents an infected tick that infects susceptible hosts at a rate $\beta_1 \frac{\Phi_H}{\mu_s}$ during its lifetime $\frac{1}{\nu_1}$; on the other hand, an infected host can infect susceptible ticks at a rate $\gamma_1 \frac{\Phi_T}{\nu_s}$ during the time frame $\frac{1}{\mu_1+\varphi_1}$ it is infected. The second term is due to co-feeding: an infected tick can infect a susceptible vector at a rate $\alpha_1 \frac{\Phi_T}{\nu_s}$ during its lifetime $\frac{1}{\nu_1}$.
One notes that the main difference between the deterministic model defined in Section 5.1.1 and the branching process approximation presented in Section 5.1.2 is that the stochastic approach enables the computation of the probability of extinction of infected individuals also in the case of virus establishment; that is $\lambda > 1$, or, equivalently $R_0 > 1$.

5.1.4 Considering depletion of susceptible species

The branching process approximation presented in Section 5.1.2 can be seen as a stochastic version of the deterministic model provided in Section 5.1.1 under the assumption of large populations of susceptible individuals, and thus, independence of infected individuals. In this section, we consider instead a stochastic version of the model where the number of susceptible individuals is not in excess, and its time evolution (in particular, the depletion of susceptible individuals over time due to infection) cannot be neglected. One of the aims of this approach is to analyse the stochastic dynamics of the system in terms of a number of stochastic descriptors or summary statistics. In particular, the probabilities of extinction of infected species versus the establishment of the virus are computed, together with the conditional times to such events. The distributions of the exact number of secondary infections are also derived considering the possible routes of transmission tick-to-host, host-to-tick and tick-to-tick. These stochastic descriptors are computed making use of a technique called *first step analysis*. This is a typical technique used to compute

summary statistics of interest in a CTMC. In particular, one exploits the law of total probability and the Markov property to condition on the next event occurring in the system, which leads to a system of linear equations that can be efficiently solved. For more details, the reader is referred to Section 3.4 of Pinsky & Karlin (2010).

Since the depletion of susceptible individuals over time is taken into account to derive the probability of and conditional time to the virus-free state or to virus establishment, as well as the distribution of the exact number of secondary infections, a new infection of a host (or a tick) corresponds to the reduction of the susceptible number of hosts (or ticks) by one unit. Furthermore, as the interest is in studying the early times of the epidemic (*e.g.*, epidemic extinction versus establishment when the virus is seeded into the population), the analysis can be simplified by considering that the total population sizes of hosts and ticks are constant over time. To do this, we neglect immigration events from now on (*i.e.*, set $\Phi_H = \Phi_T = 0$), and we consider that, when an infected individual (either a tick or a host) is removed from the system (*e.g.*, due to death or viral clearance), it is instantaneously replaced by a susceptible individual of the same species (either tick or host). Note that this is a different model from the one considered in Section 5.1.2. Let N_H denote the total number of hosts, and similarly N_T is the total number of ticks. Thus, if at time t, there are n_1 infected hosts and m_1 infected ticks, the size of the population of susceptible hosts is $N_H - n_1$, whereas the number of susceptible ticks is $N_T - m_1$. Maintaining the same notation of Section 5.1.2, the random variables $H_1(t)$ and $T_1(t)$ are the number of infected hosts and ticks, respectively, at time t. The continuous time Markov chain that describes the dynamics of the infected individuals, $(H_1(t), T_1(t))_{t\geq 0}$, is defined in the rectangle

$$\Omega = \{(n_1, m_1) \in \mathbb{N}_0^2 : 0 \leq n_1 \leq N_H, 0 \leq m_1 \leq N_T\}.$$

As depicted in Figure 5.5, from a state $(n_1, m_1) \in \Omega$, the process can jump to four

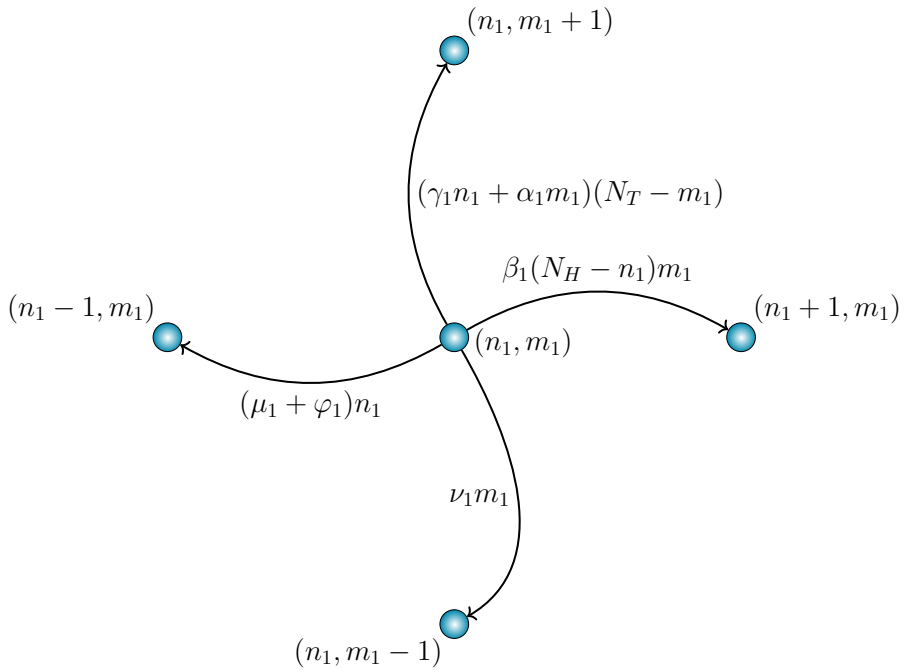

Figure 5.5: Transition diagram for the Markov chain $(H_1(t), T_1(t))_{t\geq 0}$ showing the possible states which the process can move to from a general state (n_1, m_1) and the transition rates with which these jumps occur.

adjacent states, with transition rates

$$q_{(n_1,m_1),(n_1',m_1')} = \begin{cases} \beta_1(N_H - n_1)m_1, & \text{if } (n_1', m_1') = (n_1 + 1, m_1), \\ (\gamma_1 n_1 + \alpha_1 m_1)(N_T - m_1), & \text{if } (n_1', m_1') = (n_1, m_1 + 1), \\ (\mu_1 + \varphi_1)n_1, & \text{if } (n_1', m_1') = (n_1 - 1, m_1), \\ \nu_1 m_1, & \text{if } (n_1', m_1') = (n_1, m_1 - 1). \end{cases} \tag{5.12}$$

We note that $(0, 0)$ is an absorbing state, representing epidemic extinction. A typical situation of interest is when N_T and N_H represent susceptible individuals in a particular region, where an infected tick $(T_1(0) = 1)$ or host $(H_1(0) = 1)$ is introduced. In this situation, it is of interest to compute the probability of short-term epidemic extinction (*i.e.*, the epidemic dies out without causing a large outbreak in this region) versus virus establishment (*i.e.*, a threshold number of infected individuals is achieved, leading to an outbreak). In the next subsection, we compute these probabilities, as well as the conditional times to such events. To

do this, a second absorbing macro-state E is defined by merging all the states in the sub-set $\{(n_1, m_1) \in \Omega : n_1 + m_1 = N_{\max}\}$, where, for the purposes of this chapter, $N_{\max}$ is a positive integer such that $N_{\max} \leq \min\{N_H, N_T\}$. If the total number of infected individuals, $n_1 + m_1$, hits the threshold $N_{\max}$, the virus is considered established in the populations of hosts and ticks. Hence, one notices that the state space of the Markov chain defined in equation (5.12) is actually the triangle given by

$$\hat{\Omega} = \{(n_1, m_1) \in \mathbb{N}_0^2 : 0 \leq n_1 + m_1 \leq N_{\max} - 1\} \cup E.$$

Probability of and conditional time to virus-free state and virus establishment

In order to compute the probability of short-term epidemic extinction (*i.e.*, reaching $(0, 0)$ before reaching the absorbing macro-state E), as well as the conditional time to such event, define for $(n_1, m_1) \in \hat{\Omega}$

$$\tau^{VS}_{(n_1,m_1)} = \inf\{t \geq 0 : (H_1(t), T_1(t)) = (0, 0) | (H_1(0), T_1(0)) = (n_1, m_1)\},$$

that is the time to reach the virus-free state (VS) $(0, 0)$ starting with n_1 infected hosts and m_1 infected ticks. We note that $\tau^{VS}_{(n_1,m_1)} = +\infty$ if the process, in the long term, reaches the absorbing state E instead of $(0, 0)$ (representing virus establishment instead of short-term epidemic extinction). The probability of reaching the virus-free state and the expected time to reach the virus-free state conditioned on actually reaching this fate can be computed starting from any initial state $(n_1, m_1) \in \hat{\Omega}$. This can be obtained from the Laplace-Stieltjes transform of $\tau^{VS}_{(n_1,m_1)}$ defined as

$$\phi^{VS}_{(n_1,m_1)}(z) = \mathbb{E}\left[\mathrm{e}^{-z\tau^{VS}_{(n_1,m_1)}} \mathbb{1}_{\left\{\tau^{VS}_{(n_1,m_1)} < +\infty\right\}}\right], \quad \mathrm{Re}(z) \geq 0,$$

where $\mathbb{1}_{\left\{\tau^{VS}_{(n_1,m_1)} < +\infty\right\}}$ is a random variable taking the value 1 if $\tau^{VS}_{(n_1,m_1)} < +\infty$ and 0 otherwise, so that the previous Laplace-Stieltjes transform is restricted to the

sample paths satisfying $\tau^{VS}_{(n_1,m_1)} < +\infty$. Using a first step argument, we can write

$$\begin{aligned}\phi^{VS}_{(n_1,m_1)}(z) &= \mathbb{E}\left[\mathrm{e}^{-z\tau^{VS}_{(n_1,m_1)}}\mathbb{1}_{\left\{\tau^{VS}_{(n_1,m_1)}< +\infty\right\}}\right] \\ &= \sum_{(n_1',m_1')\in\hat{\Omega}} \mathbb{E}\left[\mathrm{e}^{-z\tau^{VS}_{(n_1,m_1)}}\mathbb{1}_{\left\{\tau^{VS}_{(n_1,m_1)}< +\infty\right\}}\middle|(n_1,m_1)\to(n_1',m_1')\right]\cdot \\ &\qquad \mathbb{P}\left((n_1,m_1)\to(n_1',m_1')\right),\end{aligned}$$

where the notation $(n_1,m_1)\to(n_1',m_1')$ represents the event of moving from state (n_1,m_1) to state (n_1',m_1') in one jump. Thus, $\mathbb{P}\left((n_1,m_1)\to(n_1',m_1')\right)$ is the probability of moving from state (n_1,m_1) to state (n_1',m_1') in the next event that occurs. The states that can be possibly reached in one jump of the process starting from (n_1,m_1) are depicted in the transition diagram in Figure 5.5. If the process jumps from (n_1,m_1) to (n_1',m_1'), the random variable $\tau^{VS}_{(n_1,m_1)}$ can be split into two parts, $\tau^{VS}_{(n_1,m_1)} = t_{(n_1,m_1)\to(n_1',m_1')} + \tau^{VS}_{(n_1',m_1')}$, where $t_{(n_1,m_1)\to(n_1',m_1')}$ denotes the time taken for the process to move from state (n_1,m_1) to state (n_1',m_1') in one step, and therefore,

$$\begin{aligned}\phi^{VS}_{(n_1,m_1)}(z) = &\sum_{(n_1',m_1')\in\hat{\Omega}} \mathbb{E}\left[\mathrm{e}^{-zt_{(n_1,m_1)\to(n_1',m_1')}}\middle|(n_1,m_1)\to(n_1',m_1')\right]\cdot \\ &\mathbb{E}\left[\mathrm{e}^{-z\tau^{VS}_{(n_1',m_1')}}\mathbb{1}_{\left\{\tau^{VS}_{(n_1',m_1')}< +\infty\right\}}\right]\mathbb{P}\left((n_1,m_1)\to(n_1',m_1')\right),\end{aligned}$$

where the expectation of the product becomes the product of the expectations due to the independence given by the Markov property, and the second expectation is no longer conditional also due to the Markov property. One has

$$\mathbb{P}\left((n_1,m_1)\to(n_1',m_1')\right) = \frac{q_{(n_1,m_1),(n_1',m_1')}}{R_{(n_1,m_1)}},$$

where

$$R_{(n_1,m_1)} = q_{(n_1,m_1),(n_1+1,m_1)} + q_{(n_1,m_1),(n_1-1,m_1)} + q_{(n_1,m_1),(n_1,m_1+1)} + q_{(n_1,m_1),(n_1,m_1-1)}.$$

Then, as $t_{(n_1,m_1)\to(n_1',m_1')}|(n_1,m_1)\to(n_1',m_1')$ is exponentially distributed with rate $R_{(n_1,m_1)}$ and $\mathbb{E}\left[\mathrm{e}^{-zX}\right] = \frac{\lambda}{\lambda+z}$ if $X\sim Exp(\lambda)$,

$$\mathbb{E}\left[\mathrm{e}^{-zt_{(n_1,m_1)\to(n_1',m_1')}}\middle|(n_1,m_1)\to(n_1',m_1')\right] = \frac{R_{(n_1,m_1)}}{R_{(n_1,m_1)}+z}.$$

Thus, the following system of linear equations is derived:

$$\begin{aligned}\phi^{VS}_{(n_1,m_1)}(z) = &\frac{\beta_1(N_H-n_1)m_1}{R_{(n_1,m_1)}+z}\phi^{VS}_{(n_1+1,m_1)}(z) + \frac{(\mu_1+\varphi_1)n_1}{R_{(n_1,m_1)}+z}\phi^{VS}_{(n_1-1,m_1)}(z)\\ &+ \frac{\gamma_1(N_T-m_1)n_1+\alpha_1(N_T-m_1)m_1}{R_{(n_1,m_1)}+z}\phi^{VS}_{(n_1,m_1+1)}(z)\\ &+ \frac{\nu_1 m_1}{R_{(n_1,m_1)}+z}\phi^{VS}_{(n_1,m_1-1)}(z),\end{aligned} \tag{5.13}$$

which can be rewritten as

$$\begin{aligned}\left(R_{(n_1,m_1)}+z\right)\phi^{VS}_{(n_1,m_1)}(z) = &\beta_1(N_H-n_1)m_1\phi^{VS}_{(n_1+1,m_1)}(z)\\ &+(\mu_1+\varphi_1)n_1\phi^{VS}_{(n_1-1,m_1)}(z)\\ &+\left(\gamma_1(N_T-m_1)n_1+\alpha_1(N_T-m_1)m_1\right)\phi^{VS}_{(n_1,m_1+1)}(z)\\ &+\nu_1 m_1\phi^{VS}_{(n_1,m_1-1)}(z).\end{aligned} \tag{5.14}$$

It is interesting to notice that, for $z=0$, one has

$$\phi^{VS}_{(n_1,m_1)}(0) = \mathbb{E}\left[\mathbb{1}_{\left\{\tau^{VS}_{(n_1,m_1)}<+\infty\right\}}\right] = \mathbb{P}\left(\tau^{VS}_{(n_1,m_1)}<+\infty\right),$$

which is the probability of reaching the virus-free state starting from (n_1,m_1). We introduce the notation $p^{VS}_{(n_1,m_1)} := \mathbb{P}\left(\tau^{VS}_{(n_1,m_1)}<+\infty\right)$. Hence, evaluating equation (5.14) at $z=0$, one obtains the following system of linear equations:

$$\begin{aligned}R_{(n_1,m_1)}p^{VS}_{(n_1,m_1)} = &\beta_1(N_H-n_1)m_1p^{VS}_{(n_1+1,m_1)} + (\mu_1+\varphi_1)n_1p^{VS}_{(n_1-1,m_1)}\\ &+\left(\gamma_1(N_T-m_1)n_1+\alpha_1(N_T-m_1)m_1\right)p^{VS}_{(n_1,m_1+1)} + \nu_1m_1p^{VS}_{(n_1,m_1-1)}.\end{aligned} \tag{5.15}$$

Boundary conditions are given by $p^{VS}_{(0,0)}=1$ and $p^{VS}_{(n_1,m_1)}=0$ if $n_1+m_1=N_{\max}$. We note that reaching any state (n_1,m_1) with $n_1+m_1=N_{\max}$ represents reaching the macro-state E according to its definition. Recall that

$$\mathbb{E}\left[\left(\tau^{VS}_{(n_1,m_1)}\mathbb{1}_{\left\{\tau^{VS}_{(n_1,m_1)}<+\infty\right\}}\right)^l\right] = (-1)^l\frac{\mathrm{d}^l}{\mathrm{d}z^l}\phi^{VS}_{(n_1,m_1)}(z)\bigg|_{z=0}, \quad l\geq 0. \tag{5.16}$$

One notes that, for $l=0$, the 0th derivative of the Laplace-Stieltjes transform corresponds to the probabilities derived in equation (5.15), whereas for $l=1$,

the first derivative of the Laplace-Stieltjes transform corresponds to the first-order moments. In order to simplify the notation, denote the first-order moments as

$$M^{VS}_{(n_1,m_1)} = \mathbb{E}\left[\tau^{VS}_{(n_1,m_1)} \mathbb{1}_{\left\{\tau^{VS}_{(n_1,m_1)} < +\infty\right\}}\right].$$

Differentiating (5.14) with respect to z and evaluating it at $z = 0$, one obtains

$$\begin{aligned} R_{(n_1,m_1)} M^{VS}_{(n_1,m_1)} &= \beta_1(N_H - n_1)m_1 M^{VS}_{(n_1+1,m_1)} + (\mu_1 + \varphi_1)n_1 M^{VS}_{(n_1-1,m_1)} \\ &+ (\gamma_1(N_T - m_1)n_1 + \alpha_1(N_T - m_1)m_1) M^{VS}_{(n_1,m_1+1)} \\ &+ \nu_1 m_1 M^{VS}_{(n_1,m_1-1)} + p^{VS}_{(n_1,m_1)}. \end{aligned} \tag{5.17}$$

Boundary conditions are given by $M^{VS}_{(n_1,m_1)} = 0$ if $n_1 + m_1 = N_{\max}$ because in this case $\mathbb{1}_{\left\{\tau^{VS}_{(n_1,m_1)} < +\infty\right\}} = 0$.

Equation (5.17) shows that, in order to compute $M^{VS}_{(n_1,m_1)}$, it is necessary to first determine the value of $p^{VS}_{(n_1,m_1)}$; that is the computation of the first derivative of the Laplace-Stieltjes transform depends on the 0th derivative of the transform. More broadly, this method could be used to compute higher order moments of the random variable $\tau^{VS}_{(n_1,m_1)} \mathbb{1}_{\left\{\tau^{VS}_{(n_1,m_1)} < +\infty\right\}}$, where the lth derivative of the Laplace-Stieltjes transform depends on the $l-1$th derivative previously computed in an algorithmic fashion. However, our interest is in computing the derivatives defined in equation (5.16) for $l = 0, 1$, which correspond to the probabilities in equation (5.15) and to the first-order moments in equation (5.17), respectively.

We note that the system of equations (5.15) and (5.17) contains one equation for each possible initial state $(n_1, m_1) \in \hat{\Omega}$. Thus, in order to solve this system efficiently, one can write it in matrix form, where the structure of the corresponding matrix of coefficients depends on the ordering of the equations (*i.e.*, of the states in $\hat{\Omega}$). A particularly efficient way of doing this is to organise the state space $\hat{\Omega}$ in sub-sets (here called levels) as follows:

$$\mathscr{L}(j) = \left\{(n_1, m_1) \in \hat{\Omega} : n_1 + m_1 = j\right\}, \quad \hat{\Omega} = \bigcup_{j=1}^{N_{\max}-1} \mathscr{L}(j) \cup \{(0,0)\} \cup E. \tag{5.18}$$

The state space $\hat{\Omega}$ organised in levels is depicted in Figure 5.6. For instance, level $\mathscr{L}(3) = \{(3,0), (2,1), (1,2), (0,3)\}$ consists of the states (n_1, m_1) in $\hat{\Omega}$ such that the number of infected individuals, $n_1 + m_1$, is equal to 3. Thus, if one orders

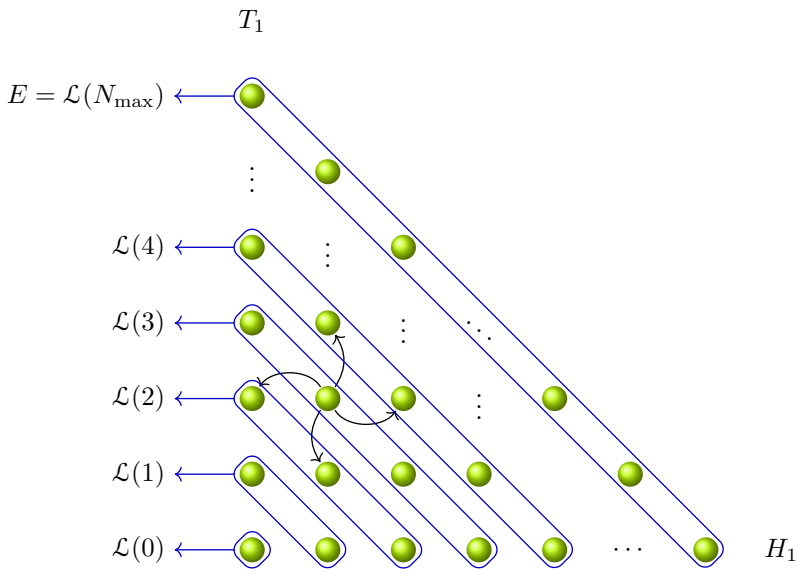

Figure 5.6: The state space $\hat{\Omega}$ is organised in levels according to equation (5.18).

the states by levels with $\mathscr{L}(0) \prec \mathscr{L}(1) \prec \cdots \prec \mathscr{L}(N_{\max} - 1)$, and the states within each level $\mathscr{L}(j)$ as $(j, 0) \prec (j-1, 1) \prec (j-2, 2) \prec \cdots \prec (0, j)$, then it is clear that only transitions between adjacent levels are allowed (see Figure 5.5). In particular, from any state (n_1, m_1) in $\mathscr{L}(j)$, the next event in the Markov chain can take the process to either a state in level $\mathscr{L}(j-1)$ through the death or the viral clearance of an infected host or the death of an infected tick, or a state in level $\mathscr{L}(j+1)$ via a new infection of either a host or a tick. Moreover, from states in level $\mathscr{L}(N_{\max} - 1)$, the process can either move to level $\mathscr{L}(N_{\max} - 2)$ or to the absorbing state E, representing virus establishment. Note that the absorbing state E can be reached only from $\mathscr{L}(N_{\max} - 1)$. On the other hand, the virus-free state $(0, 0)$ can be accessed only from level $\mathscr{L}(1)$, and the process reaching state $(0, 0)$ corresponds to epidemic extinction.

Thus, equations (5.15) and (5.17) can be rewritten in a matrix form as

$$\boldsymbol{X}^{(l)}(VS) = \boldsymbol{A}\boldsymbol{X}^{(l)}(VS) + \boldsymbol{b}^{(l)}(VS), \quad l = 0, 1, \tag{5.19}$$

where VS stands for virus-free state, and where

$$\boldsymbol{X}^{(l)}(VS) = \begin{pmatrix} \boldsymbol{X}_1^{(l)}(VS) \\ \boldsymbol{X}_2^{(l)}(VS) \\ \boldsymbol{X}_3^{(l)}(VS) \\ \vdots \\ \boldsymbol{X}_{N_{\max}-1}^{(l)}(VS) \end{pmatrix}, \qquad \boldsymbol{b}^{(l)}(VS) = \begin{pmatrix} \boldsymbol{b}_1^{(l)}(VS) \\ \boldsymbol{b}_2^{(l)}(VS) \\ \boldsymbol{b}_3^{(l)}(VS) \\ \vdots \\ \boldsymbol{b}_{N_{\max}-1}^{(l)}(VS) \end{pmatrix},$$

$$\boldsymbol{A} = \begin{pmatrix} \mathbf{0} & \boldsymbol{A}_{1,2} & \mathbf{0} & \cdots & \mathbf{0} & \mathbf{0} \\ \boldsymbol{A}_{2,1} & \mathbf{0} & \boldsymbol{A}_{2,3} & \cdots & \mathbf{0} & \mathbf{0} \\ \mathbf{0} & \boldsymbol{A}_{3,2} & \mathbf{0} & \cdots & \mathbf{0} & \mathbf{0} \\ \vdots & \ddots & \ddots & \ddots & \vdots & \vdots \\ \mathbf{0} & \mathbf{0} & \mathbf{0} & \cdots & \mathbf{0} & \boldsymbol{A}_{N_{\max}-2,N_{\max}-1} \\ \mathbf{0} & \mathbf{0} & \mathbf{0} & \cdots & \boldsymbol{A}_{N_{\max}-1,N_{\max}-2} & \mathbf{0} \end{pmatrix}.$$

The sub-vectors $\boldsymbol{X}_j^{(l)}(VS)$ and $\boldsymbol{b}_j^{(l)}(VS)$ that constitute the vectors $\boldsymbol{X}^{(l)}(VS)$ and $\boldsymbol{b}^{(l)}(VS)$ respectively, $l = 0, 1$, have dimensions $j + 1$, with $j = 1, \ldots, N_{\max} - 1$. For $l = 0$, which corresponds to the probabilities in equation (5.15), the sub-vectors $\boldsymbol{X}_j^{(0)}(VS)$ that comprise $\boldsymbol{X}^{(0)}(VS)$ are defined as

$$\boldsymbol{X}_j^{(0)}(VS) = \begin{pmatrix} p_{(j,0)}^{VS} \\ p_{(j-1,1)}^{VS} \\ \vdots \\ p_{(0,j)}^{VS} \end{pmatrix}, \quad j = 1, \ldots, N_{\max} - 1,$$

whereas $\boldsymbol{b}_j^{(0)}(VS) = \mathbf{0}$ if $j > 1$ and

$$\boldsymbol{b}_1^{(0)}(VS) = \begin{pmatrix} \dfrac{\mu_1 + \varphi_1}{R_{(1,0)}} \\ \dfrac{\nu_1}{R_{(0,1)}} \end{pmatrix}.$$

In the instance of equations (5.17), which correspond to $l = 1$, the sub-vectors in $\boldsymbol{X}^{(1)}(VS)$ are given by

$$\boldsymbol{X}_j^{(1)}(VS) = \begin{pmatrix} M_{(j,0)}^{VS} \\ M_{(j-1,1)}^{VS} \\ \vdots \\ M_{(0,j)}^{VS} \end{pmatrix}, \quad j = 1, \ldots, N_{\max} - 1,$$

and $\boldsymbol{b}^{(1)}(VS)$ consists of sub-vectors defined as

$$\boldsymbol{b}_j^{(1)}(VS) = \begin{pmatrix} \dfrac{p^{VS}_{(j,0)}}{R_{(j,0)}} \\ \dfrac{p^{VS}_{(j-1,1)}}{R_{(j-1,1)}} \\ \vdots \\ \dfrac{p^{VS}_{(0,j)}}{R_{(0,j)}} \end{pmatrix}, \quad j = 1, \ldots, N_{\max} - 1.$$

The blocks that comprise the matrix $\boldsymbol{A}$, $\boldsymbol{A}_{k+1,k}$ and $\boldsymbol{A}_{k,k+1}$, have dimensions $(k+2) \times (k+1)$ and $(k+1) \times (k+2)$ respectively, and are defined as follows:

- For $k = 1, \ldots, N_{\max} - 2$:

$$(\boldsymbol{A}_{k+1,k})_{i+1,j+1} = \begin{cases} \dfrac{(k+1-i)(\mu_1 + \varphi_1)}{R_{(k+1-i,i)}}, & \text{if } i = j, \\ \dfrac{i\nu_1}{R_{(k+1-i,i)}}, & \text{if } i = j+1, \\ 0, & \text{otherwise,} \end{cases}$$

  where $i = 0, \ldots, k+1$ and $j = 0, \ldots, k$.

- For $k = 1, \ldots, N_{\max} - 2$:

$$(\boldsymbol{A}_{k,k+1})_{i+1,j+1} = \begin{cases} \dfrac{((k-i)\gamma_1 + i\alpha_1)(N_T - i)}{R_{(k-i,i)}}, & \text{if } i = j-1, \\ \dfrac{i\beta_1(N_H + i - k)}{R_{(k-i,i)}}, & \text{if } i = j, \\ 0, & \text{otherwise,} \end{cases}$$

  where $i = 0, \ldots, k$ and $j = 0, \ldots, k+1$.

Let $\boldsymbol{I}_k$ denote the identity matrix of order k. Equation (5.19) can then be solved efficiently using Algorithm 4 based on a forward-elimination backward-substitution solution suggested by Ciarlet *et al.* (1989) (see page 144) to obtain $p^{VS}_{(n_1,m_1)}$ and $M^{VS}_{(n_1,m_1)}$ for any initial state $(n_1, m_1) \in \hat{\Omega}$.

Algorithm 4 Probability of $(l = 0)$, and conditional time to $(l = 1)$, virus-free state

$\boldsymbol{H}_2 = (\boldsymbol{I}_3 - \boldsymbol{A}_{2,1}\boldsymbol{A}_{1,2})^{-1}$.
$\boldsymbol{J}_2^{(l)} = \boldsymbol{A}_{2,1}\boldsymbol{b}_1^{(l)} + \boldsymbol{b}_2^{(l)}$.
for $k = 3, \ldots, N_{\max} - 1$ **do**:
    $\boldsymbol{H}_k = (\boldsymbol{I}_{k+1} - \boldsymbol{A}_{k,k-1}\boldsymbol{H}_{k-1}\boldsymbol{A}_{k-1,k})^{-1}$.
    $\boldsymbol{J}_k^{(l)} = \boldsymbol{A}_{k,k-1}\boldsymbol{H}_{k-1}\boldsymbol{J}_{k-1}^{(l)} + \boldsymbol{b}_k^{(l)}$.
end for
$\boldsymbol{X}_{N_{\max}-1}^{(l)} = \boldsymbol{H}_{N_{\max}-1}\boldsymbol{J}_{N_{\max}-1}^{(l)}$.
for $k = N_{\max} - 2, \ldots, 1$ **do**:
    $\boldsymbol{X}_k^{(l)} = \boldsymbol{H}_k(\boldsymbol{J}_k^{(l)} + \boldsymbol{A}_{k,k+1}\boldsymbol{X}_{k+1}^{(l)})$.
end for
return $\boldsymbol{X}^{(l)} = ((\boldsymbol{X}_1^{(l)})^T, \ldots, (\boldsymbol{X}_{N_{\max}-1}^{(l)})^T)^T$.

Once $M_{(n_1,m_1)}^{VS}$ is at hand, invoking the law of total expectation, one has

$$\begin{aligned} M_{(n_1,m_1)}^{VS} &= \mathbb{E}\left[\tau_{(n_1,m_1)}^{VS}\mathbb{1}_{\left\{\tau_{(n_1,m_1)}^{VS} < +\infty\right\}}\middle|\tau_{(n_1,m_1)}^{VS} < +\infty\right]\mathbb{P}\left(\tau_{(n_1,m_1)}^{VS} < +\infty\right) \\ &+ \mathbb{E}\left[\tau_{(n_1,m_1)}^{VS}\mathbb{1}_{\left\{\tau_{(n_1,m_1)}^{VS} < +\infty\right\}}\middle|\tau_{(n_1,m_1)}^{VS} = +\infty\right]\mathbb{P}\left(\tau_{(n_1,m_1)}^{VS} = +\infty\right) \\ &= \mathbb{E}\left[\tau_{(n_1,m_1)}^{VS}\middle|\tau_{(n_1,m_1)}^{VS} < +\infty\right]\mathbb{P}\left(\tau_{(n_1,m_1)}^{VS} < +\infty\right), \end{aligned}$$

which yields

$$\mathcal{T}_{(n_1,m_1)}^{VS} = \mathbb{E}\left[\tau_{(n_1,m_1)}^{VS}\middle|\tau_{(n_1,m_1)}^{VS} < +\infty\right] = \frac{M_{(n_1,m_1)}^{VS}}{p_{(n_1,m_1)}^{VS}}, \tag{5.20}$$

that represents the conditional expected time to reach the virus-free state from any initial state $(n_1, m_1) \in \hat{\Omega}$ conditioned on the process actually reaching this absorbing state.

Figures 5.7 and 5.8 show respectively the probability of reaching the virus-free state $(0, 0)$ and the expected time to reach the virus-free state conditioned on the process actually reaching this absorbing state for different values of the transmission parameters β_1, γ_1 and α_1, and initial conditions. The parameter that encapsulates co-feeding transmission, α_1, varies as 10^{-6} (left column), 10^{-5} (central column) and 10^{-4} (right column). The stochastic descriptors are computed starting with

only one infected host (first row), two infected hosts (second row) and three infected hosts (third row). The values of γ_1 and β_1 vary between 0 and 5×10^{-3} along the x-axis and y-axis of each plot. As shown in Figure 5.7, one observes that the virus-free state $(0, 0)$ is more likely to be reached when the parameters α_1, β_1 and γ_1 are small (as in the yellow area of the plots of the left and central columns). In the left and central column plots, the curve that marks the sharp gradient from the yellow area to the green/blue one represents the combination of parameters for which the basic reproduction number R_0 is equal to 1. Thus, when $R_0 < 1$ (yellow area), the process reaches the virus-free state, whereas for $R_0 > 1$ (green/blue area) the virus may become endemic. Conversely to the deterministic model in Section 5.1.1, the stochastic approach presented here allows us to compute the probability of virus extinction even when $R_0 > 1$. On the other hand, for larger values of the co-feeding transmission α_1 (right column), R_0 is always greater than 1, and the host-to-tick transmission parameter γ_1 affects the probability $p^{VS}_{(n_1,m_1)}$ more than β_1, which corresponds to tick-to-host transmission. This is explained by the initial conditions, that consider only infected hosts. Indeed in this situation, there are no infected ticks that can transmit the virus to susceptible hosts. It is also interesting to notice that, when the initial number of infected hosts increases (second and third row), the system more closely resembles the deterministic behaviour. Indeed, the gradient decay from yellow to blue (*i.e.*, $R_0 < 1$ and $R_0 > 1$, respectively) is sharper for increasing values of the initial number of hosts, n_1. On the contrary, when the virus is introduced into the system through a single infected host (first row), the stochasticity of the potential short-term extinction event is more significant. Regarding the conditional time to reach the virus-free state conditioned on actually reaching this fate depicted in Figure 5.8, one notes that the process takes a long time to reach the virus-free state for those parameter values such that $R_0 \approx 1$, particularly when γ_1 increases. Indeed, more ticks become infected for larger values of γ_1. Conversely to hosts, ticks remain infected for their lifetime. Thus, a longer time is needed for the system to become virus-free because of the time infected ticks require to be removed. Overall, the factors that affect the most the probability of virus extinction (*i.e.*, the process reaching the absorbing state $(0, 0)$) and the timescale to reach this fate is the basic reproduction number R_0 being smaller or greater than 1 and the initial conditions.

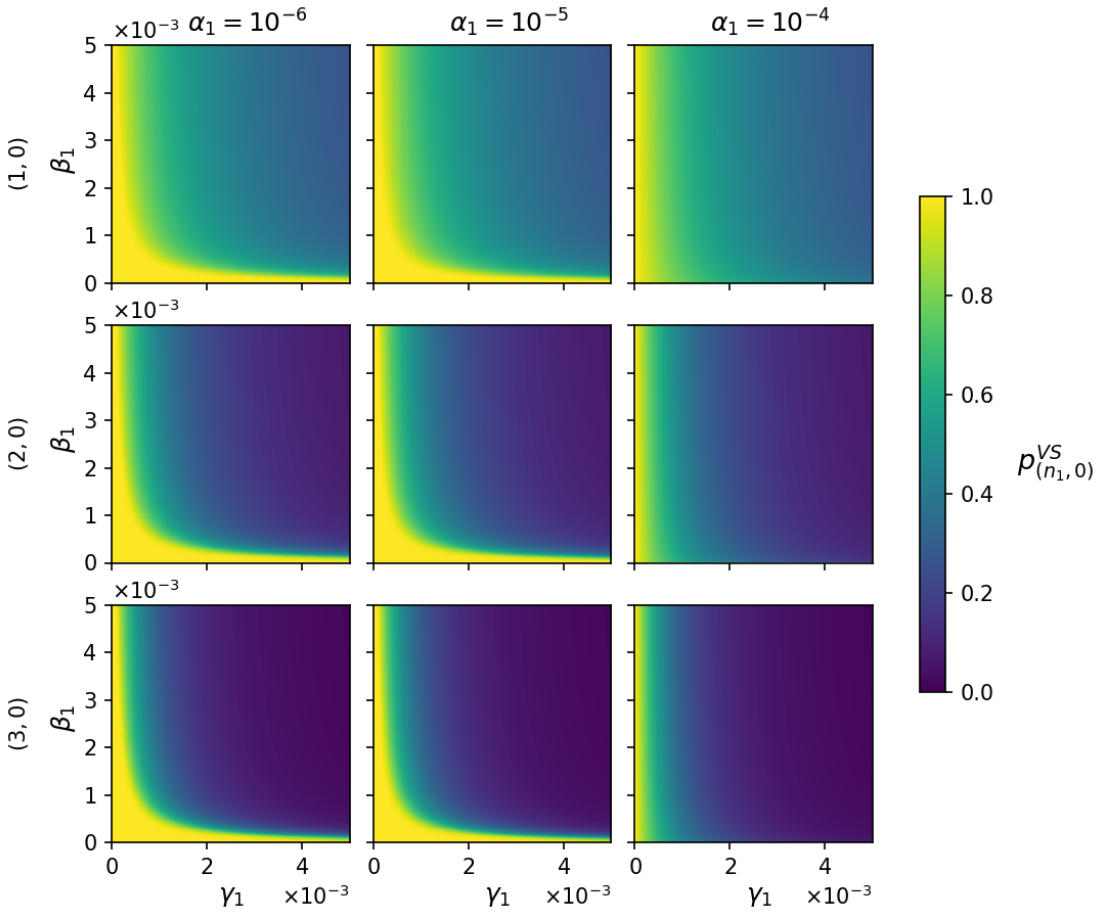

Figure 5.7: The probability of reaching the virus-free state, $p^{VS}_{(n_1,m_1)}$, computed in equation (5.19) for $l = 0$, is plotted for different values of the transmission parameters α_1 (1/Days/Tick), β_1 (1/Days/Tick) and γ_1 (1/Days/Host), and initial conditions. The co-feeding transmission parameter, α_1, varies as 10^{-6} (left column), 10^{-5} (central column) and 10^{-4} (right column). The probability $p^{VS}_{(n_1,m_1)}$ is computed starting with only one infected host (first row), two infected hosts (second row) and three infected hosts (third row). The values of γ_1 and β_1 vary between 0 and 5×10^{-3} along the x-axis and y-axis of each plot. The other parameters are fixed as follows: $N_H = 20$, $N_T = 10^2$, $N_{\max} = 20$, $\mu_1 = 1/(4 \times 365)$ 1/Days, $\varphi_1 = 1/6$ 1/Days and $\nu_1 = 1/200$ 1/Days.

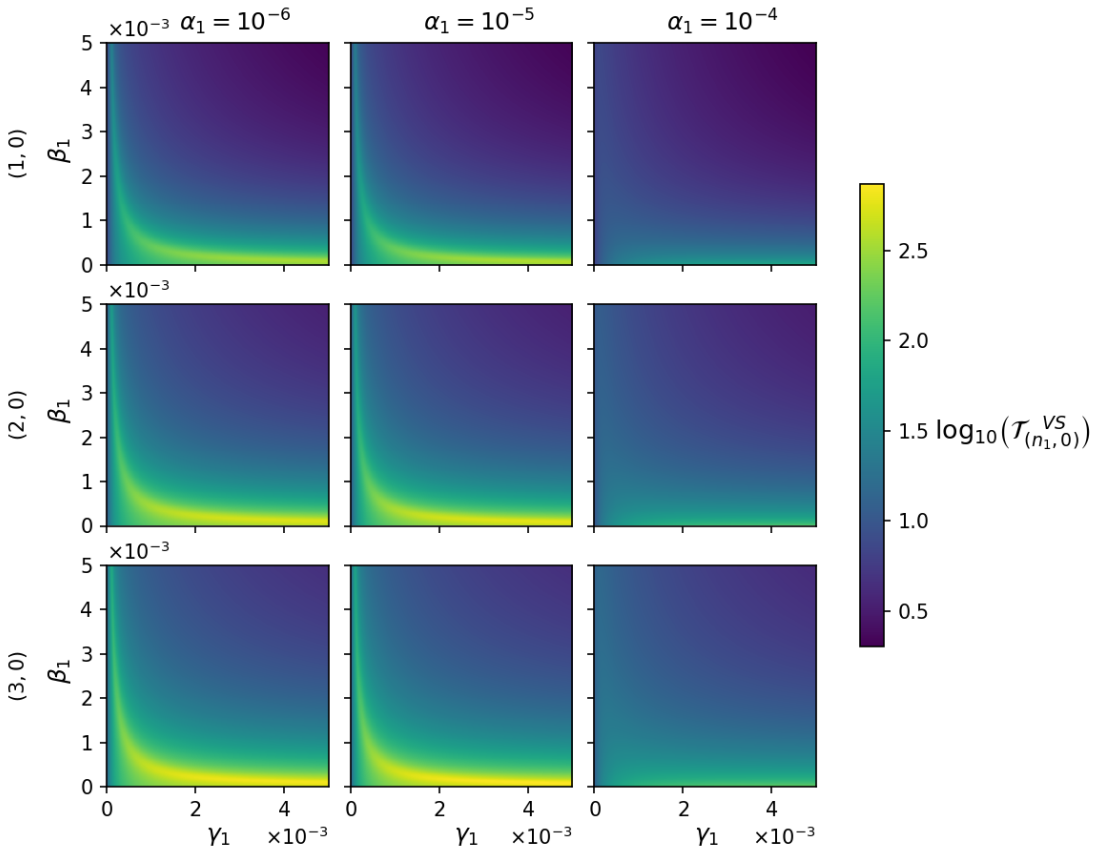

Figure 5.8: The expected time to reach the virus-free state $(0, 0)$ conditioned on actually reaching this fate, $\mathfrak{T}^{VS}_{(n_1,m_1)}$, computed in equation (5.20), is plotted for different values of the transmission parameters α_1 (1/Days/Tick), β_1 (1/Days/Tick) and γ_1 (1/Days/Host), and initial conditions. The co-feeding transmission parameter, α_1, varies as 10^{-6} (left column), 10^{-5} (central column) and 10^{-4} (right column). The conditional time $\mathfrak{T}^{VS}_{(n_1,m_1)}$ is computed starting with only one infected host (first row), two infected hosts (second row) and three infected hosts (third row). The values of γ_1 and β_1 vary between 0 and 5×10^{-3} along the x-axis and y-axis of each plot. The other parameters are fixed as follows: $N_H = 20$, $N_T = 10^2$, $N_{\max} = 20$, $\mu_1 = 1/(4 \times 365)$ 1/Days, $\varphi_1 = 1/6$ 1/Days and $\nu_1 = 1/200$ 1/Days.

On the other hand, one could define for $(n_1, m_1) \in \hat{\Omega}$

$$\tau^E_{(n_1,m_1)} = \inf\{t \geq 0 : H_1(t) + T_1(t) = N_{\max} | (H_1(0), T_1(0)) = (n_1, m_1)\},$$

that is the time to reach the absorbing macro-state E (*i.e.*, virus establishment) starting with n_1 infected hosts and m_1 infected ticks. The probability of virus establishment and the expected time to virus establishment conditioned on actually reaching this fate can be computed starting from any initial state $(n_1, m_1) \in \hat{\Omega}$. This can be obtained from the Laplace-Stieltjes transform of $\tau^E_{(n_1,m_1)}$ defined as

$$\phi^E_{(n_1,m_1)}(z) = \mathbb{E}\left[\mathrm{e}^{-z\tau^E_{(n_1,m_1)}} \mathbb{1}_{\left\{\tau^E_{(n_1,m_1)} < +\infty\right\}}\right], \quad \mathrm{Re}(z) \geq 0.$$

Similarly to the case of virus-free state, define

$$\begin{aligned} M^E_{(n_1,m_1)} &= \mathbb{E}\left[\tau^E_{(n_1,m_1)} \mathbb{1}_{\left\{\tau^E_{(n_1,m_1)} < +\infty\right\}}\right], \\ p^E_{(n_1,m_1)} &= \mathbb{P}\left(\tau^E_{(n_1,m_1)} < +\infty\right). \end{aligned}$$

Following the same steps illustrated for $\phi^{VS}_{(n_1,m_1)}(z)$, one obtains the analogous system of linear equations derived in equations (5.15) and (5.17) for $p^E_{(n_1,m_1)}$ and $M^E_{(n_1,m_1)}$ respectively. Note that

$$p^E_{(n_1,m_1)} = 1 - p^{VS}_{(n_1,m_1)}, \quad \text{for all } (n_1, m_1) \in \hat{\Omega},$$

therefore only the analogous of system (5.17) has to be solved to find $M^E_{(n_1,m_1)}$. This system of equations can be rewritten in matrix form using the order of the state space described in equation (5.18) as

$$\boldsymbol{X}^{(l)}(E) = \boldsymbol{A}\boldsymbol{X}^{(l)}(E) + \boldsymbol{b}^{(l)}(E), \quad l = 1. \tag{5.21}$$

The same matrix $\boldsymbol{A}$ is derived, whereas the sub-vectors that comprise $\boldsymbol{X}^{(1)}(E)$ are defined as

$$\boldsymbol{X}^{(1)}_j(E) = \begin{pmatrix} M^E_{(j,0)} \\ M^E_{(j-1,1)} \\ \vdots \\ M^E_{(0,j)} \end{pmatrix}, \quad j = 1, \ldots, N_{\max} - 1,$$

whereas the sub-vectors of $\boldsymbol{b}^{(1)}(E)$ are given by

$$\boldsymbol{b}_j^{(1)}(E) = \begin{pmatrix} \dfrac{p^E_{(j,0)}}{R_{(j,0)}} \\ \dfrac{p^E_{(j-1,1)}}{R_{(j-1,1)}} \\ \vdots \\ \dfrac{p^E_{(0,j)}}{R_{(0,j)}} \end{pmatrix}, \quad j = 1, \ldots, N_{\max} - 1.$$

Note that the sub-vectors $\boldsymbol{X}_j^{(1)}(E)$ and $\boldsymbol{b}_j^{(1)}(E)$ have dimension $j+1$, with $j = 1, \ldots, N_{\max} - 1$. Algorithm 4 can be then adapted to solve equation (5.21) to compute $M^E_{(n_1,m_1)}$, as well as the expected time to reach an endemic state conditioned on the process actually reaching this absorbing state, for any initial state $(n_1, m_1) \in \hat{\Omega}$.

Distribution of the exact number of secondary infections

In Section 5.1.1, the basic reproduction number, that is, the average number of new infections generated by one infected individual in a susceptible population, is computed by means of the next-generation matrix approach. From an epidemiological perspective, one could also be interested in deriving the distribution of the exact number of secondary infections directly caused by a *marked* infected individual (Artalejo & Lopez-Herrero, 2013). To this end, let us define the following random variables

- $\Lambda^T(T)$ = number of ticks directly infected by a marked infected tick until the marked tick is removed, or the process is absorbed in E.
- $\Lambda^T(H)$ = number of hosts directly infected by a marked infected tick until the marked tick is removed, or the process is absorbed in E.
- $\Lambda^H(T)$ = number of ticks directly infected by a marked infected host until the marked host is removed, or the process is absorbed in E.

Note that, when the threshold of the total number of infected individuals $N_{\max}$ is sufficiently large, the three random variables defined above represent the exact number of secondary infections caused by a marked individual. Also, by defining the random variables above in this way, and in those situations where the virus becomes established in the population (*i.e.*, trajectories where the threshold number of infected individuals $N_{\max}$ is reached), these random variables allow us to quantify the contribution that the marked individual of interest makes to reach this threshold value.

For $n \in \mathbb{N}_0$ and any state $(n_1, m_1) \in \hat{\Omega}$, define the probabilities

$$\begin{aligned}
\rho^{TT}_{(n_1,m_1)}(n) &= \mathbb{P}\left(\Lambda^T(T) = n \middle| (H_1(0), T_1(0)) = (n_1, m_1), m_1 \neq 0\right), \\
\rho^{TH}_{(n_1,m_1)}(n) &= \mathbb{P}\left(\Lambda^T(H) = n \middle| (H_1(0), T_1(0)) = (n_1, m_1), m_1 \neq 0\right), \\
\rho^{HT}_{(n_1,m_1)}(n) &= \mathbb{P}\left(\Lambda^H(T) = n \middle| (H_1(0), T_1(0)) = (n_1, m_1), n_1 \neq 0\right).
\end{aligned}$$

For example, if $n = 4$, $\rho^{TT}_{(n_1,m_1)}(4)$ is the probability that a marked infected tick transmits the virus to exactly 4 susceptible ticks during its lifetime (or before the macro-state E is reached). Let first analyse $\rho^{TT}_{(n_1,m_1)}(n)$. When considering the possible stochastic events representing the infection of a susceptible tick or the death of an infected tick, two different scenarios are distinguished. In particular, if there are m_1 infected ticks and a susceptible tick becomes infected, this new infection is caused by the marked tick with probability $1/m_1$ (since all the infected ticks are identical in our stochastic process). Similarly, if an infected tick dies, one considers that the marked tick is the one that dies with probability $1/m_1$. In light of this and by means of a first step argument, one obtains for $n = 0$

$$\begin{aligned}
\rho^{TT}_{(n_1,m_1)}(0) = {} & \frac{\beta_1(N_H - n_1)m_1}{R_{(n_1,m_1)}}\rho^{TT}_{(n_1+1,m_1)}(0) + \frac{(\mu_1 + \varphi_1)n_1}{R_{(n_1,m_1)}}\rho^{TT}_{(n_1-1,m_1)}(0) \\
& + \frac{\gamma_1(N_T - m_1)n_1 + \alpha_1(N_T - m_1)(m_1 - 1)}{R_{(n_1,m_1)}}\rho^{TT}_{(n_1,m_1+1)}(0) \\
& + \frac{\nu_1(m_1 - 1)}{R_{(n_1,m_1)}}\rho^{TT}_{(n_1,m_1-1)}(0) + \frac{\nu_1}{R_{(n_1,m_1)}},
\end{aligned} \tag{5.22}$$

with boundary conditions $\rho^{TT}_{(0,0)}(0) = 1$ and $\rho^{TT}_E(0) = 1$. On the other hand, for

$n \geq 1$, one has

$$\begin{aligned}\rho^{TT}_{(n_1,m_1)}(n) = &\frac{\beta_1(N_H - n_1)m_1}{R_{(n_1,m_1)}}\rho^{TT}_{(n_1+1,m_1)}(n) + \frac{(\mu_1+\varphi_1)n_1}{R_{(n_1,m_1)}}\rho^{TT}_{(n_1-1,m_1)}(n)\\ &+ \frac{\gamma_1(N_T - m_1)n_1 + \alpha_1(N_T - m_1)(m_1-1)}{R_{(n_1,m_1)}}\rho^{TT}_{(n_1,m_1+1)}(n)\\ &+ \frac{\alpha_1(N_T - m_1)}{R_{(n_1,m_1)}}\rho^{TT}_{(n_1,m_1+1)}(n-1) + \frac{\nu_1(m_1-1)}{R_{(n_1,m_1)}}\rho^{TT}_{(n_1,m_1-1)}(n),\end{aligned} \tag{5.23}$$

with boundary conditions $\rho^{TT}_{(0,0)}(n) = 0$ and $\rho^{TT}_{E}(n) = 0$. A direct inspection of equations (5.22) and (5.23) shows that one can start by solving (5.22) for $n = 0$, and then solve equation (5.23) sequentially for $n = 1$, then $n = 2, 3, \ldots$. Similarly to the approach showed for the other stochastic descriptors in the previous section, equations (5.22) and (5.23) are rewritten in a matrix form. In order to do so, the state space is organised as illustrated in equation (5.18). Note that the distribution of $\Lambda^T(T)$ can be derived for any initial state $(n_1, m_1) \in \hat{\Omega}$ such that $m_1 \neq 0$ because at least one infected tick is required by definition (since $\Lambda^T(T)$ is defined for a marked infected tick). Thus, equations (5.22) and (5.23) can be rewritten in matrix form as

$$\boldsymbol{Y}^{TT}(n) = \boldsymbol{B}^{TT}\boldsymbol{Y}^{TT}(n) + \boldsymbol{b}^{TT}(n), \quad n \in \mathbb{N}_0, \tag{5.24}$$

where

$$\boldsymbol{Y}^{TT}(n) = \begin{pmatrix} \boldsymbol{Y}^{TT}_1(n) \\ \boldsymbol{Y}^{TT}_2(n) \\ \boldsymbol{Y}^{TT}_3(n) \\ \vdots \\ \boldsymbol{Y}^{TT}_{N_{\max}-1}(n) \end{pmatrix}, \qquad \boldsymbol{b}^{TT}(n) = \begin{pmatrix} \boldsymbol{b}^{TT}_1(n) \\ \boldsymbol{b}^{TT}_2(n) \\ \boldsymbol{b}^{TT}_3(n) \\ \vdots \\ \boldsymbol{b}^{TT}_{N_{\max}-1}(n) \end{pmatrix},$$

and the matrix $\boldsymbol{B}^{TT}$ is defined as

$$\boldsymbol{B}^{TT} = \begin{pmatrix} \boldsymbol{0} & \boldsymbol{B}^{TT}_{1,2} & \boldsymbol{0} & \cdots & \boldsymbol{0} & \boldsymbol{0} \\ \boldsymbol{B}^{TT}_{2,1} & \boldsymbol{0} & \boldsymbol{B}^{TT}_{2,3} & \cdots & \boldsymbol{0} & \boldsymbol{0} \\ \boldsymbol{0} & \boldsymbol{B}^{TT}_{3,2} & \boldsymbol{0} & \cdots & \boldsymbol{0} & \boldsymbol{0} \\ \vdots & \ddots & \ddots & \ddots & \vdots & \vdots \\ \boldsymbol{0} & \boldsymbol{0} & \boldsymbol{0} & \cdots & \boldsymbol{0} & \boldsymbol{B}^{TT}_{N_{\max}-2,N_{\max}-1} \\ \boldsymbol{0} & \boldsymbol{0} & \boldsymbol{0} & \cdots & \boldsymbol{B}^{TT}_{N_{\max}-1,N_{\max}-2} & \boldsymbol{0} \end{pmatrix}.$$

The sub-vectors $\boldsymbol{Y}_j^{TT}(n)$ and $\boldsymbol{b}_j^{TT}(n)$ that constitute the vectors $\boldsymbol{Y}^{TT}(n)$ and $\boldsymbol{b}^{TT}(n)$ respectively, have dimension j, with $j = 1, \ldots, N_{\max} - 1$. In particular, the sub-vectors $\boldsymbol{Y}_j^{TT}(n)$, $n \in \mathbb{N}_0$, are defined as

$$\boldsymbol{Y}_j^{TT}(n) = \begin{pmatrix} \rho_{(j-1,1)}^{TT}(n) \\ \rho_{(j-2,2)}^{TT}(n) \\ \vdots \\ \rho_{(0,j)}^{TT}(n) \end{pmatrix}, \quad j = 1, \ldots, N_{\max} - 1.$$

Vector $\boldsymbol{b}^{TT}(n)$, $n \in \mathbb{N}_0$, is organised in sub-vectors $\boldsymbol{b}_j^{TT}(n)$ of dimension j, $j = 1, \ldots, N_{\max} - 1$. If $n \geq 1$, one has

$$\boldsymbol{b}_j^{TT}(n) = \begin{pmatrix} \dfrac{\alpha_1(N_T - 1)\rho_{(j-1,2)}^{TT}(n-1)}{R_{(j-1,1)}} \\ \dfrac{\alpha_1(N_T - 2)\rho_{(j-2,3)}^{TT}(n-1)}{R_{(j-2,2)}} \\ \vdots \\ \dfrac{\alpha_1(N_T - j)\rho_{(0,j+1)}^{TT}(n-1)}{R_{(0,j)}} \end{pmatrix}, \quad j = 1, \ldots, N_{\max} - 2.$$

For $j = N_{\max} - 1$, the sub-vector $\boldsymbol{b}_{N_{\max}-1}^{TT}(n) = \boldsymbol{0}$ if $n \geq 2$, whereas

$$\boldsymbol{b}_{N_{\max}-1}^{TT}(1) = \begin{pmatrix} \dfrac{\alpha_1(N_T - 1)}{R_{(N_{\max}-2,1)}} \\ \dfrac{\alpha_1(N_T - 2)}{R_{(N_{\max}-3,2)}} \\ \vdots \\ \dfrac{\alpha_1(N_T - N_{\max} + 1)}{R_{(0,N_{\max}-1)}} \end{pmatrix}.$$

If $n = 0$, one has

$$\boldsymbol{b}_j^{TT}(0) = \begin{pmatrix} \dfrac{\nu_1}{R_{(j-1,1)}} \\ \dfrac{\nu_1}{R_{(j-2,2)}} \\ \vdots \\ \dfrac{\nu_1}{R_{(0,j)}} \end{pmatrix}, \; j = 1, \ldots, N_{\max} - 2,$$

and

$$\boldsymbol{b}^{TT}_{N_{\max}-1}(0) = \begin{pmatrix} \dfrac{\nu_1 + (N_{\max}-2)\gamma_1(N_T-1)}{R_{(N_{\max}-2,1)}} \\ \dfrac{\nu_1 + ((N_{\max}-3)\gamma_1 + \alpha_1)(N_T-2)}{R_{(N_{\max}-3,2)}} \\ \vdots \\ \dfrac{\nu_1 + (N_{\max}-1)\alpha_1(N_T-N_{\max}+1)}{R_{(0,N_{\max}-1)}} \end{pmatrix}.$$

The blocks that comprise the matrix $\boldsymbol{B}^{TT}$, $\boldsymbol{B}^{TT}_{k+1,k}$ and $\boldsymbol{B}^{TT}_{k,k+1}$, have dimensions $(k+1)\times k$ and $k\times(k+1)$ respectively, and are defined as follows:

- For $k = 1,\ldots,N_{\max}-2$:

$$(\boldsymbol{B}^{TT}_{k+1,k})_{i+1,j+1} = \begin{cases} \dfrac{(k-i)(\mu_1+\varphi_1)}{R_{(k-i,i+1)}}, & \text{if } i=j, \\ \dfrac{i\nu_1}{R_{(k-i,i+1)}}, & \text{if } i=j+1, \\ 0, & \text{otherwise,} \end{cases}$$

  where $i = 0,\ldots,k$ and $j = 0,\ldots,k-1$.

- For $k = 1,\ldots,N_{\max}-2$:

$$(\boldsymbol{B}^{TT}_{k,k+1})_{i+1,j+1} = \begin{cases} \dfrac{(i+1)\beta_1(N_H-k+i+1)}{R_{(k-i-1,i+1)}}, & \text{if } i=j, \\ \dfrac{((k-j)\gamma_1+i\alpha_1)(N_T-i-1)}{R_{(k-i-1,i+1)}}, & \text{if } i=j-1, \\ 0, & \text{otherwise,} \end{cases}$$

  where $i = 0,\ldots,k-1$ and $j = 0,\ldots,k$.

Equation (5.24) can then be solved efficiently by means of Algorithm 5, which is an adaptation of Algorithm 4, to obtain the probability distribution of $\Lambda^T(T)$. The underlying idea is to compute first $\rho^{TT}_{(n_1,m_1)}(0)$, and then $\rho^{TT}_{(n_1,m_1)}(n)$ for $n \geq 1$. Consider now $\rho^{TH}_{(n_1,m_1)}(n)$. When considering the possible stochastic events representing the infection of a susceptible host, or the death of an infected tick, two different scenarios are distinguished. In particular, if there are m_1 infected ticks and a susceptible host becomes infected, this new infection is caused by the marked tick with probability $1/m_1$. Similarly, if an infected tick dies, one considers that

Algorithm 5 Distribution of $\Lambda^T(T)$

Define $\tilde{n}$ as the maximum $n \in \mathbb{N}_0$ for which $\rho^{TT}_{(n_1,m_1)}(n)$ is computed.
for $n = 0, \dots, \tilde{n}$ **do**:
    $\boldsymbol{H}_2 = (\boldsymbol{I}_2 - \boldsymbol{B}^{TT}_{2,1}\boldsymbol{B}^{TT}_{1,2})^{-1}$.
    $\boldsymbol{J}_2(n) = \boldsymbol{B}^{TT}_{2,1}\boldsymbol{b}^{TT}_1(n) + \boldsymbol{b}^{TT}_2(n)$.
    for $k = 3, \dots, N_{\max} - 1$ **do**:
        $\boldsymbol{H}_k = (\boldsymbol{I}_{k+1} - \boldsymbol{B}^{TT}_{k,k-1}\boldsymbol{H}_{k-1}\boldsymbol{B}^{TT}_{k-1,k})^{-1}$.
        $\boldsymbol{J}_k(n) = \boldsymbol{B}^{TT}_{k,k-1}\boldsymbol{H}_{k-1}\boldsymbol{J}_{k-1}(n) + \boldsymbol{b}^{TT}_k(n)$.
    end for
    $\boldsymbol{Y}^{TT}_{N_{\max}-1}(n) = \boldsymbol{H}_{N_{\max}-1}\boldsymbol{J}_{N_{\max}-1}(n)$.
    for $k = N_{\max} - 2, \dots, 1$ **do**:
        $\boldsymbol{Y}^{TT}_k(n) = \boldsymbol{H}_k(\boldsymbol{J}_k(n) + \boldsymbol{B}^{TT}_{k,k+1}\boldsymbol{Y}^{TT}_{k+1}(n))$.
    end for
    return $\boldsymbol{Y}^{TT}(n) = ((\boldsymbol{Y}^{TT}_1(n))^T, \dots, (\boldsymbol{Y}^{TT}_{N_{\max}-1}(n))^T)^T$.
end for

the marked tick is the one that dies with probability $1/m_1$. Thus, the first step equation for $\rho^{TH}_{(n_1,m_1)}(0)$ is obtained as

$$\begin{aligned}\rho^{TH}_{(n_1,m_1)}(0) = {} & \frac{\gamma_1(N_T - m_1)n_1 + \alpha_1(N_T - m_1)m_1}{R_{(n_1,m_1)}}\rho^{TH}_{(n_1,m_1+1)}(0) \\ & + \frac{\nu_1(m_1-1)}{R_{(n_1,m_1)}}\rho^{TH}_{(n_1,m_1-1)}(0) + \frac{(\mu_1+\varphi_1)n_1}{R_{(n_1,m_1)}}\rho^{TH}_{(n_1-1,m_1)}(0) \\ & + \frac{\beta_1(N_H - n_1)(m_1-1)}{R_{(n_1,m_1)}}\rho^{TH}_{(n_1+1,m_1)}(0) + \frac{\nu_1}{R_{(n_1,m_1)}}.\end{aligned} \tag{5.25}$$

with boundary conditions $\rho^{TH}_{(0,0)}(0) = 1$ and $\rho^{TH}_E(0) = 1$. On the other hand, for $n \geq 1$, a first step argument yields

$$\begin{aligned}\rho^{TH}_{(n_1,m_1)}(n) = {} & \frac{\gamma_1(N_T - m_1)n_1 + \alpha_1(N_T - m_1)m_1}{R_{(n_1,m_1)}}\rho^{TH}_{(n_1,m_1+1)}(n) \\ & + \frac{\nu_1(m_1-1)}{R_{(n_1,m_1)}}\rho^{TH}_{(n_1,m_1-1)}(n) + \frac{(\mu_1+\varphi_1)n_1}{R_{(n_1,m_1)}}\rho^{TH}_{(n_1-1,m_1)}(n) \\ & + \frac{\beta_1(N_H - n_1)}{R_{(n_1,m_1)}}\rho^{TH}_{(n_1+1,m_1)}(n-1) + \frac{\beta_1(N_H - n_1)(m_1-1)}{R_{(n_1,m_1)}}\rho^{TH}_{(n_1+1,m_1)}(n),\end{aligned} \tag{5.26}$$

with boundary conditions $\rho^{TH}_{(0,0)}(n) = 0$ and $\rho^{TH}_{E}(n) = 0$. We will first derive $\rho^{TH}_{(n_1,m_1)}(0)$ and then sequentially $\rho^{TH}_{(n_1,m_1)}(n)$ for $n \geq 1$. In order to write the previous equations (5.25) and (5.26) in matrix form, the state space is organised as illustrated in equation (5.18). Observe that the distribution of $\Lambda^T(H)$ can be derived for any initial state $(n_1, m_1) \in \hat{\Omega}$ such that $m_1 \neq 0$ because at least one infected tick is required by definition (since $\Lambda^T(H)$ is defined for a marked infected tick). Thus, equations (5.25) and (5.26) can be rewritten in matrix form as

$$\boldsymbol{Y}^{TH}(n) = \boldsymbol{B}^{TH}\boldsymbol{Y}^{TH}(n) + \boldsymbol{b}^{TH}(n), \quad n \in \mathbb{N}_0, \tag{5.27}$$

where

$$\boldsymbol{Y}^{TH}(n) = \begin{pmatrix} \boldsymbol{Y}^{TH}_1(n) \\ \boldsymbol{Y}^{TH}_2(n) \\ \boldsymbol{Y}^{TH}_3(n) \\ \vdots \\ \boldsymbol{Y}^{TH}_{N_{\max}-1}(n) \end{pmatrix}, \qquad \boldsymbol{b}^{TH}(n) = \begin{pmatrix} \boldsymbol{b}^{TH}_1(n) \\ \boldsymbol{b}^{TH}_2(n) \\ \boldsymbol{b}^{TH}_3(n) \\ \vdots \\ \boldsymbol{b}^{TH}_{N_{\max}-1}(n) \end{pmatrix},$$

and the matrix $\boldsymbol{B}^{TH}$ is defined as

$$\boldsymbol{B}^{TH} = \begin{pmatrix} \mathbf{0} & \boldsymbol{B}^{TH}_{1,2} & \mathbf{0} & \cdots & \mathbf{0} & \mathbf{0} \\ \boldsymbol{B}^{TH}_{2,1} & \mathbf{0} & \boldsymbol{B}^{TH}_{2,3} & \cdots & \mathbf{0} & \mathbf{0} \\ \mathbf{0} & \boldsymbol{B}^{TH}_{3,2} & \mathbf{0} & \cdots & \mathbf{0} & \mathbf{0} \\ \vdots & \ddots & \ddots & \ddots & \vdots & \vdots \\ \mathbf{0} & \mathbf{0} & \mathbf{0} & \cdots & \mathbf{0} & \boldsymbol{B}^{TH}_{N_{\max}-2,N_{\max}-1} \\ \mathbf{0} & \mathbf{0} & \mathbf{0} & \cdots & \boldsymbol{B}^{TH}_{N_{\max}-1,N_{\max}-2} & \mathbf{0} \end{pmatrix}.$$

The sub-vectors $\boldsymbol{Y}^{TH}_j(n)$ and $\boldsymbol{b}^{TH}_j(n)$ that constitute the vectors $\boldsymbol{Y}^{TH}(n)$ and $\boldsymbol{b}^{TH}(n)$ respectively, have dimension j, with $j = 1, \ldots, N_{\max} - 1$. In particular, the sub-vectors $\boldsymbol{Y}^{TH}_j(n)$, $n \in \mathbb{N}_0$, are defined as

$$\boldsymbol{Y}^{TH}_j(n) = \begin{pmatrix} \rho^{TH}_{(j-1,1)}(n) \\ \rho^{TH}_{(j-2,2)}(n) \\ \vdots \\ \rho^{TH}_{(0,j)}(n) \end{pmatrix}, \quad j = 1, \ldots, N_{\max} - 1.$$

Vector $\boldsymbol{b}^{TH}(n)$, $n \in \mathbb{N}_0$, is organised in sub-vectors $\boldsymbol{b}^{TH}_j(n)$ of dimension j, $j =$

$1, \ldots, N_{\max} - 1$. If $n \geq 1$, one has

$$\boldsymbol{b}_j^{TH}(n) = \begin{pmatrix} \dfrac{\beta_1(N_H - j + 1)\rho_{(j,1)}^{TH}(n-1)}{R_{(j-1,1)}} \\ \dfrac{\beta_1(N_H - j + 2)\rho_{(j-1,2)}^{TH}(n-1)}{R_{(j-2,2)}} \\ \vdots \\ \dfrac{\beta_1 N_H \rho_{(1,j)}^{TH}(n-1)}{R_{(0,j)}} \end{pmatrix}, \quad j = 1, \ldots, N_{\max} - 2.$$

For $j = N_{\max} - 1$, the sub-vector $\boldsymbol{b}_{N_{\max}-1}^{TH}(n) = \mathbf{0}$ if $n \geq 2$, whereas

$$\boldsymbol{b}_{N_{\max}-1}^{TH}(1) = \begin{pmatrix} \dfrac{\beta_1(N_H - j + 1)}{R_{(j-1,1)}} \\ \dfrac{\beta_1(N_H - j + 2)}{R_{(j-2,2)}} \\ \vdots \\ \dfrac{\beta_1 N_H}{R_{(0,N_{\max}-1)}} \end{pmatrix}.$$

If $n = 0$, one has

$$\boldsymbol{b}_j^{TH}(0) = \begin{pmatrix} \dfrac{\nu_1}{R_{(j-1,1)}} \\ \dfrac{\nu_1}{R_{(j-2,2)}} \\ \vdots \\ \dfrac{\nu_1}{R_{(0,j)}} \end{pmatrix}, \; j = 1, \ldots, N_{\max} - 2,$$

and

$$\boldsymbol{b}_{N_{\max}-1}^{TH}(0) = \begin{pmatrix} \dfrac{\nu_1 + ((N_{\max} - 2)\gamma_1 + \alpha_1)(N_T - 1)}{R_{(N_{\max}-2,1)}} \\ \dfrac{\nu_1 + ((N_{\max} - 3)\gamma_1 + 2\alpha_1)(T - 2) + \beta_1(N_H - N_{\max} + 3)}{R_{(N_{\max}-3,2)}} \\ \vdots \\ \dfrac{\nu_1 + (N_{\max} - 1)\alpha_1(N_T - N_{\max} + 1) + (N_{\max} - 2)\beta_1 N_H}{R_{(0,N_{\max}-1)}} \end{pmatrix}.$$

The blocks that comprise the matrix $\boldsymbol{B}^{TH}$, $\boldsymbol{B}_{k+1,k}^{TH}$ and $\boldsymbol{B}_{k,k+1}^{TH}$, have dimensions $(k+1) \times k$ and $k \times (k+1)$ respectively, and are defined as follows:

- For $k = 1, \ldots, N_{\max} - 2$:

$$(\boldsymbol{B}^{TH}_{k+1,k})_{i+1,j+1} = \begin{cases} \dfrac{(k-i)(\mu_1+\varphi_1)}{R_{(k-i,i+1)}}, & \text{if } i = j, \\ \dfrac{i\nu_1}{R_{(k-i,i+1)}}, & \text{if } i = j+1, \\ 0, & \text{otherwise,} \end{cases}$$

  where $i = 0, \ldots, k$ and $j = 0, \ldots, k-1$.

- For $k = 1, \ldots, N_{\max} - 2$:

$$(\boldsymbol{B}^{TH}_{k,k+1})_{i+1,j+1} = \begin{cases} \dfrac{i\beta_1(N_H - k + i + 1)}{R_{(k-i-1,i+1)}}, & \text{if } i = j, \\ \dfrac{((k-i-1)\gamma_1 + (i+1)\alpha_1)(N_T - i - 1)}{R_{(k-i-1,i+1)}}, & \text{if } i = j-1, \\ 0, & \text{otherwise,} \end{cases}$$

  where $i = 0, \ldots, k-1$ and $j = 0, \ldots, k$.

Equation (5.27) can then be solved efficiently by adapting Algorithm 5 to obtain the probability distribution of $\Lambda^T(H)$.

Lastly, $\rho^{HT}_{(n_1,m_1)}(n)$ is analysed. When considering the possible stochastic events representing the infection of a susceptible tick, or the death of an infected host, two different scenarios are distinguished. In particular, if there are n_1 infected hosts and a susceptible tick becomes infected, this new infection is caused by the marked host with probability $1/n_1$. Similarly, if an infected host dies, one considers that the marked host is the one that dies with probability $1/n_1$. In light of this and by means of a first step argument, one obtains for $\rho^{HT}_{(n_1,m_1)}(0)$

$$\begin{aligned} \rho^{HT}_{(n_1,m_1)}(0) = {} & \frac{(\mu_1+\varphi_1)(n_1-1)}{R_{(n_1,m_1)}}\rho^{HT}_{(n_1-1,m_1)}(0) + \frac{\nu_1 m_1}{R_{(n_1,m_1)}}\rho^{HT}_{(n_1,m_1-1)}(0) \\ & + \frac{\gamma_1(N_T-m_1)(n_1-1) + \alpha_1(N_T-m_1)m_1}{R_{(n_1,m_1)}}\rho^{HT}_{(n_1,m_1+1)}(n) \\ & + \frac{\beta_1(N_H-n_1)m_1}{R_{(n_1,m_1)}}\rho^{HT}_{(n_1+1,m_1)}(0) + \frac{\mu_1+\varphi_1}{R_{(n_1,m_1)}}, \end{aligned} \tag{5.28}$$

with boundary conditions $\rho^{HT}_{(0,0)}(0) = 1$ and $\rho^{HT}_{E}(0) = 1$. On the other hand, for

$n \geq 1$, the first step equation for $\rho^{HT}_{(n_1,m_1)}(n)$ is given by

$$\begin{aligned}\rho^{HT}_{(n_1,m_1)}(n) = &\frac{(\mu_1+\varphi_1)(n_1-1)}{R_{(n_1,m_1)}}\rho^{HT}_{(n_1-1,m_1)}(n) + \frac{\nu_1 m_1}{R_{(n_1,m_1)}}\rho^{HT}_{(n_1,m_1-1)}(n)\\ &+ \frac{\beta_1(N_H-n_1)m_1}{R_{(n_1,m_1)}}\rho^{HT}_{(n_1+1,m_1)}(n) + \frac{\gamma_1(N_T-m_1)}{R_{(n_1,m_1)}}\rho^{HT}_{(n_1,m_1+1)}(n-1)\\ &+ \frac{\gamma_1(N_T-m_1)(n_1-1)+\alpha_1(N_T-m_1)m_1}{R_{(n_1,m_1)}}\rho^{HT}_{(n_1,m_1+1)}(n).\end{aligned} \tag{5.29}$$

with boundary conditions $\rho^{HT}_{(0,0)}(n) = 0$ and $\rho^{HT}_{E}(n) = 0$. First, the probabilities $\rho^{HT}_{(n_1,m_1)}(0)$ will be computed, and then sequentially the probabilities $\rho^{HT}_{(n_1,m_1)}(n)$ for $n \geq 1$. In order to write equations (5.28) and (5.29) in matrix form, the state space is organised as illustrated in equation (5.18). Notice that the distribution of $\Lambda^H(T)$ can be derived for any initial state $(n_1, m_1) \in \hat{\Omega}$ such that $n_1 \neq 0$ because at least one infected host is required by definition (since $\Lambda^H(T)$ is defined for a marked infected host). Thus, equations (5.28) and (5.29) can be rewritten in matrix form as

$$\boldsymbol{Y}^{HT}(n) = \boldsymbol{B}^{HT}\boldsymbol{Y}^{HT}(n) + \boldsymbol{b}^{HT}(n), \quad n \in \mathbb{N}_0, \tag{5.30}$$

where

$$\boldsymbol{Y}^{HT}(n) = \begin{pmatrix} \boldsymbol{Y}^{HT}_1(n) \\ \boldsymbol{Y}^{HT}_2(n) \\ \boldsymbol{Y}^{HT}_3(n) \\ \vdots \\ \boldsymbol{Y}^{HT}_{N_{\max}-1}(n) \end{pmatrix}, \qquad \boldsymbol{b}^{HT}(n) = \begin{pmatrix} \boldsymbol{b}^{HT}_1(n) \\ \boldsymbol{b}^{HT}_2(n) \\ \boldsymbol{b}^{HT}_3(n) \\ \vdots \\ \boldsymbol{b}^{HT}_{N_{\max}-1}(n) \end{pmatrix},$$

and the matrix $\boldsymbol{B}^{HT}$ is defined as

$$\boldsymbol{B}^{HT} = \begin{pmatrix} \boldsymbol{0} & \boldsymbol{B}^{HT}_{1,2} & \boldsymbol{0} & \cdots & \boldsymbol{0} & \boldsymbol{0} \\ \boldsymbol{B}^{HT}_{2,1} & \boldsymbol{0} & \boldsymbol{B}^{HT}_{2,3} & \cdots & \boldsymbol{0} & \boldsymbol{0} \\ \boldsymbol{0} & \boldsymbol{B}^{HT}_{3,2} & \boldsymbol{0} & \cdots & \boldsymbol{0} & \boldsymbol{0} \\ \vdots & \ddots & \ddots & \ddots & \vdots & \vdots \\ \boldsymbol{0} & \boldsymbol{0} & \boldsymbol{0} & \cdots & \boldsymbol{0} & \boldsymbol{B}^{HT}_{N_{\max}-2,N_{\max}-1} \\ \boldsymbol{0} & \boldsymbol{0} & \boldsymbol{0} & \cdots & \boldsymbol{B}^{HT}_{N_{\max}-1,N_{\max}-2} & \boldsymbol{0} \end{pmatrix}.$$

The sub-vectors $\boldsymbol{Y}^{HT}_j(n)$ and $\boldsymbol{b}^{HT}_j(n)$ that constitute the vectors $\boldsymbol{Y}^{HT}(n)$ and $\boldsymbol{b}^{HT}(n)$ respectively, have dimension j, with $j = 1, \ldots, N_{\max} - 1$. In particular,

the sub-vectors $\boldsymbol{Y}_j^{HT}(n)$, $n \in \mathbb{N}_0$, are defined as

$$\boldsymbol{Y}_j^{HT}(n) = \begin{pmatrix} \rho_{(j,0)}^{HT}(n) \\ \rho_{(j-2,2)}^{HT}(n) \\ \vdots \\ \rho_{(1,j-1)}^{HT}(n) \end{pmatrix}, \quad j = 1, \ldots, N_{\max} - 1.$$

Vector $\boldsymbol{b}^{HT}(n)$, $n \in \mathbb{N}_0$, is organised in sub-vectors $\boldsymbol{b}_j^{HT}(n)$ of dimension j, $j = 1, \ldots, N_{\max} - 1$. If $n \geq 1$, one has

$$\boldsymbol{b}_j^{HT}(n) = \begin{pmatrix} \dfrac{\gamma_1 N_T \rho_{(j,1)}^{HT}(n-1)}{R_{(j,0)}} \\ \dfrac{\gamma_1 (N_T - 1) \rho_{(j-1,2)}^{HT}(n-1)}{R_{(j-1,1)}} \\ \vdots \\ \dfrac{\gamma_1 (N_T - j) \rho_{(1,j)}^{HT}(n-1)}{R_{(1,j-1)}} \end{pmatrix}, \quad j = 1, \ldots, N_{\max} - 2.$$

For $j = N_{\max} - 1$, the sub-vector $\boldsymbol{b}_{N_{\max}-1}^{HT}(n) = \boldsymbol{0}$ if $n \geq 2$, whereas

$$\boldsymbol{b}_{N_{\max}-1}^{HT}(1) = \begin{pmatrix} \dfrac{\gamma_1 N_T}{R_{(j,0)}} \\ \dfrac{\gamma_1 (N_T - 1)}{R_{(j-1,1)}} \\ \vdots \\ \dfrac{\gamma_1 (N_T - N_{\max} + 2)}{R_{(1,N_{\max}-2)}} \end{pmatrix}.$$

If $n = 0$, one has

$$\boldsymbol{b}_j^{HT}(0) = \begin{pmatrix} \dfrac{\mu_1 + \varphi_1}{R_{(j,0)}} \\ \dfrac{\mu_1 + \varphi_1}{R_{(j-1,1)}} \\ \vdots \\ \dfrac{\mu_1 + \varphi_1}{R_{(1,j-1)}} \end{pmatrix}, \; j = 1, \ldots, N_{\max} - 2,$$

and

$$\boldsymbol{b}^{HT}_{N_{\max}-1}(0) = \begin{pmatrix} \dfrac{\mu_1+\varphi_1+(N_{\max}-2)\gamma_1 N_T}{R_{(N_{\max}-1,0)}} \\ \dfrac{\mu_1+\varphi_1+((N_{\max}-3)\gamma_1+2\alpha_1)(N_T-2)+2\beta_1(N_H-N_{\max}+2)}{R_{(N_{\max}-2,1)}} \\ \vdots \\ \dfrac{\mu_1+\varphi_1+(N_{\max}-2)\alpha_1(N_T-N_{\max}+2)+(N_{\max}-2)\beta_1(N_H-1)}{R_{(1,N_{\max}-2)}} \end{pmatrix}.$$

The blocks that comprise the matrix $\boldsymbol{B}^{HT}$, $\boldsymbol{B}^{HT}_{k+1,k}$ and $\boldsymbol{B}^{HT}_{k,k+1}$, have dimensions $(k+1)\times k$ and $k\times(k+1)$ respectively, and are defined as follows:

- For $k = 1,\dots,N_{\max}-1$:

$$(\boldsymbol{B}^{HT}_{k+1,k})_{i+1,j+1} = \begin{cases} \dfrac{(k-i)(\mu_1+\varphi_1)}{R_{(k-i+1,i)}} & \text{if } i=j, \\ \dfrac{i\nu_1}{R_{(k-i+1,i)}} & \text{if } i=j+1, \\ 0 & \text{otherwise,} \end{cases}$$

  where $i = 0,\dots,k$ and $j = 0,\dots,k-1$.

- For $k = 1,\dots,N_{\max}-1$:

$$(\boldsymbol{B}^{HT}_{k,k+1})_{i+1,j+1} = \begin{cases} \dfrac{i\beta_1(N_H-k+i)}{R_{(k-i,i)}} & \text{if } i=j, \\ \dfrac{((k-i-1)\gamma_1+i\alpha_1)(N_T-i)}{R_{(k-i,i)}} & \text{if } i=j-1, \\ 0 & \text{otherwise,} \end{cases}$$

  where $i = 0,\dots,k-1$ and $j = 0,\dots,k$.

Equation (5.30) can then be solved efficiently by adapting Algorithm 5 to obtain the probability distribution of $\Lambda^H(T)$.
Figure 5.9 depicts the probabilities $\rho^{TT}_{(0,1)}(n)$, $\rho^{TH}_{(0,1)}(n)$ and $\rho^{HT}_{(1,0)}(n)$, $n = 0,\dots,39$, in blue, red and green respectively, for different values of the transmission parameters α_1, β_1 and γ_1, while all the other parameters in the model are fixed. In particular, the threshold $N_{\max}$ is fixed at 10^2 infected individuals, with an initial number of susceptible hosts $N_H = 10^2$ and susceptible ticks $N_T = 10^3$. In the first row, the

value of the co-feeding transmission parameter α_1 varies as 10^{-6} (first column) and 10^{-4} (second column). As one would expect, α_1 mainly affects $\rho^{TT}_{(0,1)}(n)$: for small values of α_1, the marked tick infects at most one other tick before the process ends, whereas when α_1 is increased, the marked tick can infect up to six susceptible ticks. On the other hand, α_1 does not have a significant effect on the number of secondary infections caused by systemic transmission. In the second row, the value of the tick-to-host transmission parameter β_1 is 10^{-4} in the first column and 10^{-2} in the second one. For larger values of β_1, the marked tick infects a larger number of hosts, as our intuition would suggest. Moreover, the number of ticks infected by the marked tick decreases for larger values of β_1 because the marked tick is more likely to infect a host during its lifetime. We also observe that a marked host infects fewer ticks when β_1 is increased. This can be explained by noting that, when the marked host infects a tick, this tick will transmit the virus to several susceptible hosts since the value of β_1 is large. Consequently, when a new infection of a tick occurs, it will be less likely that this infection is caused by the marked host as there are many infected hosts. In the third row, the value of the host-to-tick transmission parameter γ_1 varies as 10^{-4} (first column) and 10^{-2} (second column). When the value of γ_1 increases, a marked host infects a significantly larger number of ticks, as expected. We also note that a marked tick infects fewer hosts for larger values of γ_1. Indeed, as soon as the marked tick infects a host, this host will infect several ticks since the value of γ_1 is large. Thus, when a new infection of a host occurs, the probability that this infection is caused by the marked tick is low because the number of infected ticks is large.

5.2 Co-infection dynamics

Consider a population of ticks interacting with a population of hosts, *e.g.*, small or large vertebrates, which are in an endemic state due to a viral strain V_1. We will refer to V_1 as *resident* strain. As described in Section 5.1, the infection with V_1 can be transmitted through three different routes: tick-to-host, host-to-tick and tick-to-tick. A second viral strain V_2 is introduced in the system through a given number of ticks or hosts infected with V_2. We will refer to V_2 as *invasive* strain. Similarly to the infection with the resident strain, the infection with the

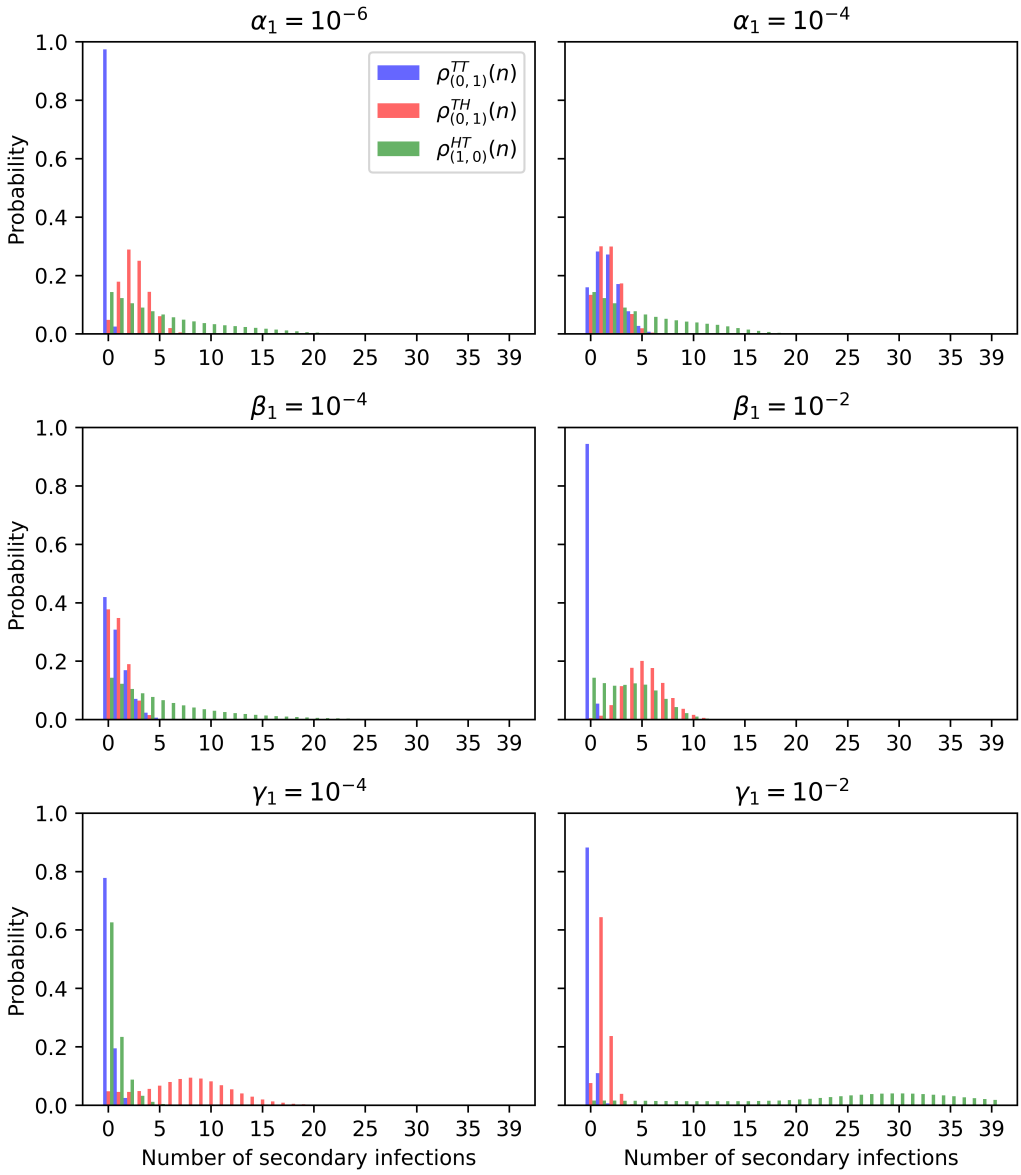

Figure 5.9: The probabilities $\rho^{TT}_{(0,1)}(n)$, $\rho^{TH}_{(0,1)}(n)$ and $\rho^{HT}_{(1,0)}(n)$, $n = 0, \ldots, 39$, are depicted in blue, red and green respectively, for different values of the transmission parameters α_1 (first row), β_1 (second row) and γ_1 (third row). The threshold $N_{\max}$ is fixed at 10^2 infected individuals, with an initial number of susceptible hosts $N_H = 10^2$ and susceptible ticks $N_T = 10^3$. The transmission parameters are: $\gamma_1 = \beta_1 = 10^{-3}$ in the first row; $\gamma_1 = 10^{-3}$ and $\alpha_1 = 10^{-5}$ in the second row; $\beta_1 = 10^{-3}$ and $\alpha_1 = 10^{-5}$ in the third row. The other parameters in the model are fixed as follows: $\varphi_1 = 1/6$ per day, $\nu_s = \nu_1 = 1/200$ per day and $\mu_s = \mu_1 = 1/(4 \times 365)$ per day.

Variable	Description	Population size
H_s	Susceptible hosts	n_s
H_1	Hosts infected with V_1	n_1
H_2	Hosts infected with V_2	n_2
H_c	Co-infected hosts	n_c
T_s	Susceptible ticks	m_s
T_1	Ticks infected with V_1	m_1
T_2	Ticks infected with V_2	m_2
T_c	Co-infected ticks	m_c

Table 5.2: Summary of the variables in the model of co-infection dynamics.

invasive strain can be transmitted via three routes: tick-to-host, host-to-tick and tick-to-tick. For both strains, once a tick contracts the virus, the infection lasts for its lifetime (Gargili *et al.*, 2017), whereas vertebrate animals are characterised by short lasting viremia (Gonzalez *et al.*, 1998; Hoch *et al.*, 2018).
Given the presence of two different viral strains, a single host, or a single tick, is either susceptible, or infected with V_1, or infected with V_2, or co-infected with both viral strains. Table 5.2 summarises the notation for susceptible, infected and co-infected hosts and ticks. Thus, we need to account for many infection events when modelling the dynamics of susceptible, infected and co-infected individuals in the presence of the three routes of transmission. In order to shed light on the role of co-transmission, a simplified scenario is considered in Section 5.2.1, where we propose a deterministic model that takes into account only co-feeding transmission. Indeed, as shown in Section 5.1.1, co-feeding is the only route of transmission that is able to maintain an epidemic with no other route of transmission. In Section 5.2.2, we propose a stochastic model of the invasive viral strain dynamics to derive some descriptors of interest and study the factors that affect co-infection events.

5.2.1 Co-feeding and co-transmission: a deterministic model

In this section, a simplified scenario that accounts for only co-feeding transmission is studied. Thus, we consider a population of ticks susceptible to the infection of a resident viral strain V_1. An invasive viral strain V_2 is introduced in the

Parameter	Event	Range	Units	Reference
α_1	$T_1 + T_s \to T_1 + T_1$	$[10^{-6}, 10^{-3}]$	1/Days/Tick	Norman *et al.* (2004)
α_2	$T_2 + T_s \to T_2 + T_2$	$[10^{-6}, 10^{-3}]$	1/Days/Tick	Norman *et al.* (2004)
ϵ_1	$T_c + T_s \to T_c + T_1$	$[10^{-6}, 10^{-3}]$	1/Days/Tick	Norman *et al.* (2004)
ϵ_2	$T_c + T_s \to T_c + T_2$	$[10^{-6}, 10^{-3}]$	1/Days/Tick	Norman *et al.* (2004)
ϵ_c	$T_c + T_s \to T_c + T_c$	$[10^{-6}, 10^{-3}]$	1/Days/Tick	Norman *et al.* (2004)
ξ_1	$T_1 + T_2 \to T_1 + T_c$	$[10^{-6}, 10^{-3}]$	1/Days/Tick	Norman *et al.* (2004)
ξ_2	$T_2 + T_1 \to T_2 + T_c$	$[10^{-6}, 10^{-3}]$	1/Days/Tick	Norman *et al.* (2004)
$\eta_2 + \eta_c$	$T_c + T_1 \to T_c + T_c$	$[10^{-6}, 10^{-3}]$	1/Days/Tick	Norman *et al.* (2004)
$\eta_1 + \eta_c$	$T_c + T_2 \to T_c + T_c$	$[10^{-6}, 10^{-3}]$	1/Days/Tick	Norman *et al.* (2004)
ν_s	Death rate of T_s	$[6 \times 10^{-3}, 3.8 \times 10^{-2}]$	1/Days	Lou *et al.* (2014)
ν_1	Death rate of T_1	$[6 \times 10^{-3}, 3.8 \times 10^{-2}]$	1/Days	Lou *et al.* (2014)
ν_2	Death rate of T_2	$[6 \times 10^{-3}, 3.8 \times 10^{-2}]$	1/Days	Lou *et al.* (2014)
ν_c	Death rate of T_c	$[6 \times 10^{-3}, 3.8 \times 10^{-2}]$	1/Days	Lou *et al.* (2014)
Φ_T	Arrival of ticks	$[0.5, 3.5]$	Tick/Days	Sutton *et al.* (2012)

Table 5.3: Summary of the parameters in the deterministic co-infection model accounting for only co-feeding transmission.

population through a given number of ticks infected with V_2. We are interested in deriving a condition for the invasion (or establishment) of the invasive strain V_2 in a system where the virus V_1 is endemic. In particular, we compute the invasion reproduction number of the invasive viral strain V_2 in a system where the resident strain V_1 is in equilibrium by means of the next generation matrix. To this end, let $m_s(t)$, $m_1(t)$, $m_2(t)$ and $m_c(t)$ be the number of susceptible, infected with V_1, infected with V_2 and co-infected ticks at time t. Figure 5.10 illustrates the dynamics considered in this mathematical model, whereas Table 5.3 summarises the parameters in the model. In particular, susceptible ticks immigrate in the population with rate Φ_T and their average lifetime is $\frac{1}{\nu_s}$ days. Ticks infected with V_1, or V_2, or co-infected, die with death rate ν_1, ν_2 and ν_c, respectively. The infection is transmitted tick-to-tick through co-feeding. One notes that co-transmission events are allowed in this setting; that is a susceptible tick can acquire both infections simultaneously when interacting with a co-infected tick, becoming co-infected itself. The events illustrated in Figure 5.10 are combined in the following system of ordinary differential equations that describe the time evolution of susceptible, infected with the resident viral strain V_1, infected with

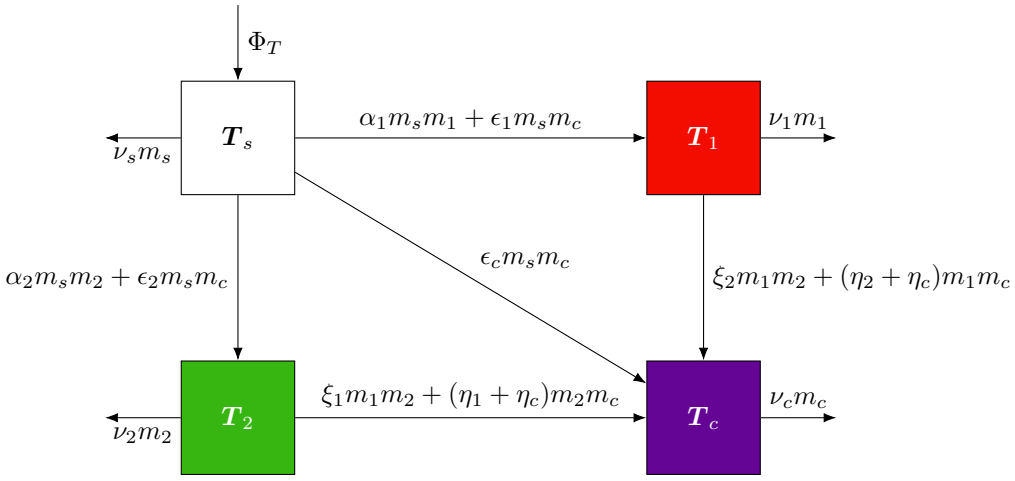

Figure 5.10: Diagram for the dynamics of susceptible, infected and co-infected ticks in the deterministic model of co-feeding and co-transmission. Model parameters are summarised in Table 5.3.

the invasive viral strain V_2 and co-infected ticks:

$$\begin{aligned}
\frac{\mathrm{d}m_s}{\mathrm{d}t} &= \Phi_T - \nu_s m_s - \alpha_1 m_s m_1 - \alpha_2 m_s m_2 - (\epsilon_1 + \epsilon_2 + \epsilon_c) m_s m_c, \\
\frac{\mathrm{d}m_1}{\mathrm{d}t} &= -\nu_1 m_1 + \alpha_1 m_s m_1 + \epsilon_1 m_s m_c - (\eta_2 + \eta_c) m_1 m_c - \xi_2 m_2 m_1, \\
\frac{\mathrm{d}m_2}{\mathrm{d}t} &= -\nu_2 m_2 + \alpha_2 m_s m_2 + \epsilon_2 m_s m_c - (\eta_1 + \eta_c) m_2 m_c - \xi_1 m_2 m_1, \\
\frac{\mathrm{d}m_c}{\mathrm{d}t} &= -\nu_c m_c + \epsilon_c m_s m_c + \xi_1 m_2 m_1 + \xi_2 m_1 m_2 + (\eta_1 + \eta_c) m_2 m_c + (\eta_2 + \eta_c) m_1 m_c.
\end{aligned} \tag{5.31}$$

Note that the previous system has a virus-free equilibrium E_0 given by

$$E_0 = \left(\frac{\Phi_T}{\nu_s}, 0, 0, 0 \right).$$

Linearising system (5.31) about the virus-free equilibrium and making use of the next generation matrix approach by following the same steps illustrated in Sec-

tion 5.1.1, one obtains the next generation matrix $F^{E_0}(V^{E_0})^{-1}$ as

$$F^{E_0}(V^{E_0})^{-1} = \begin{pmatrix} \frac{\alpha_1\Phi_T}{\nu_1\nu_s} & 0 & \frac{\epsilon_1\Phi_T}{\nu_c\nu_s} \\ 0 & \frac{\alpha_2\Phi_T}{\nu_2\nu_s} & \frac{\epsilon_2\Phi_T}{\nu_c\nu_s} \\ 0 & 0 & \frac{\epsilon_c\Phi_T}{\nu_c\nu_s} \end{pmatrix},$$

where the component

$$F^{E_0} = \begin{pmatrix} \frac{\alpha_1\Phi_T}{\nu_s} & 0 & \frac{\epsilon_1\Phi_T}{\nu_s} \\ 0 & \frac{\alpha_2\Phi_T}{\nu_s} & \frac{\epsilon_2\Phi_T}{\nu_s} \\ 0 & 0 & \frac{\epsilon_c\Phi_T}{\nu_s} \end{pmatrix},$$

accounts for new infections, whereas the matrix

$$V^{E_0} = \begin{pmatrix} \nu_1 & 0 & 0 \\ 0 & \nu_2 & 0 \\ 0 & 0 & \nu_c \end{pmatrix},$$

considers the changes in the state of the infected populations. Thus, the basic reproduction number R_0 associated with the model (5.31) is defined as the largest eigenvalue of the next generation matrix $F^{E_0}(V^{E_0})^{-1}$, *i.e.*, $R_0 = \max\{R_1, R_2, R_c\}$, where

$$R_1 = \frac{\alpha_1\Phi_T}{\nu_s\nu_1}, \quad R_2 = \frac{\alpha_2\Phi_T}{\nu_s\nu_2}, \quad R_c = \frac{\epsilon_c\Phi_T}{\nu_s\nu_c}.$$

We observe that R_1 represents the average number of new infections with V_1 directly caused by a tick infected with V_1 introduced in a population of susceptible ticks. The epidemiological interpretation of R_2 is similar: R_2 is the average number of new infections with V_2 directly caused by a tick infected with V_2 introduced in a population of susceptible ticks. On the other hand, R_c accounts for co-transmission of both strains representing the average number of new infections with both strains directly caused by a co-infected tick introduced in a population of susceptible ticks. In order to derive a condition for the establishment of the invasive strain in a system where the strain V_1 is in equilibrium, the invasion reproduction number of

the invasive strain V_2, $R_{\text{inv}}(V_2|V_1)$, is computed by means of the next generation matrix (Gao *et al.*, 2016; Van den Driessche & Watmough, 2002). The invasion reproduction number $R_{\text{inv}}(V_2|V_1)$ is defined as the average number of infections with V_2 that are produced when a tick infected by V_2 is introduced into the system comprised of susceptible ticks, and ticks infected with the resident strain V_1, where V_1 is in equilibrium. Thus, $R_{\text{inv}}(V_2|V_1)$ is a threshold value: if $R_{\text{inv}}(V_2|V_1) < 1$, the invasive strain goes extinct without generating an epidemic; on the contrary, when $R_{\text{inv}}(V_2|V_1) > 1$, the invasive strain invades the system where the resident strain is in equilibrium, causing an outbreak. We note that, from the perspective of the invasive viral strain V_2, susceptible individuals are both susceptible ticks and ticks infected with the resident viral strain. Thus the sub-system of susceptible individuals (obtained by setting $m_2 = m_c = 0$ in system (5.31)) is given by

$$\begin{aligned} \frac{\mathrm{d}m_s}{\mathrm{d}t} &= \Phi_T - \nu_s m_s - \alpha_1 m_s m_1, \\ \frac{\mathrm{d}m_1}{\mathrm{d}t} &= -\nu_1 m_1 + \alpha_1 m_s m_1, \end{aligned} \tag{5.32}$$

and has an equilibrium with the presence of only the resident strain V_1. We will refer to this equilibrium as E_1, which is given by

$$E_1 = \left(\frac{\nu_1}{\alpha_1}, \frac{\alpha_1 \Phi_T - \nu_s \nu_1}{\alpha_1 \nu_1}, 0, 0 \right). \tag{5.33}$$

Note that E_1 exists if and only if $\frac{\alpha_1 \Phi_T - \nu_s \nu_1}{\alpha_1 \nu_1} > 0$, or equivalently $R_1 > 1$, which means that the resident viral strain V_1 is established in the system.
The sub-system of ticks infected with V_2 is

$$\begin{aligned} \frac{\mathrm{d}m_2}{\mathrm{d}t} &= -\nu_2 m_2 + \alpha_2 m_s m_2 + \epsilon_2 m_s m_c - (\eta_1 + \eta_c) m_2 m_c - \xi_1 m_2 m_1, \\ \frac{\mathrm{d}m_c}{\mathrm{d}t} &= -\nu_c m_c + \epsilon_c m_s m_c + \xi_1 m_2 m_1 + \xi_2 m_1 m_2 + (\eta_1 + \eta_c) m_2 m_c + (\eta_2 + \eta_c) m_1 m_c. \end{aligned}$$

The previous system is linearised about the equilibrium E_1 and rewritten as $\dot{y} = (F^{E_1} - V^{E_1})y$, where $y = (m_2, m_c)^T$, F^{E_1} is the transmission component which accounts for the production of new infections with V_2, and V^{E_1} is the transition component that considers the changes in the state of the infected populations. Since the interest is in measuring the ability of the invasive strain V_2 to invade an

equilibrium of the resident strain V_1, only new infections with V_2 are regarded as such, whereas new infections with V_1 are considered as changes in the state of the infected populations. For example, a susceptible tick that becomes infected with V_1 is not considered a new infection, and consequently not accounted for in the matrix F^{E_1}. Conversely, a susceptible tick that becomes infected with V_2 is a new infection, and thus included in F^{E_1}. Therefore, the matrix F^{E_1} is given by

$$F^{E_1} = \begin{pmatrix} \dfrac{\alpha_2\nu_1}{\alpha_1} & \dfrac{\epsilon_2\nu_1}{\alpha_1} \\ \dfrac{\xi_2(\nu_s\nu_1 - \alpha_1\Phi_T)}{\nu_1\alpha_1} & \dfrac{\epsilon_c\nu_1 - (\eta_2+\eta_c)\nu_s}{\alpha_1} + \dfrac{(\eta_2+\eta_c)\Phi_T}{\nu_1} \end{pmatrix},$$

and

$$V^{E_1} = \begin{pmatrix} \nu_2 + \dfrac{\xi_1\Phi_T}{\nu_1} - \dfrac{\nu_s\xi_1}{\alpha_1} & 0 \\ \dfrac{\xi_1(\nu_s\nu_1 - \alpha_1\Phi_T)}{\nu_1\alpha_1} & \nu_c \end{pmatrix}.$$

Under the assumption that the infection does not affect the death rate (Gao *et al.*, 2016), *i.e.*,

$$\nu = \nu_s = \nu_1 = \nu_2 = \nu_c, \tag{5.34}$$

neither does it affect the susceptibility of ticks, that is

$$\alpha_1 = \xi_1, \quad \alpha_2 = \xi_2, \quad \epsilon_1 = \eta_1, \quad \epsilon_2 = \eta_2, \quad \epsilon_c = \eta_c, \tag{5.35}$$

the maximum eigenvalue of the next generation matrix $F^{E_1}(V^{E_1})^{-1}$, that is the invasion reproduction number $R_{\text{inv}}(V_2|V_1)$, is computed as

$$R_{\text{inv}}(V_2|V_1) = \frac{\alpha_2 - \epsilon_2}{2\alpha_1 R_1} + \frac{\epsilon_2\Phi_T}{2\nu^2} + \frac{R_c}{2} + \sqrt{\left(\frac{\epsilon_2 - \alpha_2}{2\alpha_1 R_1} - \frac{\epsilon_2\Phi_T}{2\nu^2} - \frac{R_c}{2}\right)^2 - \frac{\alpha_2\epsilon_c}{\alpha_1^2}}.$$

One would expect that $R_{\text{inv}}(V_1|V_1)$, which is the invasion reproduction number when resident and invasive strains are identical, is equal to 1 (neutrality) when a population in an endemic equilibrium with the resident strain V_1 is invaded with V_1. However, as argued by Alizon (2008, 2013a), the invasive strain always has an advantage: it can infect both susceptible individuals and individuals infected with the resident strain, whereas the resident strain can only infect susceptible individuals as the individuals infected by the invasive strain V_2 are rare (Alizon, 2013a).

One notes that this assumes that the invasive strain V_2 has at least the same fitness as the resident strain V_1. The first mathematical model of co-infection to overcome the intrinsic bias of the invasive strain was proposed by van Baalen & Sabelis (1995), who considered individuals co-infected twice with the resident viral strain V_1 and individuals co-infected twice with the invasive viral strain V_2. This solution might seem counter-intuitive from a biological perspective as one could wonder about the biological meaning of individuals infected twice with the same strain (Alizon, 2013a). When dealing with micro or macro-parasites, co-infection with the same strain can be thought of as individuals with a double parasite load (Alizon, 2013a). One challenge with the co-infection model proposed by van Baalen & Sabelis (1995) is that the mathematical analysis becomes generally more complicated, especially when considering both systemic and non-systemic transmission. Thus, we propose here the alternative to normalise $R_{\text{inv}}(V_2|V_1)$ by $R_{\text{inv}}(V_1|V_1)$, where $R_{\text{inv}}(V_1|V_1)$ is computed as $R_{\text{inv}}(V_2|V_1)$ (under hypotheses (5.34) and (5.35)) assuming that $\alpha_2 = \alpha_1$ and $\epsilon_2 = \epsilon_1$, which means that V_1 and V_2 are the same strain. This yields

$$R_{\text{inv}}(V_1|V_1) = \frac{\alpha_1 - \epsilon_1}{2\alpha_1 R_1} + \frac{\epsilon_1 \Phi_T}{2\nu^2} + \frac{R_c}{2} + \sqrt{\left(\frac{\epsilon_1 - \alpha_1}{2\alpha_1 R_1} - \frac{\epsilon_1 \Phi_T}{2\nu^2} - \frac{R_c}{2}\right)^2 - \frac{\epsilon_c}{\alpha_1}}.$$

Hence, the normalised expression of the invasion reproduction number, denoted as $\widetilde{R}_{\text{inv}}(V_2|V_1)$, is given by

$$\widetilde{R}_{\text{inv}}(V_2|V_1) = \frac{R_{\text{inv}}(V_2|V_1)}{R_{\text{inv}}(V_1|V_1)}.$$

This normalisation guarantees that the neutrality condition; that is the invasion reproduction number is equal to 1 when resident and invasive strains are identical, is satisfied. However, it would be interesting to compare the normalised invasion reproduction number $\widetilde{R}_{\text{inv}}(V_2|V_1)$ proposed here with the one computed when considering also individuals co-infected twice by the same strain (Alizon, 2013a,b; van Baalen & Sabelis, 1995). In this case, the variables in the model would be susceptible ticks, ticks infected by V_1, ticks infected twice by V_1, ticks infected by V_2, ticks infected twice by V_2 and ticks co-infected simultaneously with V_1 and V_2. After describing their dynamics over time by means of ordinary differential equations, one could derive the invasion reproduction number by making use of the next generation matrix. This is the aim of future work.

5.2.2 A stochastic approach

In this section, we propose a stochastic model that accounts for all the routes of transmission (*i.e.*, tick-to-host, host-to-tick and tick-to-tick) in the presence of two different viral strains, V_1 and V_2. Since we are interested in studying the early dynamics of the invasive viral strain V_2 in a system where the resident strain V_1 is endemic, the populations of susceptible individuals and individuals infected with V_1 are assumed to be large. Thus, the depletion of susceptible individuals, as well as individuals infected with V_1, due to infection with the invasive viral strain V_2 is not taken into account. Thus, vertebrates and ticks infected with V_2 behave independently of each other. One of the main objectives of this approach is to analyse the stochastic dynamics of the invasive viral strain in terms of a number of stochastic descriptors. In particular, the probabilities of extinction of individuals infected with V_2, establishment of the invasive viral strain, and co-infection events (*i.e.*, co-infection of a vertebrate or co-infection of a tick) are computed, together with the expected conditional times to such events. Co-infection events are important for the aim of this chapter because they could lead to re-assortment. Thus, in this section, we compute the probability of a co-infection event occurring in early times after the introduction of the invasive viral strain V_2, and the timescales for this type of event to occur. Similarly to the analyses described in Section 5.1.4, these stochastic descriptors are derived by making use of first step arguments (Pinsky & Karlin, 2010).

As the individuals infected with V_2 behave independently of each other, one can assume that the populations infected with the invasive strain behave as a branching process. However, as shown in Section 5.1.2, this approach would only allow the computation of the probabilities of extinction and establishment of V_2, whereas we are also interested in deriving the probabilities of co-infection events, as well as the conditional times to such events. Indeed, since co-infection is a necessary condition for reassortment, these descriptors are relevant to estimate the probability and timescales of potential reassortment events.

In order to compute the stochastic descriptors mentioned above, define the following random variables:

- $H_2(t)$ is the number of hosts infected by the invasive strain V_2 at time t;

Parameter	Event	Range	Units	Reference
β_2	$T_2 + H_s \to T_2 + H_2$	$[10^{-4}, 10^{-1}]$	1/Days/Tick	Norman *et al.* (2004)
γ_2	$H_2 + T_s \to H_2 + T_2$	$[10^{-4}, 10^{-1}]$	1/Days/Host	Norman *et al.* (2004)
α_2	$T_2 + T_s \to T_2 + T_2$	$[10^{-6}, 10^{-3}]$	1/Days/Tick	Norman *et al.* (2004)
ν_2	Death rate of T_2	$[6 \times 10^{-3}, 3.8 \times 10^{-2}]$	1/Days	Lou *et al.* (2014)
μ_2	Death rate of H_2	$[1/3600, 1/360]$	1/Days	Mpeshe *et al.* (2011)
ζ_1	$T_1 + H_2 \to T_1 + H_c$	$[10^{-4}, 10^{-1}]$	1/Days/Tick	Norman *et al.* (2004)
ζ_2	$T_2 + H_1 \to T_2 + H_c$	$[10^{-4}, 10^{-1}]$	1/Days/Tick	Norman *et al.* (2004)
ξ_1	$T_1 + T_2 \to T_1 + T_c$	$[10^{-6}, 10^{-3}]$	1/Days/Tick	Norman *et al.* (2004)
ξ_2	$T_2 + T_1 \to T_2 + T_c$	$[10^{-6}, 10^{-3}]$	1/Days/Tick	Norman *et al.* (2004)
λ_1	$H_1 + T_2 \to H_1 + T_c$	$[10^{-4}, 10^{-1}]$	1/Days/Tick	Norman *et al.* (2004)
λ_2	$H_2 + T_1 \to H_2 + T_c$	$[10^{-4}, 10^{-1}]$	1/Days/Tick	Norman *et al.* (2004)
φ_2	$H_2 \to H_s$	$[1/7, 1/5]$	1/Days	Hoch *et al.* (2018)

Table 5.4: Summary of the parameters in the stochastic co-infection model accounting for all the routes of transmission.

- $T_2(t)$ is the number of ticks infected by the invasive strain V_2 at time t.

The process $(H_2(t), T_2(t))_{t\geq 0}$ defines a continuous time Markov chain that describes the dynamics of individuals infected with the invasive viral strain V_2. Figure 5.11 illustrates the dynamics considered in the mathematical model presented in this section. We note that only the dynamics of hosts and ticks infected with the invasive strain V_2 are modelled, whereas the populations of susceptible individuals and individuals infected with V_1 are assumed to be large and their depletion is not taken into account. On the other hand, the dynamics of co-infected individuals are not modelled: the probabilities of the first co-infection of a host or a tick, as well as the conditional times to such events, are computed through the definition of two absorbing states representing the first time that a co-infection of a vertebrate or a tick occurs.

The state $(0, 0)$ is an absorbing state, representing V_2 extinction. Since it is of interest to compute the probability of V_2 establishment, as well as the probability of a co-infection event occurring before V_2 extinction or establishment occurs, the following absorbing states are defined:

- The macro-state E_2 defined as

$$E_2 = \{(n_2, m_2) \in \mathbb{N}_0^2 : n_2 + m_2 = \overline{N}_{\max}\}, \quad \overline{N}_{\max} \in \mathbb{N},$$

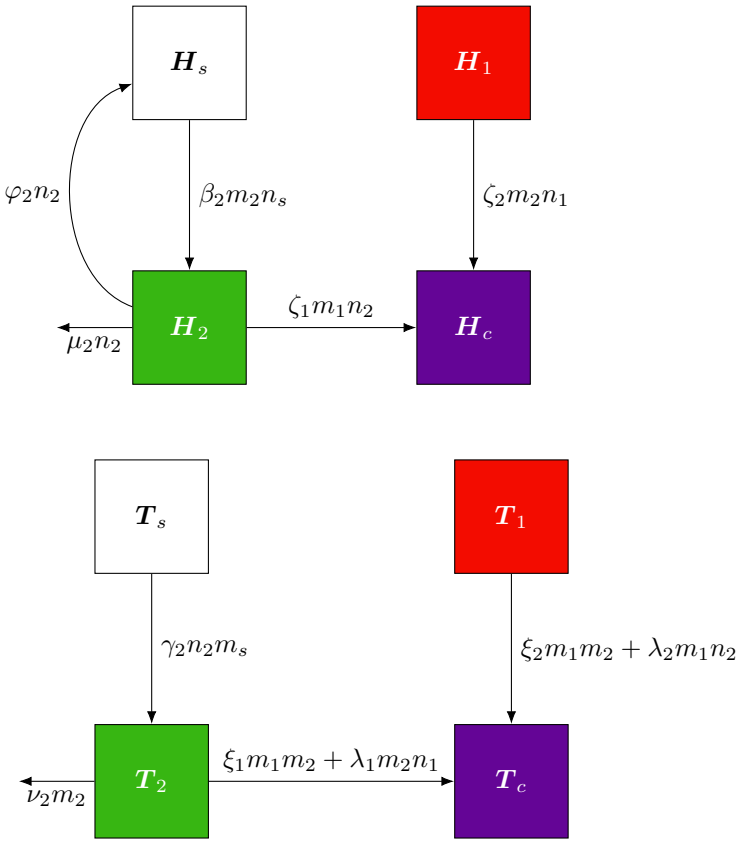

Figure 5.11: Diagram for the dynamics of susceptible, infected and co-infected hosts (**top**) and ticks (**below**). Model parameters are summarised in Table 5.4.

representing the establishment of the invasive viral strain V_2. Note that n_2 denotes hosts infected with V_2, whereas m_2 refers to ticks infected with V_2. If the total number of individuals infected with V_2, $n_2 + m_2$, hits the threshold $\overline{N}_{\max}$, the invasive strain is considered established in the population of hosts and ticks.

- C_H, representing the first time that a co-infection of a vertebrate occurs.
- C_T, representing the first time that a co-infection of a tick occurs.

Thus, one notices that the state space of the Markov chain $(H_2(t), T_2(t))_{t\geq 0}$ is given by

$$\Omega_2 = \{(n_2, m_2) \in \mathbb{N}_0^2 : 0 \leq n_2 + m_2 \leq \overline{N}_{\max} - 1\} \cup E_2 \cup C_H \cup C_T.$$

As depicted in Figure 5.12, from a state $(n_2, m_2) \in \Omega_2$, the process can jump to four adjacent states or to the absorbing states C_H and C_T with transition rates

$$q_{(n_2,m_2),(n_2',m_2')} = \begin{cases} \beta_2 m_2 n_s, & \text{if } (n_2', m_2') = (n_2 + 1, m_2), \\ (\gamma_2 n_2 + \alpha_2 m_2) m_s, & \text{if } (n_2', m_2') = (n_2, m_2 + 1), \\ (\mu_2 + \varphi_2) n_2, & \text{if } (n_2', m_2') = (n_2 - 1, m_2), \\ \nu_2 m_2, & \text{if } (n_2', m_2') = (n_2, m_2 - 1), \\ \zeta_1 m_1 n_2 + \zeta_2 m_2 n_1, & \text{if } (n_2', m_2') = C_H, \\ (\xi_1 + \xi_2) m_1 m_2 + \lambda_1 n_1 m_2 + \lambda_2 n_2 m_1, & \text{if } (n_2', m_2') = C_T, \end{cases} \tag{5.36}$$

where the model parameters are summarised in Table 5.4.

Probability and conditional time to V_2 extinction and establishment

In order to compute the probability of short-term extinction of the invasive strain V_2 (*i.e.*, reaching $(0, 0)$ before reaching any other absorbing state E_2, C_H and C_T), as well as the conditional time to such event, define for $(n_2, m_2) \in \Omega_2$

$$\tau_{(n_2,m_2)}^{VS_2} = \inf\{t \geq 0 : (H_2(t), T_2(t)) = (0, 0) | (H_2(0), T_2(0)) = (n_2, m_2)\},$$

that is the time to the extinction of the invasive viral strain V_2 starting with n_2 infected hosts and m_2 infected ticks. One observes that, in this scenario, the fact

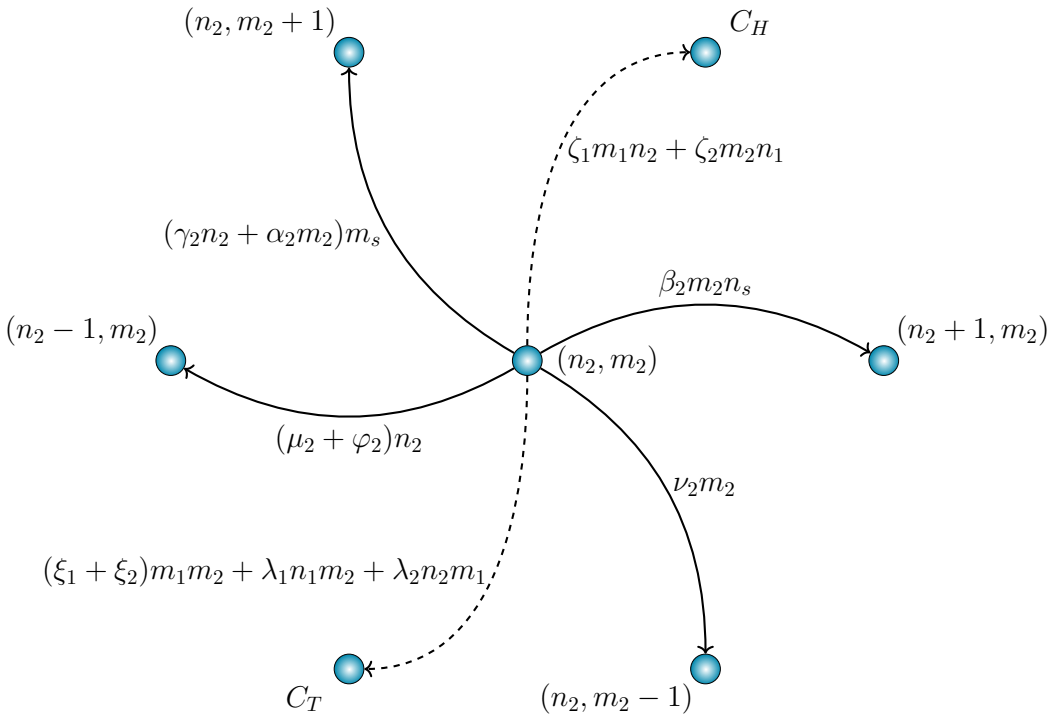

Figure 5.12: Transition diagram for the Markov chain $(H_2(t), T_2(t))_{t\geq 0}$ showing the possible states which the process can move to from a general state (n_2, m_2) and the transition rates with which these jumps occur. C_H and C_T denote the first co-infection of a host and the first co-infection of a tick, respectively, and are absorbing states.

that the process does not reach the absorbing state $(0,0)$ does not mean that V_2 will become established. Indeed, either the invasive strain V_2 becomes established or a co-infection event occurs. We note that $\tau^{VS_2}_{(n_2,m_2)} = +\infty$ if the process, in the long term, reaches any of the absorbing states E_2, C_H or C_T instead of $(0,0)$. The probability of V_2 extinction and the expected time to reach the V_2 virus-free state conditioned on actually reaching this fate can be computed starting from any initial state $(n_2, m_2) \in \Omega_2$. This can be obtained from the Laplace-Stieltjes transform of $\tau^{VS_2}_{(n_2,m_2)}$ defined as

$$\phi^{VS_2}_{(n_2,m_2)}(z) = \mathbb{E}\left[\mathrm{e}^{-z\tau^{VS_2}_{(n_2,m_2)}} \mathbb{1}_{\left\{\tau^{VS_2}_{(n_2,m_2)} < +\infty\right\}}\right], \quad \mathrm{Re}(z) \geq 0,$$

where $\mathbb{1}_{\left\{\tau^{VS_2}_{(n_2,m_2)} < +\infty\right\}}$ is a random variable taking the value 1 if $\tau^{VS_2}_{(n_2,m_2)} < +\infty$ and 0 otherwise, so that the previous Laplace-Stieltjes transform is restricted to the sample paths satisfying $\tau^{VS_2}_{(n_2,m_2)} < +\infty$. Using a first step argument, it can be written that

$$\begin{aligned}\phi^{VS_2}_{(n_2,m_2)}(z) &= \mathbb{E}\left[\mathrm{e}^{-z\tau^{VS_2}_{(n_2,m_2)}} \mathbb{1}_{\left\{\tau^{VS_2}_{(n_2,m_2)} < +\infty\right\}}\right] \\ &= \sum_{(n_2',m_2')\in\Omega_2} \mathbb{E}\left[\mathrm{e}^{-z\tau^{VS_2}_{(n_2,m_2)}} \mathbb{1}_{\left\{\tau^{VS_2}_{(n_2,m_2)} < +\infty\right\}} \middle| (n_2,m_2) \to (n_2',m_2')\right] \cdot \\ &\qquad \mathbb{P}\left((n_2,m_2) \to (n_2',m_2')\right),\end{aligned}$$

where the notation $(n_2,m_2) \to (n_2',m_2')$ represents the event of moving from state (n_2,m_2) to state (n_2',m_2') in one jump. Thus, $\mathbb{P}\left((n_2,m_2) \to (n_2',m_2')\right)$ is the probability of moving from state (n_2,m_2) to state (n_2',m_2'). The states that can be possibly reached in one jump of the process starting from (n_2,m_2) are depicted in the transition diagram in Figure 5.12. If the process jumps from (n_2,m_2) to (n_2',m_2'), the random variable $\tau^{VS_2}_{(n_2,m_2)}$ can be split into two parts, $\tau^{VS_2}_{(n_2,m_2)} = t_{(n_2,m_2)\to(n_2',m_2')} + \tau^{VS_2}_{(n_2',m_2')}$, where $t_{(n_2,m_2)\to(n_2',m_2')}$ denotes the time taken for the process to move from state (n_2,m_2) to state (n_2',m_2') in one step, and therefore,

$$\begin{aligned}\phi^{VS_2}_{(n_2,m_2)}(z) = \sum_{(n_2',m_2')\in\Omega_2} &\mathbb{E}\left[\mathrm{e}^{-zt_{(n_2,m_2)\to(n_2',m_2')}} \middle| (n_2,m_2) \to (n_2',m_2')\right] \cdot \\ &\mathbb{E}\left[\mathrm{e}^{-z\tau^{VS_2}_{(n_2',m_2')}} \mathbb{1}_{\left\{\tau^{VS_2}_{(n_2',m_2')} < +\infty\right\}}\right] \mathbb{P}\left((n_2,m_2) \to (n_2',m_2')\right),\end{aligned}$$

where the expectation of the product becomes the product of the expectations due to the independence given by the Markov property, and the second expectation is no longer conditional also due to the Markov property. One has

$$\mathbb{P}\left((n_2, m_2) \to (n_2', m_2')\right) = \frac{q_{(n_2,m_2),(n_2',m_2')}}{R_{(n_2,m_2)}},$$

where

$$\begin{aligned} R_{(n_2,m_2)} = {} & q_{(n_2,m_2),(n_2+1,m_2)} + q_{(n_2,m_2),(n_2-1,m_2)} + q_{(n_2,m_2),(n_2,m_2+1)} \\ & + q_{(n_2,m_2),(n_2,m_2-1)} + q_{(n_2,m_2),C_H} + q_{(n_2,m_2),C_T}. \end{aligned}$$

Then, as $t_{(n_2,m_2)\to(n_2',m_2')} | (n_2, m_2) \to (n_2', m_2')$ is exponentially distributed with rate $R_{(n_2,m_2)}$ and $\mathbb{E}\left[\mathrm{e}^{-zX}\right] = \frac{\lambda}{\lambda+z}$ if $X \sim Exp(\lambda)$,

$$\mathbb{E}\left[\mathrm{e}^{-zt_{(n_2,m_2)\to(n_2',m_2')}} \middle| (n_2, m_2) \to (n_2', m_2')\right] = \frac{R_{(n_2,m_2)}}{R_{(n_2,m_2)} + z}.$$

Thus, the following system of linear equations is derived:

$$\begin{aligned} \phi^{VS_2}_{(n_2,m_2)}(z) = {} & \frac{\beta_2 n_s m_2}{R_{(n_2,m_2)} + z} \phi^{VS_2}_{(n_2+1,m_2)}(z) + \frac{(\mu_2 + \varphi_2) n_2}{R_{(n_2,m_2)} + z} \phi^{VS_2}_{(n_2-1,m_2)}(z) \\ & + \frac{\gamma_2 n_2 m_s + \alpha_2 m_s m_2}{R_{(n_2,m_2)} + z} \phi^{VS_2}_{(n_2,m_2+1)}(z) \\ & + \frac{\nu_2 m_2}{R_{(n_2,m_2)} + z} \phi^{VS_2}_{(n_2,m_2-1)}(z), \end{aligned} \tag{5.37}$$

which can be rewritten as

$$\begin{aligned} \left(R_{(n_2,m_2)} + z\right) \phi^{VS_2}_{(n_2,m_2)}(z) = {} & \beta_2 n_s m_2 \phi^{VS_2}_{(n_2+1,m_2)}(z) \\ & + (\mu_2 + \varphi_2) n_2 \phi^{VS_2}_{(n_2-1,m_2)}(z) \\ & + \left(\gamma_2 n_2 m_s + \alpha_2 m_s m_2\right) \phi^{VS_2}_{(n_2,m_2+1)}(z) \\ & + \nu_2 m_2 \phi^{VS_2}_{(n_2,m_2-1)}(z). \end{aligned} \tag{5.38}$$

Note that $\phi^{VS_2}_{C_H}(z) = \phi^{VS_2}_{C_T}(z) = 0$. Moreover, for $z = 0$, one has

$$\phi^{VS_2}_{(n_2,m_2)}(0) = \mathbb{E}\left[\mathbb{1}_{\left\{\tau^{VS_2}_{(n_2,m_2)} < +\infty\right\}}\right] = \mathbb{P}\left(\tau^{VS_2}_{(n_2,m_2)} < +\infty\right),$$

which is the probability of reaching the extinction of the invasive viral strain V_2 starting from (n_2, m_2), before any other fate (*i.e.*, E_2, C_T or C_H) is reached. We

introduce the notation $p^{VS_2}_{(n_2,m_2)} := \mathbb{P}\left(\tau^{VS_2}_{(n_2,m_2)} < +\infty\right)$. Hence, evaluating equation (5.38) at $z = 0$, one obtains the following system of linear equations:

$$\begin{aligned} R_{(n_2,m_2)}p^{VS_2}_{(n_2,m_2)} &= \beta_2 n_s m_2 p^{VS_2}_{(n_2+1,m_2)} + (\mu_2+\varphi_2)n_2 p^{VS_2}_{(n_2-1,m_2)} \\ &\quad + (\gamma_2 n_2 m_s + \alpha_2 m_s m_2)p^{VS_2}_{(n_2,m_2+1)} + \nu_2 m_2 p^{VS_2}_{(n_2,m_2-1)}. \end{aligned} \tag{5.39}$$

Boundary conditions are given by $p^{VS_2}_{(0,0)} = 1$ and $p^{VS_2}_{(n_2,m_2)} = 0$ if $n_2 + m_2 = \overline{N}_{\max}$. We note that reaching any state (n_2, m_2) with $n_2 + m_2 = \overline{N}_{\max}$ represents reaching the macro-state E_2 according to its definition. Recall that

$$\mathbb{E}\left[\left(\tau^{VS_2}_{(n_2,m_2)}\mathbb{1}_{\left\{\tau^{VS_2}_{(n_2,m_2)} < +\infty\right\}}\right)^l\right] = (-1)^l \frac{\mathrm{d}^l}{\mathrm{d}z^l}\phi^{VS_2}_{(n_2,m_2)}(z)\Big|_{z=0}, \quad l \geq 0. \tag{5.40}$$

One notes that, for $l = 0$, the 0th derivative of the Laplace-Stieltjes transform corresponds to the probabilities derived in equation (5.39), whereas for $l = 1$, the first derivative of the Laplace-Stieltjes transform corresponds to the first-order moments. In order to simplify the notation, denote the first-order moments as

$$M^{VS_2}_{(n_2,m_2)} = \mathbb{E}\left[\tau^{VS_2}_{(n_2,m_2)}\mathbb{1}_{\left\{\tau^{VS_2}_{(n_2,m_2)} < +\infty\right\}}\right].$$

Differentiating (5.38) with respect to z and evaluating it at $z = 0$, one obtains

$$\begin{aligned} R_{(n_2,m_2)}M^{VS_2}_{(n_2,m_2)} &= \beta_2 n_s m_2 M^{VS_2}_{(n_2+1,m_2)} + (\mu_2+\varphi_2)n_2 M^{VS_2}_{(n_2-1,m_2)} \\ &\quad + (\gamma_2 n_2 m_s + \alpha_2 m_s m_2)M^{VS_2}_{(n_2,m_2+1)} \\ &\quad + \nu_2 m_2 M^{VS_2}_{(n_2,m_2-1)} + p^{VS_2}_{(n_2,m_2)}. \end{aligned} \tag{5.41}$$

Boundary conditions are given by $M^{VS_2}_{(n_2,m_2)} = 0$ if $n_2 + m_2 = \overline{N}_{\max}$ because in this case $\mathbb{1}_{\left\{\tau^{VS_2}_{(n_2,m_2)} < +\infty\right\}} = 0$.

Equations (5.41) show that, in order to compute $M^{VS_2}_{(n_2,m_2)}$, it is necessary to first determine the value of $p^{VS_2}_{(n_2,m_2)}$, that is the computation of the first derivative of the Laplace-Stieltjes transform depends on the 0th derivative of the transform. More broadly, this method could be used to compute higher order moments of the random variable $\tau^{VS_2}_{(n_2,m_2)}\mathbb{1}_{\left\{\tau^{VS_2}_{(n_2,m_2)} < +\infty\right\}}$, where the lth derivative of the Laplace-Stieltjes transform depends on the $l-1$th derivative previously computed in an algorithmic fashion. However, our interest is in computing the derivatives defined

in equation (5.40) for $l = 0, 1$, which correspond to the probabilities in equations (5.39) and to the first-order moments in equations (5.41), respectively.
In order to write equations (5.39) and (5.41) in matrix form, the state space Ω_2 is organised in sub-sets (here called levels) as follows:

$$\begin{aligned} \mathscr{L}(j) &= \{(n_2, m_2) \in \Omega_2 : n_2 + m_2 = j\}, \\ \Omega_2 &= \bigcup_{j=1}^{\overline{N}_{\max}-1} \mathscr{L}(j) \cup \{(0,0)\} \cup E_2 \cup C_H \cup C_T. \end{aligned} \tag{5.42}$$

Note that equations (5.39) and (5.41) represent a system of linear equations with one equation per (initial) state in Ω_2. Thus, if one orders the states by levels with $\mathscr{L}(0) \prec \mathscr{L}(1) \prec \cdots \prec \mathscr{L}(\overline{N}_{\max} - 1)$, and the states within each level $\mathscr{L}(j)$ as $(j, 0) \prec (j-1, 1) \prec (j-2, 2) \prec \cdots \prec (0, j)$, then it is clear that only transitions to adjacent levels and to the absorbing states C_H and C_T are allowed (see Figure 5.12). In particular, from any state (n_2, m_2) in $\mathscr{L}(j)$, the next event in the Markov chain can take the process to either a state in level $\mathscr{L}(j-1)$ through the death or V_2 clearance of a host infected with V_2 or the death of a tick infected with the invasive strain, or a state in level $\mathscr{L}(j+1)$ via a new infection with V_2 of either a host or a tick. Moreover, from states in level $\mathscr{L}(\overline{N}_{\max} - 1)$, the process can either move to level $\mathscr{L}(\overline{N}_{\max} - 2)$ or to the absorbing states E_2, C_H and C_T, representing virus establishment and co-infection events. Note that the absorbing state E_2 can be reached only from $\mathscr{L}(\overline{N}_{\max} - 1)$, whereas the co-infection absorbing states can be reached from any $(n_2, m_2) \in \Omega_2$. On the other hand, the extinction of the invasive strain represented by the state $(0, 0)$ can be accessed only from level $\mathscr{L}(1)$.
Thus, equations (5.39) and (5.41) can be rewritten in a matrix form as

$$\boldsymbol{X}^{(l)}(VS_2) = \boldsymbol{C}\boldsymbol{X}^{(l)}(VS_2) + \boldsymbol{b}^{(l)}(VS_2), \quad l = 0, 1, \tag{5.43}$$

where

$$\boldsymbol{X}^{(l)}(VS_2) = \begin{pmatrix} \boldsymbol{X}_1^{(l)}(VS_2) \\ \boldsymbol{X}_2^{(l)}(VS_2) \\ \boldsymbol{X}_3^{(l)}(VS_2) \\ \vdots \\ \boldsymbol{X}_{\overline{N}_{\max}-1}^{(l)}(VS_2) \end{pmatrix}, \qquad \boldsymbol{b}^{(l)}(VS_2) = \begin{pmatrix} \boldsymbol{b}_1^{(l)}(VS_2) \\ \boldsymbol{b}_2^{(l)}(VS_2) \\ \boldsymbol{b}_3^{(l)}(VS_2) \\ \vdots \\ \boldsymbol{b}_{\overline{N}_{\max}-1}^{(l)}(VS_2) \end{pmatrix},$$

$$\boldsymbol{C} = \begin{pmatrix} \mathbf{0} & \boldsymbol{C}_{1,2} & \mathbf{0} & \cdots & \mathbf{0} & \mathbf{0} \\ \boldsymbol{C}_{2,1} & \mathbf{0} & \boldsymbol{C}_{2,3} & \cdots & \mathbf{0} & \mathbf{0} \\ \mathbf{0} & \boldsymbol{C}_{3,2} & \mathbf{0} & \cdots & \mathbf{0} & \mathbf{0} \\ \vdots & \ddots & \ddots & \ddots & \vdots & \vdots \\ \mathbf{0} & \mathbf{0} & \mathbf{0} & \cdots & \mathbf{0} & \boldsymbol{C}_{\overline{N}_{\max}-2,\overline{N}_{\max}-1} \\ \mathbf{0} & \mathbf{0} & \mathbf{0} & \cdots & \boldsymbol{C}_{\overline{N}_{\max}-1,\overline{N}_{\max}-2} & \mathbf{0} \end{pmatrix}.$$

The sub-vectors $\boldsymbol{X}_j^{(l)}(VS_2)$ and $\boldsymbol{b}_j^{(l)}(VS_2)$ that constitute the vectors $\boldsymbol{X}^{(l)}(VS_2)$ and $\boldsymbol{b}^{(l)}(VS_2)$ respectively, $l = 0, 1$, have dimensions $j+1$, with $j = 1, \ldots, \overline{N}_{\max}-1$.

For $l = 0$, which corresponds to the probabilities in equation (5.39), the sub-vectors $\boldsymbol{X}_j^{(0)}(VS_2)$ that comprise $\boldsymbol{X}^{(0)}(VS_2)$ are defined as

$$\boldsymbol{X}_j^{(0)}(VS_2) = \begin{pmatrix} p_{(j,0)}^{VS_2} \\ p_{(j-1,1)}^{VS_2} \\ \vdots \\ p_{(0,j)}^{VS_2} \end{pmatrix}, \quad j = 1, \ldots, \overline{N}_{\max} - 1,$$

whereas $\boldsymbol{b}_j^{(0)}(VS_2) = \mathbf{0}$ if $j > 1$ and

$$\boldsymbol{b}_1^{(0)}(VS_2) = \begin{pmatrix} \dfrac{\mu_2 + \varphi_2}{R_{(1,0)}} \\ \dfrac{\nu_2}{R_{(0,1)}} \end{pmatrix}.$$

In the instance of equations (5.41), which correspond to $l = 1$, the sub-vectors in $\boldsymbol{X}^{(1)}(VS_2)$ are given by

$$\boldsymbol{X}_j^{(1)}(VS_2) = \begin{pmatrix} M_{(j,0)}^{VS_2} \\ M_{(j-1,1)}^{VS_2} \\ \vdots \\ M_{(0,j)}^{VS_2} \end{pmatrix}, \quad j = 1, \ldots, \overline{N}_{\max} - 1,$$

and $\boldsymbol{b}^{(1)}$ consists of sub-vectors defined as

$$\boldsymbol{b}_j^{(1)}(VS_2) = \begin{pmatrix} \dfrac{p^{VS_2}_{(j,0)}}{R_{(j,0)}} \\ \dfrac{p^{VS_2}_{(j-1,1)}}{R_{(j-1,1)}} \\ \vdots \\ \dfrac{p^{VS_2}_{(0,j)}}{R_{(0,j)}} \end{pmatrix}, \quad j = 1, \dots, \overline{N}_{\max} - 1,$$

The blocks that comprise the matrix $\boldsymbol{C}$, $\boldsymbol{C}_{k+1,k}$ and $\boldsymbol{C}_{k,k+1}$, have dimensions $(k+2) \times (k+1)$ and $(k+1) \times (k+2)$ respectively, and are defined as follows:

- For $k = 1, \dots, \overline{N}_{\max} - 2$:

$$(\boldsymbol{C}_{k+1,k})_{i+1,j+1} = \begin{cases} \dfrac{(k+1-i)(\mu_2+\varphi_2)}{R_{(k+1-i,i)}}, & \text{if } i = j, \\ \dfrac{i\nu_2}{R_{(k+1-i,i)}}, & \text{if } i = j+1, \\ 0, & \text{otherwise,} \end{cases}$$

  where $i = 0, \dots, k+1$ and $j = 0, \dots, k$.

- For $k = 1, \dots, \overline{N}_{\max} - 2$:

$$(\boldsymbol{C}_{k,k+1})_{i+1,j+1} = \begin{cases} \dfrac{((k-i)\gamma_2 + i\alpha_2)m_s}{R_{(k-i,i)}}, & \text{if } i = j-1, \\ \dfrac{i\beta_2 n_s}{R_{(k-i,i)}}, & \text{if } i = j, \\ 0, & \text{otherwise,} \end{cases}$$

  where $i = 0, \dots, k$ and $j = 0, \dots, k+1$.

Equation (5.43) can then be solved efficiently adapting Algorithm 4 to obtain $p^{VS_2}_{(n_2,m_2)}$ and $M^{VS_2}_{(n_2,m_2)}$ for any initial state $(n_2, m_2) \in \Omega_2$.
Once $M^{VS_2}_{(n_2,m_2)}$ is at hand, invoking the law of total expectation, one has

$$\begin{aligned} M^{VS_2}_{(n_2,m_2)} &= \mathbb{E}\left[\tau^{VS_2}_{(n_2,m_2)} \mathbb{1}_{\left\{\tau^{VS_2}_{(n_2,m_2)} < +\infty\right\}} \middle| \tau^{VS_2}_{(n_2,m_2)} < +\infty\right] \mathbb{P}\left(\tau^{VS_2}_{(n_2,m_2)} < +\infty\right) \\ &+ \mathbb{E}\left[\tau^{VS_2}_{(n_2,m_2)} \mathbb{1}_{\left\{\tau^{VS_2}_{(n_2,m_2)} < +\infty\right\}} \middle| \tau^{VS_2}_{(n_2,m_2)} = +\infty\right] \mathbb{P}\left(\tau^{VS_2}_{(n_2,m_2)} = +\infty\right) \\ &= \mathbb{E}\left[\tau^{VS_2}_{(n_2,m_2)} \middle| \tau^{VS_2}_{(n_2,m_2)} < +\infty\right] \mathbb{P}\left(\tau^{VS_2}_{(n_2,m_2)} < +\infty\right), \end{aligned}$$

which yields

$$\mathbb{E}\left[\tau^{VS_2}_{(n_2,m_2)}\middle|\tau^{VS_2}_{(n_2,m_2)} < +\infty\right] = \frac{M^{VS_2}_{(n_2,m_2)}}{p^{VS_2}_{(n_2,m_2)}},$$

that represents the conditional expected time to reach the virus-free state from any initial state $(n_2, m_2) \in \Omega_2$ contioned on the process actually reaching this absorbing state.

On the other hand, one could define for $(n_2, m_2) \in \Omega_2$

$$\tau^{E_2}_{(n_2,m_2)} = \inf\{t \geq 0 : H_2(t) + T_2(t) = \overline{N}_{\max} | (H_2(0), T_2(0)) = (n_2, m_2)\},$$

that is the time to reach the absorbing macro-state E_2 (*i.e.*, establishment of the invasive strain V_2) starting with n_2 hosts and m_2 ticks infected with V_2. In this case, the fact that the absorbing state E_2 is not reached does not necessarily mean that the invasive viral strain establishment does not occur. Indeed, a co-infection event might happen first. The probability of V_2 strain establishment and the expected time to V_2 strain establishment conditioned on actually reaching this fate can be computed starting from any initial state $(n_2, m_2) \in \Omega_2$. This can be obtained from the Laplace-Stieltjes transform of $\tau^{E_2}_{(n_2,m_2)}$ defined as

$$\phi^{E_2}_{(n_2,m_2)}(z) = \mathbb{E}\left[\mathrm{e}^{-z\tau^{E_2}_{(n_2,m_2)}} \mathbb{1}_{\left\{\tau^{E_2}_{(n_2,m_2)} < +\infty\right\}}\right], \quad \mathrm{Re}(z) \geq 0.$$

Similarly to the case of virus-free state for the invasive viral strain V_2, define

$$\begin{aligned} M^{E_2}_{(n_2,m_2)} &= \mathbb{E}\left[\tau^{E_2}_{(n_2,m_2)} \mathbb{1}_{\left\{\tau^{E_2}_{(n_2,m_2)} < +\infty\right\}}\right], \\ p^{E_2}_{(n_2,m_2)} &= \mathbb{P}\left(\tau^{E_2}_{(n_2,m_2)} < +\infty\right). \end{aligned}$$

Following the same steps illustrated for $\phi^{VS_2}_{(n_2,m_2)}(z)$, one obtains the analogous system of linear equations derived in equations (5.39) and (5.41) for $p^{E_2}_{(n_2,m_2)}$ and $M^{E_2}_{(n_2,m_2)}$ respectively. This systems of equations can be rewritten in matrix form using the order of the state space described in equation (5.42). This yields

$$\boldsymbol{X}^{(l)}(E_2) = \boldsymbol{C}\boldsymbol{X}^{(l)}(E_2) + \boldsymbol{b}^{(l)}(E_2), \quad l = 0, 1. \tag{5.44}$$

The same matrix $\boldsymbol{C}$ is derived, whereas the sub-vectors that comprise $\boldsymbol{X}^{(0)}(E_2)$ and $\boldsymbol{X}^{(1)}(E_2)$ are defined as

$$\boldsymbol{X}_j^{(0)}(E_2) = \begin{pmatrix} p_{(j,0)}^{E_2} \\ p_{(j-1,1)}^{E_2} \\ \vdots \\ p_{(0,j)}^{E_2} \end{pmatrix}, \quad j = 1, \ldots, \overline{N}_{\max} - 1,$$

and

$$\boldsymbol{X}_j^{(1)}(E_2) = \begin{pmatrix} M_{(j,0)}^{E_2} \\ M_{(j-1,1)}^{E_2} \\ \vdots \\ M_{(0,j)}^{E_2} \end{pmatrix}, \quad j = 1, \ldots, \overline{N}_{\max} - 1,$$

respectively. On the other hand, the sub-vectors of $\boldsymbol{b}^{(1)}(E_2)$ are given by

$$\boldsymbol{b}_j^{(1)}(E_2) = \begin{pmatrix} \dfrac{p_{(j,0)}^{E_2}}{R_{(j,0)}} \\ \dfrac{p_{(j-1,1)}^{E_2}}{R_{(j-1,1)}} \\ \vdots \\ \dfrac{p_{(0,j)}^{E_2}}{R_{(0,j)}} \end{pmatrix}, \quad j = 1, \ldots, \overline{N}_{\max} - 1.$$

whereas $\boldsymbol{b}_j^{(0)}(E_2) = \boldsymbol{0}$ if $j < \overline{N}_{\max} - 1$ and

$$\boldsymbol{b}_{\overline{N}_{\max}-1}^{(0)}(E_2) = \begin{pmatrix} \dfrac{\gamma_2(\overline{N}_{\max} - 1)}{R_{(\overline{N}_{\max}-1,0)}} \\ \dfrac{\gamma_2 m_s(\overline{N}_{\max} - 2) + \beta_2 n_s + \alpha_2 m_s}{R_{(\overline{N}_{\max}-2,1)}} \\ \vdots \\ \dfrac{(\beta_2 n_s + \alpha_2 m_s)(\overline{N}_{\max} - 1)}{R_{(0,\overline{N}_{\max}-1))}} \end{pmatrix}.$$

Algorithm 4 can be then adapted to compute $p_{(n_2,m_2)}^{E_2}$ and $M_{(n_2,m_2)}^{E_2}$, as well as the expected time to reach an endemic state conditioned on the process actually reaching this absorbing state, for any initial state $(n_2, m_2) \in \Omega_2$.

Probability and conditional time to co-infection events

We are interested in computing the probability of the first co-infection events, that is the first co-infection of a vertebrate or the first co-infection of a tick, as well as the conditional times to such events because they can be used to estimate the probability and the timescale of potential reassortment events. We note that in the stochastic model presented in this section, co-transmission (*i.e.*, a susceptible individual can become co-infected in one time step) is not considered.
In order to compute the probability of the first host co-infection, define for $(n_2, m_2) \in \Omega_2$

$$\tau^{C_H}_{(n_2,m_2)} = \inf\{t \geq 0 : \text{process visits } C_H | (H_2(0), T_2(0)) = (n_2, m_2)\},$$

that is the time to have a co-infected vertebrate for the first time starting with n_2 hosts and m_2 ticks infected with the invasive viral strain V_2. The probability of the first co-infection of a host and the expected time to the first co-infection of a host conditioned on actually reaching this fate can be computed starting from any initial state $(n_2, m_2) \in \Omega_2$. This can be obtained from the Laplace-Stieltjes transform of $\tau^{C_H}_{(n_2,m_2)}$ defined as

$$\phi^{C_H}_{(n_2,m_2)}(z) = \mathbb{E}\left[\mathrm{e}^{-z\tau^{C_H}_{(n_2,m_2)}} \mathbb{1}_{\left\{\tau^{C_H}_{(n_2,m_2)} < +\infty\right\}}\right], \quad \mathrm{Re}(z) \geq 0.$$

Similarly to the case of the virus-free state and the establishment of the invasive viral strain V_2 analysed in the previous section, define

$$M^{C_H}_{(n_2,m_2)} = \mathbb{E}\left[\tau^{C_H}_{(n_2,m_2)} \mathbb{1}_{\left\{\tau^{C_H}_{(n_2,m_2)} < +\infty\right\}}\right],$$
$$p^{C_H}_{(n_2,m_2)} = \mathbb{P}\left(\tau^{C_H}_{(n_2,m_2)} < +\infty\right).$$

Following the same steps illustrated for $\phi^{VS_2}_{(n_2,m_2)}(z)$, one obtains the analogous system of linear equations derived in equations (5.39) and (5.41) for $p^{C_H}_{(n_2,m_2)}$ and $M^{C_H}_{(n_2,m_2)}$ respectively. This systems of equations can be rewritten in matrix form using the order of the state space described in equation (5.42). This yields

$$\boldsymbol{X}^{(l)}(C_H) = \boldsymbol{C}\boldsymbol{X}^{(l)}(C_H) + \boldsymbol{b}^{(l)}(C_H), \quad l = 0, 1. \tag{5.45}$$

The same matrix $\boldsymbol{C}$ is derived, whereas the sub-vectors that comprise $\boldsymbol{X}^{(0)}(C_H)$ and $\boldsymbol{X}^{(1)}(C_H)$ are defined as

$$\boldsymbol{X}_j^{(0)}(C_H) = \begin{pmatrix} p_{(j,0)}^{C_H} \\ p_{(j-1,1)}^{C_H} \\ \vdots \\ p_{(0,j)}^{C_H} \end{pmatrix}, \quad j = 1, \ldots, \overline{N}_{\max} - 1,$$

and

$$\boldsymbol{X}_j^{(1)}(C_H) = \begin{pmatrix} M_{(j,0)}^{C_H} \\ M_{(j-1,1)}^{C_H} \\ \vdots \\ M_{(0,j)}^{C_H} \end{pmatrix}, \quad j = 1, \ldots, \overline{N}_{\max} - 1,$$

respectively. On the other hand, the sub-vectors of $\boldsymbol{b}^{(1)}(C_H)$ are given by

$$\boldsymbol{b}_j^{(1)}(C_H) = \begin{pmatrix} \dfrac{p_{(j,0)}^{C_H}}{R_{(j,0)}} \\ \dfrac{p_{(j-1,1)}^{C_H}}{R_{(j-1,1)}} \\ \vdots \\ \dfrac{p_{(0,j)}^{C_H}}{R_{(0,j)}} \end{pmatrix}, \quad j = 1, \ldots, \overline{N}_{\max} - 1.$$

whereas

$$\boldsymbol{b}_j^{(0)}(C_H) = \begin{pmatrix} \dfrac{j\zeta_1 m_1}{R_{(j,0)}} \\ \dfrac{(j-1)\zeta_1 m_1 + \zeta_2 n_1}{R_{(j-1,1)}} \\ \vdots \\ \dfrac{j\zeta_2 n_1}{R_{(0,j)}} \end{pmatrix}, \quad j = 1, \ldots, \overline{N}_{\max} - 1.$$

Algorithm 4 can be then adapted to compute $p_{(n_2,m_2)}^{C_H}$ and $M_{(n_2,m_2)}^{C_H}$ for any initial state $(n_2, m_2) \in \Omega_2$. Then, the expected time to the first co-infection of a host conditioned on the process actually reaching this absorbing state is derived as

$$\mathcal{T}_{(n_2,m_2)}^{C_H} = \mathbb{E}\left[\tau_{(n_2,m_2)}^{C_H} \middle| \tau_{(n_2,m_2)}^{C_H} < +\infty\right] = \frac{M_{(n_2,m_2)}^{C_H}}{p_{(n_2,m_2)}^{C_H}}. \tag{5.46}$$

Finally, in order to compute the probability of the first tick co-infection, define for $(n_2, m_2) \in \Omega_2$

$$\tau^{C_T}_{(n_2,m_2)} = \inf\{t \geq 0 : \text{process visits } C_T | (H_2(0), T_2(0)) = (n_2, m_2)\},$$

that is the time to have a co-infected tick for the first time starting with n_2 hosts and m_2 ticks infected with the invasive viral strain V_2. The probability of the first co-infection of a tick and the expected time to the first co-infection of a tick conditioned on actually reaching this fate can be computed starting from any initial state $(n_2, m_2) \in \Omega_2$. This can be obtained from the Laplace-Stieltjes transform of $\tau^{C_T}_{(n_2,m_2)}$ defined as

$$\phi^{C_T}_{(n_2,m_2)}(z) = \mathbb{E}\left[\mathrm{e}^{-z\tau^{C_T}_{(n_2,m_2)}} \mathbb{1}_{\left\{\tau^{C_T}_{(n_2,m_2)} < +\infty\right\}}\right], \quad \mathrm{Re}(z) \geq 0.$$

Similarly to the case of the virus-free state and the establishment of the invasive viral strain V_2 analysed in the previous section, define

$$M^{C_T}_{(n_2,m_2)} = \mathbb{E}\left[\tau^{C_T}_{(n_2,m_2)} \mathbb{1}_{\left\{\tau^{C_T}_{(n_2,m_2)} < +\infty\right\}}\right],$$
$$p^{C_T}_{(n_2,m_2)} = \mathbb{P}\left(\tau^{C_T}_{(n_2,m_2)} < +\infty\right).$$

Following the same steps illustrated for $\phi^{VS_2}_{(n_2,m_2)}(z)$, one obtains the analogous system of linear equations derived in equations (5.39) and (5.41) for $p^{C_T}_{(n_2,m_2)}$ and $M^{C_T}_{(n_2,m_2)}$ respectively. Note that

$$p^{C_T}_{(n_2,m_2)} = 1 - p^{VS_2}_{(n_2,m_2)} - p^{E_2}_{(n_2,m_2)} - p^{C_H}_{(n_2,m_2)}, \quad \text{for all } (n_2, m_2) \in \Omega_2,$$

therefore only the analogous of system (5.41) has to be solved to find $M^{C_T}_{(n_2,m_2)}$. This system of equations can be rewritten in matrix form using the order of the state space described in equation (5.42). One obtains

$$\boldsymbol{X}^{(l)}(C_T) = \boldsymbol{C}\boldsymbol{X}^{(l)}(C_T) + \boldsymbol{b}^{(l)}(C_T), \quad l = 1. \tag{5.47}$$

The same matrix $\boldsymbol{C}$ is derived, whereas the sub-vectors that comprise $\boldsymbol{X}^{(1)}(C_T)$ are defined as

$$\boldsymbol{X}^{(1)}_j(C_T) = \begin{pmatrix} M^{C_T}_{(j,0)} \\ M^{C_T}_{(j-1,1)} \\ \vdots \\ M^{C_T}_{(0,j)} \end{pmatrix}, \quad j = 1, \ldots, \overline{N}_{\max} - 1,$$

On the other hand, the sub-vectors of $\boldsymbol{b}^{(1)}(C_T)$ are given by

$$\boldsymbol{b}_j^{(1)}(C_T) = \begin{pmatrix} \dfrac{p^{C_T}_{(j,0)}}{R_{(j,0)}} \\ \dfrac{p^{C_T}_{(j-1,1)}}{R_{(j-1,1)}} \\ \vdots \\ \dfrac{p^{C_T}_{(0,j)}}{R_{(0,j)}} \end{pmatrix}, \quad j = 1, \ldots, \overline{N}_{\max} - 1.$$

Algorithm 4 can be then adapted to compute $M^{C_T}_{(n_2,m_2)}$ for any initial state $(n_2, m_2) \in \Omega_2$. This enables the computation of the expected time to have the first tick co-infection conditioned on the process actually reaching this absorbing state as

$$\mathcal{T}^{C_T}_{(n_2,m_2)} = \mathbb{E}\left[\tau^{C_T}_{(n_2,m_2)} \middle| \tau^{C_T}_{(n_2,m_2)} < +\infty\right] = \frac{M^{C_T}_{(n_2,m_2)}}{p^{C_T}_{(n_2,m_2)}}. \tag{5.48}$$

Figure 5.13 shows the probability of reaching the first co-infection of a host (panel **A**) or a tick (panel **B**), whereas Figure 5.14 depicts the expected time to reach the first co-infection of a host (panel **A**) or a tick (panel **B**) conditioned on the process actually reaching these absorbing states, for different values of the transmission parameters ζ_1, ξ_1 and λ_2, and initial conditions. The parameter ξ_1, which models a tick infected with V_1 infecting a tick infected with V_2, leading to a co-infected tick, affects the probabilities $p^{C_H}_{(n_2,m_2)}$ and $p^{C_T}_{(n_2,m_2)}$, as well as the conditional times $\mathcal{T}^{C_H}_{(n_2,m_2)}$ and $\mathcal{T}^{C_T}_{(n_2,m_2)}$, only when the invasive strain is introduced in the system through infected ticks. Indeed, when the invasive strain is introduced in the system through infected hosts, there are no ticks infected with V_2 that can be infected by a tick infected with V_1. On the other hand, the parameters ζ_1 (representing a tick infected with V_1 infecting a host infected with V_2, yielding a co-infected host) and λ_2 (modelling a host infected with V_2 infecting a tick infected with V_1, resulting in the co-infection of a tick) affect the probabilities $p^{C_H}_{(n_2,m_2)}$ and $p^{C_T}_{(n_2,m_2)}$, and the conditional times $\mathcal{T}^{C_H}_{(n_2,m_2)}$ and $\mathcal{T}^{C_T}_{(n_2,m_2)}$, only when the invasive strain is introduced in the system through infected hosts. Indeed, when the invasive strain is introduced in the system through infected ticks, there are no hosts infected with V_2 that can be infected by, or infect, a tick infected with V_1.

In Figure 5.13, when V_2 is introduced in the populations through infected hosts, larger values of λ_2 correspond to a smaller probability of reaching a co-infected host (first row of panel **A**). This is explained by the fact that increasing λ_2 while keeping the other parameters fixed and considering the same initial conditions, determines an increment of the probability of the co-infection of a tick occurring first, as shown in panel **B** of Figure 5.13. Considering the same initial conditions, one observes that larger values of ζ_1 increase the probability of reaching the first co-infection of a host, while decreasing the probability of the first co-infection of a tick occurring, as our intuition would suggest. On the other hand, when the invasive strain V_2 is introduced in the system through infected ticks, an increase of ξ_1 makes the first co-infection of a tick more likely to occur (see the second row of panel **B**), as one would expect.

In Figure 5.14, it is interesting to observe that, when starting with hosts infected with V_2, the conditional time to reach the first co-infection of a host (first row of panel **A**) is short, particularly for larger values of λ_2, as one would expect. On the other hand, when the invasive strain is introduced through infected ticks (second row of panel **A**), the conditional time to reach the first co-infection of a host is significantly longer. Indeed, in this model, we are not considering co-transmission and the parameters ζ_2 (which represents the infection of a host infected with V_1 by a tick infected with V_2) and β_2 (which models the infection of a susceptible host by a tick infected with V_2) are small. Thus, in those few cases when the co-infection of a host is reached starting with only ticks infected with V_2 (since the probability $p^{C_H}_{(n_2,m_2)}$ is low), a longer time is needed to reach the first co-infection of a host before other absorbing states.

Regarding the conditional time to reach the first co-infection of a tick depicted in panel **B** of Figure 5.14, one notes that the process takes on average a short time to reach the first co-infection of a tick for all the parameter values but when starting with only hosts infected by V_2 and $\lambda_2 = 10^{-4}$. In this instance, the parameter ζ_1 is inversely proportional to $\mathcal{T}^{C_T}_{(n_2,m_2)}$. This can be explained by the fact that the process takes also a shorter time to be absorbed by C_H when ζ_1 is larger. Thus, in order to observe first the co-infection of a tick, the process has to reach this absorbing state quicker when ζ_1 increases.

In summary, the results in Figures 5.13 and 5.14 suggest that the main factors (*i.e.*, the main parameters) affecting the probability and conditional time to reach the first co-infection of a host or a tick significantly depend on how the invasive strain is introduced into the population. When V_2 enters the system through infected ticks, the process is more likely to reach the first co-infection of a tick before the first co-infection of a host. Instead, when the invasive strain is introduced via infected hosts, the fate of the process depends significantly on the value of λ_2. Regarding the conditional times to reach the first co-infection event, we observe that the timescale to reach the first co-infection of a tick is on average shorter than the timescale required to have the first co-infected host.

5.3 Discussion

Interacting populations of ticks and hosts are considered to describe the transmission of tick-borne viral infections. The focus of the work presented here is on three fundamental aspects: co-feeding, co-infection and co-transmission. The virus can be transmitted tick-to-host, host-to-tick and tick-to-tick through co-feeding (Gonzalez *et al.*, 1992; Matser *et al.*, 2009). With the aim of characterising the role of different routes of transmission, we propose a deterministic model of single infection dynamics. As the model presents more than one type of infectious individuals, the basic reproduction number is derived by means of the next generation matrix approach (Diekmann *et al.*, 2010; Van den Driessche & Watmough, 2002), considering all the possible routes of transmission and under some simplified scenarios. This study allows us to prove that co-feeding and systemic transmission are two distinguished routes of transmission, with co-feeding being the only route able to maintain an epidemic with no other route of transmission in place. The deterministic model is then approximated making use of the branching processes theory (Allen, 2010), which enables the derivation of a condition for the epidemic extinction equivalent to the basic reproduction number R_0 computed in the deterministic setting. Then, a stochastic approach that accounts for the depletion of susceptible individuals due to infection allows us to derive the probability of virus extinction versus epidemic establishment, as well as the conditional times to

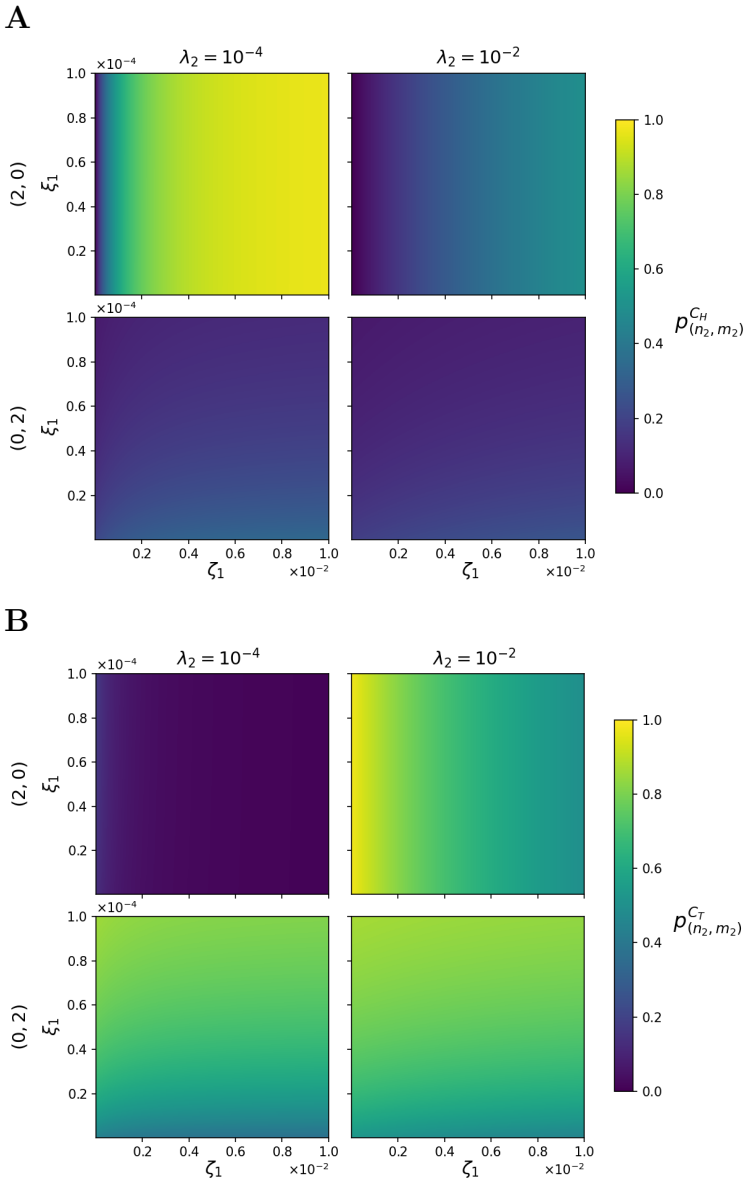

Figure 5.13: The probabilities of reaching the first co-infection of a host $p^{C_H}_{(n_2,m_2)}$ (**A**), and the first co-infection of a tick $p^{C_T}_{(n_2,m_2)}$ (**B**) are plotted for different values of the transmission parameters ζ_1, ξ_1 and λ_2, and initial conditions. The transmission parameter λ_2 varies as 10^{-4} (left column) and 10^{-2} (right column). The probabilities $p^{C_H}_{(n_2,m_2)}$ and $p^{C_T}_{(n_2,m_2)}$ are computed starting with two infected hosts (first row of **A** and **B**) or two infected ticks (second row of **A** and **B**). The parameter ζ_1 varies between 10^{-5} and 10^{-2} along the x-axis, whereas ξ_1 varies between 10^{-7} and 10^{-4} along the y-axis. The other parameters are fixed as follows: $\overline{N}_{\max} = 20$, $n_s = n_1 = 10$, $m_s = m_1 = 10^2$, $\beta_2 = \gamma_2 = \zeta_2 = \lambda_1 = 10^{-4}$, $\alpha_2 = \xi_2 = 10^{-5}$, $\mu_2 = 1/(4 \times 365)$ and $\nu_2 = 1/200$.

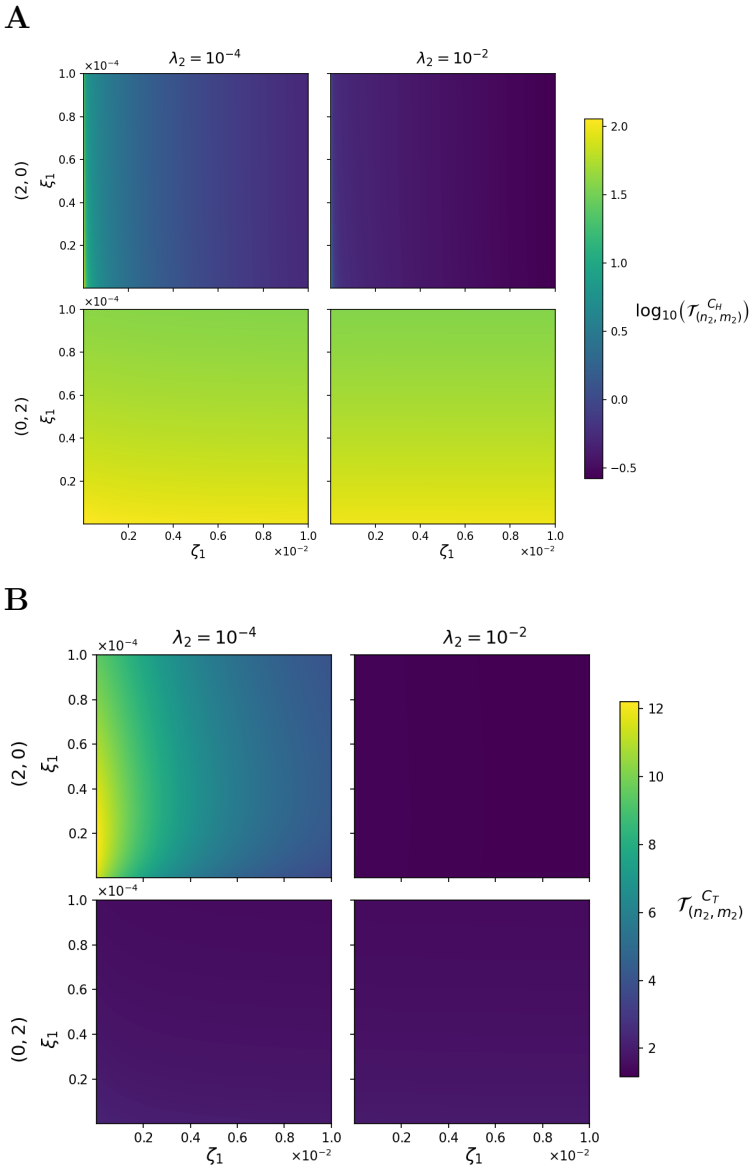

Figure 5.14: The conditional times to reach the first co-infection of a host $\mathcal{T}_{(n_2,m_2)}^{C_H}$ (**A**), and the first co-infection of a tick $\mathcal{T}_{(n_2,m_2)}^{C_T}$ (**B**) are plotted for different values of the transmission parameters ζ_1, ξ_1 and λ_2, and initial conditions. The transmission parameter λ_2 varies as 10^{-4} (left column) and 10^{-2} (right column). The conditional times $\mathcal{T}_{(n_2,m_2)}^{C_H}$ and $\mathcal{T}_{(n_2,m_2)}^{C_T}$ are computed starting with two infected hosts (first row of **A** and **B**) or two infected ticks (second row of **A** and **B**). The parameter ζ_1 varies between 10^{-5} and 10^{-2} along the x-axis, whereas ξ_1 varies between 10^{-7} and 10^{-4} along the y-axis. The other parameters are fixed as follows: $\overline{N}_{\max} = 20$, $n_s = n_1 = 10$, $m_s = m_1 = 10^2$, $\beta_2 = \gamma_2 = \zeta_2 = \lambda_1 = 10^{-4}$, $\alpha_2 = \xi_2 = 10^{-5}$, $\mu_2 = 1/(4 \times 365)$ and $\nu_2 = 1/200$.

such events. In this setting, we also derive the distribution of the exact number of secondary infections (Artalejo & Lopez-Herrero, 2013).

On the other hand, as co-infection is a necessary condition for reassortment, it is interesting to study the different factors affecting the probability and timescales of the first co-infection events occurring. Assuming that ticks and hosts are susceptible to the infection of two different strains of the same virus, V_1 and V_2 (resident and invasive respectively), we propose a deterministic model of co-feeding transmission that accounts for co-transmission (Alizon, 2013a). The basic reproduction number and the invasion reproduction number of the invasive viral strain V_2 in an endemic equilibrium of the resident strain V_1 are computed by making use of the next generation matrix. Since our model does not account for individuals infected twice with the same viral strain, the invasive virus V_2 possesses an intrinsic advantage over the invasive strain (Alizon, 2013a,b). Indeed, the invasive strain can infect both susceptible individuals and individuals infected with V_1, whereas the resident strain can only infect susceptible individuals as hosts and ticks infected by V_2 are rare. In order to overcome this issue, we propose a normalisation for the invasion reproduction number of the invasive viral strain V_2 in an endemic equilibrium of the resident strain V_1. We are interested in comparing our solution with the invasion reproduction number computed in the model where co-infection with the same strain is allowed (Alizon, 2013a; van Baalen & Sabelis, 1995). A challenge of this alternative might be the complexity of the analysis, particularly when considering both systemic and non-systemic transmission. The comparison of the invasion reproduction number computed under these different assumptions is the aim of future work.

A stochastic approach is also proposed to compute some stochastic descriptors of interest, such as the probability of the establishment of the invasive viral strain versus its extinction, and the probability of the first co-infection events, as well as the expected conditional times to such events. Our analyses of these stochastic descriptors show that the main parameters that affect the probability and timescale to the first co-infection of a tick or a host depend on how the invasive strain is introduced in the system (either through ticks or hosts infected with V_2). Moreover, the conditional time required to reach the first co-infection of a tick is on average shorter than the conditional time to have the first co-infected host.

We note that this stochastic approach does not account for co-transmission, *i.e.*, an individual cannot become infected with both strains simultaneously. It is the aim of future work to include in the model this type of transmission, analysing how co-transmission affects the stochastic descriptors. From an epidemiological perspective, it would be also interesting to compute the distribution of the exact number of secondary infections directly caused by a tick or a host infected with the invasive viral strain V_2, similarly to the analysis carried out in Section 5.1.4 for a single infection.

One could also think to parametrise the mathematical models presented here making use of experimental data, for example, antibody seroprevalence data (Monsalve-Arteaga *et al.*, 2020; Nurettin *et al.*, 2022; Phonera *et al.*, 2021). The assumptions on the parameters, especially in the case of co-infection with two different viruses or viral strains, would depend on the quantity and the quality of the data, as well as on the specific questions that one would be interested in answering. Personally, given the challenge that I faced when looking for the values of infection transmission parameters (for example, α_1, β_1 and γ_1 in the instance of single infection dynamics), I would be interested in providing a sensible estimation for them.

In summary, the work presented in this chapter provides several tools to better characterise co-infection dynamics in tick-borne virus transmission and to understand the role that different routes of transmission play in the spread of the virus. Beyond the future research that I mentioned above, a natural prosecution of this study would consist in the definition of mathematical models of the intracellular life cycle of Bunyaviruses with reassortment as the co-infection of a single cell is a necessary condition for reassortment.

Appendix A

Akaike Information Criterion for model selection

In Chapter 3 I made use of the corrected version of the Akaike's information criterion (AIC_C) to compare statistically the performance of the exponential and the Erlang MS-G models accounting for the extra parameters N_0 and N when assuming Erlang times to division and death. The approach in Anderson & Burnham (2004); Burnham & Anderson (2004) was followed to derive the expression of AIC_C.

The general Akaike's information criterion (AIC), introduced for the first time in 1973 (see *e.g.* Akaike (1998)), is defined as

$$\text{AIC} = -2\log\left(\mathcal{L}(\hat{\theta})\right) + 2K,$$

in which $\mathcal{L}(\hat{\theta})$ is the maximum likelihood estimate and K is the number of parameters in the model. However, when the number of parameters is high compared to the size of the data set n, i.e. $n/K < 40$, the performance of AIC may be poor. Therefore, a second order correcting factor was introduced in 1978 by Hurvich & Tsai (1989); Sugiura (1978) and led to the definition of AIC_C as

$$\text{AIC}_C = \text{AIC} + \frac{2K(K+1)}{n-K-1}. \tag{A.1}$$

In order to derive the expression of AIC_C, let $\boldsymbol{\theta} = (C_0, N_0, N, \lambda_0, \lambda, \alpha)$, and $x_M^g(\boldsymbol{\theta}, t)$ represent the prediction given by the mathematical model with parameter values $\boldsymbol{\theta}$ for the number of cells in generation g at time t. Notice that

$x_M^g(\boldsymbol{\theta}, t) = x_M^g(t) = M^g(t)$ in the notation of Chapter 3. The parameters $\boldsymbol{\theta}$ have been added as variables to highlight their role when computing AIC_C. Then, let $x_D^g(t)$ denote the experimentally determined mean of cells in generation g at time t. Hence, one has

$$x_D^g(t) = x_M^g(\boldsymbol{\theta}, t) + \xi^g(t), \ t \in \mathscr{T}, \ g \geq G,$$

where $\mathscr{T}$ is the set of the time points. The errors, $\xi^g(t)$, are assumed to be independent and normally distributed with mean 0 and standard deviation $\sigma_D^g(t)$, which depends on the time point t and the generation g and is given with the data. Notice that Anderson & Burnham (2004); Burnham & Anderson (2004) assume that the errors are normally distributed with mean 0 and constant standard deviation σ. The hypothesis that the standard deviation varies with time and generations is due to the structure of the data set: for each time point and generation, a number of mice between 3 and 7 were considered, making possible to compute the standard deviation.

Given that the errors are independent and normally distributed, their joint distribution is

$$f(\xi^g(t)|\boldsymbol{\theta}, \sigma_D^g(t)) = \prod_{g=0}^{G} \prod_{t \in \mathscr{T}} \frac{1}{\sqrt{2\pi}\sigma_D^g(t)} \exp\left(-\frac{1}{2}\left(\frac{\xi^g(t)}{\sigma_D^g(t)}\right)^2\right),$$

and therefore the likelihood is given by

$$\mathcal{L}(\boldsymbol{\theta}) = \frac{1}{(2\pi)^{n/2}} \frac{1}{\prod_{g=0}^{G} \prod_{t \in \mathscr{T}} \sigma_D^g(t)} \exp\left(-\frac{1}{2} \sum_{g=0}^{G} \sum_{t \in \mathscr{T}} \left(\frac{\xi^g(t)}{\sigma_D^g(t)}\right)^2\right). \tag{A.2}$$

Switching to the logarithm and neglecting the terms which do not depend on $\xi^g(t)$, equation (A.2) becomes

$$\log\left(\mathcal{L}(\boldsymbol{\theta})\right) = -\frac{1}{2} \sum_{g=0}^{G} \sum_{t \in \mathscr{T}} \left(\frac{x_D^g(t) - x_M^g(\boldsymbol{\theta}, t)}{\sigma_D^g(t)}\right)^2. \tag{A.3}$$

Therefore, the parameters $\hat{\boldsymbol{\theta}}$ that maximise the (log)likelihood are the same that minimise the distance (3.41) used in the ABC-SMC algorithm implemented in

Chapter 3. Replacing the value of $\log\left(\mathcal{L}(\hat{\boldsymbol{\theta}})\right)$ derived in (A.3) in the formula of the AIC_C (A.1), one obtains

$$\mathrm{AIC}_C = \sum_{g=0}^{G} \sum_{t \in \mathscr{T}} \left(\frac{x_D^g(t) - x_M^g(\hat{\boldsymbol{\theta}}, t)}{\sigma_D^g(t)} \right)^2 + \frac{2Kn}{n - K - 1}. \tag{A.4}$$

Formula (A.4) was used to determine the values of AIC_C shown in Table 3.2.

References

Ablowitz, M.J., Fokas, A.S. & Fokas, A.S. (2003). *Complex variables: introduction and applications*. Cambridge University Press. 94

Abramowitz, M., Stegun, I.A. & Romer, R.H. (1988). Handbook of mathematical functions with formulas, graphs, and mathematical tables. 88, 91, 92

Abudurexiti, A., Adkins, S., Alioto, D., Alkhovsky, S.V., Avšič-Županc, T., Ballinger, M.J., Bente, D.A., Beer, M., Bergeron, É., Blair, C.D. *et al.* (2019). Taxonomy of the order bunyavirales: update 2019. *Archives of virology*, **164**, 1949–1965. 129

Akaike, H. (1998). Information theory and an extension of the maximum likelihood principle. In *Selected papers of hirotugu akaike*, 199–213, Springer. 207

Alizon, S. (2008). Decreased overall virulence in coinfected hosts leads to the persistence of virulent parasites. *The American Naturalist*, **172**, E67–E79. 181

Alizon, S. (2013a). Co-infection and super-infection models in evolutionary epidemiology. *Interface focus*, **3**, 20130031. 7, 181, 182, 204

Alizon, S. (2013b). Parasite co-transmission and the evolutionary epidemiology of virulence. *Evolution: International Journal of Organic Evolution*, **67**, 921–933. 182, 204

Allen, L.J. (2010). *An introduction to stochastic processes with applications to biology*. CRC press. xi, 7, 9, 16, 18, 19, 21, 23, 25, 26, 48, 77, 84, 95, 116, 126, 143, 145, 146, 201

Allen, L.J. (2015). Applications of multi-type branching processes. In *Stochastic Population and Epidemic Models*, 21–27, Springer. 75

Allen, L.J., Bokil, V.A., Cunniffe, N.J., Hamelin, F.M., Hilker, F.M. & Jeger, M.J. (2019). Modelling vector transmission and epidemiology of co-infecting plant viruses. *Viruses*, **11**, 1153. 133, 139

Anderson, D. & Burnham, K. (2004). Model selection and multi-model inference. *Second. NY: Springer-Verlag*, **63**, 10. 61, 66, 207, 208

Anderson, D. & Watson, R. (1980). On the spread of a disease with gamma distributed latent and infectious periods. *Biometrika*, **67**, 191–198. 136

Andrews, G.E., Askey, R., Roy, R., Roy, R. & Askey, R. (1999). *Special functions*, vol. 71. Cambridge university press Cambridge. 92

Antal, T. & Krapivsky, P. (2010). Exact solution of a two-type branching process: clone size distribution in cell division kinetics. *Journal of Statistical Mechanics: Theory and Experiment*, **2010**, P07028. 77, 80, 85, 89, 93, 94, 126

Antal, T. & Krapivsky, P. (2011). Exact solution of a two-type branching process: models of tumor progression. *Journal of Statistical Mechanics: Theory and Experiment*, **2011**, P08018. 75

Antia, R., Ganusov, V.V. & Ahmed, R. (2005). The role of models in understanding cd8+ t-cell memory. *Nature Reviews Immunology*, **5**, 101–111. 2, 33

Ariza, A., Tanner, S.J., Walter, C.T., Dent, K.C., Shepherd, D.A., Wu, W., Matthews, S.V., Hiscox, J.A., Green, T.J., Luo, M. *et al.* (2013). Nucleocapsid protein structures from orthobunyaviruses reveal insight into ribonucleoprotein architecture and rna polymerization. *Nucleic acids research*, **41**, 5912–5926. 129

Artalejo, J.R. & Lopez-Herrero, M.J. (2013). On the exact measure of disease spread in stochastic epidemic models. *Bulletin of mathematical biology*, **75**, 1031–1050. 7, 132, 162, 204

Asmussen, S. & Albrecher, H. (2010). *Ruin probabilities*, vol. 14. World scientific. 23

Athreya, K.B., Ney, P.E. & Ney, P. (2004). *Branching processes*. Courier Corporation. 5, 25, 75, 143

Bartoszyński, R. (1967). Branching processes and the theory of epidemics. In *Proceedings of the Berkeley Symposium on Mathematical Statistics and Probability*, vol. 4, 259, University of California Press. 141

Belli, A., Sarr, A., Rais, O., Rego, R.O. & Voordouw, M.J. (2017). Ticks infected via co-feeding transmission can transmit lyme borreliosis to vertebrate hosts. *Scientific Reports*, **7**, 1–13. 6, 131

Belluccini, G., López-García, M., Lythe, G. & Molina-París, C. (2022). Counting generations in birth and death processes with competing erlang and exponential waiting times. *Scientific Reports*, **12**, 1–20. 4, 5, 77, 97, 101, 116, 122, 126

Berger, Q., Caravenna, F. & Dai Pra, P. (2021). *Probabilità*. Springer. 9

Bhowmick, S., Kasi, K.K., Gethmann, J., Fischer, S., Conraths, F.J., Sokolov, I.M. & Lentz, H.H. (2022). Ticks on the run: A mathematical model of crimean-congo haemorrhagic fever (cchf)—key factors for transmission. *Epidemiologia*, **3**, 116–134. 131

Bittanti, S., Laub, A.J. & Willems, J.C. (2012). *The Riccati Equation*. Springer Science & Business Media. 85

Brouwer, A.F. (2022). Why the spectral radius? an intuition-building introduction to the basic reproduction number. *Bulletin of Mathematical Biology*, **84**, 96. 138

Bruss, F.T. & Duerinckx, M. (2015). Resource dependent branching processes and the envelope of societies. *The Annals of Applied Probability*, **25**, 324–372. 127

Burnham, K.P. & Anderson, D.R. (2004). Multimodel inference: understanding aic and bic in model selection. *Sociological methods research*, **33**, 261–304. 61, 66, 207, 208

Callard, R. & Hodgkin, P. (2007). Modeling t-and b-cell growth and differentiation. *Immunological reviews*, **216**, 119–129. 73

Callard, R.E., Stark, J. & Yates, A.J. (2003). Fratricide: a mechanism for t memory-cell homeostasis. *Trends in immunology*, **24**, 370–375. 74

Chao, H.X., Fakhreddin, R.I., Shimerov, H.K., Kedziora, K.M., Kumar, R.J., Perez, J., Limas, J.C., Grant, G.D., Cook, J.G., Gupta, G.P. *et al.* (2019). Evidence that the human cell cycle is a series of uncoupled, memoryless phases. *Molecular systems biology*, **15**, e8604. 35

Cheek, D. & Antal, T. (2018). Mutation frequencies in a birth–death branching process. *The Annals of Applied Probability*, **28**, 3922–3947. 75

Cheon, H., Prevedello, G., Oostindie, S.C., Dovedi, S.J., Hawkins, E.D., Marchingo, J.M., Heinzel, S., Duffy, K.R. & Hodgkin, P.D. (2021). Cyton2: A model of immune cell population dynamics that includes familial instructional inheritance. *Frontiers in Bioinformatics*, 50. 5, 35, 74, 78, 117, 126

Ciarlet, P.G., Miara, B. & Thomas, J.M. (1989). *Introduction to numerical linear algebra and optimisation*. Cambridge university press. 156

Coldman, A. & Goldie, J. (1986). A stochastic model for the origin and treatment of tumors containing drug-resistant cells. *Bulletin of mathematical biology*, **48**, 279–292. 76

Coldman, A.J., Goldie, J.H. & Ng, V. (1985). The effect of cellular differentiation on the development of permanent drug resistance. *Mathematical Biosciences*, **74**, 177–198. 76

Cox, F. (2001). Concomitant infections, parasites and immune responses. *Parasitology*, **122**, S23–S38. 6, 129

Csilléry, K., Blum, M.G., Gaggiotti, O.E. & François, O. (2010). Approximate bayesian computation (abc) in practice. *Trends in ecology & evolution*, **25**, 410–418. 27

De Boer, R.J. & Perelson, A.S. (2005). Estimating division and death rates from cfse data. *Journal of computational and applied mathematics*, **184**, 140–164. 51, 72, 73, 127

De Boer, R.J. & Perelson, A.S. (2013). Quantifying t lymphocyte turnover. *Journal of theoretical biology*, **327**, 45–87. 73

De Boer, R.J., Ganusov, V.V., Milutinović, D., Hodgkin, P.D. & Perelson, A.S. (2006). Estimating lymphocyte division and death rates from cfse data. *Bulletin of mathematical biology*, **68**, 1011–1031. 34, 61, 127

Deenick, E.K., Gett, A.V. & Hodgkin, P.D. (2003). Stochastic model of t cell proliferation: a calculus revealing il-2 regulation of precursor frequencies, cell cycle time, and survival. *The Journal of Immunology*, **170**, 4963–4972. 33, 55

den Braber, I., Mugwagwa, T., Vrisekoop, N., Westera, L., Mögling, R., de Boer, A.B., Willems, N., Schrijver, E.H., Spierenburg, G., Gaiser, K. *et al.* (2012). Maintenance of peripheral naive t cells is sustained by thymus output in mice but not humans. *Immunity*, **36**, 288–297. 33

Dessalles, R., Pan, Y., Xia, M., Maestrini, D., D'Orsogna, M.R. & Chou, T. (2021). How naive t-cell clone counts are shaped by heterogeneous thymic output and homeostatic proliferation. *Frontiers in immunology*, **12**. 74

Diekmann, O., Heesterbeek, J.A.P. & Metz, J.A. (1990). On the definition and the computation of the basic reproduction ratio r 0 in models for infectious diseases in heterogeneous populations. *Journal of mathematical biology*, **28**, 365–382. 135, 136

Diekmann, O., Heesterbeek, J. & Roberts, M.G. (2010). The construction of next-generation matrices for compartmental epidemic models. *Journal of the royal society interface*, **7**, 873–885. 132, 136, 201

Dohm, D.J., Logan, T.M., Linthicum, K.J., Rossi, C.A. & Turell, M.J. (2014). Transmission of crimean-congo hemorrhagic fever virus by hyalomma impeltatum (acari: Ixodidae) after experimental infection. *Journal of medical entomology*, **33**, 848–851. 134

Dowling, M.R., Kan, A., Heinzel, S., Zhou, J.H., Marchingo, J.M., Wellard, C.J., Markham, J.F. & Hodgkin, P.D. (2014). Stretched cell cycle model for proliferating lymphocytes. *Proceedings of the National Academy of Sciences*, **111**, 6377–6382. 5, 34, 74, 117

Duffy, K.R. & Hodgkin, P.D. (2012). Intracellular competition for fates in the immune system. *Trends in cell biology*, **22**, 457–464. 5, 35, 74, 117, 119

Duffy, K.R. & Subramanian, V.G. (2009). On the impact of correlation between collaterally consanguineous cells on lymphocyte population dynamics. *Journal of mathematical biology*, **59**, 255–285. 5, 34, 35, 74, 117

Duffy, K.R., Wellard, C.J., Markham, J.F., Zhou, J.H., Holmberg, R., Hawkins, E.D., Hasbold, J., Dowling, M.R. & Hodgkin, P.D. (2012). Activation-induced b cell fates are selected by intracellular stochastic competition. *Science*, **335**, 338–341. 5, 34, 74, 117

El-Aouar Filho, R.A., Nicolas, A., De Paula Castro, T.L., Deplanche, M., De Carvalho Azevedo, V.A., Goossens, P.L., Taieb, F., Lina, G., Le Loir, Y. & Berkova, N. (2017). Heterogeneous family of cyclomodulins: smart weapons that allow bacteria to hijack the eukaryotic cell cycle and promote infections. *Frontiers in cellular and infection microbiology*, **7**, 208. xi, 3, 4

Ganusov, V.V., Milutinović, D. & De Boer, R.J. (2007). Il-2 regulates expansion of cd4+ t cell populations by affecting cell death: insights from modeling cfse data. *The Journal of Immunology*, **179**, 950–957. 39, 61, 65, 73, 122, 127

Gao, D., Porco, T.C. & Ruan, S. (2016). Coinfection dynamics of two diseases in a single host population. *Journal of mathematical analysis and applications*, **442**, 171–188. 133, 141, 180, 181

Gargili, A., Estrada-Peña, A., Spengler, J.R., Lukashev, A., Nuttall, P.A. & Bente, D.A. (2017). The role of ticks in the maintenance and transmission of crimean-congo hemorrhagic fever virus: A review of published field and laboratory studies. *Antiviral research*, **144**, 93–119. 131, 134, 176

Gett, A.V. & Hodgkin, P.D. (2000). A cellular calculus for signal integration by t cells. *Nature immunology*, **1**, 239–244. 34, 72, 73

Gillespie, D.T. (1976). A general method for numerically simulating the stochastic time evolution of coupled chemical reactions. *Journal of computational physics*, **22**, 403–434. 2, 26, 33, 46, 53, 73, 78, 104, 126

Gillespie, D.T. (1977). Exact stochastic simulation of coupled chemical reactions. *The journal of physical chemistry*, **81**, 2340–2361. 2, 26, 33, 46, 53, 73, 78, 104, 126

Goggans, P.M., Cao, L. & Henderson, R.W. (2014). Assigning priors for parameters constrained to a simplex region. In *AIP Conference Proceedings*, vol. 1636, 94–99, American Institute of Physics. 96, 123

Gómez-Corral, A. & García, M.L. (2014). Maximum queue lengths during a fixed time interval in the m/m/c retrial queue. *Applied Mathematics and Computation*, **235**, 124–136. 43

Gómez-Corral, A. & López García, M. (2013). Maximum population sizes in host–parasitoid models. *International Journal of Biomathematics*, **6**, 1350002. 43

Gonzalez, J.P., Camicas, J.L., Cornet, J.P., Faye, O. & Wilson, M. (1992). Sexual and transovarian transmission of crimean-congo haemorrhagic fever virus in hyalomma truncatum ticks. *Research in virology*, **143**, 23–28. 6, 131, 133, 201

Gonzalez, J.P., Camicas, J.L., Cornet, J.P. & Wilson, M. (1998). Biological and clinical responses of west african sheep to crimean-congo haemorrhagic fever virus experimental infection. *Research in virology*, **149**, 445–455. 131, 133, 176

Gunnarsson, E.B., De, S., Leder, K. & Foo, J. (2020). Understanding the role of phenotypic switching in cancer drug resistance. *Journal of theoretical biology*, **490**, 110162. 75

Guo, Z., Zhang, Z., Prajapati, M. & Li, Y. (2021). Lymphopenia caused by virus infections and the mechanisms beyond. *Viruses*, **13**, 1876. 61

Haccou, P., Haccou, P., Jagers, P., Vatutin, V.A. & Vatutin, V. (2005). *Branching processes: variation, growth, and extinction of populations*. 5, Cambridge university press. 25

Harris, T.E. *et al.* (1963). *The theory of branching processes*, vol. 6. Springer Berlin. 25, 26

Hart, Y., Reich-Zeliger, S., Antebi, Y.E., Zaretsky, I., Mayo, A.E., Alon, U. & Friedman, N. (2014). Paradoxical signaling by a secreted molecule leads to homeostasis of cell levels. *Cell*, **158**, 1022–1032. 74

Hasbold, J., Gett, A., Rush, J., Deenick, E., Avery, D., Jun, J. & Hodgkin, P.D. (1999). Quantitative analysis of lymphocyte differentiation and proliferation in vitro using carboxyfluorescein diacetate succinimidyl ester. *Immunology and cell biology*, **77**, 516–522. 34

Hawkins, E., Markham, J., McGuinness, L. & Hodgkin, P. (2009). A single-cell pedigree analysis of alternative stochastic lymphocyte fates. *Proceedings of the National Academy of Sciences*, **106**, 13457–13462. 5, 34, 74, 76, 78, 79, 117, 126

Hawkins, E.D., Turner, M.L., Dowling, M.R., Van Gend, C. & Hodgkin, P.D. (2007). A model of immune regulation as a consequence of randomized lymphocyte division and death times. *Proceedings of the National Academy of Sciences*, **104**, 5032–5037. 4, 35, 55, 56, 65, 72, 73, 78

He, Q.M. (2014). *Fundamentals of matrix-analytic methods*, vol. 365. Springer. 4, 9, 16, 23

Hoch, T., Breton, E. & Vatansever, Z. (2018). Dynamic modeling of crimean congo hemorrhagic fever virus (cchfv) spread to test control strategies. *Journal of Medical Entomology*, **55**, 1124–1132. 131, 134, 135, 176, 184

Hogan, T., Shuvaev, A., Commenges, D., Yates, A., Callard, R., Thiebaut, R. & Seddon, B. (2013). Clonally diverse t cell homeostasis is maintained by a common program of cell-cycle control. *The Journal of Immunology*, **190**, 3985–3993. xiii, 4, 34, 36, 60, 61, 62, 63, 64, 68, 72, 74

Hurvich, C.M. & Tsai, C.L. (1989). Regression and time series model selection in small samples. *Biometrika*, **76**, 297–307. 207

Jacob, C. (2010). Branching processes: their role in epidemiology. *International journal of environmental research and public health*, **7**, 1186–1204. 141

Jacod, J. & Protter, P. (2004). *Probability essentials*. Springer Science & Business Media. 9

Karlin, S. & Taylor, H. (1975). *A First Course in Stochastic Processes*, vol. 1. Gulf Professional Publishing. 15, 16, 143

Kendall, D.G. (1948). On the role of variable generation time in the development of a stochastic birth process. *Biometrika*, **35**, 316–330. 35

Kimmel, M. & Axelrod, D.E. (2002). *Branching processes in biology*. Springer, New York, NY. 25, 26

Kinjyo, I., Qin, J., Tan, S.Y., Wellard, C.J., Mrass, P., Ritchie, W., Doi, A., Cavanagh, L.L., Tomura, M., Sakaue-Sawano, A. *et al.* (2015). Real-time tracking of cell cycle progression during cd8+ effector and memory t-cell differentiation. *Nature communications*, **6**, 1–13. 34, 65, 72, 73, 78

Klempa, B. (2018). Reassortment events in the evolution of hantaviruses. *Virus genes*, **54**, 638–646. xvi, 130

Kulkarni, V.G. (2016). *Modeling and analysis of stochastic systems*. Chapman and Hall/CRC. 16, 17

Lambert, A. (2005). The branching process with logistic growth. *The Annals of Applied Probability*, **15**, 1506–1535. 127

Lee, H.Y. & Perelson, A.S. (2008). Modeling t cell proliferation and death in vitro based on labeling data: generalizations of the smith–martin cell cycle model. *Bulletin of mathematical biology*, **70**, 21–44. 34, 73

León, K., Faro, J. & Carneiro, J. (2004). A general mathematical framework to model generation structure in a population of asynchronously dividing cells. *Journal of theoretical biology*, **229**, 455–476. 35

Lou, Y., Wu, J. & Wu, X. (2014). Impact of biodiversity and seasonality on lyme-pathogen transmission. *Theoretical Biology and Medical Modelling*, **11**, 1–25. 131, 135, 177, 184

Lovell-Read, F.A., Shen, S. & Thompson, R.N. (2022). Estimating local outbreak risks and the effects of non-pharmaceutical interventions in age-structured populations: Sars-cov-2 as a case study. *Journal of Theoretical Biology*, **535**, 110983. 75

Lowen, A.C. (2017). Constraints, drivers, and implications of influenza a virus reassortment. *Annual review of virology*, **4**, 105–121. 6, 129

Lowen, A.C. (2018). It's in the mix: Reassortment of segmented viral genomes. *PLoS Pathogens*, **14**, e1007200. 6, 129

Luzyanina, T. & Bocharov, G.A. (2018). Markov chain monte carlo parameter estimation of the ode compartmental cell growth model. *Mathematical biology and bioinformatics*, **13**, 376–391. 51, 73

Luzyanina, T., Mrusek, S., Edwards, J.T., Roose, D., Ehl, S. & Bocharov, G. (2007). Computational analysis of cfse proliferation assay. *Journal of mathematical biology*, **54**, 57–89. 35, 51, 53, 73

Lyons, A.B. & Parish, C.R. (1994). Determination of lymphocyte division by flow cytometry. *Journal of immunological methods*, **171**, 131–137. 34, 38

Lythe, G., Callard, R.E., Hoare, R.L. & Molina-París, C. (2016). How many tcr clonotypes does a body maintain? *Journal of theoretical biology*, **389**, 214–224. 1

Ma, W., Lager, K., Vincent, A., Janke, B., Gramer, M. & Richt, J. (2009). The role of swine in the generation of novel influenza viruses. *Zoonoses and public health*, **56**, 326–337. 129

Mackillop, J., Ciampi, A., E. Till, J. & N. Buick, R. (1983). A stem cell model of human tumor growth: implications for tumor cell clonogenic assays. *Journal of the national cancer institute*, **70**, 9–16. 75, 76

Markham, J.F., Wellard, C.J., Hawkins, E.D., Duffy, K.R. & Hodgkin, P.D. (2010). A minimum of two distinct heritable factors are required to explain correlation structures in proliferating lymphocytes. *Journal of the Royal Society Interface*, **7**, 1049–1059. xvi, 5, 34, 35, 65, 72, 73, 74, 76, 78, 79, 117, 118, 120, 123, 127

Matser, A., Hartemink, N., Heesterbeek, H., Galvani, A. & Davis, S. (2009). Elasticity analysis in epidemiology: an application to tick-borne infections. *Ecology Letters*, **12**, 1298–1305. 6, 131, 133, 201

Mazzocco, P., Bernard, S. & Pujo-Menjouet, L. (2017). Estimates and impact of lymphocyte division parameters from cfse data using mathematical modelling. *Plos one*, **12**, e0179768. 65, 73, 122

McDonald, S.M., Nelson, M.I., Turner, P.E. & Patton, J.T. (2016). Reassortment in segmented rna viruses: mechanisms and outcomes. *Nature Reviews Microbiology*, **14**, 448–460. 6, 129

Mehand, M.S., Al-Shorbaji, F., Millett, P. & Murgue, B. (2018). The who r&d blueprint: 2018 review of emerging infectious diseases requiring urgent research and development efforts. *Antiviral research*, **159**, 63–67. 6, 130

Michalakis, Y. & Blanc, S. (2020). The curious strategy of multipartite viruses. *Annual Review of Virology*, **7**, 203–218. 130

Míguez, D.G. (2015). A branching process to characterize the dynamics of stem cell differentiation. *Scientific reports*, **5**, 1–13. 127

Moler, C. & Van Loan, C. (1978). Nineteen dubious ways to compute the exponential of a matrix. *SIAM review*, **20**, 801–836. 20, 43

Moler, C. & Van Loan, C. (2003). Nineteen dubious ways to compute the exponential of a matrix, twenty-five years later. *SIAM review*, **45**, 3–49. 20, 43

Monsalve-Arteaga, L., Alonso-Sardón, M., Muñoz Bellido, J.L., Vicente Santiago, M.B., Vieira Lista, M.C., López Abán, J., Muro, A. & Belhassen-García, M. (2020). Seroprevalence of crimean-congo hemorrhagic fever in humans in the world health organization european region: A systematic review. *PLoS neglected tropical diseases*, **14**, e0008094. 205

Mpeshe, S.C., Haario, H. & Tchuenche, J.M. (2011). A mathematical model of rift valley fever with human host. *Acta biotheoretica*, **59**, 231–250. 135, 184

Negredo, A., Sánchez-Arroyo, R., Díez-Fuertes, F., de Ory, F., Budiño, M.A., Vázquez, A., Garcinuño, Á., Hernández, L., De la Hoz González, C., Gutiérrez-Arroyo, A. *et al.* (2021). Fatal case of crimean-congo hemorrhagic fever caused by reassortant virus, spain, 2018. *Emerging infectious diseases*, **27**, 1211. 130

Norman, R., Bowers, R., Begon, M. & Hudson, P.J. (1999). Persistence of tick-borne virus in the presence of multiple host species: tick reservoirs and parasite mediated competition. *Journal of theoretical biology*, **200**, 111–118. 134

Norman, R., Ross, D., Karen Laurenson, M. & Hudson, P.J. (2004). The role of non-viraemic transmission on the persistence and dynamics of a tick borne virus–louping ill in red grouse (lagopus lagopus scoticus) and mountain hares (lepus timidus). *Journal of Mathematical Biology*, **48**, 119–134. 135, 177, 184

Norris, J.R. (1998). *Markov chains*. 2, Cambridge university press. 9, 18, 25

Nurettin, C., Engin, B., Sukru, T., Munir, A., Zati, V. & Aykut, O. (2022). The seroprevalence of crimean-congo hemorrhagic fever in wild and domestic animals: An epidemiological update for domestic animals and first seroevidence in wild animals from turkiye. *Veterinary Sciences*, **9**, 462. 205

Ogden, N., Bigras-Poulin, M., O'callaghan, C., Barker, I., Lindsay, L., Maarouf, A., Smoyer-Tomic, K., Waltner-Toews, D. & Charron, D. (2005). A dynamic population model to investigate effects of climate on geographic range and seasonality of the tick ixodes scapularis. *International journal for parasitology*, **35**, 375–389. 131

Pandit, A. & De Boer, R.J. (2019). Stochastic inheritance of division and death times determines the size and phenotype of cd8+ t cell families. *Frontiers in immunology*, **10**, 436. 4, 34

Pereira, J.P., Girard, R., Chaby, R., Cumano, A. & Vieira, P. (2003). Monoallelic expression of the murine gene encoding toll-like receptor 4. *Nature immunology*, **4**, 464–470. 33, 55

Perveen, N. & Khan, G. (2022). Crimean–congo hemorrhagic fever in the arab world: A systematic review. *Frontiers in Veterinary Science*, **9**. xvi, 132

Phonera, M.C., Simuunza, M.C., Kainga, H., Ndebe, J., Chembensofu, M., Chatanga, E., Kanyanda, S., Changula, K., Muleya, W., Mubemba, B. *et al.* (2021). Seroprevalence and risk factors of crimean-congo hemorrhagic fever in cattle of smallholder farmers in central malawi. *Pathogens*, **10**, 1613. 205

Pinchover, Y., Rubinstein, J. *et al.* (2005). *An introduction to partial differential equations*, vol. 10. Cambridge university press. 83

Pinsky, M. & Karlin, S. (2010). *An introduction to stochastic modeling*. Academic press. 7, 77, 95, 132, 148, 183

Pritchard, J.K., Seielstad, M.T., Perez-Lezaun, A. & Feldman, M.W. (1999). Population growth of human y chromosomes: a study of y chromosome microsatellites. *Molecular biology and evolution*, **16**, 1791–1798. 28

Quah, B.J. & Parish, C.R. (2012). New and improved methods for measuring lymphocyte proliferation in vitro and in vivo using cfse-like fluorescent dyes. *Journal of immunological methods*, **379**, 1–14. 34

Revy, P., Sospedra, M., Barbour, B. & Trautmann, A. (2001). Functional antigen-independent synapses formed between t cells and dendritic cells. *Nature immunology*, **2**, 925–931. 51, 73

Roberts, M. & Heesterbeek, J. (2003). A new method for estimating the effort required to control an infectious disease. *Proceedings of the Royal Society of London. Series B: Biological Sciences*, **270**, 1359–1364. 139

Rochman, Y., Spolski, R. & Leonard, W.J. (2009). New insights into the regulation of t cells by γc family cytokines. *Nature Reviews Immunology*, **9**, 480–490. 2

Rosà, R., Pugliese, A., Norman, R. & Hudson, P.J. (2003). Thresholds for disease persistence in models for tick-borne infections including non-viraemic transmission, extended feeding and tick aggregation. *Journal of theoretical biology*, **224**, 359–376. 131

Shutt, D.P., Manore, C.A., Pankavich, S., Porter, A.T. & Del Valle, S.Y. (2017). Estimating the reproductive number, total outbreak size, and reporting rates for zika epidemics in south and central america. *Epidemics*, **21**, 63–79. 140

Smith, J. & Martin, L. (1973). Do cells cycle? *Proceedings of the National Academy of Sciences*, **70**, 1263–1267. 34

Sompayrac, L.M. (2022). *How the immune system works*. John Wiley & Sons. 1

Spengler, J.R. & Estrada-Peña, A. (2018). Host preferences support the prominent role of hyalomma ticks in the ecology of crimean-congo hemorrhagic fever. *PLoS neglected tropical diseases*, **12**, e0006248. 131

Spengler, J.R., Bergeron, É. & Rollin, P.E. (2016). Seroepidemiological studies of crimean-congo hemorrhagic fever virus in domestic and wild animals. *PLoS neglected tropical diseases*, **10**, e0004210. 131

Spengler, J.R., Bergeron, É. & Spiropoulou, C.F. (2019). Crimean-congo hemorrhagic fever and expansion from endemic regions. *Current opinion in virology*, **34**, 70–78. 130, 131

Stirzaker, D. (2005). *Stochastic processes and models*. OUP Oxford. 9, 16

Sugiura, N. (1978). Further analysts of the data by akaike's information criterion and the finite corrections: Further analysts of the data by akaike's. *Communications in Statistics-theory and Methods*, **7**, 13–26. 207

Sutton, A., Karagenc, T., Bakirci, S., Sarali, H., Pekel, G. & Medley, G. (2012). Modelling the transmission dynamics of theileria annulata: model structure and validation for the turkish context. *Parasitology*, **139**, 441–453. 135, 177

Takahashi, M. (1966). Theoretical basis for cell cycle analysis i. labelled mitosis wave method. *Journal of Theoretical Biology*, **13**, 202–211. 34

Takahashi, M. (1968). Theoretical basis for cell cycle analysis: Ii. further studies on labelled mitosis wave method. *Journal of theoretical biology*, **18**, 195–209. 35

Teschl, G. (2012). *Ordinary differential equations and dynamical systems*, vol. 140. American Mathematical Soc. 90

Till, J.E., McCulloch, E.A. & Siminovitch, L. (1964). A stochastic model of stem cell proliferation, based on the growth of spleen colony-forming cells. *Proceedings of the National Academy of Sciences of the United States of America*, **51**, 29. 75, 76

Toni, T., Welch, D., Strelkowa, N., Ipsen, A. & Stumpf, M.P. (2009). Approximate bayesian computation scheme for parameter inference and model selection in dynamical systems. *Journal of the Royal Society Interface*, **6**, 187–202. 4, 5, 28, 29, 30, 36, 63, 64

van Baalen, M. & Sabelis, M.W. (1995). The dynamics of multiple infection and the evolution of virulence. *The American Naturalist*, **146**, 881–910. 182, 204

Van den Driessche, P. (2017). Reproduction numbers of infectious disease models. *Infectious Disease Modelling*, **2**, 288–303. 7, 132, 136, 139

Van den Driessche, P. & Watmough, J. (2002). Reproduction numbers and sub-threshold endemic equilibria for compartmental models of disease transmission. *Mathematical biosciences*, **180**, 29–48. 135, 136, 137, 180, 201

Vittadello, S.T., McCue, S.W., Gunasingh, G., Haass, N.K. & Simpson, M.J. (2019). Mathematical models incorporating a multi-stage cell cycle replicate normally-hidden inherent synchronization in cell proliferation. *Journal of the Royal Society Interface*, **16**, 20190382. 35

Weber, T.S., Jaehnert, I., Schichor, C., Or-Guil, M. & Carneiro, J. (2014). Quantifying the length and variance of the eukaryotic cell cycle phases by a stochastic model and dual nucleoside pulse labelling. *PLoS computational biology*, **10**, e1003616. 35

Wellard, C., Markham, J., Hawkins, E. & Hodgkin, P. (2010). The effect of correlations on the population dynamics of lymphocytes. *Journal of Theoretical Biology*, **264**, 443–449. 5, 34, 74, 78, 117

Wellard, C., Markham, J.F., Hawkins, E.D. & Hodgkin, P.D. (2011). The cyton model for lymphocyte proliferation and differentiation. In *Mathematical Models and Immune Cell Biology*, 107–120, Springer. 34

Westera, L., Drylewicz, J., Den Braber, I., Mugwagwa, T., Van Der Maas, I., Kwast, L., Volman, T., Van De Weg-Schrijver, E.H., Bartha, I., Spierenburg, G. *et al.* (2013). Closing the gap between t-cell life span estimates from stable isotope-labeling studies in mice and humans. *Blood, The Journal of the American Society of Hematology*, **122**, 2205–2212. 33

Whittaker, E.T. (1903). An expression of certain known functions as generalized hypergeometric functions. *Bulletin of the American Mathematical Society*, **10**, 125–134. 87

Yates, C.A., Ford, M.J. & Mort, R.L. (2017). A multi-stage representation of cell proliferation as a markov process. *Bulletin of mathematical biology*, **79**, 2905–2928. 2, 4, 35, 36, 38, 44, 46, 47, 97, 101, 107

Zhang, X., Zheng, P., Prestwood, T.R., Zhang, H., Carmi, Y., Tolentino, L.L., Wu, N., Choi, O., Winer, D.A., Strober, S. *et al.* (2020). Human regulatory dendritic cells develop from monocytes in response to signals from regulatory and helper t cells. *Frontiers in Immunology*, **11**, 1982. xi, 39

Zhu, H., Webby, R., Lam, T.T., Smith, D.K., Peiris, J.S. & Guan, Y. (2011). History of swine influenza viruses in asia. *Swine influenza*, 57–68. 129

Zilman, A., Ganusov, V.V. & Perelson, A.S. (2010). Stochastic models of lymphocyte proliferation and death. *PLoS one*, **5**, e12775. 2, 35, 43, 61, 65, 72, 73, 126